

EXPLOITING THE SUPRAMOLECULAR CHEMISTRY OF CARBON NANOHOOPS AND
THEIR POTENTIAL IN AQUEOUS APPLICATIONS

by

CLAIRE ELIZABETH OTTESON

A DISSERTATION

Presented to the Department of Chemistry and Biochemistry
and the Division of Graduate Studies of the University of Oregon
in partial fulfillment of the requirements for the degree of
Doctor of Philosophy

September 2022

DISSERTATION APPROVAL PAGE

Student: Claire Elizabeth Otteson

Title: Exploiting the Supramolecular Chemistry of Carbon Nanohoops and Their Potential in Aqueous Applications

This dissertation has been accepted and approved in partial fulfillment of the requirements for the Doctor of Philosophy degree in the Department of Chemistry and Biochemistry by:

Michael Haley	Chairperson
Ramesh Jasti	Advisor
Michael Pluth	Core Member
Juliet Baxter	Institutional Representative

and

Krista Chronister	Vice Provost for Graduate Studies
-------------------	-----------------------------------

Original approval signatures are on file with the University of Oregon Division of Graduate Studies.

Degree awarded September 2022

© 2022 Claire Elizabeth Otteson

This work is licensed under a Creative Commons

Attribution (United States) License.



DISSERTATION ABSTRACT

Claire Elizabeth Otteson

Doctor of Philosophy

Department of Chemistry and Biochemistry

September 2022

Title: Exploiting the Supramolecular Chemistry of Carbon Nanohoops and Their Potential in Aqueous Applications

Carbon nanomaterials have a wide variety of proposed applications spanning across many different fields. Since their fairly recent isolation, many of these applications are actively being investigated, however those that take place in aqueous media remain relatively underexplored due to challenges with solubility. Carbon nanohoops or [n]CPPs are small molecules that can be synthesized in atom precise ways not possible with other carbon nanomaterials and are therefore poised to serve as model systems to explore aqueous applications of carbon nano-systems.

Chapter **I** provides a discussion of the supramolecular chemistry of CPPs and their derivatives. Chapter **II** describes the development of a modular synthesis of fully water-soluble carbon nanohoops of varying sizes. The following chapter (**III**) will delve into the study of these water soluble nanohoops as hosts for other carbon nanomaterials in water and other polar environments towards better understanding how carbon nanomaterials behave in aqueous media. Chapter **IV** will discuss the development of a nanohoop-based rotaxane as a fluorescent sensor for biologically relevant analyte hydrosulfide anion. Chapter **V** will detail the further development of the rotaxane sensors as a modular family of sensors for a variety of different biological analytes. In summary the findings in this dissertation provide synthetic strategies for the development of carbon nanohoops towards use in biological and aqueous systems.

This dissertation includes previously published and unpublished co-authored material.

CURRICULUM VITAE

NAME OF AUTHOR: Claire Elizabeth Otteson

GRADUATE AND UNDERGRADUATE SCHOOLS ATTENDED:

University of Oregon, Eugene
Carroll University, Waukesha

DEGREES AWARDED:

Doctor of Philosophy, Chemistry, 2022, University of Oregon
Bachelor of Science, Chemistry, 2015, Carroll University

AREAS OF SPECIAL INTEREST:

Synthetic Organic Chemistry
Physical Organic Chemistry
Chemical Biology

PROFESSIONAL EXPERIENCE:

Instructor of Note, University of Oregon, 2021
Teaching Fellow, University of Oregon, 2017-2020

GRANTS, AWARDS, AWARDS AND HONORS:

NSF Research Traineeship, University of Oregon, Materials Science Institute 2020
Excellence in the Teaching of Chemistry Award, University of Oregon, 2019 and 2021
Thronson International Scholarship, Carroll University, 2015

PUBLICATIONS:

Patrick, C. W.; Woods, J. F.; Gaweel, P.; Otteson, C. E.; Thompson, A. L.; Claridge, T. D. W.; Jasti, R.; Anderson, H. L. Polyynes [3]rotaxanes: Synthesis via dicobalt carbonyl complexes and enhanced stability. *Angew. Chem. Int. Ed.* **2022**, *61* (10), e202116897.

Lovell, T. C.; Bolton, S. G.; Kenison, J. P.; Shangguan, J.; Otteson, C. E.; Civitci, F.; Nan, X.; Pluth, M. D.; Jasti, R. Biocompatible, intracellularly targeted nanohoop for one- and two-photon live cell imaging. *ACS Nano*. **2021**, *15* (9), 15285.

Otteson, C. E.; Levinn C. M.; Van Raden, J. M.; Pluth, M. D.; Jasti, R. Nanohoop rotaxane design to enhance selectivity of reaction-based probes: a proof-of-principle study. *Org. Lett.* **2021**, *23* (12), 4608.

Gilbert, A. K.; Zhao, Y.; Otteson, C. E.; Pluth, M. D. Development of Acid-Mediated H₂S/COS Donors That Respond to a Specific pH Window. *J. Org. Chem.* **2019**, *84* (22), 14469.

ACKNOWLEDGEMENTS

Firstly, I would like to acknowledge all the teachers and mentors that encouraged me throughout the years. Dr. Gail Vojta is an incredible role model as a woman in science and a wonderful teacher, without whose encouragement I would not have pursued a graduate degree. Further I would like to thank all the faculty and staff in the Department of Chemistry at Carroll University who fostered my love for both teaching and chemistry, as well as Professor David Amabilino for giving me my first opportunity to perform research. Professors Mike Pluth and Mike Haley, thank you for your guidance and support throughout my graduate career. And above all, I want to thank Professor Ramesh Jasti for all the support and guidance he has lent me for the past five years. He is an incredibly kind and thoughtful mentor and person who welcomed me into his lab and always encouraged and supported – I could not have asked for a better advisor.

I would also like to thank my fellow graduate students and postdoctoral researchers who have mentored, collaborated, or otherwise supported me through my journey. Dr. Yu Zhao, Dr. Terri Lovell, Dr. Tobias Shaub, and Dr. Justin Dressler were all wonderful friends and mentors who each taught me so much during my first year in Oregon and beyond. Former lab mates, Dr. Brittney White, Dr. Jeff Van Raden, Dr. Tobias Shaub, Dr. Erik Leonhardt, Dr. Curtis Colwell, Dr. Terri Lovell, and Dr. Ruth Maust welcomed me into the lab and were excellent lab mates, friends, and mentors who each contributed to my research and my life. I would also like to thank the current Jasti lab for their continued support and kindness. Beyond that, I have made many wonderful friends here who made this process much more fun; specifically, I want to thank Thaís De Faria and Terri Lovell, whose friendship is unflinching.

Finally, I want to thank my family, particularly my parents Amy and Dean Otteson for always supporting me in every area of my life. Their love and support have made me who I am

today, and I cannot thank them enough for all they have done for me. I would also like to thank my wonderful partner Dr. Dan Seidenkranz, who has been a pillar of support for me in both my graduate career and my life outside of UO - thank you for always believing in me. Finally, I want to thank my dogs, Green Bean and Cora, for simply being, especially Beans who has been by my side from the very beginning and never fails to make me smile.

Dedicated to Green Bean, my best friend, my adventure buddy, my emotional support system -
my dog.

TABLE OF CONTENTS

Chapter		Page
I.	THE PROPERTIES AND POTENTIAL OF CARBON NANOHOOPS IN SUPRAMOLECULAR CHEMISTRY	1
	1.1. Introduction	1
	1.2. Fullerene Guests	3
	1.3. Nanohoop and Nanotube Guests	7
	1.3.1. Saturn Systems	7
	1.3.2. Carbon Nanotubes	9
	1.4. Small Molecule Guests	10
	1.4.1. Polycyclic Aromatic Hydrocarbons	10
	1.4.2. Charged Guests	11
	1.5. Mechanically Interlocked Molecules	13
	1.6. Outlook	16
	1.7. Bridge to Chapter II	17
II.	THE DEVELOPMENT OF A MODULAR SYNTHESIS FOR WATER-SOLUBLE CARBON NANOHOOPS	18
	2.1. Introduction	18
	2.2. Results and Discussion	21
	2.3. Conclusion	26
	2.4. Experimental Sections	27
	2.4.1. General Experimental Details	27
	2.4.2. Synthesis and Characterization	28
	2.4.3. Cell Imaging	45

2.5. Bridge to Chapter III	48
III. EXPLORING THE SUPRAMOLECULAR CHEMISTRY OF WATER-SOLUBLE CARBON NANOHOOPS.	49
3.1. Introduction	49
3.2. Results and Discussion	52
3.3. Conclusion	56
3.4. Experimental Sections	57
3.4.1. General Experimental Details	57
3.4.2. Photophysical Studies	60
3.5. Bridge to Chapter IV	82
IV. NANOHOOP ROTAXANE DESIGN TO ENHANCE THE SELECTIVITY OF REACTION-BASED PROBES: A PROOF-OF-PRINCIPLE STUDY	83
4.1. Introduction	83
4.2. Results and Discussion	85
4.3. Conclusion	90
4.4. Experimental Sections	90
4.4.1. General Experimental Details	90
4.4.2. Synthesis and Characterization	91
4.4.3. ¹ H NMR Studies	94
4.4.4. Photophysical Studies	97
4.5. Bridge to Chapter V	110
V. TOWARDS THE DEVELOPMENT OF MODULAR NANOHOOP- [2]ROTAXANES FOR BIOLOGICAL SENSING APPLICATIONS.....	111

5.1. Introduction	111
5.2. Results and Discussion	113
5.2.1. Work Towards Biological Compatibility	113
5.2.2. Work Towards Exploring Modularity	115
5.3. Conclusion	117
5.4. Experimental Sections	118
5.4.1. General Experimental Details	118
5.4.2. Synthesis and Characterization	119
CONCLUDING REMARKS	126
REFERENCES CITED	127

LIST OF FIGURES

Figure	Page
1.1. Well established macrocyclic hosts used in supramolecular chemistry, cyclodextrins and cucurbiturils, contain a variety of functional groups making them capable of hosting a range of guests via multiple types of supramolecular interactions. In comparison, carbon nanohoops are functionally simple molecules, however their unique make-up gives rise to a radially oriented pi-system (bottom right) capable of interacting with suitable guests.	2
1.2. Carbon nanohoops represent the smallest cross-section of arm-chair carbon nanotubes, as such it was predicted that similar to CNTs, CPPs should be capable of hosting C ₆₀	4
1.3. Association constants (K _a) for [10]CPP derivatives with C ₆₀ all measured in toluene. 1) unfunctionalized [10]CPP ²⁵ ; 2) porphyrin-appended [10]CPP for charge transfer ²⁸ ; 3) π-extended [10]CPP derivatives ²⁷ ; 4) pyridine- and pyridinium-[10]CPP ³⁰ ; 5) BT-[10]CPP. ²⁹	5
1.4. Nanohoop-based “Saturn” complexes have been predicted to form with the general formula [n+5]CPP⊂[n]CPP (i.e. [12]CPP⊂[7]CPP, left), while isolation has proven challenging systems including the ternary complex of [15]CPP⊂[10]CPP⊂C ₆₀ (right) have been identified by NMR spectroscopy. ³⁹ ...	8
1.5. Theoretical work predicts complexation of nanohoops with CNTs. ⁴⁴	10
1.6. An [11]CPP⊂coronene complex – one amongst a series of CPP-aromatic hydrocarbon complexes recently described by the Bruns group – is stabilized by CH-π interactions. ⁴⁵	11
1.7. Left: 1,4-DMB[8]CPP effectively hosts NMP ⁺ via electrostatic interactions. ⁴⁷ Right: dodecamethoxy[9]CPP plays host to a number of cationic molecules due to functionalization with electron donating methyl ether groups. ⁴⁸	12
1.8. (Top) a fullerene-based thread interlocked within [10]CPP was templated using convex-concave π-π interactions between host and guest, ⁵³ (bottom) an alternative passive template approach to interlocked nanohoops is based on the incorporation of nitrogen into the backbone. ⁶¹	14
1.9. Active template synthesis of nanohoop-[2]rotaxanes is achieved through the use of a meta-pyridyl moiety. These MIMs have promise for use in fluorescent sensing as illustrated by the metal-sensing abilities of the triazole-containing macrocycle. ⁶²	15
2.1. Carbon nanohoops are small molecules analogues of 3D CNMs; [5]CPP maps on to [5,5]-CNT (armchair) and C ₆₀ fullerene.	19

Figure	Page
2.2. Biocompatible CPPs are taken into cells due to different functionality: sulfonates allow for general cell uptake ³¹ , folic acid targets folate receptors overexpressed on cancer cells ³¹ , and a PEG chain confers solubility while morpholine targets the lysosome. ⁴²	20
2.3. Retro-synthetic analysis of initial target molecule II.12 for the development of water-soluble nano hoops based on key intermediate II.3	21
2.4. Top: Synthesis of optimized target molecule II.16 for the development of water-soluble nano hoops based on incorporation of ethyl ester moieties. Bottom: water soluble carboxylate-nano hoop II.16* absorbance and fluorescence spectra of [10]CPP and ester- acid- and carboxylate derivatives.	23
2.5. Live imaging of HeLa cells co-incubated with ester derivative II.15 and NucRed; (a) DIC channel shows surviving cells, (b) DAPI, (c) DAPI-longpass and (d) Cy5 channel show no fluorescence from the NucRed or CPP dyes.	46
2.6. Live imaging of HeLa cells co-incubated with II.16 and NucRed; (a) DIC channel shows surviving cells, (b) DAPI, (c) DAPI-longpass and (d) Cy5 channel show no fluorescence from the NucRed or CPP dyes. The dim fluorescence seen in the DAPI (b) channel shows some II.16 clinging to the outside of cells was not completely removed even with washes.	47
2.7. Live imaging of HeLa cells co-incubated with II.18 and NucRed; (a) DIC channel Y5 and DAPI-long pass channels with (top) and without II.18 (b) zoom in on DAPI-long pass channel showing non-cell permeable aggregates of II.18	48
3.1. a) Molecular “tweezers” developed to host fullerenes through maximizing convex-concave π - π interactions ³⁰ ; b) formation of a 2:1 complex of gamma-cyclodextrin (CD) with C ₆₀ requires high temperature for extended time ²⁴	50
3.2. In this work the development of water-soluble nano hoops III.2* and III.3* can be used to host carbon nanomaterials, like C ₆₀ , and other nano hoops in water. ..	51
3.3. Left: Nano hoops hosts used in this study include [10]- and [12]CPP and functionalized derivatives III.1 , III.2(*) , III.3(*) can be used to host fullerenes like C ₆₀ and PCBM. Right: fluorescence quenching of III.2* by C ₆₀ in 20% ethanol/water solution is used to obtain association constants K _a and K _{SV}	52
3.4. Top: fluorescence titration of C ₆₀ ([G] = 3.89x10 ⁻⁶ M) into [10]CPP in toluene ([H] = 2.89x10 ⁻⁷ M); the changes in fluorescence intensity of [10]CPP at 470 nm were measured. Bottom: correlations of the fluorescence intensity of [10]CPP in toluene as a function of guest concentration to obtain (left) K _a = (5.44±0.19)x10 ⁶ M ⁻¹ and (right) K _{SV} = (4.47±0.02)x10 ⁶ M ⁻¹ for the system.	61

Figure	Page
3.5. Top: fluorescence titration of PCBM ($[G] = 4.39 \times 10^{-6}$ M) into [10]CPP in toluene ($[H] = 2.89 \times 10^{-7}$ M); the changes in fluorescence intensity of [10]CPP at 470 nm were measured. Bottom: correlations of the fluorescence intensity of [10]CPP in toluene as a function of guest concentration to obtain (left) $K_a = (8.82 \pm 0.04) \times 10^5$ M ⁻¹ and (right) $K_{SV} = (6.26 \pm 0.06) \times 10^5$ M ⁻¹ for the system.	62
3.6. Top: fluorescence titration of C ₆₀ ($[G] = 6.66 \times 10^{-5}$ M) into [12]CPP in toluene ($[H] = 3.29 \times 10^{-6}$ M); the changes in fluorescence intensity of [12]CPP at 450 nm were measured. Bottom: correlations of the fluorescence intensity of [12]CPP in toluene as a function of guest concentration to obtain (left) $K_a = (9.27 \pm 1.11) \times 10^5$ M ⁻¹ and (right) $K_{SV} = (1.38 \pm 0.06) \times 10^6$ M ⁻¹ for the system.	63
3.7. Top: fluorescence titration of PCBM ($[G] = 6.59 \times 10^{-5}$ M) into (CO ₂ Et) ₄ -[10]CPP (III.1) in DMSO ($[H] = 1.36 \times 10^{-5}$ M); the changes in fluorescence intensity of III.1 at 509 nm were measured. Bottom: correlations of the fluorescence intensity of III.1 in DMSO as a function of guest concentration to obtain (left) $K_a = (2.19 \pm 0.34) \times 10^4$ M ⁻¹ and (right) $K_{SV} = (3.11 \pm 0.06) \times 10^4$ M ⁻¹ for the system.	64
3.8. Top: fluorescence titration of PCBM ($[G] = 1.45 \times 10^{-4}$ M) into (CO ₂) ₄ -[10]CPP (III.2*) in DMSO ($[H] = 1.71 \times 10^{-5}$ M); the changes in fluorescence intensity of III.2* at 490 nm were measured. Bottom: correlations of the fluorescence intensity of III.2* in DMSO as a function of guest concentration to obtain (left) $K_a = (1.72 \pm 0.19) \times 10^6$ M ⁻¹ and (right) $K_{SV} = (2.17 \pm 0.09) \times 10^6$ M ⁻¹ for the system.	65
3.9. Top: fluorescence titration of C ₆₀ ($[G] = 4.16 \times 10^{-5}$ M) into (CO ₂) ₄ -[10]CPP (III.2*) in 20% EtOH/H ₂ O ($[H] = 3.20 \times 10^{-6}$ M); the changes in fluorescence intensity of III.2* at 470 nm were measured. Bottom: correlations of the fluorescence intensity of III.2* in 20% EtOH/H ₂ O as a function of guest concentration to obtain (left) $K_a = (2.03 \pm 0.52) \times 10^6$ M ⁻¹ and (right) $K_{SV} = (4.70 \pm 0.46) \times 10^4$ M ⁻¹ for the system.	66
3.10. Top: fluorescence titration of PCBM ($[G] = 1.76 \times 10^{-5}$ M) into (CO ₂) ₄ -[10]CPP (III.2*) in 20% EtOH/H ₂ O ($[H] = 5.43 \times 10^{-6}$ M); the changes in fluorescence intensity of III.2* at 470 nm were measured. Bottom: correlations of the fluorescence intensity of III.2* in 20% EtOH/H ₂ O as a function of guest concentration to obtain (left) $K_a = (1.78 \pm 0.29) \times 10^7$ M ⁻¹ and (right) $K_{SV} = (2.39 \pm 0.13) \times 10^6$ M ⁻¹ for the system.	67
3.11. Top: fluorescence titration of C ₆₀ ($[G] = 1.39 \times 10^{-4}$ M) into (CO ₂) ₆ -[12]CPP (III.3*) in 20% EtOH/H ₂ O ($[H] = 1.09 \times 10^{-5}$ M); the changes in fluorescence intensity of III.3* at 455 nm were measured. Bottom: correlations of the fluorescence intensity of III.3* in 20% EtOH/H ₂ O as a function of guest concentration to obtain (left) $K_a = (1.85 \pm 0.46) \times 10^6$ M ⁻¹ and (right) $K_{SV} = (2.93 \pm 0.51) \times 10^5$ M ⁻¹ for the system.	68

Figure	Page
3.12. Top: fluorescence titration of PCBM ($[G] = 6.59 \times 10^{-5} \text{ M}$) into $(\text{CO}_2^-)_6$ -[12]CPP (III.3*) in 20% EtOH/H ₂ O ($[H] = 1.09 \times 10^{-5} \text{ M}$); the changes in fluorescence intensity of III.3* at 455 nm were measured. Bottom: correlations of the fluorescence intensity of III.3* in 20% EtOH/H ₂ O as a function of guest concentration to obtain (left) $K_a = (1.63 \pm 0.29) \times 10^7 \text{ M}^{-1}$ and (right) $K_{SV} = (7.50 \pm 0.99) \times 10^5 \text{ M}^{-1}$ for the system.	69
3.13. Top: fluorescence titration of PCBM ($[G] = 7.47 \times 10^{-5} \text{ M}$) into $(\text{CO}_2^-)_6$ -[12]CPP (III.3*) in H ₂ O ($[H] = 8.42 \times 10^{-6} \text{ M}$); the changes in fluorescence intensity of III.3* at 450 nm were measured. Bottom: correlations of the fluorescence intensity of III.3* in H ₂ O as a function of guest concentration to obtain (left) $K_a = (8.35 \pm 3.24) \times 10^5 \text{ M}^{-1}$ and (right) $K_{SV} = (1.12 \pm 0.27) \times 10^3 \text{ M}^{-1}$ for the system. ...	70
3.14. Top: fluorescence titration of [5]CPP ($[G] = 1.16 \times 10^{-4} \text{ M}$) into [10]CPP in toluene ($[H] = 1.05 \times 10^{-5} \text{ M}$); the changes in fluorescence intensity of [10]CPP at 470 nm were measured. Bottom: correlations of the fluorescence intensity of [10]CPP in toluene as a function of guest concentration to obtain (left) $K_a = (6.91 \pm 1.54) \times 10^5 \text{ M}^{-1}$ and (right) $K_{SV} = (1.06 \pm 0.04) \times 10^5 \text{ M}^{-1}$ for the system.	71
3.15. Top: fluorescence titration of [7]CPP ($[G] = 9.77 \times 10^{-5} \text{ M}$) into [10]CPP in toluene ($[H] = 2.37 \times 10^{-6} \text{ M}$); the changes in fluorescence intensity of [10]CPP at 470 nm were measured. Bottom: correlations of the fluorescence intensity of [10]CPP in toluene as a function of guest concentration to obtain (left) $K_a = (1.54 \pm 0.06) \times 10^6 \text{ M}^{-1}$ and (right) $K_{SV} = (3.91 \pm 0.25) \times 10^6 \text{ M}^{-1}$ for the system.	72
3.16. Top: fluorescence titration of [7]CPP ($[G] = 5.26 \times 10^{-5} \text{ M}$) into [12]CPP in toluene ($[H] = 6.58 \times 10^{-6} \text{ M}$); the changes in fluorescence intensity of [12]CPP at 450 nm were measured. Bottom: correlations of the fluorescence intensity of [10]CPP in toluene as a function of guest concentration to obtain (left) $K_a = (3.64 \pm 0.21) \times 10^6 \text{ M}^{-1}$ and (right) $K_{SV} = (6.58 \pm 0.33) \times 10^6 \text{ M}^{-1}$ for the system.	73
3.17. Top: fluorescence titration of [5]CPP ($[G] = 4.21 \times 10^{-5} \text{ M}$) into $(\text{CO}_2^-)_4$ -[10]CPP (III.2*) in H ₂ O ($[H] = 9.62 \times 10^{-6} \text{ M}$); the changes in fluorescence intensity of III.2* at 470 nm were measured. Bottom: correlations of the fluorescence intensity of III.2* in H ₂ O as a function of guest concentration to obtain (left) $K_a = (3.20 \pm 1.01) \times 10^5 \text{ M}^{-1}$ and (right) $K_{SV} = (6.25 \pm 0.33) \times 10^5 \text{ M}^{-1}$ for the system. ...	74
3.18. Top: fluorescence titration of [7]CPP ($[G] = 9.77 \times 10^{-5} \text{ M}$) into $(\text{CO}_2^-)_4$ -[10]CPP (III.2*) in H ₂ O ($[H] = 9.62 \times 10^{-6} \text{ M}$); the changes in fluorescence intensity of III.2* at 470 nm were measured. Bottom: correlations of the fluorescence intensity of III.2* in H ₂ O as a function of guest concentration to obtain (left) $K_a = (1.64 \pm 0.43) \times 10^6 \text{ M}^{-1}$ and (right) $K_{SV} = (2.99 \pm 0.18) \times 10^5 \text{ M}^{-1}$ for the system. ...	75
3.19. Top: fluorescence titration of [8]CPP ($[G] = 2.96 \times 10^{-5} \text{ M}$) into $(\text{CO}_2^-)_4$ -[10]CPP (III.2*) in H ₂ O ($[H] = 6.35 \times 10^{-6} \text{ M}$); the changes in fluorescence intensity of III.2* at 470 nm were measured. Bottom: correlations of the fluorescence intensity of III.2* in H ₂ O as a function of guest concentration to obtain (left) $K_a = (2.59 \pm 1.10) \times 10^6 \text{ M}^{-1}$ and (right) $K_{SV} = (6.39 \pm 0.56) \times 10^5 \text{ M}^{-1}$ for the system. ...	76

Figure	Page
3.20. Top: fluorescence titration of [9]CPP ([G] = 2.92×10^{-5} M) into (CO ₂ ⁻) ₄ -[10]CPP (III.2*) in H ₂ O ([H] = 6.35×10^{-6} M); the changes in fluorescence intensity of III.2* at 470 nm were measured. Bottom: correlations of the fluorescence intensity of III.2* in H ₂ O as a function of guest concentration could not be reasonably fit to equations III.1 and III.2, respectively.	77
3.21. Top: fluorescence titration of [6]CPP ([G] = 3.51×10^{-5} M) into (CO ₂ ⁻) ₆ -[12]CPP (III.3*) in H ₂ O ([H] = 6.50×10^{-6} M); the changes in fluorescence intensity of III.3* at 450 nm were measured. Bottom: correlations of the fluorescence intensity of III.3* in H ₂ O as a function of guest concentration to obtain (left) $K_a = (8.48 \pm 1.38) \times 10^6 \text{ M}^{-1}$ and (right) $K_{SV} = (1.34 \pm 0.05) \times 10^6 \text{ M}^{-1}$ for the system.	78
3.22. Top: fluorescence titration of aza-[6]CPP ([G] = 7.87×10^{-5} M) into (CO ₂ ⁻) ₆ -[12]CPP (III.3*) in H ₂ O ([H] = 6.50×10^{-6} M); the changes in fluorescence intensity of III.3* at 450 nm were measured. Bottom: correlations of the fluorescence intensity of III.3* in H ₂ O as a function of guest concentration to obtain (left) $K_a = (5.60 \pm 1.56) \times 10^6 \text{ M}^{-1}$ and (right) $K_{SV} = (6.45 \pm 1.37) \times 10^5 \text{ M}^{-1}$ for the system.	79
3.23. Top: fluorescence titration of [7]CPP ([G] = 6.26×10^{-5} M) into (CO ₂ ⁻) ₆ -[12]CPP (III.3*) in H ₂ O ([H] = 8.42×10^{-6} M); the changes in fluorescence intensity of III.3* at 450 nm were measured. Bottom: correlations of the fluorescence intensity of III.3* in H ₂ O as a function of guest concentration to obtain (left) $K_a = (9.83 \pm 1.27) \times 10^5 \text{ M}^{-1}$ and (right) $K_{SV} = (1.86 \pm 0.04) \times 10^4 \text{ M}^{-1}$ for the system. ...	80
3.24. Top: fluorescence titration of [9]CPP ([G] = 6.42×10^{-5} M) into (CO ₂ ⁻) ₆ -[12]CPP (III.3*) in H ₂ O ([H] = 8.42×10^{-6} M); the changes in fluorescence intensity of III.3* at 450 nm were measured. Bottom: correlations of the fluorescence intensity of III.3* in H ₂ O as a function of guest concentration to obtain (left) $K_a = (3.55 \pm 0.95) \times 10^6 \text{ M}^{-1}$ and (right) $K_{SV} = (2.38 \pm 0.63) \times 10^4 \text{ M}^{-1}$ for the system. ...	81
3.25. Fluorescence titration of [5,6]CNT into (CO ₂ ⁻) ₆ -[12]CPP (III.3*) in H ₂ O ([H] = 6.50×10^{-6} M); as guest concentration increases fluorescence is quenched (red arrow, see inlay), however at high concentration of guest fluorescence increases dramatically (green arrow).	82
4.1. Classic examples of (a) size selective ¹² and (b) reaction-based sensing platforms. ¹⁶ (c) A previously published nanohoop[2]-rotaxane-based fluorescent fluoride sensor. ²⁸	84
4.2. (a) Synthesis of rotaxane IV.4 and free thread IV.5 , (b) proposed mechanism of rotaxane dethreading in the presence of HS ⁻ , and (c) ¹ H NMR spectra (aromatic region) of rotaxane IV.4 in CD ₃ CN, before and after addition of 1 equiv of NBu ₄ SH, compared with free macrocycle IV.1 and DNT in the presence of NBu ₄ SH.	87

Figure	Page
4.3. Time-course fluorescence (excitation 310 nm) of IV.4 (25 μ M in acetonitrile) before and after addition of 10 equiv of NBu ₄ SH over 120 min. Inlay: integrated fluorescence of IV.4 over 120 min in the presence of 10 equiv of NBu ₄ SH, NBu ₄ <i>St</i> -Bu, or NBu ₄ SBn.	88
4.4. Time-course UV-vis spectra of IV.4 with 10 equiv of NBu ₄ SH (top) and of IV.5 with 10 equiv of NBu ₄ SH followed by addition of DNT (middle) and IV.5 with 10 equiv of NBu ₄ <i>St</i> -Bu (bottom). All probe concentrations are 25 μ M each in acetonitrile.	89
4.5. Rotaxane prior to addition of NBu ₄ SH in MeCN- <i>d</i> ₃	94
4.6. Rotaxane after addition of NBu ₄ SH in MeCN- <i>d</i> ₃	95
4.7. Aromatic region of ¹ H NMR of (top) IV.4 , (middle) IV.4 and NBu ₄ SH, and (bottom) IV.4 , NBu ₄ SH and DNT.	96
4.8. Aromatic region of ¹ H NMR of (top) DNT and NBu ₄ SH and (bottom) IV.4 , NBu ₄ SH and DNT.	96
4.9. Aromatic region of ¹ H NMR of (top) DNT in the presence of NBu ₄ SH and (bottom) DNT.	96
4.10. Fluorescence of IV.4 over time with 10 equiv of NBu ₄ SH added.	98
4.11. Absorbance of IV.4 over time with 10 equiv of NBu ₄ SH added.	98
4.12. Fluorescence of IV.4 over time with 50 equiv of NBu ₄ SH added.	98
4.13. Absorbance of IV.4 over time with 50 equiv of NBu ₄ SH added.	99
4.14. Fluorescence of IV.4 over time with 100 equiv of NBu ₄ SH added.	99
4.15. Absorbance of IV.4 over time with 100 equiv of NBu ₄ SH added.	99
4.16. Comparison of integrated emission vs. time for IV.4 with varying concentrations of NBu ₄ SH.	100
4.17. Fluorescence of IV.4 over time with 10 equiv of NBu ₄ <i>St</i> -Bu over time. Inlay: integrated fluorescence over time.	100
4.18. Absorbance of IV.4 over time with 10 equiv of NBu ₄ <i>St</i> -Bu over time.	101
4.19. Fluorescence of IV.4 over time with 100 equiv of NBu ₄ <i>St</i> -Bu over time. The sharp signal at 620 nm is an artifact of the fluorimeter.	101
4.20. Absorbance of IV.4 over time with 100 equiv of NBu ₄ <i>St</i> -Bu over time, spiked with thread IV.5 after 120 minutes to ensure thiolate remains reactive.	101
4.21. Fluorescence of IV.4 over time with 10 equiv of NBu ₄ SBn over time. Inlay: integrated fluorescence over time. The sharp signal at 620 nm is an artifact of the fluorimeter.	102
4.22. Absorbance of IV.4 over time with 10 equiv of NBu ₄ SBn over time.	102

Figure	Page
4.23. Comparison of integrated emission vs. time for IV.4 with 10 equiv of NBu ₄ SH, NBu ₄ St-Bu, and NBu ₄ SBn.	102
4.24. Fluorescence of IV.5 before and after 10 equiv of NBu ₄ SH was added. The sharp signal at 620 nm is an artifact of the fluorimeter.	103
4.25. Absorbance over time of IV.5 with 10 equiv of NBu ₄ SH.	103
4.26. Fluorescence of IV.5 before and after 10 equiv of NBu ₄ St-Bu was added. The sharp signal at 620 nm is an artifact of the fluorimeter.	104
4.27. Absorbance over time of IV.5 with 10 equiv of NBu ₄ St-Bu was added.	104
4.28. Fluorescence of IV.5 before and after 10 equiv of NBu ₄ SBn was added. The sharp signal at 620 nm is an artifact of the fluorimeter.	104
4.29. Absorbance over time of IV.5 before and after 10 equiv of NBu ₄ SBn was added.	105
4.30. Fluorescence over time of IV.4 and IV.5 with NBu ₄ St-Bu. The sharp signal at 620 nm is an artifact of the fluorimeter.	105
4.21. Absorbance over time of IV.4 and IV.5 with NBu ₄ St-Bu.	105
4.32. Fluorescence over time of IV.4 and IV.5 with NBu ₄ SBn. The sharp signal at 620 nm is an artifact of the fluorimeter.	106
4.33. Absorbance over time of IV.4 and IV.5 with NBu ₄ SBn. DNT added 30 minutes after the addition of thiolate.	106
4.34. Absorbance of thread IV.5 with NBu ₄ SH and DNT.	107
4.35. Absorbance of thread IV.5 with NBu ₄ St-Bu and DNT.	107
4.36. Fluorescence of macrocycle IV.1 with NBu ₄ SH over time; inlay: integrated fluorescence.	108
4.37. Fluorescence of macrocycle IV.1 with increasing equiv (10-100) of NBu ₄ Cl.	108
4.38. Stern-Volmer analysis of fluorescence quenching of IV.1 of NBu ₄ SH. Stock solutions of IV.1 (1.8 μM) in 1% DCM/MeCN and NBu ₄ SH (8.5 μL) in dry MeCN were prepared. To a 2.0 mL solution of IV.1 were added aliquots of NBu ₄ SH and the change in fluorescent intensity of IV.1 at 520 nm was measured. K _{SV} was determined by using the following Equation IV.1.	109
4.39. Absorbance of 250 μM NBu ₄ St-Bu in MeCN.	109
4.40. Absorbance of 150 μM NBu ₄ SBn in MeCN.	109
4.41. Absorbance of 150 μM NBu ₄ SH in MeCN.	110

Figure	Page
5.1. A) Previously developed nanohoop-[2]rotaxane sensors for fluoride ²⁶ (left) and hydrosulfide ¹⁴ (right) highlight the potential for this scaffold in sensing; b) the rotaxane design offers a modular synthesis comprised of three components: a nanohoop fluorophore also serves as protection for a reactive thread, a dinitro-substituted aromatic ring serves as stopper and quencher when interlocked, and a second stopper could serve as a trigger and/or potentially a payload for theranostic applications in the future. C) The small, rigid nanohoop provides substantially better protection for a reactive poly-yne thread than the larger, more flexible M2 . ¹⁷	112
5.2. Synthesis of a PEG-functionalized water-soluble <i>m</i> N[6]CPP compatible nanohoop, V.1 , for use in the development of biologically compatible nanohoop-rotaxane sensors based on previous work with <i>m</i> -[6]CPP used for cell imaging. ²⁵	114
5.3. Progress towards a nanohoop-[2]rotaxane ROS probe (top) based on a benzil trigger motif (bottom) highlights the potential modularity of the sensing scaffold.	116

LIST OF TABLES

Table		Page
3.1.	Comparison of fullerene guests binding (K_a and Stern-Volmer constant (K_{SV})) with water soluble nano hoops; *previously published data ³⁶ measured via the same titration method used herein.	53
3.2.	Comparison of nano hoop guests binding (K_a and K_{SV}) with 10- and 12[CPP] hosts.	55

LIST OF SCHEMES

Scheme		Page
2.1.	Synthesis of aromatized precursors to target molecule II.12 for the development of water-soluble nano hoops via MOM-ether or TBS protected, or unprotected benzylic alcohols.	22
2.2.	Synthesis of derivatives of II.15 and II.16 illustrates the utility of ester functionalized nano hoops for broader applications.	24
2.3.	Synthesis of larger [12]CPP derivative II.23 using the same tetra-ester functionalized key intermediate.	26
4.1.	Synthesis of thread component IV.3 , rotaxane IV.4 (using macrocycle IV.1) and free thread IV.5	91
5.1	Progress towards synthesizing a biologically compatible nano hoop-[2]rotaxane for sensing HS ⁻ in cells has been complicated by challenges with late-stage functionalization of the interlocked system.	117

CHAPTER I

THE PROPERTIES AND POTENTIAL OF CARBON NANOHOOPS IN SUPRAMOLECULAR CHEMISTRY

This chapter includes unpublished material, it was written by myself, with editorial assistance from Professor Ramesh Jasti.

Chapter **II** includes unpublished co-authored material, it was written by myself, with editorial assistance from Professor Ramesh Jasti. Experimental work in this chapter was performed by myself with experimental guidance provided by Professor Ramesh Jasti.

Chapter **III** includes unpublished co-authored material, it was written by myself, with editorial assistance from Professor Ramesh Jasti. Experimental work in this chapter was performed by myself with experimental guidance provided by Professor Ramesh Jasti.

Chapter **IV** includes co-authored material published in *Organic Letters*. The manuscript was written by myself, with contributions from Carolyn M. Levinn, and with editorial assistance from Professor Ramesh Jasti, and Professor Michael D. Pluth. Experimental work in this chapter was performed by myself, Carolyn M. Levinn, and Jeff M. Van Raden. Experimental guidance was provided by Professor Ramesh Jasti, and Professor Michael D. Pluth.

Chapter **V** includes unpublished co-authored material, it was written by myself, with editorial assistance from Professor Ramesh Jasti. Experimental work in this chapter was performed by myself or Phyllis Liao under my direction, with experimental guidance provided by Professor Ramesh Jasti.

1.1. Introduction

Supramolecular chemistry is the area of chemistry which specializes in non-covalent interactions (*i.e.* van der Waals forces, hydrogen bonds, hydrophobic forces, metal-ligand coordination, *etc.*) that drive self-assembly, and more generally, the construction of complex materials of two or more chemical species. Emil Fischer first described the “lock-and-key” model of supramolecular systems (still used today) in 1894 to describe the interactions of proteins and ligands, whereby only a correctly fitting ligand (key) could fit into the complex pocket of a protein (lock).¹ While this idea has changed and grown since Fischer’s initial description, the broad idea

of complementarity between interacting chemical species holds true and has become a vast, complex field of research. Importantly, the field of supramolecular chemistry was spurred forward by the discovery of crown ethers and their ability to host metals in solution, as reported by Pedersen in 1976.² This discovery, alongside analogous work by Cram and Lehn, was later acknowledged when all three shared the Nobel Prize in chemistry in 1987 for “their development and use of molecules with structure-specific interactions of high selectivity.”³ While the field has developed substantially since the 1980s, the importance of macrocycles like crown ethers as supramolecular hosts has remained an integral part. Common macrocycles used in supramolecular chemistry include cyclodextrins, cucurbiturils, pillararenes, calixarenes, resorcinarenes and others, and systems produced with these macrocycles have found countless applications spanning many fields.⁴⁻¹⁴

A relatively new family of macrocycles first synthesized in 2008, $[n]$ cycloparaphenylenes or carbon nano hoops (so called due to their relationship to carbon nanotubes,) were long-standing synthetic targets due largely to interest in their unique electronic properties.¹⁵ Now that the synthesis of nano hoops and their derivatives has been well established, focus has shifted towards

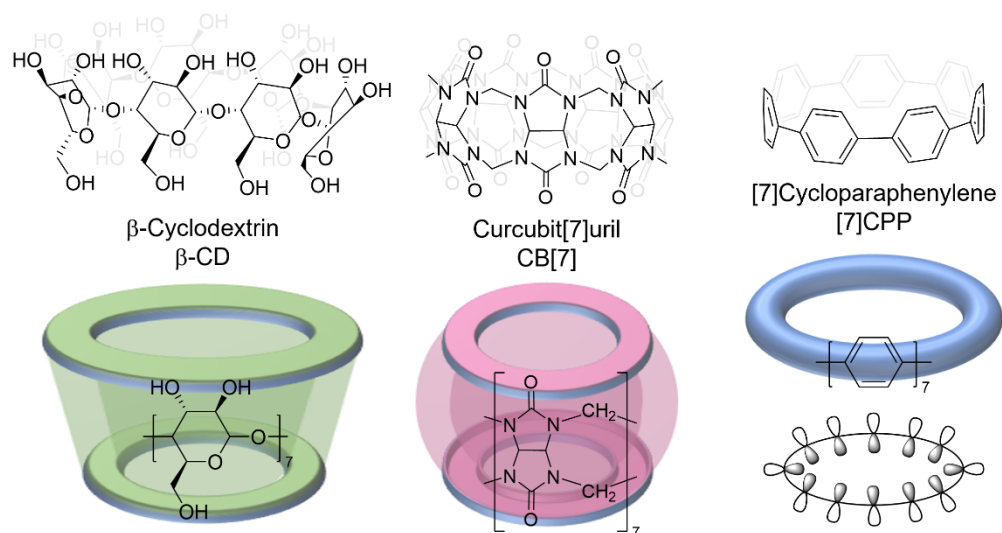


Figure 1.1. Well established macrocyclic hosts used in supramolecular chemistry, cyclodextrins and cucurbiturils, contain a variety of functional groups making them capable of hosting a range of guests via multiple types of supramolecular interactions. In comparison, carbon nano hoops are functionally simple molecules, however their unique make-up gives rise to a radially oriented π -system (bottom right) capable of interacting with suitable guests.

their applications. Cycloparaphenylenes (CPPs) are macrocycles composed entirely of phenylene units arranged in a macrocyclic array. As such, these molecules are fully conjugated and display bright fluorescence and tunable HOMO-LUMO gaps, which have been leveraged for applications in imaging, sensing, and electronics.¹⁶⁻¹⁷ Furthermore, the unique phenylene-based macrocycles are rigid with a shape-persistent pore and a radially oriented π -system (**Figure I.1**, right) capable of interacting with complementary guests. However, in comparison to other more commonly used macrocycles like cucurbiturils (CBs) and cyclodextrins (CDs) nano hoops are functionally simple, non-polar small molecules. This inherent simplicity limits their interactions with guests to those mediated by π systems (i.e. π - π stacking, cation- π , anion- π , or CH- π interactions). Yet, part of what makes these macrocycles so interesting as supramolecular hosts, is that despite this simplicity, they are still capable of achieving strong binding with appropriate guests. In contrast, CBs for example have carbonyl moieties at the top and bottom of the macrocyclic cavities (**Figure I.1**, center) which are useful for complexation with cations via ion-dipole interactions, while their interior is quite hydrophobic and is well-suited for complexation with aromatic and alkyl guests.⁹ Alternatively, naturally occurring sugar-based CDs (**Figure I.1**, left) are capable of dipole-dipole, hydrogen bonding, charge transfer, van der Waals, and hydrophobic interactions allowing for complexation with a wide variety of guests.¹⁰ In contrast, although nano hoops are perhaps more interesting macrocycles due to their optical and electronic properties, their host-guest chemistry is currently quite limited, and relatively underexplored. Herein, recent progress towards exploiting nano hoops as macrocyclic hosts in host-guest supramolecular chemistry is discussed.

1.2. Fullerene Guests

The creation of receptors for fullerenes has long been a very active area of research in large part due to the unique properties of these molecules that could be useful for many applications if successfully incorporated into supramolecular assemblies.¹⁸⁻²⁰ Much of this work focused on the creation of large π -systems that could interact with the convex π -surface of C_{60} and other fullerenes. In the late 90s it was reported that carbon nanotubes (CNTs) were capable of hosting fullerenes in “peapod” like structures, and soon after the complexation of fullerenes with cycloparaphenylene-acetylenes (CPPAs), nano hoops with alternating phenylene and acetylene units in a macrocyclic array, were also capable hosts for fullerenes due to their concave π -systems.²¹⁻²⁴ When the synthesis of carbon nano hoops was finally achieved in 2008, it is therefore

unsurprising that complexation with C_{60} followed soon after. As mentioned above, the unique structure of nanohoops gives rise to a radially oriented π -system within the shape-persistent pore, which is poised to interact with fullerenes via convex-concave π - π interactions.

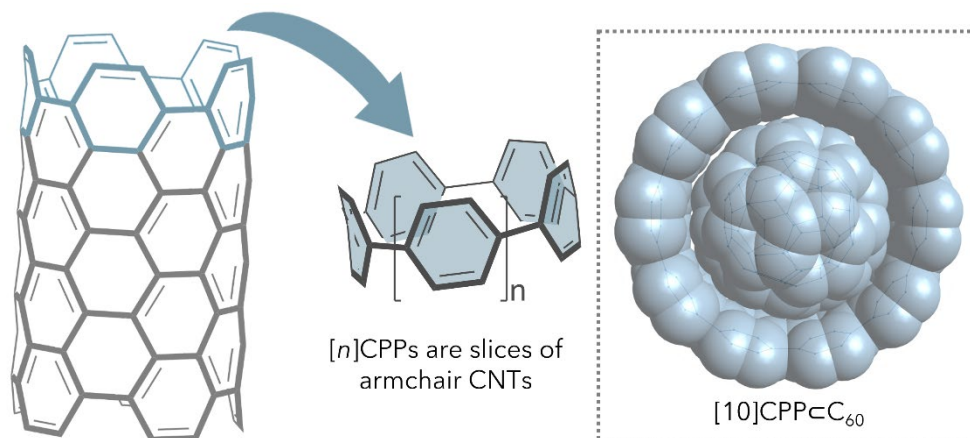


Figure 1.2. Carbon nanohoops represent the smallest cross-section of arm-chair carbon nanotubes, as such it was predicted that similar to CNTs, CPPs should be capable of hosting C_{60} .

The first such study was published by Yamago et al. just three years after CPPs were first synthesized and reported encapsulation of C_{60} by [10]CPP with an association/binding constant (K_a) of $2.79 \pm 0.03 \times 10^6 \text{ M}^{-1}$.²⁵ They found that when excess C_{60} was mixed with [8]-[12]CPP in $CDCl_3$, only the resonance of [10]CPP showed a downfield shift in proton NMR suggesting exceptionally selective complexation. This was followed by UV-Vis and fluorescence titrations, which also illustrated the quenching of nanohoop fluorescence by the electron poor fullerene upon complexation and allowing for measurement of binding affinity. The next year a crystal structure of this peapod complex was published by Jasti et al. which highlighted the beautifully matched convex-concave π - π interactions with all of the phenylenes in the nanohoop participating. From this structure it was found that the average dihedral angle between adjacent phenylenes in the macrocycle increased to $28.5 \pm 2.5^\circ$ compared to $27.3 \pm 11.7^\circ$ of free [10]CPP, with an average distance from nanohoop phenylenes to C_{60} ring centroid of $3.6 \pm 0.05 \text{ \AA}$.²⁶ Following these works, as well as the development of a variety of alternative synthetic methodologies to access nanohoops, a number of [10]CPP derivatives have since been published, with researchers often assessing complexation with fullerene whenever possible.

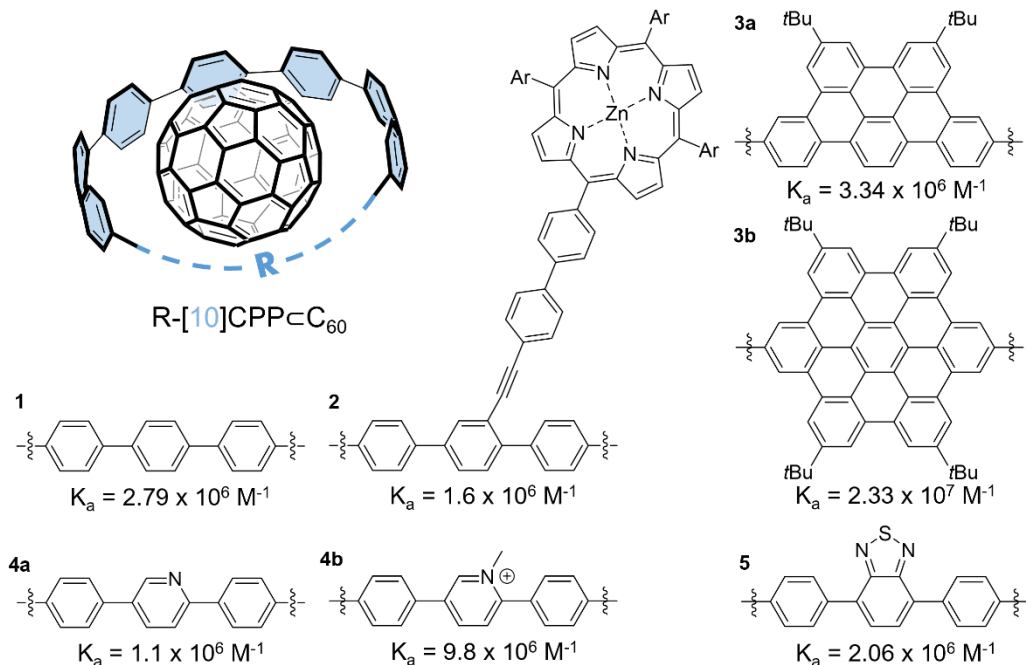


Figure 1.3. Association constants (K_a) for [10]CPP derivatives with C₆₀ all measured in toluene. 1) unfunctionalized [10]CPP²⁵; 2) porphyrin-appended [10]CPP for charge transfer²⁸; 3) π -extended [10]CPP derivatives²⁷; 4) pyridine- and pyridinium-[10]CPP³⁰; 5) BT-[10]CPP²⁹.

Due to the nature of the interaction between the π -rich donor and acceptor, one seemingly obvious route to increasing binding affinity of this system is π -extension of the [10]CPP host. This was achieved by insertion of annulated moieties onto the CPP backbone (**Figure 1.3**, 3a and 3b) by the Du group and as expected stepwise increase of the π -surface led to a similar stepwise increase in binding affinity for C₆₀.²⁷ Another interesting system, created with the technological applications of C₆₀ in mind, comprises a supramolecular junction based on the complexation of electron acceptor fullerenes with a [10]CPP functionalized with a zinc porphyrin electron donor (**Figure 1.3**, 2) created by von Delius et al. This porphyrin-appended nanohoop retained the high affinity seen with parent [10]CPP while also achieving charge-separation and recombination across the junction in a noncovalent manner.²⁸ Other manipulations of the nanohoop backbone, like the introduction of an electron-accepting benzothiadiazole (BT) unit for red-shifting CPP fluorescence showed little effect on the complexation, suggesting that a wide array of fullerene hosts can be created from the [10]CPP scaffold.²⁹ Similarly, synthesis of a pyridine-incorporated nanohoop, aza[10]CPP, and the N-methylated pyridinium analogue were recently synthesized by the von Delius group. Interestingly, they found that incorporation of the pyridine moiety led to an

increase in the binding affinity compared to the all carbon analogue, while N-methylation of the aza-[10]CPP led to an decrease in affinity compared to the parent nanohoop.³⁰ The authors also performed DFT calculations to better understand the changes in binding affinity and suggest that the greatest factor in this series is the change in torsional angle between phenylenes based on the incorporation of pyridine. While the aza[10]CPP analogue has on average lower torsional angles (25.6°) than parent [10]CPP (27.3°), this trend is opposite for the methylated analogue (28.9°) potentially reducing the π - π interaction efficiency, which agrees well with theoretical work on the effects of heteroatom incorporation in nanohoops.³¹

In addition to modifications of the nanohoop host, researchers have also studied the complexation of modified fullerene guests – *i.e.* metallo-fullerenes, azafullerenes – as well as higher order fullerenes, like C_{70} , with a variety of nanohoops. Similar to early work on [10]CPP \subset C_{60} , Yamago and coworkers were the first to study the complexation of C_{70} with carbon nanohoops and found that due to the football-like shape of the higher order fullerene, it was capable of adopting different conformations within the nanohoop pores. Due to the increase in size, C_{70} was found to fit into [10]CPP only in a “lying” orientation where the host interacts with the fullerene’s equator while the fullerene poles protrude from the nanohoop cavity. When complexed with the larger [11]CPP the guest adopts a “standing” orientation where the nanohoop interacts with guests poles.³² Not long after, reports of metallofullerene-containing peapods with Ln@ C_{82} (Ln = La, Gd, Tm and Lu₂) guests inside [11]CPP illustrated a ground-state charge-transfer interaction between host and guest while retaining high binding affinity ($K_a \approx 10^6 \text{ M}^{-1}$).³³⁻³⁴ Similarly, complexation of bis(azafullerene) ($C_{59}N$)₂ with two equivalents of [10]CPP led to the formation of a [10]CPP \subset ($C_{59}N$)₂ \supset [10]CPP complex that also showed charge-transfer phenomena, in this case with a neutral fullerene guest. Additionally, it was found that the binding of one [10]CPP to the fullerene dimer ($K_a = 8.4 \times 10^6 \text{ M}^{-1}$) stabilized the binding of the second hoop ($K_a = 3.0 \times 10^6 \text{ M}^{-1}$) via increasing π - π , and CH- π interactions.³⁵

While initial assessment of carbon nanohoops suggests their simple atomic make-up might limit their host abilities, the exploration of fullerene guests has produced evidence of not only π - π interactions but also the importance of van der Waals interactions in size-selectivity, as well as charge transfer interactions. The breadth of work produced on nanohoop-fullerene host-guest complexes, only a small selection of which has been discussed herein, has shown that nanohoops are much more capable macrocyclic hosts than perhaps previously believed, and while research on

CPP-fullerene complexes remains an active area of research, recently researchers are branching out to explore what other guests nanohoops are capable of hosting.

1.3. Nanohoop and Nanotube Guests

While a substantial amount of both theoretical and experimental work has been put forth concerning the complexation of nanohoops and fullerenes, much of this work was predated by analogous examples of fullerene complexation with CNTs and CPPAs, both of which have similar concave π -rich cavities capable of interacting with fullerene. It is no surprise then that to expand the suite of guests for CPPs inspiration could be drawn from similar work on CNTs and CPPAs with non-fullerene guests. Double- and multi-walled CNTs, reported prior to single-walled nanotubes, illustrate that the ideal distance between CNTs is roughly 0.34 nm, the same average distance reported by Jasti, between [10]CPP phenylene rings and C₆₀ in the solid state.^{26,36} The fullerene-nanohoop complexes are considered the shortest possible fullerene peapods; the shortest possible double- or multi-walled CNTs should therefore be comprised of nanohoop ring-in-ring complexes of appropriate size.

1.3.1. Saturn Systems

Similar to fullerenes, the convex surface of a guest nanohoop has excellent size and shape complementarity to a nanohoop host's concave surface. The ring-in-ring complexes, however, have a smaller π -surface for interaction between guest and host, suggesting weaker complexes will be formed than in the case of fullerenes. In part due to this reduced affinity, nanohoop ring-in-ring complexes were first explored via theoretical work. In the initial analysis, Guadarrama et al. predicted the structures of nanohoop "Russian doll" complexes suggesting that optimal interactions should be seen when the size of guest nanohoop is 5 phenylene units smaller than the host nanohoop.³⁷ This initial work suggested complexation geometries similar to DWCNTs in which the macrocycles are perfectly aligned to maximize π - π interactions between host and guest. Additionally, based on similar work regarding bowl-shaped polyarenes they suggest that the concave side of nanohoops are more negative, as seen in electrostatic potential maps of nanohoops and other curved aromatics.³⁸ This asymmetry in the π -electron density distribution between the two sides of polyarenes suggests that electrostatic interactions, in addition to expected π - π stacking, should contribute to stabilizing these complexes. A similar theoretical analysis of

nanohoop inclusion complexes published four years later provided a broader computational exploration and found that the “Russian doll” model is likely not the optimal geometry for interaction between hoops. Instead, suggesting that a planetary orbit or “Saturn” model, in which the guest nanohoop is inclined out of the host, reminiscent of the trajectory of planets about the sun (**Figure 1.4**), is more stable than the “Russian doll” conformation by 1.27 kcal mol⁻¹. The studies do agree, however, on the ideal hoop size-pairings as the optimal distance between host and guest should be 3.5 Å, which is true of complexes with the general formula [n+5]CPP⊂[n]CPP.

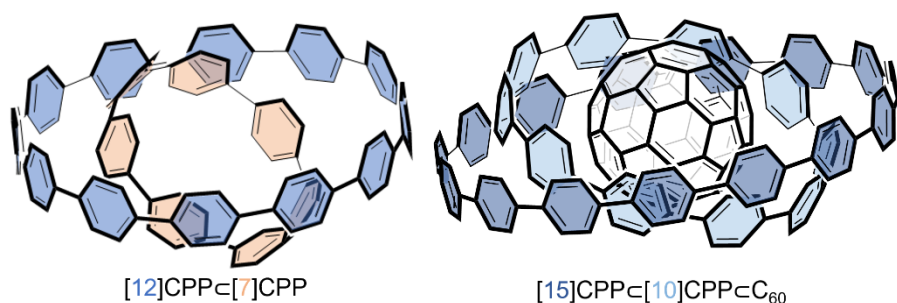


Figure 1.4. Nanohoop-based “Saturn” complexes have been predicted to form with the general formula [n+5]CPP⊂[n]CPP (*i.e.* [12]CPP⊂[7]CPP, left), while isolation has proven challenging systems including the ternary complex of [15]CPP⊂[10]CPP⊂C₆₀ (right) have been identified by NMR spectroscopy.³⁹

Due to the lower association affinity between nanohoos discussed above, evidence of the nanohoop inclusion complexes has proven more challenging to obtain than for nanohoop-fullerene complexes. Much as in the case of CPP-fullerene complexes, the first such evidence came from Yamago et al. via proton NMR experiments. They showed that introduction of [6]CPP to a mixture of [8]-[12]CPP in CDCl₃ results in a 0.05 ppm upfield shift of the resonance for [6]CPP which was only reproduced upon mixing with [11]CPP. Based on the tracking this chemical shift they were able to measure a K_a of 773±17 L mol⁻¹ for [11]CPP⊂[6]CPP in [D₂]TCE at 50 °C.³⁹ Additionally, they showed that upon addition of [13]CPP to a mixture of [8]-[12]CPPs in CDCl₃ the proton resonance of only [8]CPP signal disappeared and noted the appearance of a precipitate, which they suggest is the [13]CPP⊂[8]CPP complex, while upon addition of excess [13]CPP they note that the proton signal emerged. Though they were unable to measure the association constant for this

complex due to the lack of solubility, association constants for [10]CPP \subset [5]CPP and [12]CPP \subset [7]CPP (53 ± 10 and 97 ± 15 L mol⁻¹ respectively) were measured by NMR titrations in [D₂]TCE at 50 °C. In addition, evidence of ternary complex was found upon mixing [15]CPP with [10]CPP \subset C₆₀ in [D₂]TCE by monitoring the resonance of [10]CPP which shifted downfield (by 0.036 ppm) compared to [10]CPP and upfield (by 0.007 ppm) relative to [10]CPP \subset C₆₀. It is unsurprising, but important to note, the large reduction in binding affinity of these complexes as compared to fullerene-based complexes, attributed to the reduction of the π -surface area.

Very recently a number of similar studies have been conducted to better understand these nanohoop inclusion complexes. One such work suggests the formation of such a complex may result in protection of the smaller, more strained, guest hoop upon complexation. Alvarez et al. illustrated that pressurization of [6]CPP led to deformation of the highly strained macrocycle and resulted in an increase in the band gap upon loss of conjugation, however when a 1:1 mixture of [12] and [6]CPP was subjected to the same conditions little spectral change was seen, and the authors suggest this was a consequence of complexation.⁴⁰ The following year, the first mass spectrometry (MS)-based evidence of the inclusion complexes was reported. While this study produced no further understanding of binding energies, evidence of a variety of different complexes was observed using a new MALDI protocol including radical cation containing complexes like [[10]CPP \subset [5]CPP]⁺.⁴¹ Finally in 2021 the first solid-state structure of a nanohoop inclusion complex was obtained from a 1:1 mixture of [6] and [12]CPP in chlorobenzene.⁴² The Wang group reported that single crystals of the [12]CPP \subset [6]CPP complex demonstrated enhanced performance in a photoelectric device when compared to simple monomeric versions. Importantly, in the solid state they found that the plane of the guest hoop is tilted roughly 25° out of the plane of the larger hoop, confirming the predicted “Saturn” orientation of these ring-in-ring complexes, as opposed to the “Russian doll” conformation.

1.3.2. Carbon Nanotubes

As previously discussed, nanohoos are small molecule CNT mimics representing the smallest fragment of arm-chair carbon nanotubes. Due to successful creation of nanohoop inclusion complexes, researchers have also suggested that inclusion complexes of CNTs with nanohoos is likely possible, however research in this area is even more limited than for ring-in-

ring complexes. While there is one publication reporting the complexation of a CPPA nanohoop with a single-walled CNT, so far, no examples of CPP-based complexes have yet been reported.⁴³ A computational investigation of these systems by Yamamoto et al., however, gives some general principles regarding how one might achieve complexation. They suggest that an optimal fit is achieved when the distance between hoop and tube is roughly 3.35 Å, citing (8,8)@[12]CPP as potential complex, among others.⁴⁴ Interestingly, they also report that different complex types are likely: tube-in-ring and ring-on-tube (wherein the pore of the CPP is parallel to the long axis of the tube) and these supramolecular geometries are dominated by different interactions. As with fullerene and nanohoop guests, the tube-in-ring interaction is dominated by π - π stacking, while the ring-on-tube complex is far more dependent on CH- π interactions.

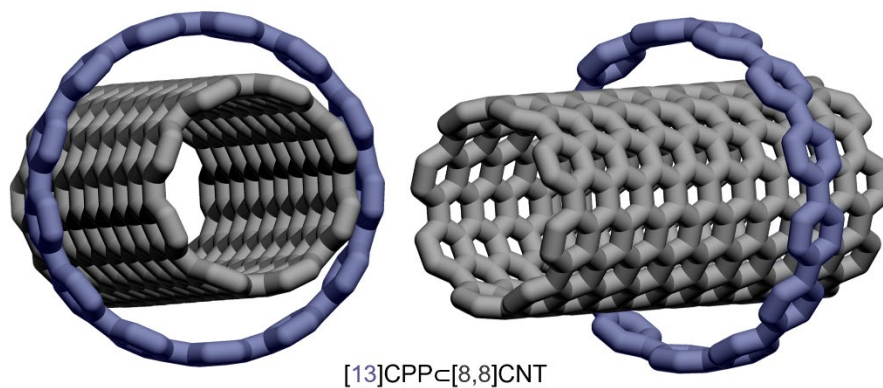


Figure 1.5. Theoretical work predicts complexation of nanohoops with CNTs.⁴⁴

1.4. Small Molecule Guests

While π -rich carbon nanomaterials and molecular analogues have been the most heavily studied guests of nanohoops due to the dominance of π - π interactions in their supramolecular complexes, there are some examples of alternative guest types that utilize alternative supramolecular interactions.

1.4.1 Polycyclic Aromatic Hydrocarbons

Without the incorporation of heteroatoms the potential supramolecular interactions of polycyclic aromatic hydrocarbons (PAHs) and similar π -rich hydrocarbons like nanohoops are limited to a handful of π -system based interactions. This includes π - π stacking as discussed previously, as well as edge-to-face (CH- π) interactions. Interactions of nanohoops with fullerenes

and nanohoops studied up to this point have relied almost entirely on the former. However, very recently work by the Bruns group has shown that CH- π interactions are also useful in the creation of nanohoop-based inclusion complexes. Via a combined DFT- and experiment-based approach they successfully identified a new family of guest molecules for nanohoop macrocycles, namely PAHs. Using DFT calculations they identified a series of PAH guests for [9]-[12]CPPs and selection criteria for future studies. To optimize interactions in such complexes, they found that the distance between a guest CH bond donor and a host π acceptor should fall between 2.35-3.05 Å based on analysis of CH- π interactions in previously published crystal structures.⁴⁵ Therefore, they suggest that the difference in nanohoop and guest diameter should be equivalent to two CH- π bond lengths, or between 4.7 and 6.1 Å. Based on this criterion they predicted the complexation of PAHs including azulene, corannulene, and coronene among others with [9]-, [10]- and [11]CPP

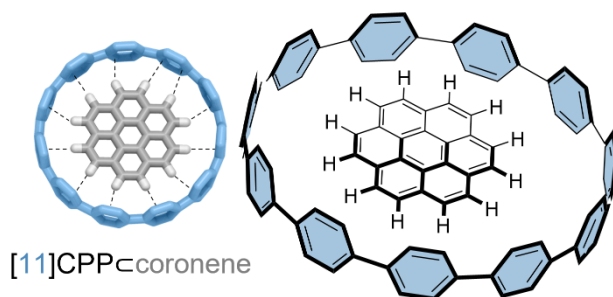


Figure 1.6. An [11]CPP-coronene complex – one amongst a series of CPP-aromatic hydrocarbon complexes recently described by the Bruns group – is stabilized by CH- π interactions.⁴⁵

respectively. These predictions were corroborated by experimental evidence obtained via ¹H NMR spectroscopy. They found that when coronene was mixed in a 1:1 ratio with [10]-, [11]-, and [12]CPP only the mixture of coronene with [11]CPP resulted in significant $\Delta\delta$ values for host and guest. They were also able to measure a K_a of $4100 \pm 1200 \text{ Mol}^{-1}$ for Cor-c[11]CPP in $\text{C}_2\text{D}_2\text{Cl}_4$ at 293 K as via NMR titrations.

1.4.2 Charged Guests

As the synthetic methodologies for nanohoops have developed, researchers have created a variety of nanohoop-derivatives via functionalization of phenylene backbone. In particular, nanohoops with appended electron-donating or with-drawing groups has proven a successful route to tailoring their electronic properties.⁴⁶ In an attempt to tailor nanohoop host properties to guests

outside of π -conjugated molecules, the Gaeta group synthesized an [8]CPP derivative where one phenylene unit was substituted with a 1,4-dimethoxybenzene (DMB) unit. They were able to show by MS and NMR analysis the complexation of this electron-donor containing [8]CPP derivative with N-methylpyridinium (NMP^+), measuring a K_a of 2200 M^{-1} in CDCl_3 . This NMR titration was repeated with the parent [8]CPP for which a much smaller binding affinity ($K_a = 700 \text{ M}^{-1}$) was measured.⁴⁷ DFT analysis of this complex suggest that it is stabilized by cation $^+$ - π , as well as CH- π , interactions. They also studied the interaction of their 1,4-DMB[8]CPP host with other pyridinium species and viologen guests, and while the other pyridinium guests gave similar results to NMP^+ , the viologen guests showed no interaction by ^1H NMR, which the authors suggest is due mostly to a steric effect as the guest is likely too large for the small macrocycle.

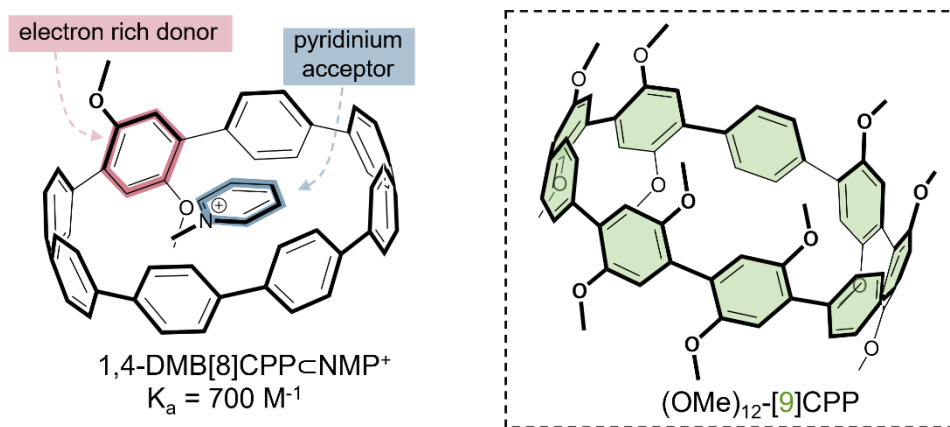


Figure 1.7. Left: 1,4-DMB[8]CPP effectively hosts NMP^+ via electrostatic interactions.⁴⁷ Right: dodecamethoxy[9]CPP plays host to a number of cationic molecules due to functionalization with electron donating methyl ether groups.⁴⁸

The following year a similar study with a dodecamethoxy-functionalized [9]CPP wherein six of the nine phenylene units were electron rich 1,4-dimethoxy-substituted units in order to create a nanohoop host for cationic molecules.⁴⁸ Complexation with a series of charged (hexadecyl trimethyl ammonium bromide, tetrabutyl ammonium bromide, and dibenzylammonium hexafluorophosphate among others) and neutral (including *p*-dinitrobenzene, 1,5-dibromopentane and benzoquinone) molecules were monitored by ^1H NMR spectroscopy. Most guests showed a small change in chemical shift of one or more proton resonances, however the direction each resonance shifted was inconsistent and relatively minor, precluding the accurate measurement of any association constants.

1.5. Mechanically Interlocked Molecules

A long considered, but only recently accessible field to emerge from supramolecular chemistry is the study of mechanically interlocked molecules (MIMs).⁴⁹⁻⁵⁰ The mechanical bond is defined as “an entanglement in space between two or more molecular entities (component parts) such that they cannot be separated without breaking or distorting chemical bonds between atoms.”⁵¹ The rational synthesis of MIMs - the prototypical examples of which are rotaxanes (a dumbbell shaped thread threaded through one or more rings) and catenanes (two or more interlocked rings) - heavily relies on the use of supramolecular interactions for bond formation, and, importantly, requires the use of a macrocycle. While early attempts at MIM synthesis were based on a statistical approach, seminal work by Sauvage showed that preorganization of the component pieces of MIM synthesis via the use of supramolecular interactions allowed for synthesis of MIMs in much better yields and with more control over the final structure. In particular, this work highlighted what has come to be known as the “template approach” to MIMs, in which preorganization of component parts via supramolecular interactions – in this case metal coordination – followed by the formation of the interlocking bond(s) to hold this structure together resulted in the synthesis of a catenane in 42% yield, a massive improvement over previous works published using a non-templated approach.⁵²

Carbon nanohoops, due to their fully conjugated π -system are inimitable macrocycles compared to many others used in supramolecular chemistry and in the synthesis of MIMs. Inclusion of such a macrocycle into a complex interlocked architecture may give rise to more unique and interesting structures with potential for use in areas like electronics and biological sensing or delivery. As such, the development of nanohoop-based MIMs has seen increased interest in the past few years. The first example of template-directed synthesis with nanohoops took advantage of the best-known supramolecular guest of nanohoops, C_{60} , for preorganization of the component pieces. Von Delius et al. reported the synthesis of a [10]CPP-fullerene based rotaxane (**Figure 1.8**, top) via a capping strategy, in which a functionalized C_{60} dimer was complexed with [10]CPP via strong concave-convex π - π interactions, then the thread was capped

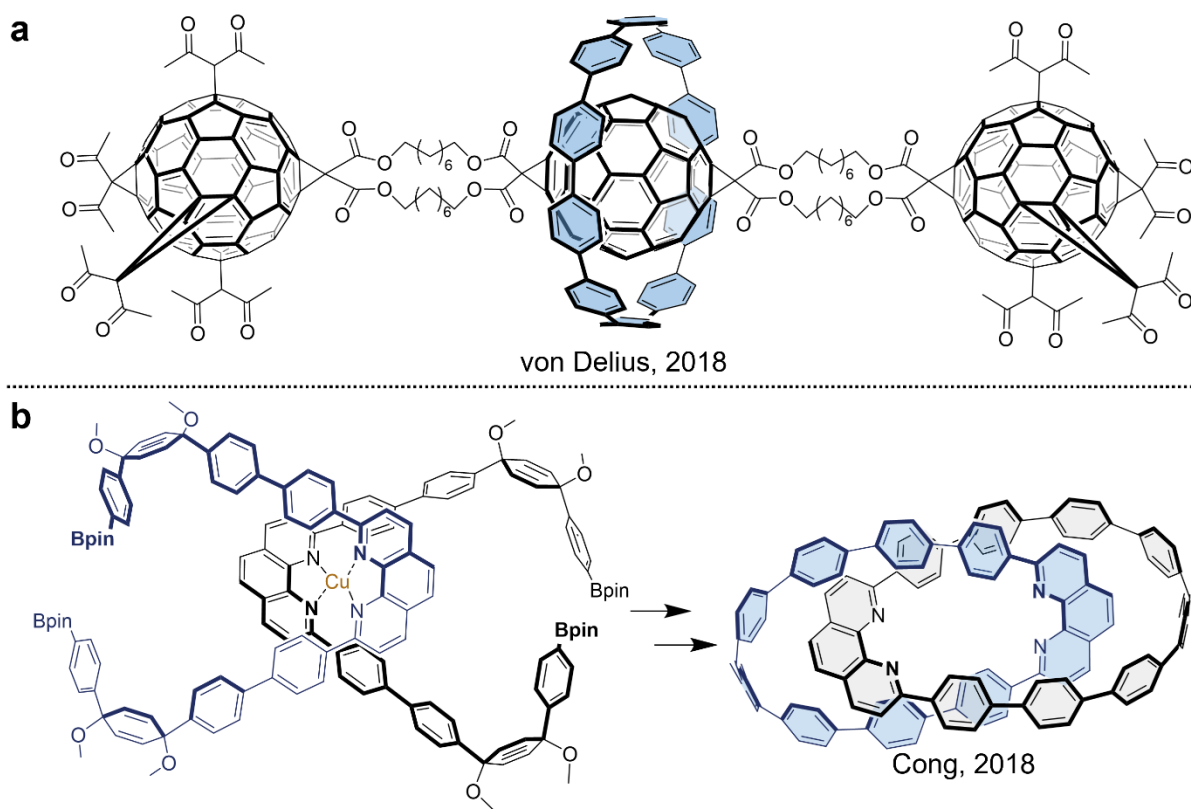


Figure 1.8. (Top) a fullerene-based thread interlocked within [10]CPP was templated using convex-concave π - π interactions between host and guest,⁵³ (bottom) an alternative passive template approach to interlocked nanohoops is based on the incorporation of nitrogen into the backbone.⁶¹

with a final ester- functionalized C₆₀ stopper group with enough functionality that the nanohoop was unable to slip off of the fullerene-based thread.⁵³ Notably, passive template synthesis such as this are achieved by incorporation of recognition motifs in the macrocycle (or macrocyclic precursor) that recognize and bind to a guest, which generally means that the final interlocked molecule retains this recognition between the two component pieces.

An alternative template strategy for the synthesis of MIMs is “active templating” first introduced independently by both the Saito and Leigh groups more than two decades after Sauvage’s introduction of templating as a general strategy.⁵⁴⁻⁵⁵ The active template (AT) strategy refers to the use of a metal to simultaneously preassemble the molecular components and catalyze the bond formation to produce an interlocked molecule. AT chemistry reduces the need for recognition groups in the component pieces, increasing the potential structural diversity of MIMs

made in this way, it also allows for the use of catalytic rather than stoichiometric amounts of metal, and can be applied to many metal-catalyzed reactions.⁵⁶⁻⁵⁷

While it is not immediately obvious how nano hoops might be utilized in active template synthesis due to their lack of heteroatoms capable of ligating metals, thanks to their modular synthesis, a number of pyridine-containing aza-nano hoops have been produced and successfully applied as ligands for a variety of metals.⁵⁸⁻⁶⁰ While these initial examples of aza-nano hoops highlighted their utility as ligands, in all cases metal coordination takes place exotopically, or on the exterior of the hoop, meaning that any reaction catalyzed by the bound metal would take place outside of the hoop and result in non-interlocking molecules. To overcome this geometry problem, the Cong group incorporated phenanthroline units into an acyclic nano hoop precursor. These nitrogen-containing precursors were then preorganized via complexation with copper and the precursors were then cyclized and aromatized to yield a nano hoop-based catenane through passive metal templating (**Figure 1.8**, bottom).⁶¹

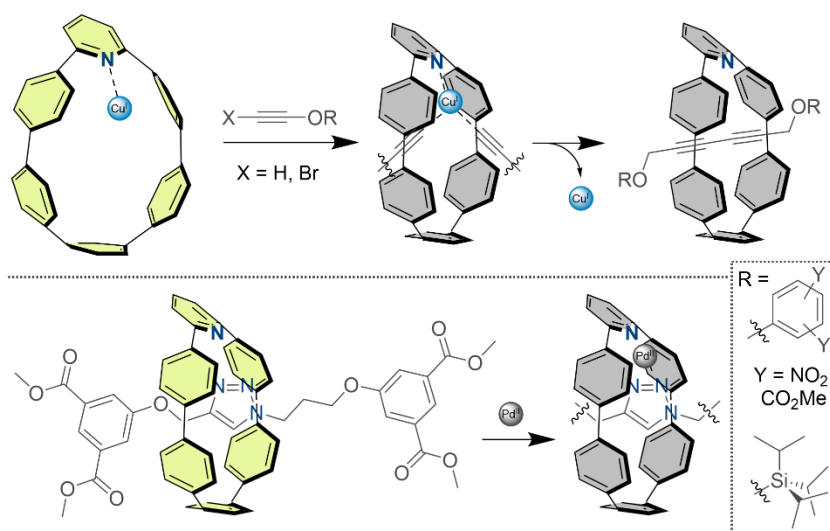


Figure 1.9. Active template synthesis of nano hoop-[2]rotaxanes is achieved through the use of a *meta*-pyridyl moiety. These MIMs have promise for use in fluorescent sensing as illustrated by the metal-sensing abilities of the triazole-containing macrocycle.⁶²

Inspired by this, but with a desire to achieve AT synthesis of a nano hoop rotaxane, our group turned to an alternative method to obtain endotopic metal coordination via synthesis of a *meta*-pyridine containing nano hoop (*mN*[6]CPP) wherein the pyridyl nitrogen points to the

nanohoop's interior (**Figure 1.9**). With the *mN*[6]CPP able to coordinate a metal in the nanohoop interior Van Raden and coauthors successfully illustrated the creation of a series of nanohoop-based rotaxanes using both copper catalyzed azide-alkyne cycloaddition (CuAAC) and Cadiot-Chodkiewicz (CC) couplings with copper catalysis. Interestingly in the case of the CuAAC-formed rotaxane, the resultant triazine moiety contained in the thread component and the pyridyl nitrogen could be exploited to coordinate metal ions resulting in the quenching of nanohoop fluorescence and highlighting the potential of these nanohoop-[2]rotaxanes (where 2 denotes the number of component pieces) for fluorescence-based sensing.⁶² This was accompanied by the synthesis of fluoride-sensing nanohoop-[2]rotaxanes in which, in contrast to the metal-sensing rotaxane, was chemically active, participating in a non-reversible dethreading of the macrocycle. In addition, in this fluoride-sensing design, while one stopper group as a trigger to initiate dethreading, the other stopper (a dinitro-substituted aromatic unit) was used to quench the fluorescence of the nanohoop when interlocked, resulting in a turn-on signal upon introduction of analyte.

1.6. Outlook

Supramolecular interactions are fundamental to life, as exemplified by the interactions of proteins and ligands, antibodies and antigens and many more similar biological processes. The fundamental nature of supramolecular interactions has prompted chemists to recognize the importance of understanding and using supramolecular systems to create complex assemblies for application in many fields. Macrocycles are integral to supramolecular chemistry, often acting as the “lock” for a well-fitting “key.” Nanohoops, amongst macrocycles, are particularly interesting due to their all-phenylene backbone giving them unique properties especially when compared to macrocycles like CBs and CDs that are far more commonly used in supramolecular chemistry. While their supramolecular chemistry may be less obvious and require tailoring, advances in the synthesis of nanohoops continues to open more opportunities for these conjugated macrocycles in the development of supramolecular systems. Despite this, nanohoop supramolecular chemistry is still in infant stages compared to the field as a whole, and much more work must be done in order for nanohoops to reach their full potential in the supramolecular world, and I look forward to their bright future.

1.6. Bridge to Chapter II

This chapter highlights the utility of carbon nanohoops as a unique class of macrocycles in supramolecular chemistry whose properties can be readily tailored towards complexation with a variety of guests. Compared to more well-established macrocycles used in the field of supramolecular chemistry, unfunctionalized or “parent” nanohoops are quite functionally simple, limiting their host-abilities mainly to interactions with fullerenes. However, thanks to general interest in this scaffold’s unique properties, synthetic developments in the fabrication of carbon nanohoops has allowed for researchers to tailor the electronic and general supramolecular properties of these macrocycles, suggesting a bright future in this field. The next chapter describes the development of water-soluble carbon nanohoop derivatives to further tailor the properties of these unique macrocyclic fluorophores.

CHAPTER II

THE DEVELOPMENT OF A MODULAR SYNTHESIS FOR WATER-SOLUBLE CARBON NANOHOOPS

This chapter includes unpublished co-authored material, it was written by myself, with editorial assistance from Professor Ramesh Jasti. Experimental work in this chapter was performed by myself with experimental guidance provided by Professor Ramesh Jasti.

In the few last decades, substantial effort has been put forth towards utilizing carbon nanomaterials for biological and medicinal applications due to their unique physicochemical properties. However, use of CNMs is often hindered by the heterogeneity inherent to their syntheses, decreasing their efficacy for many applications as well as leading to inconsistencies between studies due to the use of non-specific structures. In contrast, small molecule analogues of CNMs, for example carbon nanohoops, offer a controlled bottom-up synthetic approach allowing for atomic precision in their fabrication, meaning they can be tailor-made in ways not yet possible with CNMs. In addition to this, nanohoops have their own set of unique photophysical and supramolecular properties, suggesting they also have potential for use in biology/medicine. In 2018 our group presented the first biologically compatible nanohoop, employing them in cells for live imaging. However, this derivative was not completely water-soluble, and the synthesis was not designed for modularity nor was it high-yielding. Described herein, we sought an approach to accessing fully water-soluble nanohoops for future studies in a modular, high-yielding manner.

2.1. Introduction

Since their prediction, the proposed applications for carbon nanomaterials (CNMs) like carbon nanotubes (CNTs) are extensive and span a variety of fields.¹⁻⁷ Upon isolation of these materials, beginning with fullerene in 1985,⁸ many of these applications have been realized including use in organic electronics, materials development, and sensing.⁹⁻¹⁰ Further, CNMs have great potential in biological and medicinal applications due in large part to their small size, surface functionalization, and drug-hosting abilities, which suggest their potential as multi-functional diagnostic and therapeutic systems.¹¹⁻¹⁴ However, these applications are still in relatively early stages due to

challenges with the selective synthesis, solubility, and biocompatibility of these nanosized carbon-based structures.^{12,15-16} Currently, most CNMs are made by harsh methods that produce a wide variety of different structures which are challenging to separate. This means that bulk CNMs used for fundamental research are a mixture of structures which can lead to irreproducibility/inconsistency between studies.^{12,17} For example, toxicity profiles for CNMs differ substantially between studies; more specifically for CNTs it has been shown that the diameter, length, and mass basis (single-walled or double-walled) can all affect the toxicity but are impossible parameters to have complete control over.¹⁸⁻²² Furthermore, it has also been established that the means of solubilizing/dispersing CNMs for biological use not only affects their toxicity²³⁻²⁴, but also the intrinsic properties which make them useful for such applications.²⁵⁻²⁶

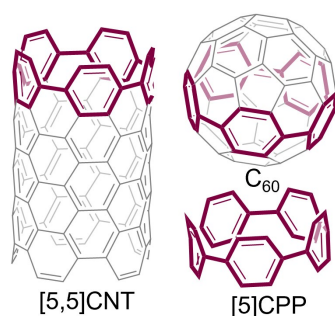


Figure 2.1. Carbon nano hoops are small molecules analogues of 3D CNMs; [5]CPP maps on to [5,5]-CNT (armchair) and C₆₀ fullerene.

Small molecule analogues of carbon nanomaterials, known as [*n*]cycloparaphenylenes ([*n*]CPPs where *n* denotes the number of phenylene units) are the smallest cross-section of an armchair carbon nanotube (**Figure 2.1**). As small molecules, these “nanohoops” offer a controlled bottom-up synthetic approach which allows for atomic precision in their synthesis, an approach not yet possible with most carbon nanomaterials. Importantly, covalent functionalization of curved CNMs (i.e. CNTs and fullerenes) disrupts the conjugated sp² network of the materials.^{16,27-29} This conjugation can be retained in nanohoops where functionality can replace protons on the hoop’s backbone, allowing them to retain their desirable properties.³⁰⁻³⁶ In addition to this, nanohoops have enhanced solubility over their linear counterparts and their own set of unique photophysical and supramolecular properties.³⁷⁻³⁸ For examples, they share a common excitation maximum across sizes, while the fluorescence emission is red shifted as hoop size decreases. Our lab and

others have also shown that discrete functionalization of these nano hoops with electron accepting units red-shifts the emission to more biologically relevant wavelengths.³⁹⁻⁴¹ Further, larger sizes have relatively high quantum yields and extinction coefficients as well as large effective stokes shifts, all of which suggests their usefulness as biological fluorophores. In 2018, our lab produced the first example of biologically compatible nano hoops via introduction of sulfonate groups or a folic-acid moiety (**Figure 2.2**).³¹ This work illustrated the idea that nano hoops can be used for live-cell imaging with no cytotoxicity up to 10 μ M. Notably, the sulfonated hoop showed pH independent fluorescence, unlike some commonly used biological dyes like fluorescein, an important property, as physiological pH can vary widely based on the intracellular compartment being studied. However, the derivative prepared was not fully water soluble, precipitates out of solution when allowed to stand for extended periods.

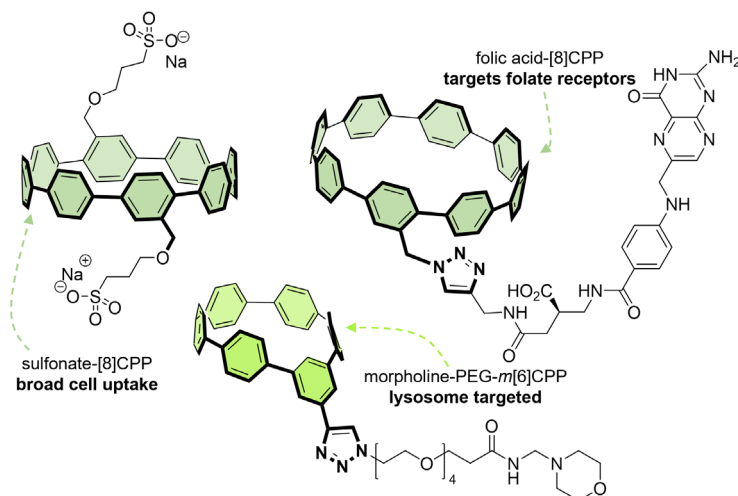


Figure 2.2. Biocompatible CPPs are taken into cells due to different functionality: sulfonates allow for general cell uptake³¹, folic acid targets folate receptors overexpressed on cancer cells³¹, and a PEG chain confers solubility while morpholine targets the lysosome.⁴²

In an alternate approach, folic acid was conjugated to the [8]CPP scaffold via an incorporated azide functionality. This derivative was also capable of cell imaging, with the folate moiety binding to folate receptors overexpressed on the surface of cancer cells. More recently, in 2021, work from our lab illustrated a more generalizable approach to creating organelle-targeted fluorophores using a *m*-[6]CPP scaffold.⁴² In this example, an alkyne was appended to the smaller nano hoop scaffold that could be coupled using the copper-catalyzed azide-alkyne cycloaddition to short PEG linkers with different end groups to modulate functionality (**Figure 2.2**). While this

approach can be carried out in higher yield when compared to the relatively challenging and low yielding sulfonation-approach, a similar result was observed regarding solubility: the derivative was not completely water soluble. While complete water-solubility is not necessary for use as a fluorophore, it is useful for other applications and further, while this approach conferred partial solubility to smallest fluorescent nanohoop (*m*-[5]CPP is very dimly fluorescent while [5]CPP is non-emissive), it is expected that larger sizes will require additional solubilizing groups to achieve the same result. While these approaches were successful and illustrated the utility of nanohoos as fluorophores, we sought to find a modular, and high-yielding route to water-soluble nanohoos for general applications in aqueous media. For this, we first target [10]CPP, as this is a well well-studied size in a variety of applications in addition to its known ability to host C₆₀.

2.2. Results and Discussion

For the initial target molecule, **II.12**, the solubilizing functionality was to be achieved via the use of four sulfonate groups, drawing upon the same types of synthetic precursors containing protected benzylic alcohols used to make sulfonate-[8]CPP. Due to the labile nature of the tertbutyl methyl silyl ether (TBS) noted in the synthesis of sulfonate-[8]CPP, a more robust methoxymethyl (MOM) ether protecting group was instead chosen for the synthesis of the target molecule. Finally, the synthesis was designed such that all the functionality was contained within only one of the coupling partners in the macrocyclization, allowing for substitution of the complementary coupling partner while retaining complete functionality for synthetic modularity. A retrosynthetic analysis of target molecule **II.12** (**Figure 2.3**) highlights key intermediate **II.3** for development of the modular synthetic route.

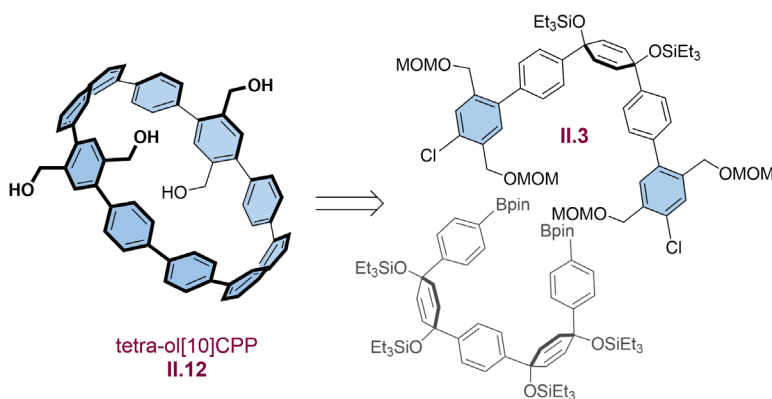
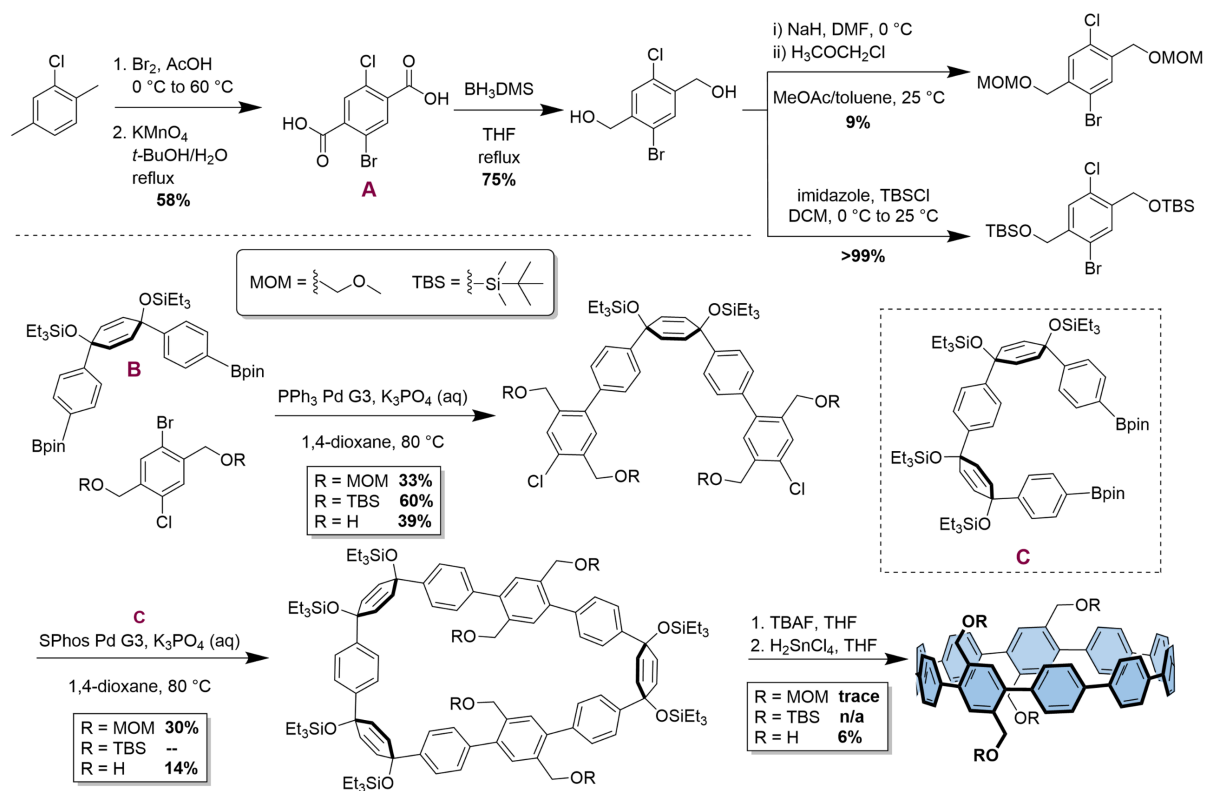


Figure 2.3. Retro-synthetic analysis of initial target molecule **II.12** for the development of water-soluble nanohoos based on key intermediate **II.3**.



Scheme 2.1. Synthesis of aromatized precursors to target molecule **II.12** for the development of water-soluble nanohoops via MOM-ether or TBS protected, or unprotected benzylic alcohols.

The synthesis began with small molecule manipulation of chloro-*para*-xylene to yield an asymmetric diol which is protected prior to incorporation into macrocyclic coupling partner **II.3** via Suzuki cross-coupling with *bis*-boronate intermediate **B** (**Scheme 2.1**) This tetra-functionalized synthon was then cyclized under dilute Suzuki coupling conditions with *bis*-boronate intermediate **C** (**Scheme 2.1**) to form the requisite macrocycle which could then be deprotected and aromatized to form tetra-functionalized nanohoop **II.6**. While the use of MOM ether protecting groups did allow access to a tetra-functionalized [10]CPP, the initial protection was low yielding (9%), suggesting this was not an amenable route to a scalable synthesis, and others were therefore tested. Due to precedence, TBS groups were studied next (**Scheme 2.1**), however as expected these labile groups were prone to base-induced deprotection prior to the intended deprotection step and were therefore abandoned at the unsuccessful macrocyclization step. Finally, the synthesis was carried out without protection of the benzylic alcohols (**Scheme 2.1**), and while, again, the fully aromatized nanohoop (**II.12**) could be synthesized, incorporation

of the asymmetric diol piece and the subsequent synthetic steps were generally low yielding and became increasingly challenging to purify, again suggesting this route was not amenable to scale-up. Notably, the sulfonation procedure developed by Dr. White was a challenging step requiring continual resubjection to sulfonate only two benzylic alcohols and resulted in a challenging purification. Due to this, and the low yielding syntheses of tetra-ol[10]CPP, it seemed wise to consider alternate methods to incorporate water solubility to nano hoops in a higher yielding, modular fashion.

To obtain the asymmetric diol used for the previously discussed syntheses, di-acid precursor **A** (Scheme 2.1) was reduced prior to incorporation, however, we considered that instead of reduction, ester protection of this intermediate might yield a robust functional group that could be manipulated in later stages of the synthesis to obtain the same target molecule, or to install a variety of other functional groups post-aromatization. Ethyl ester protection of intermediate **A** was high yielding and the resulting asymmetric diester could then be selectively coupled to familiar

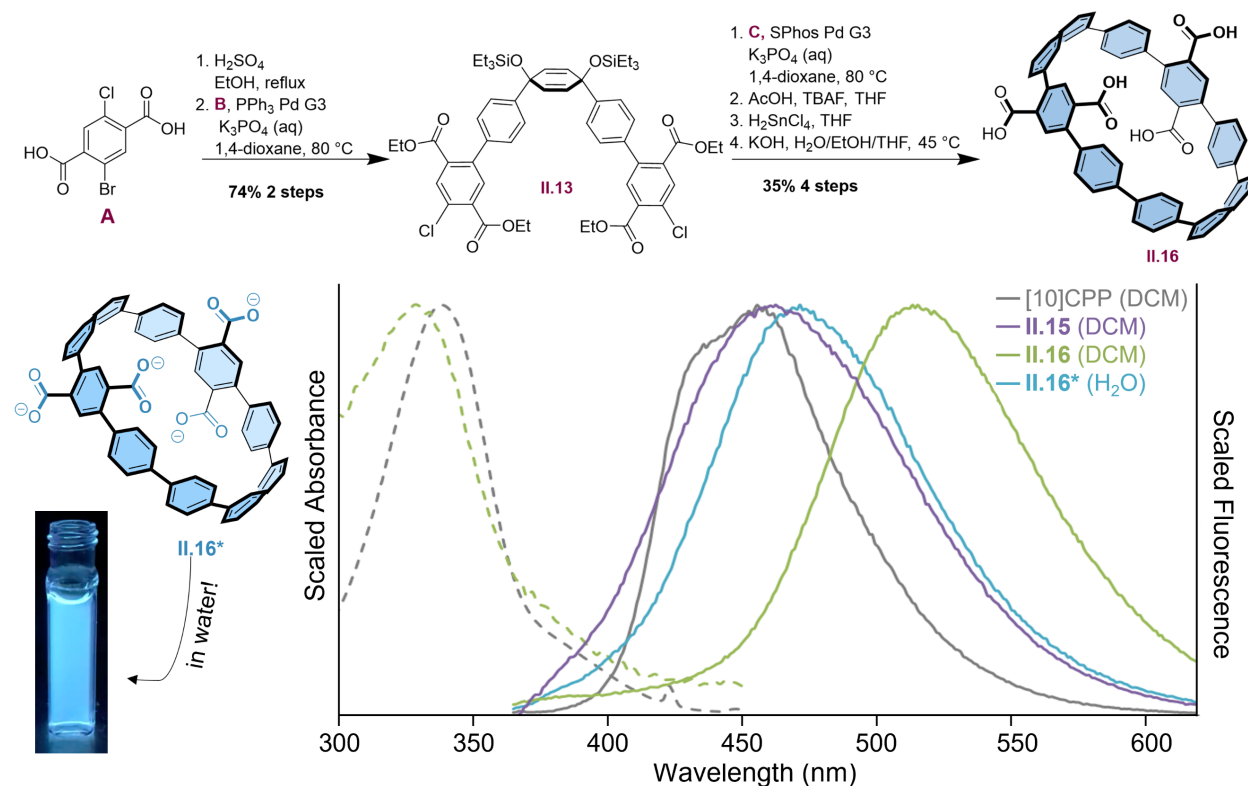
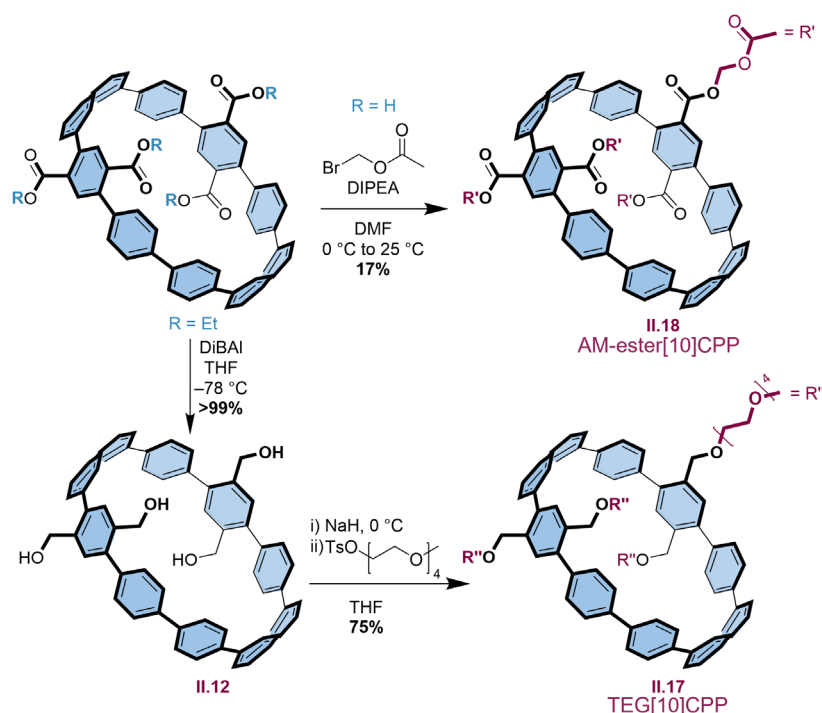


Figure 2.4. Top: Synthesis of optimized target molecule **II.16** for the development of water-soluble nano hoops based on incorporation of ethyl ester moieties. Bottom: water soluble carboxylate-nano hoop **II.16*** absorbance and fluorescence spectra of [10]CPP and ester- acid- and carboxylate derivatives.

bis-boronate **B**, to obtain the functionalized coupling partner **II.13** in nearly quantitative yield. Following the same general synthetic route described above, Suzuki macrocyclization of **II.13** with *bis*-boronate **C** gave the unaromatized macrocyclic precursor to **II.15** in more than twice the yield of even the best diol-based synthesis discussed above. Finally, after deprotection and aromatization tetraester-[10]CPP was saponified to yield tetraacid-[10]CPP (**II.16**). From here, simple deprotonation of the acid-functionalized hoop with aqueous NaOH yields a fully water soluble nanohoop.

While sulfonation could still be achieved upon reduction of the esters to alcohols and subsequent reaction with propane-sultone (as with sulfonate[8]CPP synthesis) it proved unnecessary as water-solubility could instead be conferred by the four carboxylate moieties. Further, this new synthetic route proved successful giving tetra-functionalized nanohoop **II.16** in a combined 35% yield over the final four steps (macrocyclization, deprotection, aromatization, and saponification), compared to an analogous four step yield of 5% achieved for the di-functionalized sulfonate[8]CPP (macrocyclization through sulfonation.) Further, as expected, the

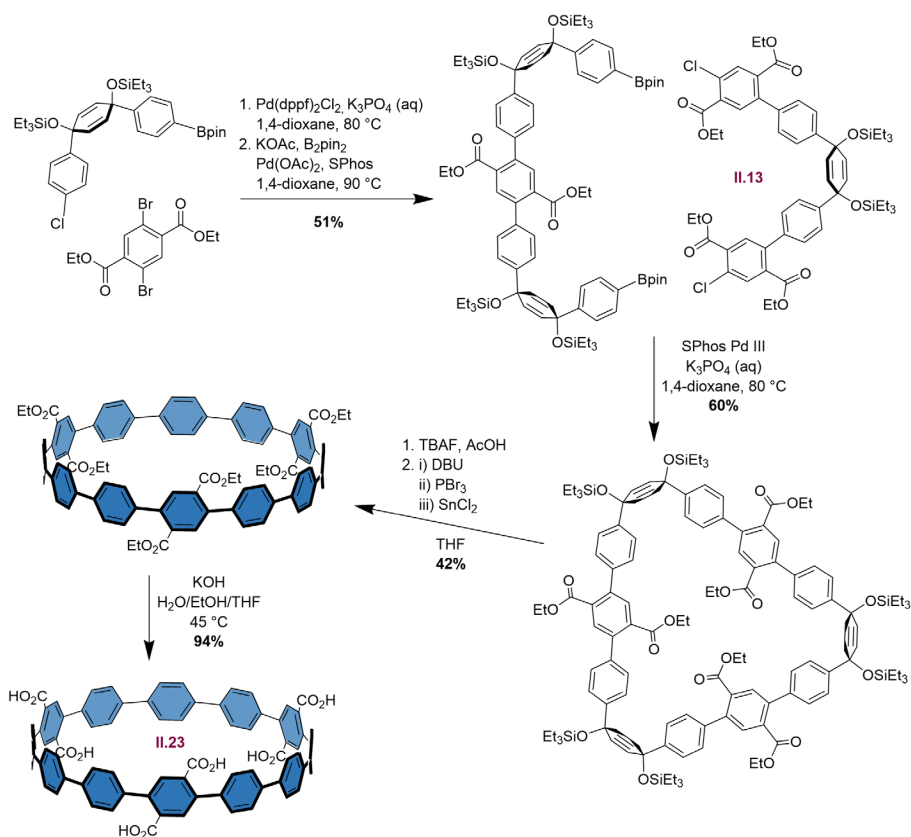


Scheme II.2. Synthesis of derivatives of **II.15** and **II.16** illustrates the utility of ester functionalized nanohoops for broader applications.

ester functionality proved a useful handle for post-aromatization manipulation of the scaffold; reduction of **II.15** with di-*isobutyl* aluminum hydride quantitatively yields the tetra-ol precursor (**II.12**) to original target sulfonate[10]CPP (**Figure 2.4**, left), which can then be further functionalized in-turn. To explore alternative functionality, of this new nano hoop a number of derivatives were investigated. From tetraol-[10]CPP **II.12** a short polyethylene glycol (PEG) linker was installed via S_N2 reaction with a tosylated triethylene glycol monomethyl ether to yield a tetraethylene glycol (TEG) functionalized [10]CPP in good yield (**Figure 2.4**, bottom). Interestingly the four short, uncharged PEG chains were not enough to confer solubility in water as expected.

Importantly, the water-soluble carboxylate-derivative **II.16***, retains its fluorescence in water with a λ_{max} of 472 nm. In fact, all the functionalized derivatives display a red-shifted emission, with the greatest shift, 48 nm, observed for **II.15** (514 nm) compared to [10]CPP (466 nm) in DCM. We next considered that these derivatives may be used for cell imaging. To study this, HeLa cells were treated with either the tetra-ester (**II.15**) or tetra-acid (**II.16**) derivative under standard conditions, however no cell uptake was seen after incubation. A commonly used functional group for the development of cell-trappable probes is the acetoxymethyl (AM) ester group, which can pass through cell membranes in its uncharged form, but upon entrance the ester group should be cleaved by esterase, leaving the charged probe trapped.⁴³⁻⁴⁴ Based on this, an AM-ester derivative of **II.16** was also synthesized (**Scheme 2.2**, top), however the uncharged species was poorly soluble in the cell culture media, and again imaging of HeLa cells was unsuccessful.

In addition to the improved yields and versatile functionality that the ester groups brought to the synthesis, the key functionalized intermediate, **II.13**, was also successfully incorporated into a water-soluble [12]CPP derivative. This was swiftly achieved via a similar synthetic route (**Scheme 2.3**). An additional ester-functionalized phenylene unit was incorporated via double Suzuki cross-coupling to asymmetric mono-boronate **D**. A subsequent Suzuki-Miyaura borylation of the ester functionalized intermediate results in a new *bis*-boronate coupling partner **II.20** for macrocyclization with **II.13**. The resulting macrocycle can then be deprotected, aromatized and saponified to reach hexa-acid[12]CPP in reasonably good yield with minimal additional synthetic steps. Although we targeted additional solubilizing groups in the synthesis of this derivative, this serves as a proof of concept that additional functionality can be incorporated into the water-soluble nano hoops via the macrocyclic coupling partner of intermediate **II.13** as anticipated.



Scheme 2.3. Synthesis of larger [12]CPP derivative **II.23** using the same tetra-ester functionalized key intermediate.

2.3. Conclusion

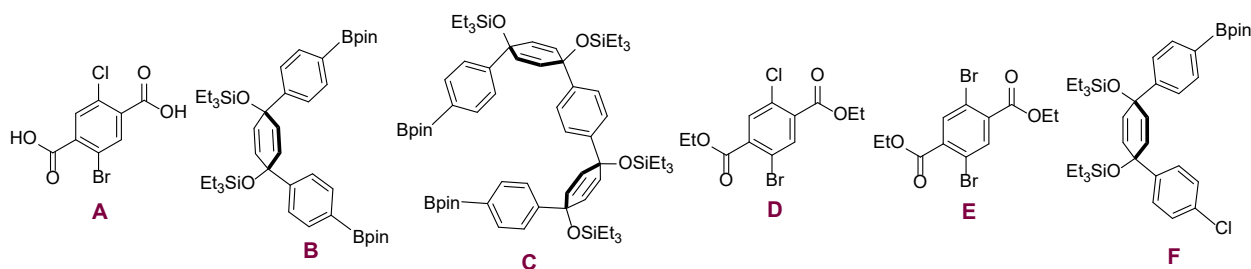
The bottom-up synthesis of nano hoops allows for the incorporation of functional groups with atom precision without interruption of the properties that make them so interesting for a variety of applications, including those in biology and medicine. While we have previously reported cell-permeable nano hoop derivatives, herein we present a higher yielding, modular approach to the synthesis of water-soluble nano hoops via the use of ester functionalized phenylene units. Not only can this synthetic approach be used to make water soluble nano hoops of varied sizes, but the robust functionality also allows for further derivatization with the well-studied carbonyl chemistry paving the way for the synthesis of other highly functionalized nano hoop derivatives.

2.4. Experimental Sections

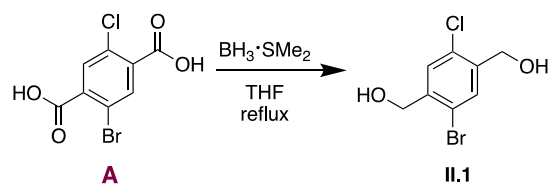
2.4.1. General Experimental Details

Moisture/air sensitive reactions were carried out under nitrogen atmosphere using standard Schlenk technique with flame-dried glassware cooled under an inert atmosphere of nitrogen. Dichloromethane, dimethylformamide, 1,4-dioxane and tetrahydrofuran used for reactions were dried by filtration through alumina and stored under an inert argon atmosphere. Silica column chromatography was conducted with Zeochem Zeoprep 60 Eco 40-63 μm silica gel and automated flash chromatography was performed using a Biotage Isolera One. Compounds A⁴⁵, B⁴⁶, C⁴⁷, D⁴⁵, E⁴⁸, F⁴⁷ (below) and PPh_3 Pd III and SPhos Pd III⁴⁹ were prepared according to literature procedure. All other reagents were obtained commercially.

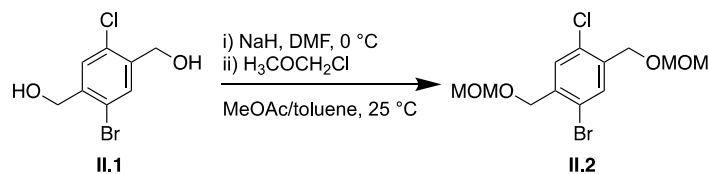
NMR spectra were recorded at 500 MHz or 600 MHz on Bruker Advance-III-HD NMR spectrometers. All ^1H NMR spectra were taken in CDCl_3 (referenced to TMS, δ 0.00 ppm), CD_2Cl_2 (references to dichloromethane, δ 5.32 ppm), $(\text{CD}_3)_2\text{CO}$ (referenced to acetone, δ 2.05 ppm), or $\text{DMSO}-d_6$ (referenced to DMSO, δ 2.50 ppm). All ^{13}C NMR spectra are referenced to either residual CDCl_3 (77.16 ppm), or $(\text{CD}_3)_2\text{CO}$ (29.84). Absorbance and fluorescence spectra were obtained in a 1 cm Quartz cuvette with dichloromethane or deionized water using an Agilent Cary 100 UV-Vis spectrometer Horiba Jobin Yvon Fluoromax-4 Fluorimeter, respectively. Cell imaging experiments were performed on a Leica DMI8 fluorescence microscope equipped with an Andor Zyla 4.2+sCMOS detector.



2.4.2. Synthesis and Characterization

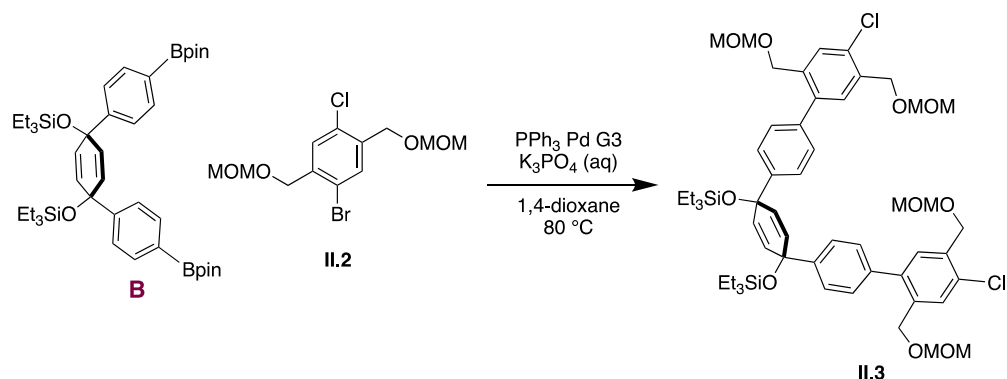


II.1. A flame dried 250 mL three-neck round bottom flask equipped with magnetic stir bar and reflux condenser was charged with **A** (5.30 g, 0.02 mol, 1.00 eq). The flask and condenser were capped with septa and refilled with nitrogen. Tetrahydrofuran (50 mL) was added to the reaction flask and the solution was stirred at 0 °C for 35 minutes. BH₃DMS (4.50 mL, 0.05 mol, 2.50 eq) was added dropwise over 10 minutes and the resulting mixture was stirred at 0 °C for 15 minutes. The reaction was allowed to come to room temperature then heated to reflux in an oil bath and stirred overnight. The reaction mixture was cooled to room temperature then quenched with methanol followed by the addition of water until the mixture became turbid. The organic solvents were removed under reduced pressure. The remaining water was removed by filtration to yield a light grey powder which was rinsed with hexanes until the color persisted. The resulting white solid (3.55 g, 75%). ¹H NMR (500 MHz, DMSO-*d*₆) δ 7.66 (s, 1H), 7.48 (s, 1H), 5.55 (s, 1H), 5.51 (s, 1H), 4.53 (d, *J* = 4.4 Hz, 2H), 4.48 (d, *J* = 4.2 Hz, 2H).

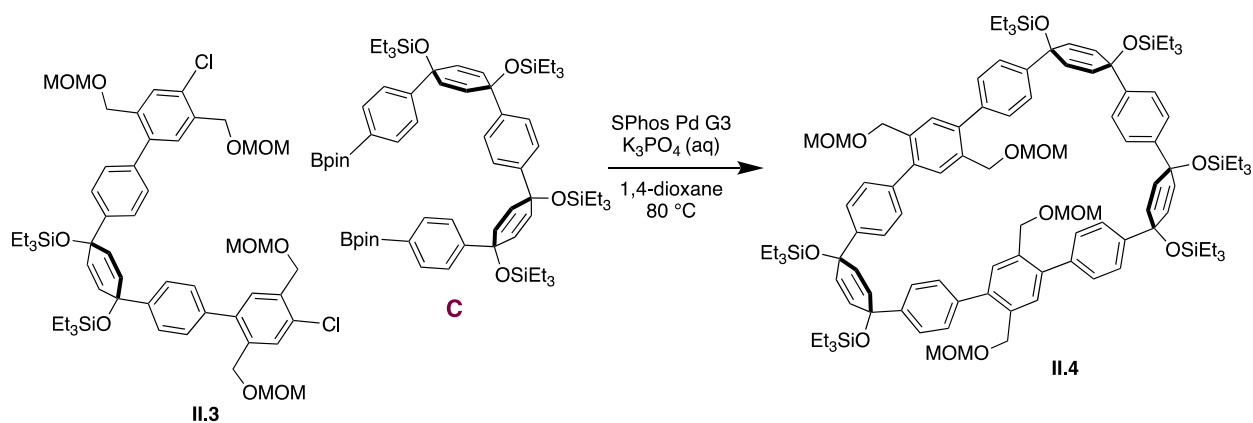


II.2. A flame dried 15 mL three-neck round bottom flask equipped with magnetic stir bar, addition funnel and reflux condenser then capped with septa and charged with 2 M ZnBr₂ in dimethoxymethane (0.22 mL). The flask was then charged with dimethoxymethane (0.65 mL, 10 mmol, 2.5 eq) and acetyl chloride (0.86 mL, 10 mmol, 2.5 eq) and the resulting solution was allowed to stir for 2 hours at room temperature. A flame-dried 50 mL round bottom flask was equipped with a stir bar and charged with **II.1** (1.0 g, 4 mmol, 1 eq) which was dissolved in dimethylformamide (5.0 mL) and stirred at 0 °C for 30 minutes. NaH (0.40 g, 10 mmol, 2.5 eq) was added in one charge then the reaction was stirred at 0 °C for 1.5 hours. The contents of flask

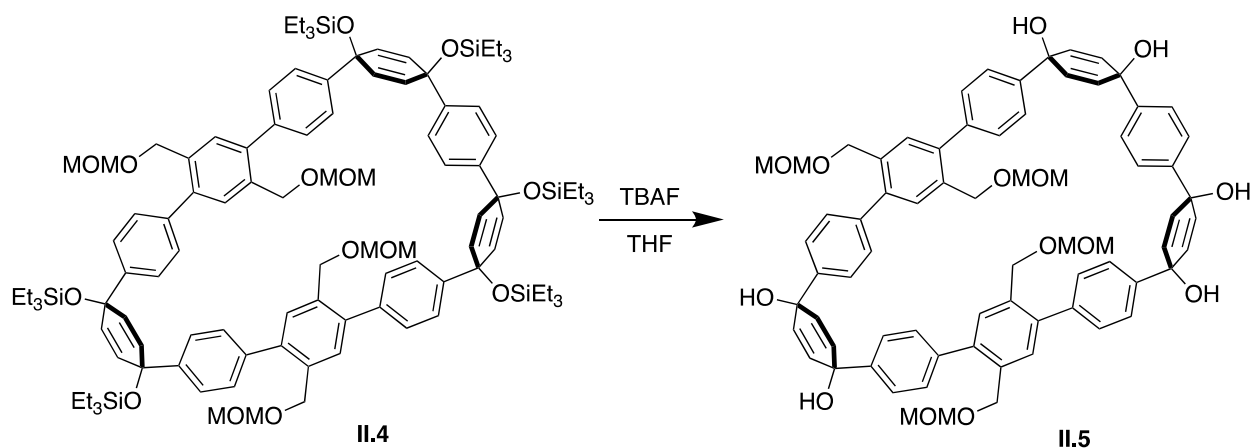
one were cannulated into the 50 mL reaction flask slowly and the resulting solution was allowed to come to room temperature and stirred for 48 hours. The reaction was quenched with a saturated solution of ammonium chloride and diluted with water. The product was extracted with ethyl acetate (3 x 50 mL) and washed with DI water (3 x 30 mL) then brine (50 mL). The organic layers were dried over sodium sulfate and concentrated to yield a tan solid which was washed with ethyl acetate and dried by vacuum filtration (120 mg, 8.9 %). ¹H NMR (600 MHz, Chloroform-*d*) δ 7.62 (s, 1H), 7.43 (s, 1H), 5.17 (s, 2H), 5.14 (s, 2H), 2.17 (s, 3H), 2.16 (s, 3H), 1.55 (s, overlapping 4H).



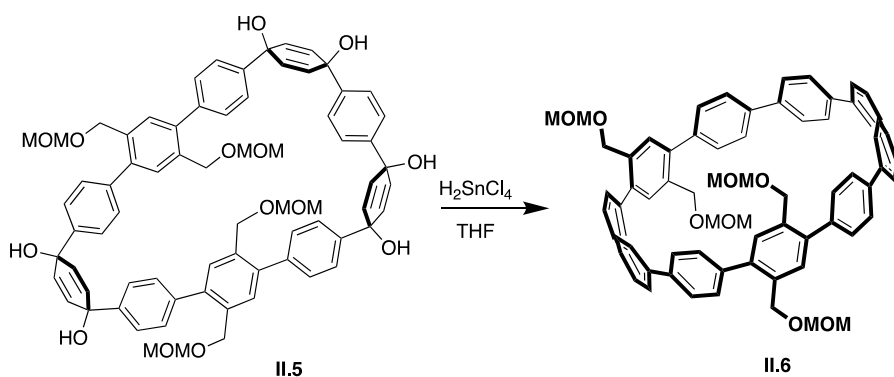
II.3. A microwave vessel was equipped with a magnetic spin vane and charged with **B** (0.10 g, 0.13 mmol, 1.0 eq), **II.2** (0.09 g, 0.27 mmol, 2.0 eq) and PPh₃ Pd G3 (0.03 g, 0.053 mmol, 0.20 eq) then purged with nitrogen for 30 minutes. 1,4-dioxane (0.90 mL) and 2M K₃PO₄ (aq) (0.35 mL) were added to the vial which was sparged for an additional 5 minutes. The reaction was stirred for 18 hours under microwave irradiation at 60 °C. The resulting dark brown reaction mixture was allowed to cool to room temperature and washed through a plug of Celite with ethyl acetate. The solution was diluted with water and the product extracted with ethyl acetate (3 x 20 mL) then washed with DI water (3 x 10 mL) and brine (20 mL). The organic layers were dried over sodium sulfate and concentrated to yield a brown oil. The crude material was purified by silica gel chromatography (0-20% ethyl acetate/hexanes) which yielded a yellow crystalline solid (44 mg, 33%). ¹H NMR (500 MHz, Chloroform-*d*) δ 7.56 (s, 2H), 7.41 (d, *J* = 8.5 Hz, 4H), 7.38 (s, 2H), 7.23 (d, *J* = 8.5 Hz, 4H), 6.06 (s, 4H), 4.73 (s, 4H), 4.70 (s, 4H), 4.61 (s, 4H), 4.43 (s, 4H), 3.40 (s, 6H), 3.29 (s, 6H), 0.96 (t, *J* = 7.9 Hz, 18H), 0.64 (q, *J* = 7.9 Hz, 12H).



II.4. Dichloride **II.3** (0.10 g, 0.09 mmol, 1.0 eq) was transferred to 50 mL flame-dried round bottom flask in minimal dichloromethane and solvent removed under vacuum. The flask was charged with **C** (0.10 g, 0.10 mmol, 1.2 eq) and Pd SPhos G3 (7.0 mg, mmol, 0.10 eq) then evacuated and refilled with nitrogen. 1,4-dioxane (30 mL) was transferred to the flask and sparged 5 minutes before being lowered into a preheated oil bath (80 °C). The reaction was allowed to come to temperature for 10 minutes before the addition of 2M K_3PO_4 (aq) (3.0 mL). The reaction was stirred overnight at 80 °C. The reaction mixture was allowed to cool to room temperature then washed through a plug of Celite with dichloromethane. The filtrate was diluted with water and the product extracted with dichloromethane (3 x 20 mL) and brine (25 mL). The organic layers were dried over sodium sulfate and concentrated to yield a brown oil. The crude material was purified by silica gel chromatography (2-5% ethyl acetate/hexanes) which yielded a waxy yellow solid (48 mg, 30 %). ^1H NMR (500 MHz, Chloroform-*d*) δ 7.46 (s, 8H), 7.40 – 7.30 (m, 12H), 6.10 (s, 4H), 6.07 – 5.98 (m, 8H), 4.62 (d, J = 4.1 Hz, 8H), 4.51 (d, J = 6.0 Hz, 8H), 3.28 (d, J = 4.1 Hz, 12H), 1.00 – 0.92 (m, overlapping 24H), 0.90 (t, J = 7.4 Hz, 24H), 0.70 – 0.64 (m, 32H), 0.58 (q, J = 7.4 Hz, 18H).

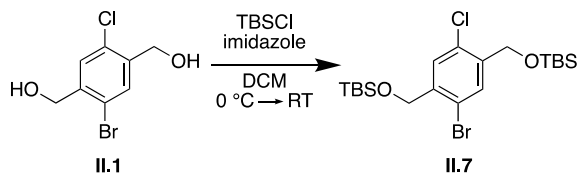


II.5. A scintillation vial containing macrocycle **II.4** (48 mg, 0.026 mmol, 1 eq) and a magnetic stir bar was dried under vacuum at 40 °C for 1 hour then capped with a septum. Tetrahydrofuran (0.26 mL) was added to the vial followed by tetra-*n*-butylammonium fluoride (0.26 mL, 1 M in tetrahydrofuran) and the reaction was allowed to stir for 2 hours at room temperature. The reaction was quenched with deionized water and the precipitate was collected via vacuum filtration. The yellow solid was rinsed with dichloromethane (30 mg, > 99%). ¹H NMR (500 MHz, DMSO-*d*₆) δ 7.52 – 7.42 (m, 8H), 7.35 (s, 16H), 5.90 (s, 12H), 4.54 (s, 8H), 4.43 (s, 8H), 3.12 (s, 12H), 0.96 – 0.93 (m, 8H).

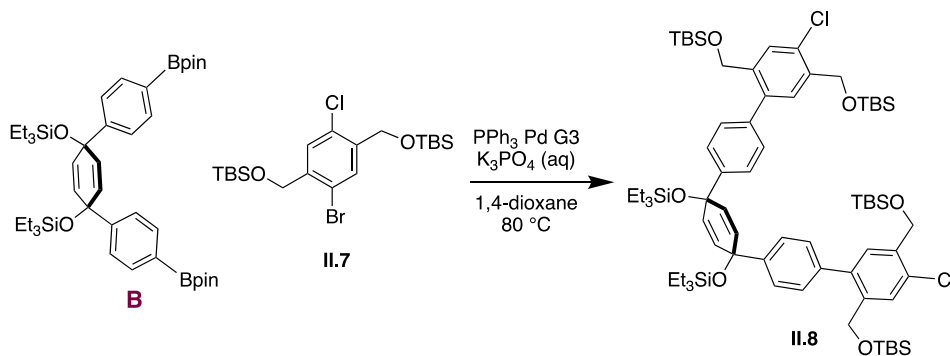


II.6. Deprotected macrocycle **II.5** (0.03 g, 0.025 mmol, 1.0 eq) was added to a 25 mL flame dried round bottom flask equipped with magnetic stir bar and capped with a septum, minimal THF was added to dissolve the macrocycle. To this solution was added 9.4 mL of the following solution: tin(II) dichloride monohydrate (0.18 g, 0.8 mmol, 2.1 eq) and concentrated hydrochloric acid (0.13 mL, 1.6 mmol, 4.2 eq) in tetrahydrofuran (20 mL). The reaction was allowed to stir for 1 hour at room temperature then quenched with saturated sodium bicarbonate (5 mL). The product was

extracted with dichloromethane (3 x 10 mL) and washed with brine (25 mL). The organic layers were dried over sodium sulfate and concentrated to give an off white solid. Crude material purified by alumina column chromatography (50-90% dichloromethane/hexanes) to yield a white solid (0.9 mg, 2.8%). ¹H NMR (600 MHz, Chloroform-*d*) δ 7.61 – 7.59 (m, 12H), 7.56 – 7.53 (m, 12H), 7.46 (s, 2H), 7.45 (s, 2H), 7.42 (d, *J* = 8.4 Hz, 4H), 7.38 – 7.36 (m, 4H), 4.72 (s, 8H), 4.55 (s, 4H), 4.51 (s, 6H), 3.41 (s, 6H), 3.40 (s, 6H).

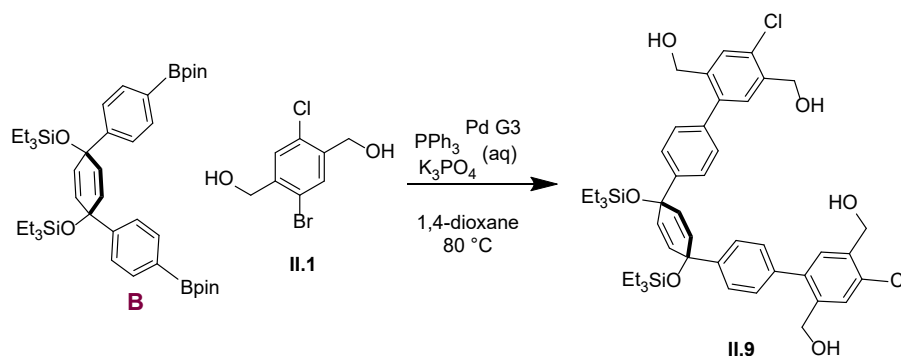


II.7. A flame dried 50 mL round bottom flask equipped with magnetic stir bar was charged with **II.1** (1.0 g, 4.0 mmol, 1.0 eq) and imidazole (1.7 g, 25 mmol, 6.4 eq) then capped with a septum. The flask was evacuated and refilled with nitrogen before the addition of dichloromethane (3.0 mL). The reaction was stirred at 0 °C for 15 minutes. *Tert*-butyldimethylsilyl chloride (4.50 mL, 0.05 mol, 2.50 eq) was added in one charge and the resulting mixture was allowed to come to room temperature overnight. The reaction was washed through a plug of silica with dichloromethane and the filtrate was concentrated to yield a yellow oil which solidified under vacuum (1.9 g, >99%). ¹H NMR (500 MHz, Chloroform-*d*) δ 7.66 (d, *J* = 0.9 Hz, 1H), 7.47 (d, *J* = 1.1 Hz, 1H), 4.74 (s, 1H), 4.68 (s, 1H), 0.97 (s, 9H), 0.97 (s, 9H), 0.14 (s, 6H), 0.13 (s, 6H).

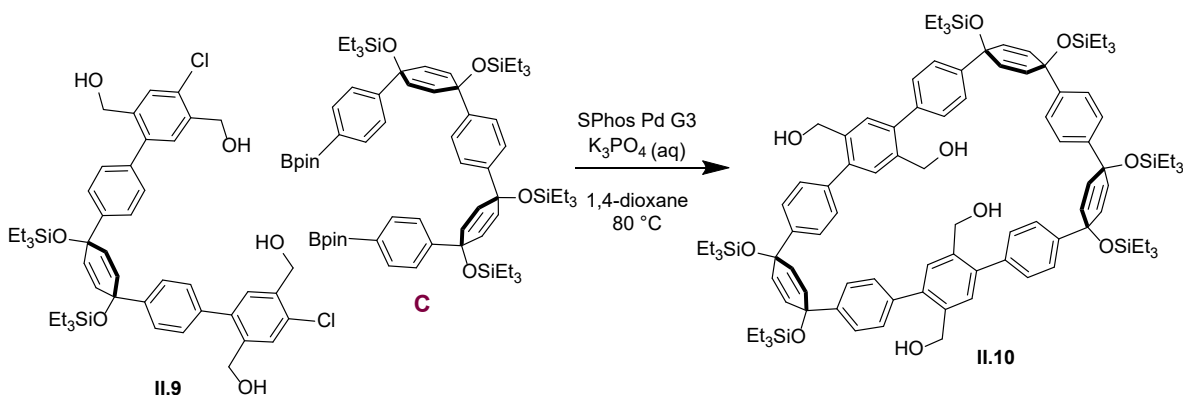


II.8. A 10 mL round bottom flask was equipped with a magnetic stir bar then charged with **B** (0.78 g, 1.0 mmol, 1.0 eq), **II.7** (1.0 g, 2.0 mmol, 2.0 eq) and PPh₃ Pd G3 (0.13 g, 0.20 mmol, 0.10 eq) then purged with nitrogen for 30 minutes. 1,4-dioxane (5.2 mL) and 2M K₃PO₄ (aq) (0.52 mL) were added to the flask and sparged for an additional 15 minutes then the reaction was heated to

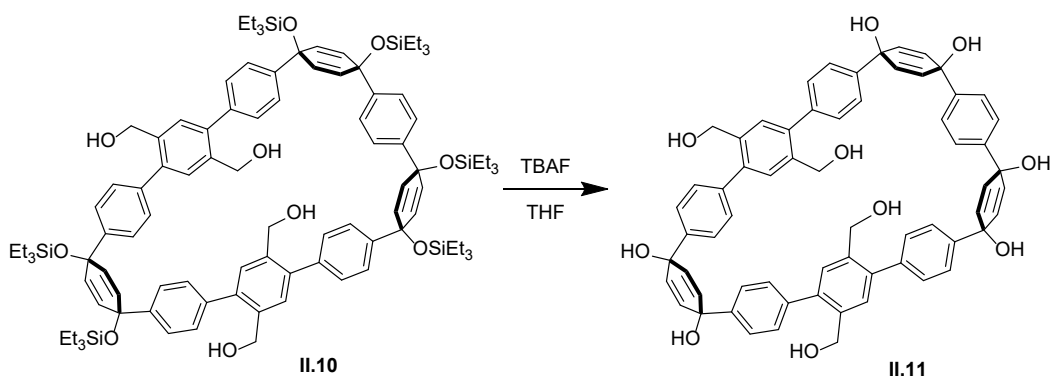
80 °C and stirred overnight. The reaction was allowed to cool to room temperature and washed through a plug of Celite with dichloromethane. The solution was diluted with water and the product extracted with dichloromethane (3 x 100 mL) then washed with DI water (3 x 50 mL) and brine (100 mL). The organic layers were dried over sodium sulfate and concentrated to yield a brown liquid. The crude material was purified by silica gel column chromatography (0-30% Ethyl Acetate/Hexanes) which yielded a light, yellow oil (0.81 g, 60%). ¹H NMR (500 MHz, Chloroform-*d*) δ 7.51 (s, 2H), 7.41 (d, *J* = 8.4 Hz, 4H), 7.37 (s, 2H), 7.19 (d, *J* = 8.3 Hz, 3H), 6.08 (s, 4H), 4.79 (s, 4H), 4.53 (s, 4H), 0.97 (t, *J* = 1.5 Hz, 18H), 0.96 (s, 18H), 0.97 – 0.91 (m, 12H), 0.64 (q, *J* = 7.7 Hz, 24H), 0.14 (d, *J* = 1.8 Hz, 12H), 0.08 (s, 12H).



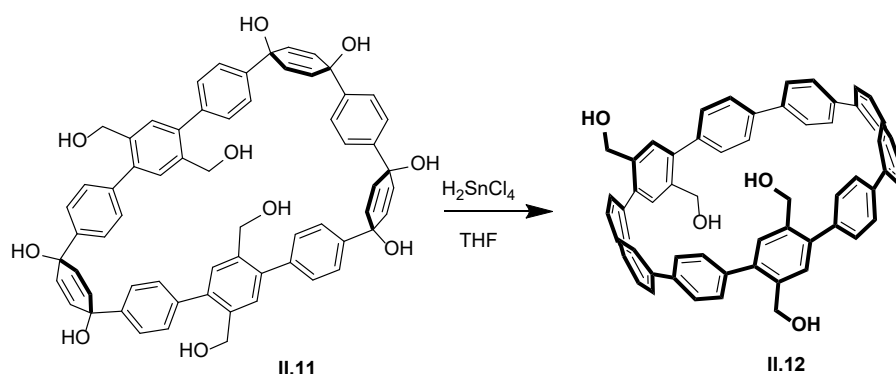
II.9. A 25 mL round bottom flask was equipped with a magnetic stir bar then charged with **B** (0.59 g, 0.79 mmol, 1.0 eq), **II.1** (0.40 g, 1.6 mmol, 2.0 eq) and PPh₃ Pd G3 (0.20 g, 0.32 mmol, 0.20 eq) then purged with nitrogen for 30 minutes. 1,4-dioxane (4.0 mL) and 2M K₃PO₄ (aq) (2.0 mL) were added to the flask and sparged for an additional 15 minutes then the reaction was heated to 80 °C and stirred overnight. The reaction was allowed to cool to room temperature and washed through a plug of Celite with ethyl acetate. The solution was diluted with water and the product extracted with ethyl acetate (3 x 100 mL) then washed with deionized water (3 x 50 mL) and brine (100 mL). The organic layers were dried over sodium sulfate and concentrated to yield a tan oil. The crude material was purified by automated flash silica gel chromatography (40-60% ethyl acetate/hexanes) which yielded a clear oil which was dissolved in minimal dichloromethane and triturated with hexanes to obtain an off-white solid (0.33 g, 50%). ¹H NMR (600 MHz, Chloroform-*d*) δ 7.56 (s, 2H), 7.38 (s, 2H), 7.37 (d, *J* = 8.3 Hz, 4H), 7.23 (d, *J* = 8.3 Hz, 4H), 6.09 (s, 4H), 4.79 (d, *J* = 6.2 Hz, 2H), 4.56 (d, *J* = 5.0 Hz, 2H), 2.09 (t, *J* = 6.3 Hz, 1H), 1.93 (t, *J* = 5.5 Hz, 1H), 0.96 (t, *J* = 7.9 Hz, 9H), 0.65 (q, *J* = 7.9 Hz, 6H).



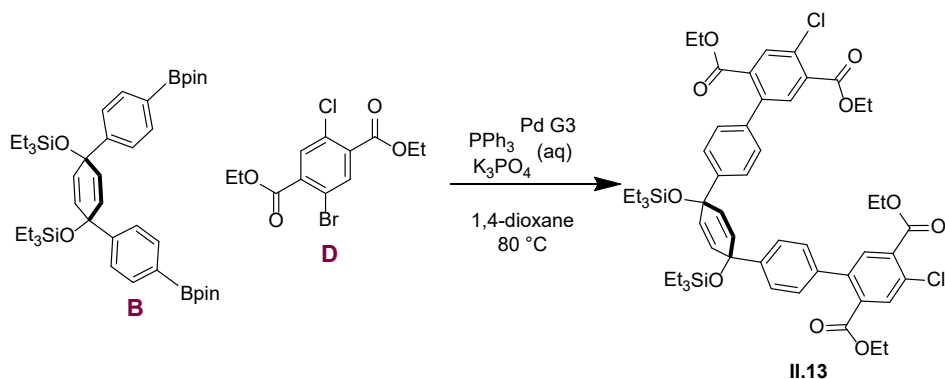
II.10. A 250 mL flame-dried round bottom flask equipped with magnetic stir bar was charged with **II.9** (0.09 g, 1.0 mmol, 1.0 eq), **C** (0.15 g, 1.2 mol, 1.2 eq) and Pd SPhos G3 (8.6 mg, 0.011 mmol, 0.1 eq) then evacuated and refilled with nitrogen. 1,4-dioxane (36 mL) was transferred to the flask and sparged 5 minutes before being lowered into a preheated oil bath (80 °C). The reaction was allowed to come to temperature for 10 minutes before the addition of 2M K₃PO₄ (aq) (3.6 mL). The reaction was stirred overnight at 80 °C. The reaction mixture was allowed to cool to room temperature then washed through a plug of Celite with dichloromethane. The filtrate was diluted with water and the product extracted with dichloromethane (3 x 20 mL) and brine (25 mL). The organic layers were dried over sodium sulfate and concentrated to yield a brown oil. The crude oil was triturated with acetone and the solid was collected by vacuum filtration then further purified using silica gel chromatography (0-50% Ethyl Acetate/Hexanes) which yielded a yellow solid (25 mg, 14%). ¹H NMR (600 MHz, Chloroform-*d*) δ 7.43 (dd, *J* = 10.3, 1.8 Hz, 4H), 7.38 – 7.33 (m, 3H), 7.31 – 7.27 (m, 1H), 7.26 – 7.21 (m, 2H), 6.13 – 5.91 (m, 12H), 4.72 (s, 4H), 4.60 (d, *J* = 6.8 Hz, 2H), 4.38 (s, 4H), 1.05 – 0.78 (m, 36H), 0.71 – 0.33 (m, 54H).



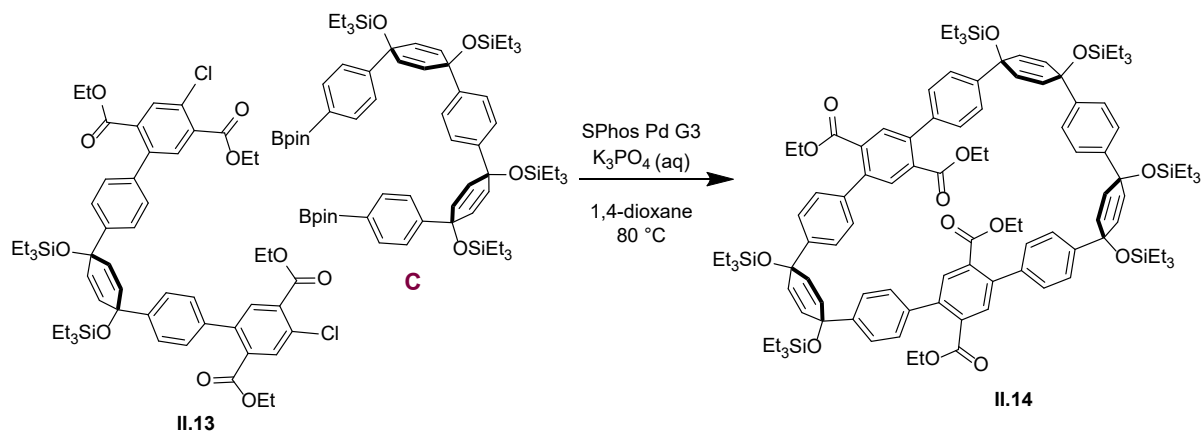
II.11. A scintillation vial containing macrocycle **II.10** (0.02 g, 0.01 mmol, 1.0 eq) and a magnetic stir bar was dried under vacuum for 1 hour then capped with a septum. Tetrahydrofuran (0.13 mL) was added to the vial followed by tetra-*n*-butylammonium fluoride (0.13 mL, 1 M in tetrahydrofuran) and the reaction was allowed to stir for 2 hours at room temperature. The reaction was quenched with deionized water (5 mL) and the precipitate was collected via vacuum filtration. The yellow solid was rinsed with dichloromethane (3.9 mg, 30%). ¹H NMR (500 MHz, Acetone-*d*₆) δ 7.63 (d, *J* = 8.3 Hz, 4H), 7.57 (s, 4H), 7.50 (d, *J* = 8.3 Hz, 4H), 7.48 (s, 2H), 7.40 (s, 2H), 7.23 (s, 8H), 6.27 (s, 4H), 6.00 – 5.90 (m, 8H), 4.55 (s, 4H), 4.50 (s, 4H).



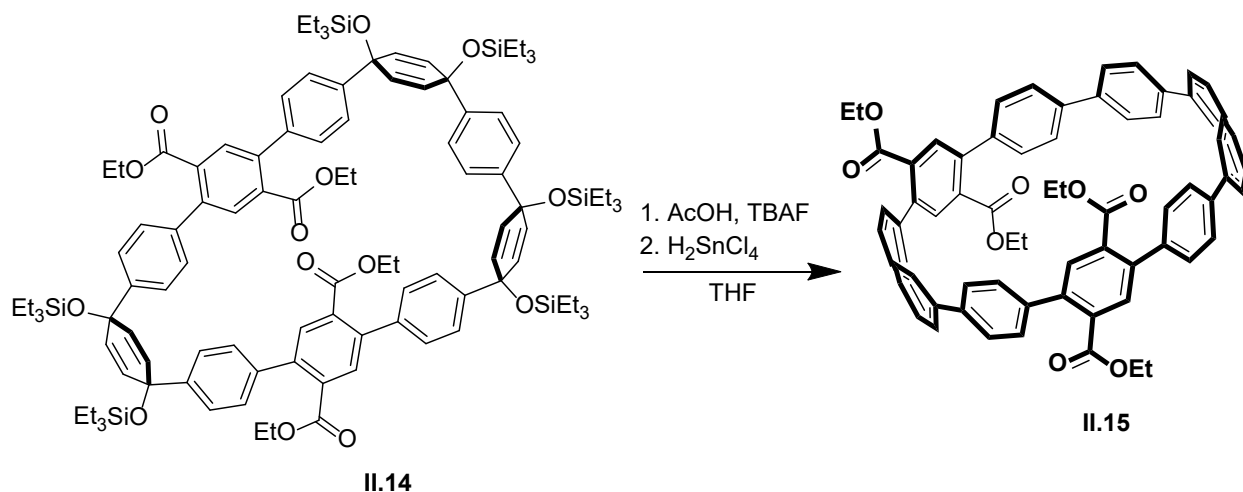
II.12. Deprotected macrocycle **II.11** (0.016 g, 0.016 mmol, 1.0 eq) was added to a 25 mL flame dried round bottom flask equipped with magnetic stir bar and capped with a septum, minimal THF was added to dissolve the macrocycle. To this solution was added 1.3 mL of the following solution: tin(II) dichloride monohydrate (0.09 g, 0.40 mmol, 2.1 eq) and concentrated hydrochloric acid (0.07 mL, 0.8 mmol, 4.2 eq) in THF (10 mL). The reaction was allowed to stir for 1 hour at room temperature then quenched with saturated sodium bicarbonate (5 mL). The product was extracted with dichloromethane (3 x 10 mL) and washed with brine (25 mL). The organic layers were dried over sodium sulfate and concentrated to give an off white solid. Crude material purified by preparative thin layer chromatography using alumina (10% methanol/dichloromethane) to yield a white solid (2.8 mg, 20%). ¹H NMR (600 MHz, Chloroform-*d*) δ 7.71 (dd, *J* = 5.6, 3.4 Hz, 1H), 7.59 (d, *J* = 3.9 Hz, 7H), 7.56 (d, *J* = 2.4 Hz, 3H), 7.54 (d, *J* = 8.5 Hz, 5H), 7.44 – 7.40 (m, 2H), 7.39 (d, *J* = 2.0 Hz, 2H), 7.37 (d, *J* = 8.5 Hz, 3H), 7.34 (s, 1H), 7.31 (d, *J* = 8.2 Hz, 4H), 4.68 (d, *J* = 5.5 Hz, 2H), 4.61 (d, *J* = 5.5 Hz, 2H), 2.13 (s, 1H), 2.04 (s, 1H).



II.13. To a 50 mL flame-dried round bottom flask equipped with a magnetic stir bar was added **D** (0.614 g, 2.44 mmol, 2.00 equiv.), **B** (1.00 g, 1.34 mmol, 1.10 equiv.), and PPh₃ Pd III (0.309 g, 0.488 mmol, 0.200 equiv.) followed by five cycles of evacuation and refill with N₂. A septum was placed on the flask followed by the addition of 1,4-dioxane (12.5 mL). The reaction was heated to 80 °C with stirring for 15 minutes followed by the addition of 2 M K₃PO₄ (0.13 mL) and stirred at temperature for 48 hours. The reaction was cooled to room temperature and the solvent was removed under reduced pressure. The resulting crude oil was dissolved in ethyl acetate (EtOAc) and passed through a plug of Celite, dried over sodium sulfate, filtered, and concentrated to yield an orange oil. The crude solid was purified by automated flash chromatography (10% EtOAc/hexanes) to obtain the product as a clear oily solid (1.10 g, 98%). ¹H NMR (600 MHz, Chloroform-*d*) δ 7.84 (s, 2H), 7.77 (s, 2H), 7.38 (d, *J* = 8.4 Hz, 4H), 7.20 (d, *J* = 8.4 Hz, 4H), 6.03 (s, 4H), 4.40 (q, *J* = 7.1 Hz, 4H), 4.07 (q, *J* = 7.2 Hz, 4H), 1.38 (t, *J* = 7.1 Hz, 6H), 0.99 (t, *J* = 7.1 Hz, 6H), 0.96 (t, *J* = 7.1 Hz, 18H), 0.64 (q, *J* = 7.9 Hz, 12H). ¹³C NMR (151 MHz, Chloroform-*d*) δ 166.76, 165.05, 145.78, 140.28, 138.25, 134.74, 133.22, 132.50, 132.31, 131.95, 131.56, 128.17, 125.76, 71.33, 61.99, 61.54, 14.20, 13.60, 7.08, 6.48 ppm. HRMS (ESI) (*m/z*): [M+Na]⁺ calcd for [C₅₄H₆₆Cl₂O₁₀Si₂]Na, 1023.3469; found, 1023.3452.

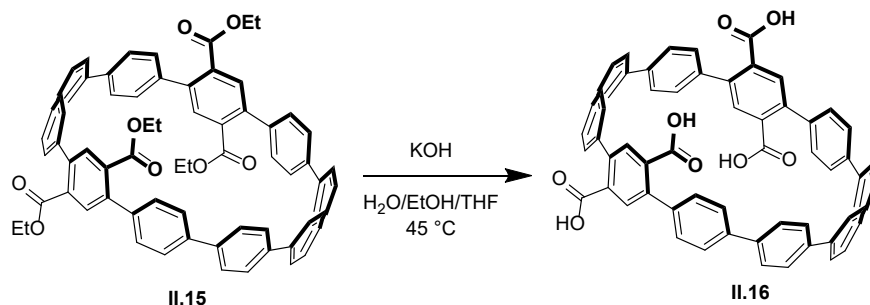


II.14. To a 500 mL flame-dried round bottom flask equipped with magnetic stir bar was added **C** (0.740 g, 0.773 mol, 1.20 equiv.), **II.13** (0.646 g, 0.644 mmol, 1.00 equiv.), and SPhos Pd III (0.077 mg, 0.097 mmol, 0.150 equiv.) followed by five cycles of evacuation and refill with N₂. A septum was placed on the flask followed by the addition of 1,4-dioxane (260 mL). The reaction was heated to 80 °C with stirring for 30 minutes followed by the addition of 2 M K₃PO₄ (26.0 mL) and stirred at temperature for 24 hours. The mixture was allowed to cool to room temperature and the solvent was removed under reduced pressure. The resulting crude oil was dissolved in DCM and passed through a pad of silica. The resulting solution was dried over sodium sulfate, filtered, and concentrated to yield a yellow solid. The crude solid was purified by automated flash chromatography (25% EtOAc/hexanes) to obtain the product as a yellow solid (0.961 g, 78%). ¹H NMR (600 MHz, Chloroform-*d*) δ 7.74 (s, 2H), 7.61 (s, 2H), 7.42 (d, *J* = 8.4 Hz, 4H), 7.40 (s, 4H), 7.29 (d, *J* = 8.3 Hz, 4H), 7.06 (s, 8H), 6.16 (s, 4H), 6.04 (d, *J* = 9.5 Hz, 4H), 5.98 (d, *J* = 10.0 Hz, 4H), 4.05 (q, *J* = 7.0 Hz, 4H), 3.94 (q, *J* = 7.1 Hz, 4H), 1.29 (t, *J* = 6.9 Hz, 6H), -1.23 (m, 60H), 0.83 (t, *J* = 7.1 Hz, 6H), 0.66 (q, *J* = 7.8 Hz, 24H), 0.57 (q, *J* = 7.9 Hz, 12H). ¹³C NMR (151 MHz, Chloroform-*d*) δ 167.87, 167.72, 145.91, 145.79, 143.36, 140.81, 140.54, 139.17, 139.08, 133.40, 133.08, 132.44, 131.99, 131.86, 131.35, 128.38, 128.02, 126.17, 125.75, 125.36, 72.30, 70.76, 70.47, 67.11, 61.16, 61.04, 13.68, 13.52, 7.13, 7.06, 6.50, 6.44. HRMS (TOF MS ES⁺) (*m/z*): [M]⁺ calcd for [C₁₀₈H₁₄₆O₁₄Si₆]Na, 1857.9226; found, 1857.9257.

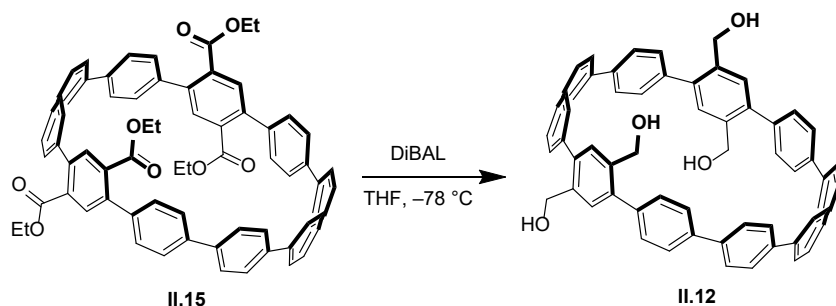


II.15. To a 50 mL flame-dried round bottom flask equipped with magnetic stir bar was added macrocycle **II.14** (0.480 g, 0.301 mmol, 1.00 equiv.) followed by five cycles of evacuation and refill with N₂. A septum was placed on the flask followed by the addition of THF (3 mL) and glacial acetic acid (0.86 mL, 15.034 mmol, 50.0 equiv.). Tetra-*n*-butylammonium fluoride (1 M in THF, 7.52 mL, 7.52 mmol, 25.0 equiv.) was added dropwise and the reaction was allowed to stir for 2 hours at room temperature. The reaction was quenched with water (10 mL), and the organic solvent was removed under reduced pressure. The resulting white precipitate was collected by vacuum filtration and rinsed with hexanes (5 mL) then transferred to a 100 mL flame-dried round bottom flask equipped with magnetic stir bar followed by five cycles of evacuation and refill with N₂. A septum was placed on the flask followed by the addition of THF (30 mL) then the dropwise addition of H₂SnCl₄ (0.040 M in THF, 24.80 mL, 0.992 mmol, 3.30 equiv.). The reaction was allowed to stir for 1 hour at room temperature, then quenched with saturated sodium bicarbonate (30 mL). Organic solvent removed under reduced pressure, then more water was added (50 mL) and extracted with DCM (3 x 50 mL). Combined organic layers washed with brine (50 mL) then dried over sodium sulfate, filtered, and concentrated to give a yellow solid. The crude material was run through a short alumina plug (100% DCM) providing **II.15** as a yellow solid (150.4 mg, 48%). ¹H NMR (600 MHz, Chloroform-*d*) δ 7.85 (s, 2H), 7.83 (s, 2H), 7.61 (d, *J* = 8.7 Hz, 4H), 7.61 (d, *J* = 8.7 Hz, 4H), 7.60 (s, 4H), 7.51 (s, 4H), 7.48 (d, *J* = 8.6 Hz, 4H), 7.43 (d, *J* = 8.6 Hz, 4H), 7.41 (d, *J* = 8.6 Hz, 4H), 7.33 (d, *J* = 8.7 Hz, 4H), 7.31 (d, *J* = 8.6 Hz, 4H), 4.23 (qd, *J* = 7.2, 1.2 Hz, 8H), 1.13 (t, *J* = 7.1 Hz, 12H). ¹³C NMR (151 MHz, Chloroform-*d*) δ 168.32, 139.97, 139.84, 139.66, 139.65, 139.37, 139.16, 138.50, 138.16, 138.12, 138.03, 133.28, 133.19, 132.62, 132.50, 129.29, 129.18, 128.10, 128.04, 127.56, 127.35, 61.74, 61.71, 13.99, 13.98, 6.95, 6.54 ppm. MS

(TOF MS ES⁺) (m/z): [M]⁺ calculated for C₇₀H₆₀O₈, 1048.3975; found, 1048.5.

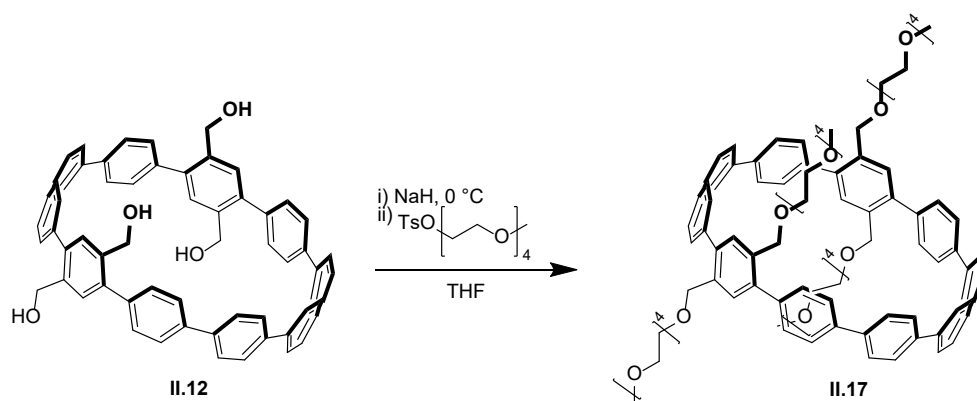


II.16. A 25 mL round bottom flask equipped with magnetic stir bar was charged with potassium hydroxide (0.120 g, 2.13 mmol, 40.0 equiv.) and H₂O (1.00 mL) and stirred until fully dissolved. Macrocycle **II.15** (0.055 g, 0.053 mmol, 1.0 equiv.), was dissolved in ethanol (5.3 mL) and tetrahydrofuran (5.3 mL) and transferred to the reaction flask. An air-cooled condenser was attached, and the reaction was heated to 45 °C with stirring. After 24 hours, the reaction was allowed to cool to room temperature and acidified with 1 M HCl (10 mL). The product was extracted with EtOAc (3 x 10 mL). The combined organic layers were washed with brine (15 mL), dried over sodium sulfate, filtered, and concentrated to yield an orange solid (44.3 mg, 91%). ¹H NMR (500 MHz, Acetone-*d*₆) δ 7.94 (s, 2H), 7.93 (s, 2H), 7.74 – 7.72 (m, 4H), 7.71 (s, 4H), 7.62 (s, 4H), 7.60 (d, *J* = 8.6 Hz, 4H), 7.56 (d, *J* = 3.0 Hz, 4H), 7.55 (d, *J* = 3.0 Hz, 4H), 7.51 (d, *J* = 4.0 Hz, 4H), 7.49 (d, *J* = 4.0 Hz, 4H), acid protons not seen. MS (TOF MS ES⁺) (m/z): [M]⁺ calculated for C₆₄H₄₀O₈, 934.2578; found, 934.5.

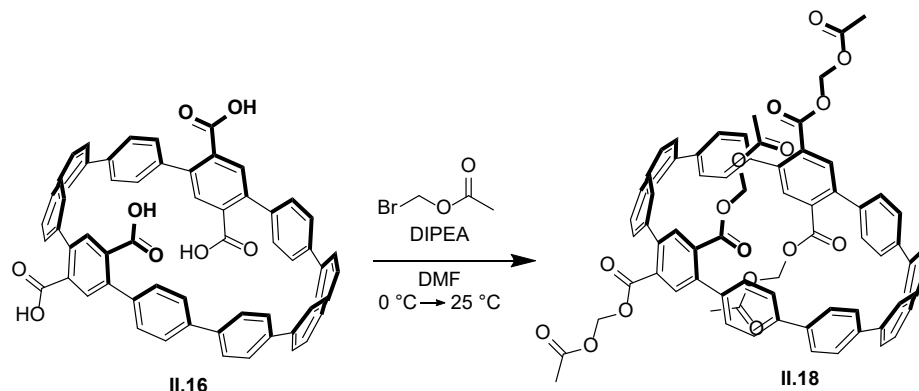


II.12. To a flame dried 5 mL round bottom flask equipped with magnetic stir bar was added **II.15** (0.029 g, 0.028 mmol, 1.00 equiv.) followed by five cycles of evacuation and refill with N₂. A septum was placed on the flask followed by the addition of THF (1.15 mL) and the solution was cooled to –78 °C with stirring. After the dropwise addition of *diisobutylaluminum* hydride (1 M in hexanes, 0.238 mL, 0.238 mmol, 8.5 equiv.) the solution was allowed to warm to room

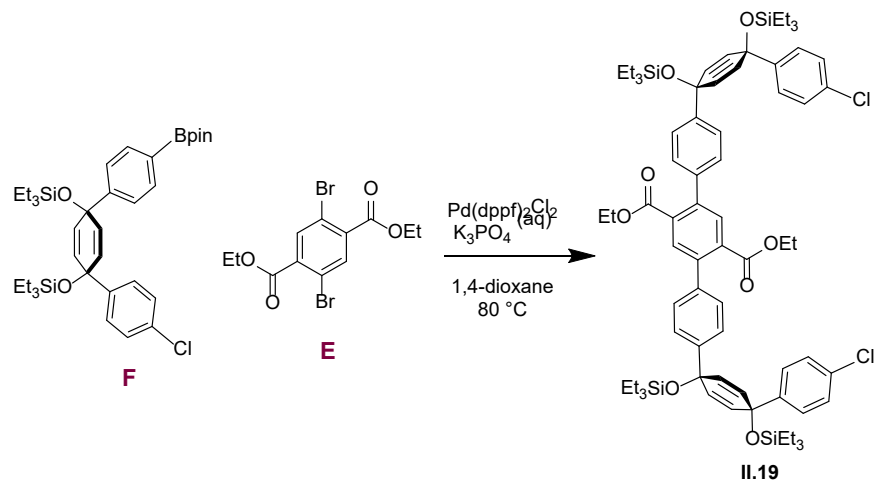
temperature. The reaction was allowed to stir at room temperature 1 hour before the addition of ethyl acetate followed by a saturated solution of Rochelle's salt. The reaction was allowed to stir one hour, then the product was extracted with ethyl acetate (3 x 5 mL). The combined organic layers were washed with brine, dried over sodium sulfate, filtered and concentrated to yield the product as a pale-yellow solid (24.1 mg, <99%). ¹H NMR (600 MHz, Chloroform-*d*) δ 7.71 (dd, *J* = 5.6, 3.4 Hz, 1H), 7.59 (d, *J* = 3.9 Hz, 7H), 7.56 (d, *J* = 2.4 Hz, 3H), 7.54 (d, *J* = 8.5 Hz, 5H), 7.44 – 7.40 (m, 2H), 7.39 (d, *J* = 2.0 Hz, 2H), 7.37 (d, *J* = 8.5 Hz, 3H), 7.34 (s, 1H), 7.31 (d, *J* = 8.2 Hz, 4H), 4.68 (d, *J* = 5.5 Hz, 2H), 4.61 (d, *J* = 5.5 Hz, 2H), 2.13 (s, 1H), 2.04 (s, 1H).



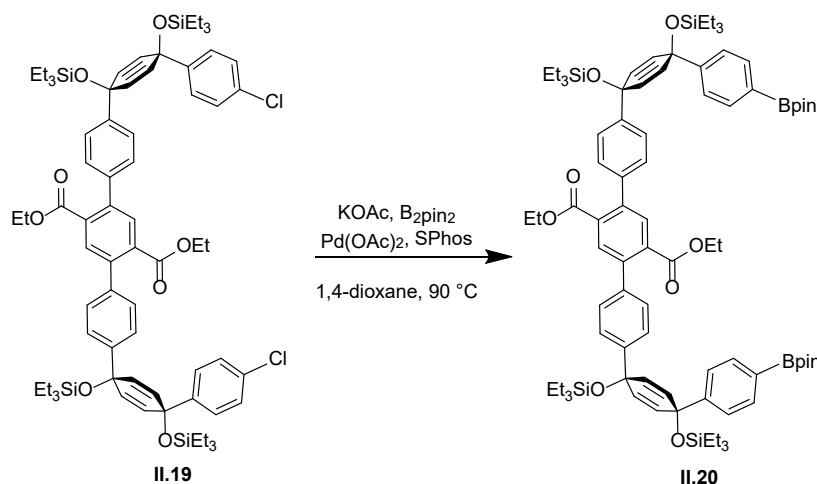
II.17. To a flame dried 10 mL round bottom flask equipped with magnetic stir bar was added **II.12** (0.005 g, 0.006 mmol, 1.00 equiv.) followed by five cycles of evacuation and refill with N₂. A septum was placed on the flask followed by the addition of THF (0.15 mL) and the solution was cooled to 0 °C with stirring. After 15 minutes, sodium hydride (0.001 mg, 0.006 mmol, 5 equiv.) was added in one shot and the resulting mixture was allowed to stir at 0 °C for 10 minutes before warming to room temperature. After 20 minutes at room temperature, tri(ethylene glycol) monomethyl ether tosylate (0.009 g, 0.0284 mmol, 5 equiv.) diluted in dry THF (0.2 mL) was added and the reaction was allowed to stir overnight. The reaction was quenched with water (1.0 mL), and the product was extracted with ethyl acetate (3 x 5 mL). The combined organic layers were washed with brine, dried over sodium sulfate, filtered, and concentrated to yield the product as a yellow oil (6.0 mg, 75%). ¹H NMR (500 MHz, Chloroform-*d*) δ 7.60 – 7.54 (m, 16H), 7.51 (m, 8H), 7.42 (d, *J* = 8.5 Hz, 4H), 7.40 (d, *J* = 8.5 Hz, 4H), 7.34 (s, 2H), 7.31 (s, 2H), 4.44 (s, 4H), 4.37 (s, 4H), 3.69 – 3.55 (m, 40H), 3.48 (q, *J* = 4.7 Hz, 4H), 3.38 (s, 4H), 3.31 (s, 6H), 3.31 (s, 6H).



11.18. A 10 mL round bottom flask equipped with magnetic stir bar was charged with **II.16** (0.044 g, 0.048 mmol, 1.00 equiv) and DMF (1.20 mL) and mixture cooled to 0 °C. Once cooled, DIPEA (0.135 mL, 0.77 mmol, 16.0 equiv) was added via syringe followed by bromomethyl acetate (0.47 mL, 0.48 mmol, 10 equiv) and reaction was allowed to come to room temperature over 12 hours. The resulting yellow solution was quenched with a saturated aqueous sodium bicarbonate solution. The product was extracted with EtOAc (3 x 10 mL). The combined organic layers were washed with sodium hydroxide (1 M, 10 mL) followed by brine (15 mL), dried over sodium sulfate, filtered, and concentrate. The resulting yellow solid was then purified via size exclusion chromatography to give the product as a light, yellow solid (8.1 mg, 17%). ¹H NMR (600 MHz, Chloroform-*d*) δ 7.95 (s, 2H), 7.93 (s, 2H), 7.62 (d, $J = 9.1$ Hz, 4H), 7.61 (d, $J = 1.0$ Hz, 4H), 7.49 (s, 4H), 7.45 (d, $J = 8.6$ Hz, 4H), 7.40 (d, $J = 8.7$ Hz, 4H), 7.38 (d, $J = 8.6$ Hz, 4H), 7.31 (d, $J = 8.6$ Hz, 4H), 7.29 (d, $J = 8.6$ Hz, 4H), 5.86 (s, 2H), 5.85 (s, 2H), 2.00 (s, 3H), 2.00 (s, 3H).

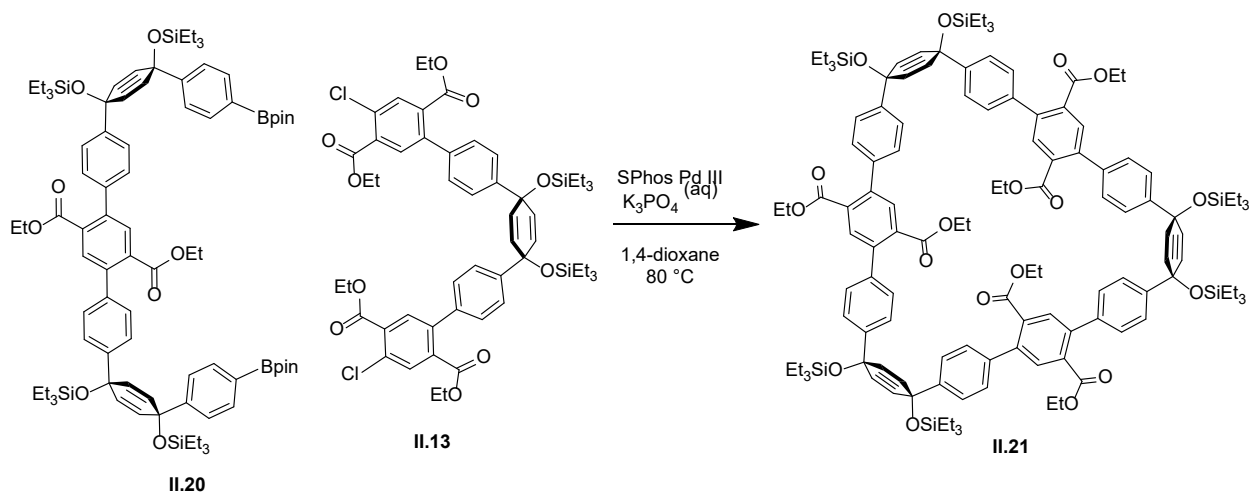


II.19. To a 50 mL flame-dried round bottom flask equipped with a magnetic stir bar was added **E** (0.175 g, 0.459 mmol, 1.00 equiv.), **F** (0.600 g, 0.918 mmol, 2.00 equiv.) and Pd(dppf)Cl₂ (0.038 g, 0.032 mmol, 0.100 equiv.) followed by five cycles of evacuation and refill with N₂. A septum was placed on the flask followed by the addition of 1,4-dioxane (2.30 mL). The reaction was heated to 80 °C with stirring for 10 minutes followed by the addition of 2 M K₃PO₄ (0.23 mL) and stirred at temperature for 48 hours. The reaction was cooled to room temperature and passed through a plug of Celite with DCM. The filtrate was dried over sodium sulfate and concentrated to yield a pale, yellow oil. The crude oil was purified by automated flash chromatography (15-50% DCM/hexanes) to obtain the product as a white solid (0.380 g, 65%). ¹H NMR (600 MHz, methylene chloride-*d*₂) δ 7.76 (s, 2H), 7.38 (d, *J* = 8.3 Hz, 4H), 7.31 (d, *J* = 8.7 Hz, 4H), 7.28 (d, *J* = 8.4 Hz, 4H), 7.26 (d, *J* = 8.7 Hz, 4H), 6.08 (d, *J* = 10.2 Hz, 4H), 6.02 (d, *J* = 10.1 Hz, 4H), 4.11 (q, *J* = 7.1 Hz, 4H), 1.02 (t, *J* = 7.1 Hz, 6H), 0.96 (m, 36H), 0.64 (m, 24H) ppm. ¹³C NMR (151 MHz, Chloroform-*d*) δ 168.23, 145.44, 144.73, 140.68, 139.18, 133.72, 133.15, 131.90, 131.87, 131.38, 128.42, 128.39, 127.44, 125.81, 71.42, 71.28, 61.43, 13.77, 7.20, 7.18, 6.60, 6.56 ppm. HRMS (ASAP+) (m/z): [M+H]⁺ calcd for C₇₂H₉₇Cl₂O₈Si₄, 1271.5368; found, 1271.5590.



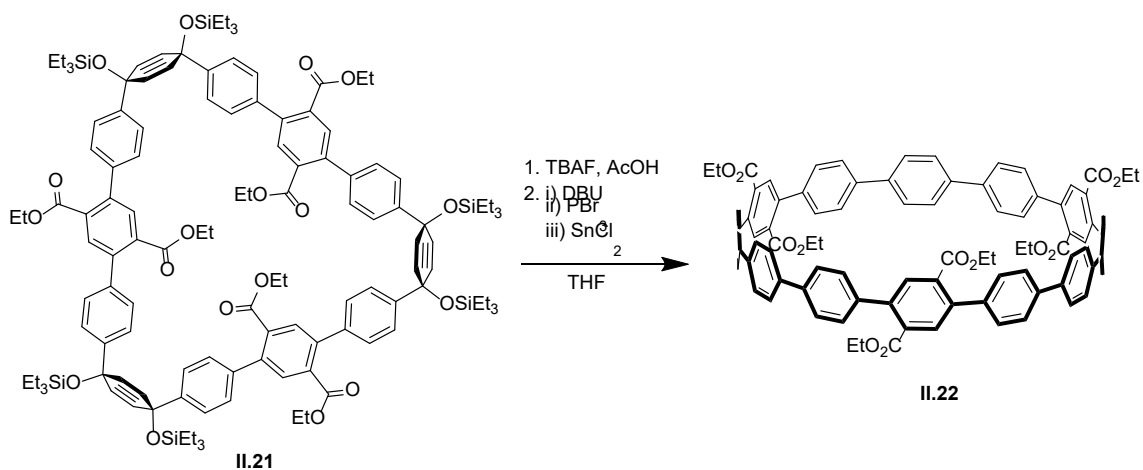
II.20. To a 25 mL flame-dried round bottom flask equipped with magnetic stir bar was added KOAc (0.278 g, 2.83 mmol, 6.60 equiv.) and flask flame-dried again. Once cooled, flask charged with **II.19** (0.545 g, 0.429 mmol, 1.00 equiv.), B₂pin₂ (0.436 g, 1.72 mol, 4.00 equiv.), Pd(OAc)₂ (0.005 g, 0.021 mol, 0.05 equiv.), and SPhos (0.022 g, 0.054 mmol, 0.125 eq) followed by five cycles of evacuation and refill with N₂. A septum was placed on the flask followed by the addition of 1,4-dioxane (1.5 mL), and the reaction was heated to 90 °C with stirring for 2 hours. The mixture

was allowed to cool to room temperature and the solvent was removed under reduced pressure. The resulting crude oil was dissolved in DCM and passed through a pad of silica topped with a pad of Celite. The resulting solution was dried over sodium sulfate and concentrated to yield a gray solid. The solid was washed with minimal cold EtOH to obtain the product as a white solid (0.511 g, 82%). ^1H NMR (600 MHz, methylene chloride- d_2) δ 7.75 (s, 2H), 7.67 (d, $J = 8.3$ Hz, 4H), 7.39 (d, $J = 8.0$ Hz, 8H), 7.28 – 7.25 (m, 4H), 6.05 (s, 8H), 4.10 (q, $J = 7.1$ Hz, 4H), 1.31 (s, 24H), 1.01 (t, $J = 7.1$ Hz, 6H), 0.98 (t, $J = 7.9$ Hz, 18H), 0.94 (t, $J = 7.9$ Hz, 18H), 0.67 (q, $J = 7.9$ Hz, 12H), 0.61 (q, $J = 7.9$ Hz, 12H) ppm. ^{13}C NMR (151 MHz, Chloroform- d) δ 168.18, 149.13, 145.47, 140.60, 138.97, 134.71, 133.60, 131.70, 131.59, 131.37, 128.22, 125.66, 125.22, 83.75, 71.51, 71.40, 61.28, 24.89, 13.62, 7.10, 7.07, 6.47 ppm. HRMS (ASAP+) (m/z): $[\text{M}]^+$ calcd for $\text{C}_{84}\text{H}_{120}\text{B}_2\text{O}_{12}\text{Si}_4$, 1454.8043; found, 1454.7815.



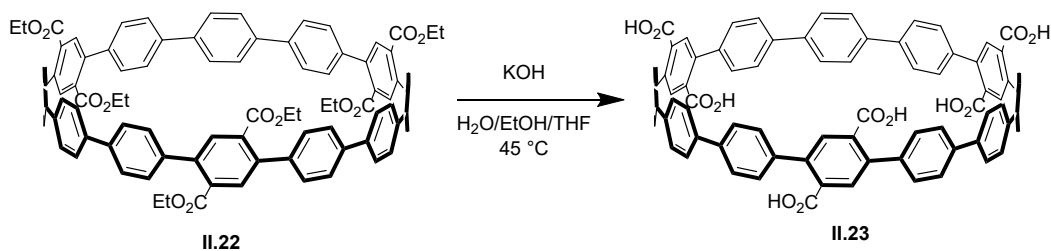
II.21. To a 100 mL flame-dried round bottom flask equipped with a magnetic stir bar was added **II.20** (0.296 g, 0.204 mmol, 1.20 equiv.), **II.13** (0.170 g, 0.170 mmol, 1.00 equiv.) and SPhos Pd III (0.020 g, 0.025 mmol, 0.150 equiv.) followed by five cycles of evacuation and refill with N_2 . A septum was placed on the flask followed by the addition of 1,4-dioxane (57 mL). The reaction was heated to 80 $^\circ\text{C}$ with stirring for 30 minutes followed by the addition of 2M K_3PO_4 (5.7 mL) and stirred at temperature for 2 hours. The reaction was cooled to room temperature and the solvent was removed under reduced pressure. The resulting crude oil was dissolved in DCM and passed through a plug of Celite. The solution was dried over sodium sulfate and concentrated to yield a yellow oil. The crude oil was purified by automated flash chromatography (10% EtOAc/hexanes) to obtain the product as a yellow solid (0.217 g, 60%). ^1H NMR (600 MHz, Chloroform- d) δ 7.76

(s, 6H), 7.41 (d, $J = 8.4$ Hz, 12H), 7.27 (d, $J = 8.3$ Hz, 12H), 6.04 (s, 12H), 4.06 (q, $J = 7.1$ Hz, 12H), 0.98 (t, $J = 7.9$ Hz, 54H), 0.95 (t, $J = 7.1$ Hz, 18H), 0.65 (q, $J = 8.0$ Hz, 36H) ppm. ^{13}C NMR (151 MHz, Chloroform- d) δ 168.13, 145.54, 140.56, 139.05, 133.57, 131.73, 131.52, 128.25, 125.64, 71.42, 61.24, 13.62, 7.10, 6.49 ppm. MS (ESI) (m/z): $[\text{M}]^+$ calculated for $\text{C}_{126}\text{H}_{163}\text{O}_{18}\text{Si}_6$, 2132.0450; found, 2132.1.



II.22. A scintillation vial equipped with magnetic stir bar was charged with macrocycle **II.21** (0.217 g, 0.102 mmol, 1.00 equiv.) followed by five cycles of evacuation and refill with N_2 . A septum was placed on the vial followed by the addition of THF (1.00 mL) and tetra-*n*-butylammonium fluoride (1 M in THF, 1.01 mL, 10.0 mmol, 10.0 equiv.) and the reaction was allowed to stir for 2 hours at room temperature. The reaction was quenched with water (10 mL), and the organic solvent was removed under reduced pressure. The product was extracted with EtOAc (3 x 10 mL). Combined organic layers washed with brine (15 mL), dried over sodium sulfate, filtered, and concentrated to yield a yellow solid (70 mg, 88%). The solid was transferred to a 10 mL flame-dried round bottom flask equipped with magnetic stir bar followed by five cycles of evacuation and refill with N_2 . After addition of THF (3.5 mL), DBU (0.121 mL, 0.813 mmol, 8 equiv.), PBr_3 (0.076 mL, 0.813 mmol, 8 equiv.), and SnCl_2 (0.154 g, 0.813 mmol, 8 equiv.) were added in rapid succession. The reaction was allowed to stir for 1 hour at room temperature, then DCM (5.0 mL) was added to the flask and the mixture was filtered through a plug of alumina, eluting with DCM. The filtrate was concentrated to give a yellow solid which was washed with hexanes to yield **II.22** as a yellow solid (57.8 mg, 42%). ^1H NMR (600 MHz, Chloroform- d) δ 7.85 (s, 6H), 7.57 (s, 12H), 7.53 – 7.49 (m, 12H), 7.39 – 7.36 (m, 12H), 4.21 (q, $J = 7.1$ Hz, 12H),

1.11 (t, $J = 7.1$ Hz, 18H) ppm. ^{13}C NMR (151 MHz, Chloroform- d) δ 168.35, 140.00, 139.92, 139.51, 138.48, 132.98, 132.96, 129.21, 128.99, 127.91, 127.78, 61.69, 13.96 ppm.



II.23. A 10 mL round bottom flask equipped with magnetic stir bar was charged with potassium hydroxide (0.045 g, 0.809 mmol, 40.0 eq) and water (0.36 mL) and stirred until fully dissolved. Macrocycle **II.22** (0.027 g, 0.020 mmol, 1.0 equiv.), was dissolved in ethanol (2.02 mL) and tetrahydrofuran (2.02 mL) and transferred to the reaction flask. An air-cooled condenser was attached, and the reaction was heated to 45 °C with stirring. After 18 hours, the reaction was allowed to cool to room temperature and acidified with 2 M HCl. The product was extracted with EtOAc (3 x 10 mL) and washed with brine (15 mL). The combined organic layers were dried over sodium sulfate and concentrated to yield a yellow solid (22.4 mg, 94%). ^1H NMR (500 MHz, Acetone- d_6) δ 7.95 (s, 6H), 7.68 (s, 12H), 7.63 (d, $J = 8.4$ Hz, 12H), 7.54 (d, $J = 8.5$ Hz, 12H).

4.4.3. Cell Imaging

HeLa cells were cultured in (DMEM) by Dr. Yu Zhao. Separate stock solutions of **II.15** (1:1 PBS:DMSO) and **II.16** (PBS buffer) were made at 10 mM concentration. The confluent cells were washed with PBS buffer then co-incubated with **II.15** (2 μL stock solution) and NucRed dye (2 drops) or **II.16** (2 μL stock solution) and NucRed dye for 30 minutes each. After incubation, the cells were again washed with PBS and finally bathed in 2 mL PBS for imaging. Cell imaging was performed on the cells using a Lecia DMI8 fluorescent microscope equipped with a Excelitas X-Cite 110LED light source. Cells were visible through the DIC channel, however no fluorescence was seen from the CPPs through the DAPI or DAPI-longpass channels, nor was the NucRed stain seen.

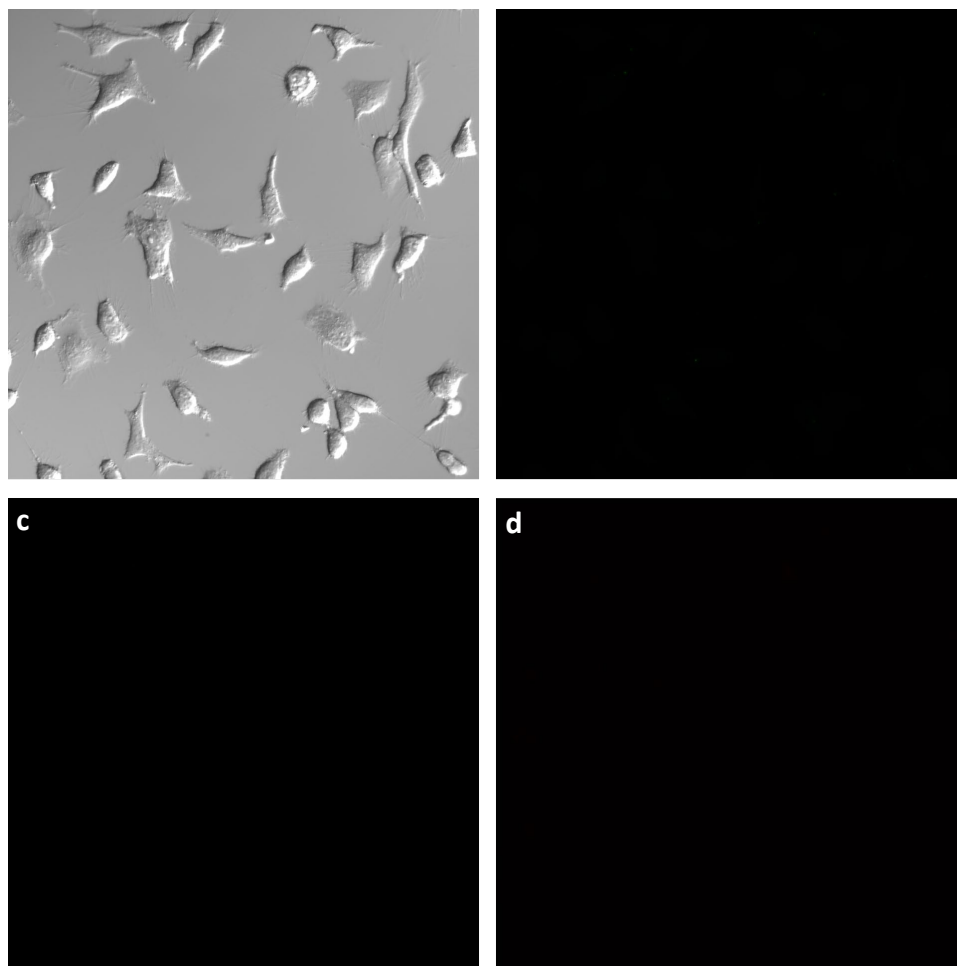


Figure 2.5. Live imaging of HeLa cells co-incubated with ester derivative **II.15** and NucRed; (a) DIC channel shows surviving cells, (b) DAPI, (c) DAPI-longpass and (d) Cy5 channel show no fluorescence from the NucRed or CPP dyes.

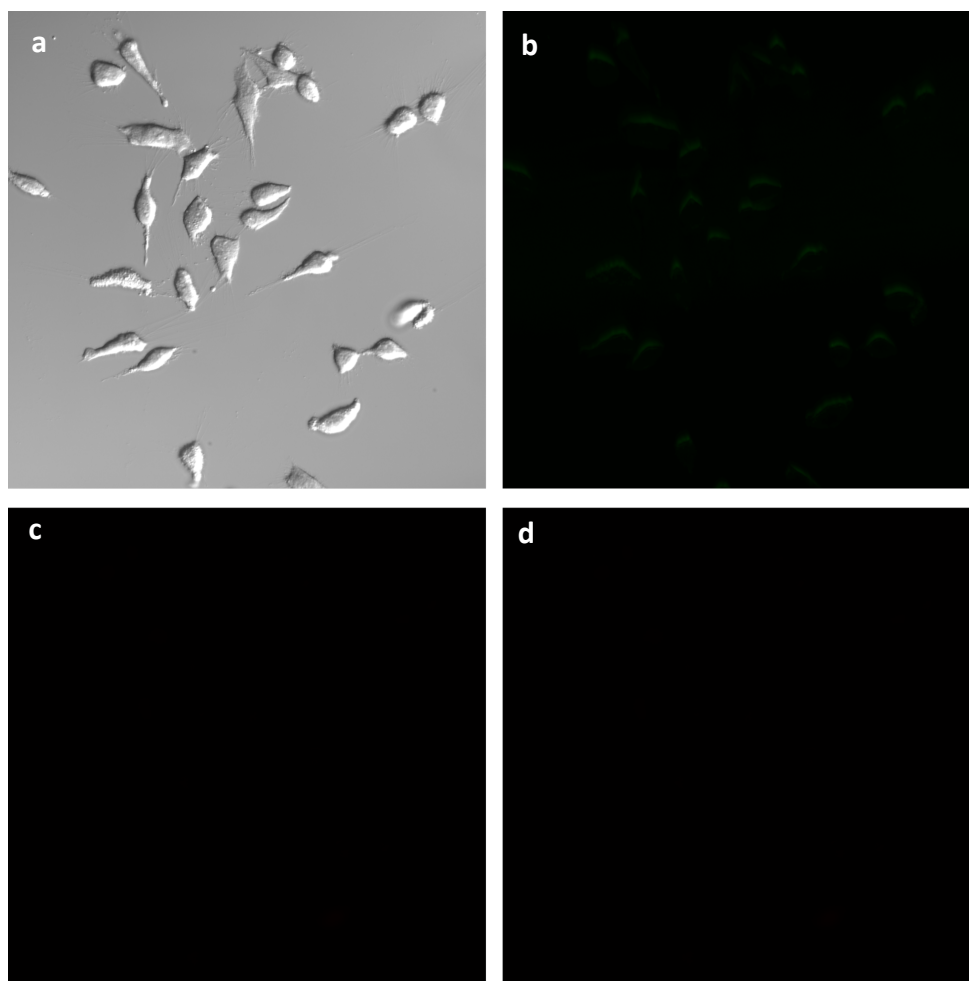


Figure 2.6. Live imaging of HeLa cells co-incubated with **II.16** and NucRed; (a) DIC channel shows surviving cells, (b) DAPI, (c) DAPI-longpass and (d) Cy5 channel show no fluorescence from the NucRed or CPP dyes. The dim fluorescence seen in the DAPI (b) channel shows some **II.16** clinging to the outside of cells was not completely removed even with washes.

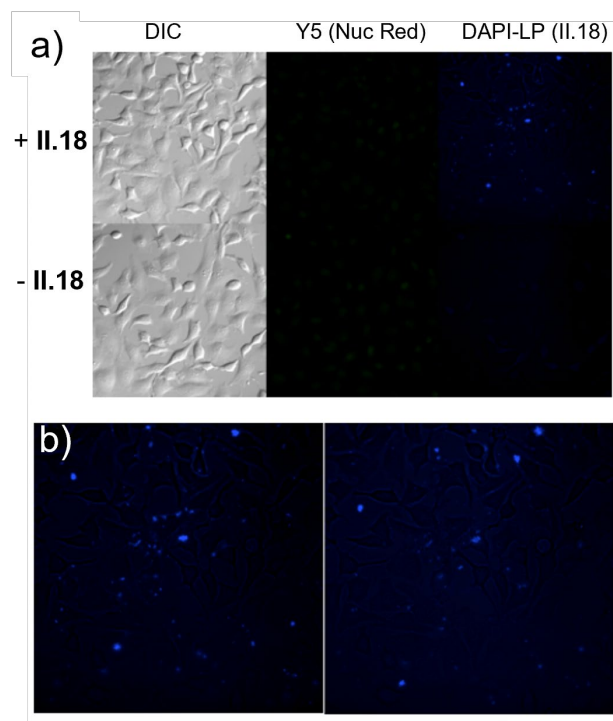


Figure 2.7. Live imaging of HeLa cells co-incubated with **II.18** and NucRed; (a) DIC channel Y5 and DAPI-long pass channels with (top) and without **II.18** (b) zoom in on DAPI-long pass channel showing non-cell permeable aggregates of **II.18**.

2.5. Bridge to Chapter III

This chapter described the development of modular synthetic methodology for the creation of water-soluble carbon nanohoop derivatives. To the best of our knowledge, this is the first example of fully water-soluble nanohoos, and the use of ester groups provides a robust functional handle for further derivatization towards a variety of applications. The next chapter discusses the supramolecular capabilities of these novel water-soluble nanohoop fluorophores, and the broad utility of the hydrophobic effect to drive complexation with a variety of guests.

CHAPTER III

EXPLORING THE SUPRAMOLECULAR CHEMISTRY OF WATER-SOLUBLE CARBON NANOHOOPS

This chapter includes unpublished co-authored material, it was written by myself, with editorial assistance from Professor Ramesh Jasti. Experimental work in this chapter was performed by myself with experimental guidance provided by Professor Ramesh Jasti.

[*n*]Cycloparaphenylenes, colloquially called carbon nanohoops, are small molecule analogues of carbon nanotubes (CNTs) with a vast range of interesting properties that make these compounds desirable for use in a variety of applications. In addition to being bright fluorophores that can be made cell-permeable, nanohoops also contain a shape-persistent pore making them interesting host compounds for use in supramolecular chemistry. However, most research on this supramolecular chemistry has been constrained to the interaction between [10]CPP with C₆₀ - due to the limited nature of the supramolecular interactions these cavitands are capable of (*i.e.* convex-concave π - π interactions) - and has only been studied in organic solvents or the solid state. We have recently developed a synthetic route to various carboxylate-functionalized nanohoops that are fully water-soluble while retaining their electronic properties. We hypothesized that these nanohoops may have enhanced host abilities compared to the parent molecules due to the hydrophobic effect that should drive guests inside the nanohoop interior. Herein we explore the supramolecular interactions of a new family of water-soluble carbon nanohoops with a variety of guest molecules including unfunctionalized nanohoops, fullerenes, CNTs, and other small molecule hydrocarbons.

3.1. Introduction

Carbon nanomaterials (CNMs) have a wealth of proposed applications spanning a variety of fields.¹⁻³ Recently, there has been substantial effort put forth towards utilizing CNMs in biomedical applications such as imaging, photo-based therapy methods and drug delivery.⁴⁻¹⁰ However, many of these proposed applications are still in relative infancy due in large part to challenges with producing biologically compatible and/or water-soluble analogues.¹¹⁻¹⁶ To overcome this issue, a

variety of methods have been explored to solubilize CNMs. For example, methods to solubilize fullerenes include: ultrasonication, which provides only metastable dispersions¹⁷⁻¹⁹ and direct functionalization, generally resulting in breaking conjugation and negatively influencing the properties of interest.²⁰⁻²² Finally, supramolecular approaches have also been explored whereby CNMs are solubilized via interaction with a host species.²³⁻²⁵ These supramolecular systems are especially promising as they require no functionalization of the pristine nanomaterial, however they currently rely heavily on popular supramolecular host macrocycles that have low affinity for CNMs like cyclodextrins and calixarenes. Complexation of C₆₀ with γ -cyclodextrin (**Figure 3.1b**), for example, is an energy intensive process that requires boiling an aqueous dispersion of C₆₀ with the host for 16-48 hours and the complex tends to precipitate out of solution once cooled.^{24,26-27}

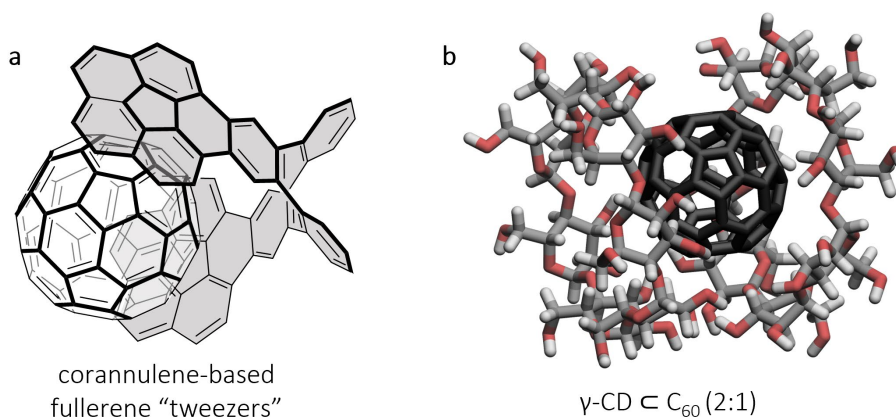


Figure 3.1. a) Molecular “tweezers” developed to host fullerenes through maximizing convex-concave π - π interactions³⁰; b) formation of a 2:1 complex of gamma-cyclodextrin (CD) with C₆₀ requires high temperature for extended time²⁴.

Another class of macrocyclic hosts, calixarenes, can also host C₆₀, however this interaction causes precipitate formation, and upon solvation results in dissolution of the complex, therefore generally limiting use to the solid-state.²⁸⁻²⁹ Alternatively, a variety of hosts specially designed for fullerene, commonly referred to as “fullerene-tweezers” are generally large π -extended organic molecules that make excellent hosts for fullerene in organic media but are insoluble in water (**Figure 3.1a**).³⁰ This solubility challenge is a particularly important hurdle to overcome, as the photophysical and photochemical properties of CNMs on which many of their potential applications rely are intrinsically linked to the nature of dispersion of the material.³¹

Due to the unique chemical make-up of CNMs like fullerenes and carbon nanotubes (CNTs), the nature of supramolecular interactions they are capable of are quite limited which explains why traditional host macrocycles are not ideal for use with CNMs. These carbon allotropes rely on Van der Waals interactions which are enhanced when the host molecule's cavity complements the concave host surface, and solvophobic interactions, whereby CNMs are attracted to π -rich interiors of a host molecule in order to limit poor interactions with bulk solvent.³² These criteria are well met by carbon nanohoops, or $[n]$ CPPs (where n denotes the number of phenylenes), the smallest radial fragment of armchair carbon nanotubes. In fact, for this relatively new class of macrocycles, C_{60} is one of few known guests, forming the shortest known "peapod" structure usually seen on complexation of fullerenes within a nanotube cavity.³²⁻³³ The shape-persistent pore of the rigid nanohoops complements the surface of C_{60} making convex-concave π - π interactions where the (as calculated) distance between host and guest (0.335 nm) aligns well with the Van der Waals distances observed for other materials with known convex-concave π - π interactions like multi-walled CNTs and the aforementioned CNT peapods.³⁴⁻³⁵ The first experimental observation of this host-guest system by Yamago et al. showed not only that C_{60} will selectively complex with $[10]$ CPP when mixed with $[8]$ - $[12]$ CPP, but also this complexation event leads to a quenching of the nanohoop's inherent fluorescence, from which an large association constant of $(2.79 \pm 0.03) \times 10^6 \text{ M}^{-1}$ was determined.³⁶

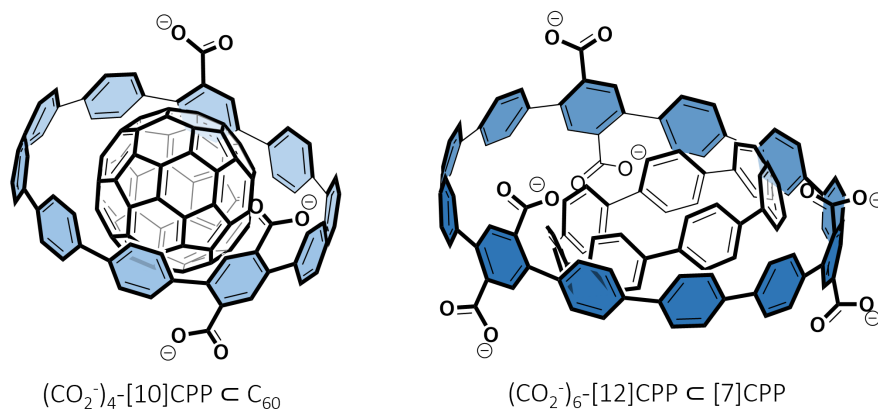


Figure 3.2. In this work the development of water-soluble nanohoops **III.2*** and **III.3*** can be used to host carbon nanomaterials, like C_{60} , and other nanohoops in water.

Since the first evidence of complexation this system has been quite extensively studied with a variety of $[10]$ CPP derivatives, the results of which have been recently reviewed.³⁷⁻³⁸ In addition

to this, researchers have also begun to study nanohoop supramolecular systems with guests with concave π -surfaces similar to C_{60} , namely smaller nanohoops (**Figure 3.2**). It has been predicted,³⁹⁻⁴¹ and more recently, experimentally observed that nanohoops can form complexes of the general formula $[n+5]CPP \subset [n]CPP$.⁴²⁻⁴⁴ These systems are interesting as potential dimeric chromophores, as well as double-walled CNT analogues, however their relatively weak associations (on the order of $10^{1-2} M^{-1}$) have made them a challenge to characterize and utilize for more advanced studies.⁴⁵ With our recently synthesized water-soluble nanohoops, we envisioned that we could utilize the hydrophobic effect to drive host-guest interactions with enhanced associations in aqueous media. Further, because the functionalization of nanohoops does not require breaking the π -conjugation (as is the case with fullerenes), the properties that make these materials so desirable can be retained in water and should also make excellent new water-soluble hosts for fullerenes and other CNMs towards realizing their long-predicted biological applications.

3.2. Results and Discussion

The ability of carbon nanohoops to play host to small molecules makes them quite unique amongst small molecule fluorophores, but current research on this family of hosts is limited to use

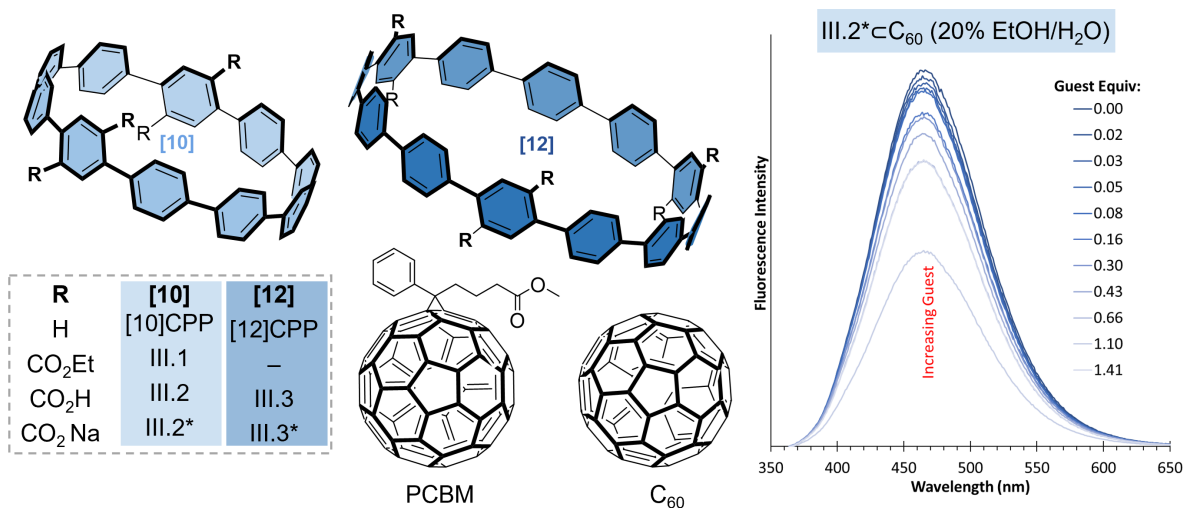


Figure 3.3. Left: Nanohoops hosts used in this study include [10]- and [12]CPP and functionalized derivatives **III.1**, **III.2(*)**, **III.3(*)** can be used to host fullerenes like C_{60} and PCBM. Right: fluorescence quenching of **III.2*** by C_{60} in 20% ethanol/water solution is used to obtain association constants K_a and K_{SV} .

in organic solvents. To determine whether our water-soluble nanohoops would bind C₆₀ in aqueous media as predicted, fluorescence titrations were attempted via the method published by Yamago et al. with which the original nanohoop peapod structure was studied, and has since been used by many others (**Figure 3.3**, right).³⁶ It should be noted that alternate titration methods were also considered or attempted but were insufficient; NMR analysis is not sensitive enough to analyze associations of magnitudes greater than 10⁶ M⁻¹, and ITC studies were prohibitive due to the partial precipitation of both C₆₀ and nanohoop-C₆₀ complexes resulting in irregular data over multiple trials. It is also of note that fluorescence titrations, while sensitive enough for this system, can produce convoluted results, as both dynamic and static quenching can decrease nanohoop fluorescence. Therefore, Stern-Volmer (SV) analyses were also carried out for each system as diagnostic tools to assess quenching modes – if the analysis yields a linear plot, this is suggestive of collisional and/or complexation-based quenching.

As an internal standard, initial titrations were carried out using [10]CPP and C₆₀ in toluene for which a binding constant of (5.44±0.19)×10⁶ M⁻¹ was calculated over three trials. Additionally, this experiment was repeated with phenyl-C₆₁-butyric acid methyl ester (PCBM, a more soluble C₆₀ derivative) as the guest molecule (**Figure 3.3**), to determine the relative binding ability of these

	Host	Host ID	Guest	Solvent	K _a (M ⁻¹)	K _{SV} (M ⁻¹)
1*	[10]CPP	–	C ₆₀	Toluene	2.79 (±0.03) × 10 ⁶	4.34 (±0.04) × 10 ⁶
2	[10]CPP	–	C ₆₀	Toluene	5.44 (±0.19) × 10 ⁶	4.47 (±0.02) × 10 ⁶
3	[10]CPP	–	PCBM	Toluene	8.82 (±0.04) × 10 ⁵	6.26 (±0.06) × 10 ⁵
4	[12]CPP	–	C ₆₀	Toluene	1.01 (±0.11) × 10 ⁶	1.70 (±0.06) × 10 ⁶
5	(CO ₂ ⁻) ₄ -[10]CPP	III.2*	C ₆₀	20% EtOH/H ₂ O	2.03 (±0.52) × 10 ⁶	4.70 (±0.46) × 10 ⁴
6	(CO ₂ ⁻) ₄ -[10]CPP	III.2*	PCBM	20% EtOH/H ₂ O	1.78 (±0.29) × 10 ⁷	2.39 (±0.13) × 10 ⁶
7	(CO ₂ ⁻) ₆ -[12]CPP	III.3*	C ₆₀	20% EtOH/H ₂ O	1.85 (±0.46) × 10 ⁶	2.93 (±0.51) × 10 ⁵
8	(CO ₂ ⁻) ₆ -[12]CPP	III.3*	PCBM	20% EtOH/H ₂ O	1.63 (±0.29) × 10 ⁷	7.50 (±0.99) × 10 ⁵
9	(CO ₂ ⁻) ₄ -[10]CPP	III.2*	PCBM	DMSO	1.82 (±0.25) × 10 ⁶	6.70 (±0.27) × 10 ⁶
10	(CO ₂ Et) ₄ -[10]CPP	III.1	PCBM	DMSO	2.19 (±0.34) × 10 ⁴	3.11 (±0.06) × 10 ⁴
11	(CO ₂ ⁻) ₆ -[12]CPP	III.3*	PCBM	Water	1.53 (±0.24) × 10 ⁶	8.89 (±1.89) × 10 ³

Table 3.1. Comparison of fullerene guests binding (K_a and Stern-Volmer constant (K_{SV})) with water soluble nanohoops; *previously published data³⁶ measured via the same titration method used herein.

guests. Due to the functionalization present on the surface of PCBM (as compared to C₆₀) the association ability of this molecule was expected to be lower, and the data agrees well with this assumption as the binding constant drops by nearly an order of magnitude under the same experimental conditions ($K_a = (8.82 \pm 0.04) \times 10^5 \text{ M}^{-1}$). In order to carry out titrations in aqueous media, solubility of both the host and guest must be achieved at the concentration regime of the experiment, which meant the use of co-solvents to work with fullerenes; the results are summarized in **Table 3.1** above.

In general, titrations not performed in toluene (**Table 3.1**, entries 5 and 7) were plagued by larger error when using C₆₀ as the guest molecule, which is likely due to poor solubility of the complexes especially at higher concentrations. PCBM, however, with its enhanced solubility over C₆₀, in general resulted in more reliable titration data (**Table 3.1**, entries 6 and 8-11). Overall, it can be seen that the association constant of these molecules when in aqueous media increases by roughly one order-of-magnitude (i.e. **Table 3.1**, entry 3 vs entries 6 and 9). One hypothesis as to why binding does not increase more substantially in water is that the carboxylate functionalized phenylenes are rotated out of the plane of the macrocycle leading to higher torsional angles between adjacent phenylenes. It has been noted that increased torsional angles in nanohoops, generally caused by substitution of a pendant proton with more sterically demanding functional group, are correlated with reduced binding affinity for C₆₀.⁴² We next repeated these experiments with the larger, more functionalized carboxylate-[12]CPP **III.3***, expecting that the larger pore of this hoop may lead to less hinderance, and potentially improve the solubility of the complex once formed. Gratifyingly, we found this to be the case, as association increased more substantially when compared to the parent [12]CPP with either guest in toluene (**Table 3.1**, entry 4 versus entries 7, 8 and 11) and relative errors simultaneously decreased.

To establish the broad utility of the hydrophobic effect as a means of driving host-guest interactions with nanohoops in water, we next turned our attention to the creation of nanohoop ring-in-ring complexes. As discussed above, while these types of complexes have been studied via theoretical models, there is far less evidence for their formation experimentally, likely in large part due to their decreased association affinity (on the order of 10¹⁻²) as reported by Yamago et al.⁴² While initial NMR experiments led to inconclusive results – this is likely due to the asymmetry of the functionalized host giving rise to a more complex proton NMR than the unfunctionalized parent CPP, making the very minor (0.02 ppm) chemical shifts noted previously difficult to

monitor – we found that fluorescence titrations once again led to characteristic fluorescence quenching as a function of guest concentration. As an initial test, we once again started with titrations in toluene using the parent [10]- and [12]CPP hosts. We were surprised to find the fluorescence quenching suggested far higher association than previously reported (**Table 3.2**, entries 12-14) based on NMR chemical shifts.

	Host	Host ID	Guest	Solvent	K_a (M^{-1})	K_{SV} (M^{-1})
12	[10]CPP	–	[5]CPP	Toluene	$6.91 (\pm 1.54) \times 10^5$	$1.06 (\pm 0.04) \times 10^5$
13	[10]CPP	–	[7]CPP	Toluene	$1.54 (\pm 0.06) \times 10^6$	$3.91 (\pm 0.25) \times 10^6$
14	[12]CPP	–	[7]CPP	Toluene	$6.67 (\pm 0.21) \times 10^6$	$6.61 (\pm 0.35) \times 10^6$
15	$(CO_2^-)_4$ -[10]CPP	III.2*	[5]CPP	H ₂ O	$3.20 (\pm 1.01) \times 10^5$	$6.25 (\pm 0.33) \times 10^5$
16	$(CO_2^-)_4$ -[10]CPP	III.2*	[7]CPP	H ₂ O	$1.64 (\pm 0.43) \times 10^6$	$2.99 (\pm 0.18) \times 10^5$
17	$(CO_2^-)_4$ -[10]CPP	III.2*	[8]CPP	H ₂ O	$2.59 (\pm 1.10) \times 10^6$	$6.39 (\pm 0.56) \times 10^5$
18	$(CO_2^-)_4$ -[10]CPP	III.2*	[9]CPP	H ₂ O	N/A	N/A
19	$(CO_2^-)_6$ -[12]CPP	III.3*	[6]CPP	H ₂ O	$7.74 (\pm 1.28) \times 10^6$	$1.28 (\pm 0.04) \times 10^6$
20	$(CO_2^-)_6$ -[12]CPP	III.3*	Aza-[6]CPP	H ₂ O	$5.60 (\pm 1.56) \times 10^6$	$6.45 (\pm 1.37) \times 10^5$
21	$(CO_2^-)_6$ -[12]CPP	III.3*	[7]CPP	H ₂ O	$9.83 (\pm 1.27) \times 10^5$	$1.86 (\pm 0.40) \times 10^4$
22	$(CO_2^-)_6$ -[12]CPP	III.3*	[9]CPP	H ₂ O	$3.55 (\pm 0.95) \times 10^6$	$2.38 (\pm 0.63) \times 10^4$

Table 3.2. Comparison of nanohoop guests binding (K_a and K_{SV}) with 10- and 12[CPP] hosts.

Excitingly, the smaller nanohoop guests were more readily solubilized in water than fullerenes, and therefore all ring-in-ring complexes created with the water-soluble hosts, **III.2*** and **III.3***, were carried out in water without the use of co-solvents. Interestingly we were able to measure substantial ($10^{5-6} M^{-1}$) association constants for **III.2*** with [5]-[8]CPP (**Table 3.2**, entries 15-18) despite calculations predicting the ideal guest size for [n]CPP being [n-5]CPP (e.g. [10]CPP \subset [5]CPP) based on van der Waals interactions. This suggests that alternate orientations of the guest nanohoos are likely possible to accommodate the larger guests. However, there still seems to be a limit to the size of guest nanohoop allowed, as [9]CPP was not solubilized by **III.2*** leading to unfittable titration data (**Figure 3.20**) although it was adequately solubilized by the larger **III.3*** (**Table 3.2**, entry 22).

Due to our success with fullerenes and nanohoos, we next hypothesized that we might be able to extend this work to carbon nanotubes. There is experimental evidence that

cycloparaphnyleneacetylenes (CPPAs, π -rich macrocycles made up of alternating phenylene and acetylene moieties) are capable of complexing nanotubes, and theory predicting that CPPs should do as well.⁴⁶⁻⁴⁷ While the results are less quantitative, as the length of the nanotubes is unknown due to the limitations in CNT synthetic methodology, making the concentration of guest unknown, we do still see the quenching of nanohoop fluorescence upon addition of chiral[5,6]CNT in water (**Figure 3.24**), however there is also a clear increase in the absorbance baseline suggesting aggregation of these species in solution rather than dissolution of the CNT. Although further work is needed this is a promising first step to complexation of nanohoops with CNTs in aqueous media.

3.3. Conclusions

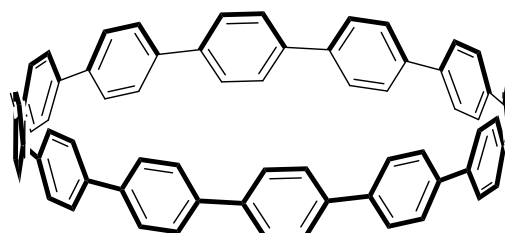
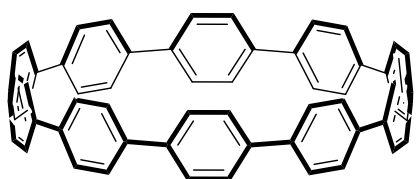
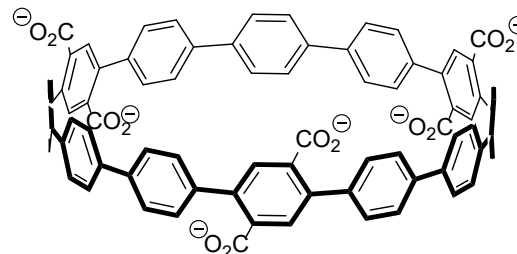
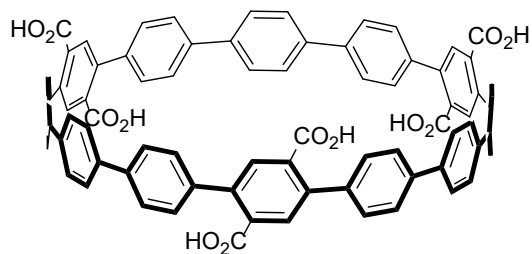
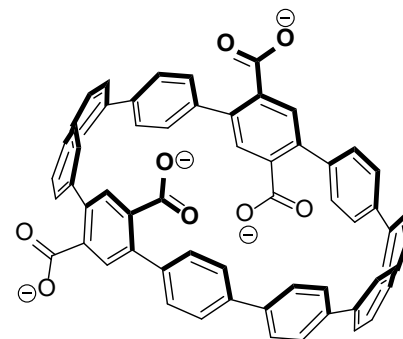
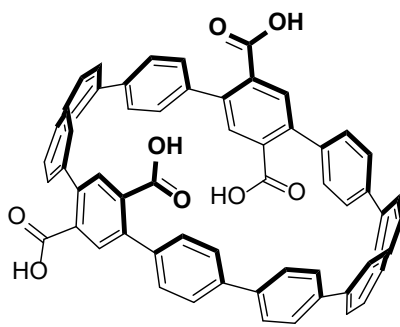
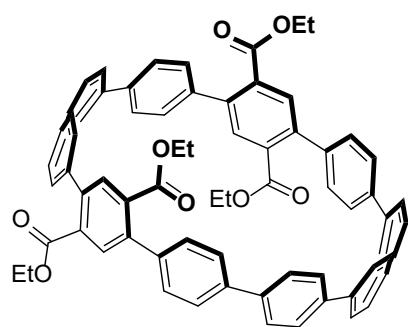
The development of water-soluble carboxylate-functionalized nanohoops has allowed for exploration of a supramolecular interaction new to nanohoops: the hydrophobic effect. Excitingly, this hydrophobic driving force seems to be a broadly applicable strategy for creation of nanohoop host-guest complexes. Importantly for nanohoop-supramolecular complexes outside of those with fullerenes, exploitation of the hydrophobic effect has a large impact on the association affinity of these complexes with K_{as} for ring-in-ring structures increasing by more than 4 orders of magnitude. In addition, studying these complexes in water offers an opportunity to learn more about the nature of π - π interactions in aqueous media which could have broader utility in the world of supramolecular chemistry. Based off the successes discussed herein, in the future we hope to explore more host-guest interactions of nanohoops in water, including the use of functionalized nanohoop guests like fluorinated- and methylated-aza[n]CPPs. Additionally, very recent work from the Bruns group has shown that small molecule polycyclic aromatic hydrocarbons can also interact with nanohoop hosts via CH- π interactions.⁴⁸ Based on this work, guests like corannulene and coronene should fit well with the water-soluble hosts discussed herein and provide further evidence of broad applicability of the hydrophobic effect for driving host-guest complexation of nanohoops.

3.4. Experimental Sections

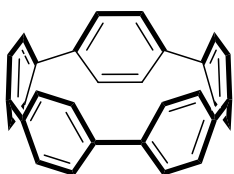
3.4.1. General Experimental Details

Compounds **III.1-III.3** (below) were prepared as described in chapter **II**, unfunctionalized hosts ([10] and [12]CPP) were prepared according to literature procedure.⁴⁹⁻⁵⁰ Guest compounds [5]-, [6]-, [7]-, [8]-, [9]-, and aza-[6]CPP were made according to literature procedure.⁴⁹⁻⁵³ Other guest compounds: fullerene, PCBM, and [5,6]CNT were all obtained commercially. Absorbance and fluorescence spectra were obtained in a 1 cm Quartz cuvette with toluene or deionized water (H₂O), dimethyl sulfoxide (DMSO), ethanol (EtOH) or mixtures of these solvents (i.e. 20% EtOH/H₂O) using an Agilent Cary 100 UV-Vis spectrometer Horiba Jobin Yvon Fluoromax-4 Fluorimeter, respectively. Excitation wavelength 340 nm was used for all fluorescence spectra with an entrance slit width of 2 nm, and spectra were collected from 350-650 or 700 nm at 1 nm increments with an exit slit width of 1 nm. All titrations were carried out in triplicate at 25 °C.

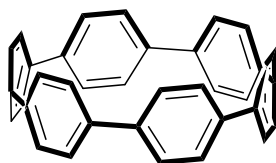
Host Compounds:



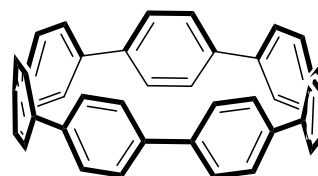
Guest Compounds:



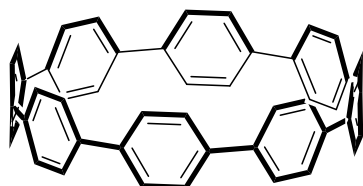
[5]CPP



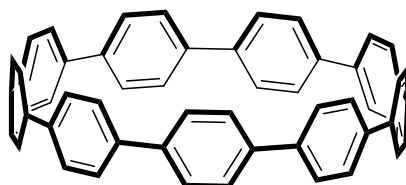
[6]CPP



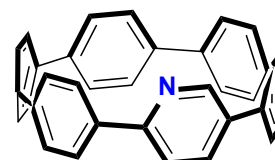
[7]CPP



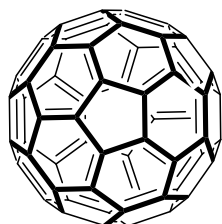
[8]CPP



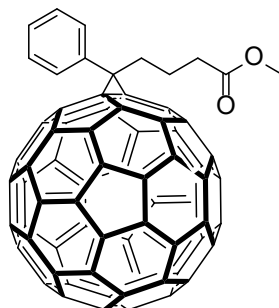
[9]CPP



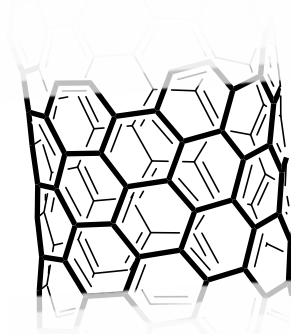
aza-[6]CPP



C₆₀



PCBM



[6,5]CNT

3.4.2. Photophysical Studies

3.4.2.1. General Procedure

All titrations were carried out with constant host concentration; all guest solutions were made from the corresponding host solution for a given experiment. Nonlinear regression analysis was performed to fit Equation III.1 by using the nonlinear-fitting function of OriginPro 2021 to obtain association constants for each system.

$$\frac{F}{F_0} = \frac{(1+AK_a[G])}{1+K_a[G]} \quad (\text{Equation III.1})$$

Where F and F₀ are fluorescence intensity, and fluorescence of CPP before addition of guest respectively; A is representative of proportionality constants of the complex and the host; K_a is the association constant and [G] is the concentration of guest.

Stern-Volmer analysis was also carried out via nonlinear regression analysis to fit Equation III.2 using the linear-fitting function of OriginPro 2021 for each system.

$$\frac{F_0}{F} = 1 + K_{SV}[G] \quad (\text{Equation III.1})$$

Where F and F₀ are fluorescence intensity, and fluorescence of CPP before addition of guest respectively; K_{SV} is the Stern-Volmer constant and [G] is the concentration of guest.

3.4.2.2. Unfunctionalized CPPs with Fullerene Guests

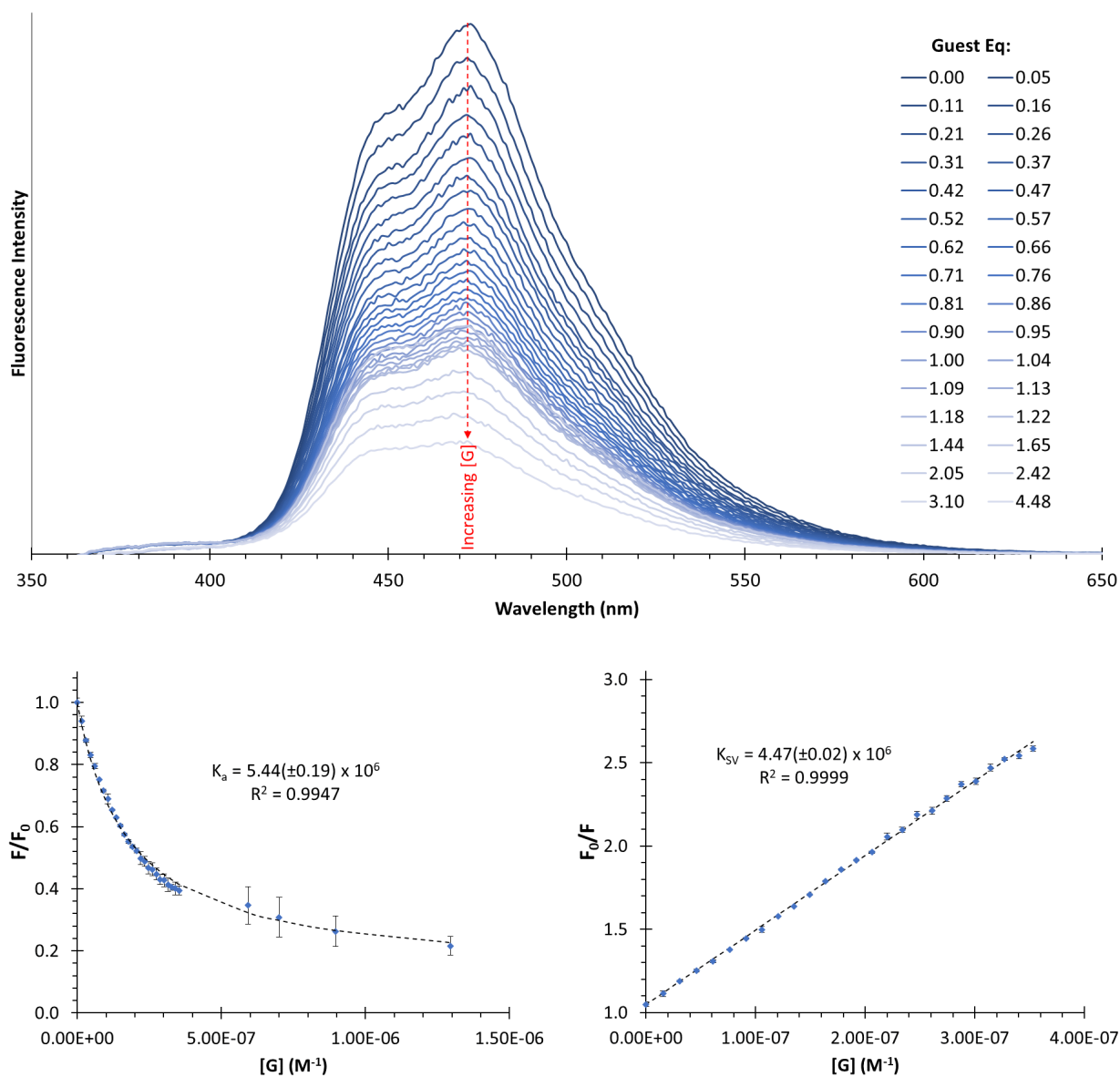


Figure 3.4. Top: fluorescence titration of C_{60} ($[G] = 3.89 \times 10^{-6} M$) into $[10]CPP$ in toluene ($[H] = 2.89 \times 10^{-7} M$); the changes in fluorescence intensity of $[10]CPP$ at 470 nm were measured. Bottom: correlations of the fluorescence intensity of $[10]CPP$ in toluene as a function of guest concentration to obtain (left) $K_a = (5.44 \pm 0.19) \times 10^6 M^{-1}$ and (right) $K_{sv} = (4.47 \pm 0.02) \times 10^6 M^{-1}$ for the system.

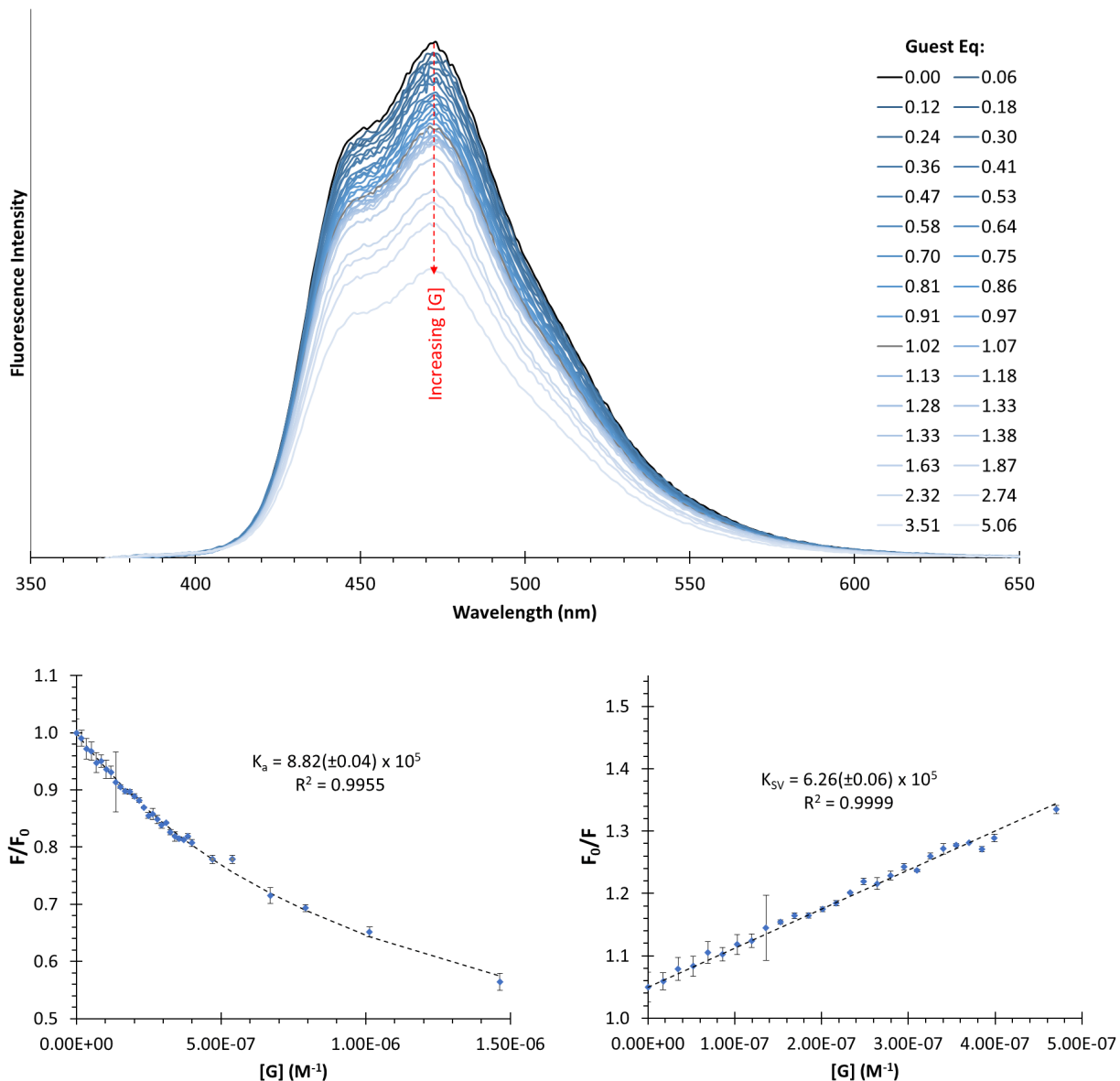


Figure 3.5. Top: fluorescence titration of PCBM ($[G] = 4.39 \times 10^{-6}$ M) into [10]CPP in toluene ($[H] = 2.89 \times 10^{-7}$ M); the changes in fluorescence intensity of [10]CPP at 470 nm were measured. Bottom: correlations of the fluorescence intensity of [10]CPP in toluene as a function of guest concentration to obtain (left) $K_a = (8.82 \pm 0.04) \times 10^5$ M^{-1} and (right) $K_{SV} = (6.26 \pm 0.06) \times 10^5$ M^{-1} for the system.

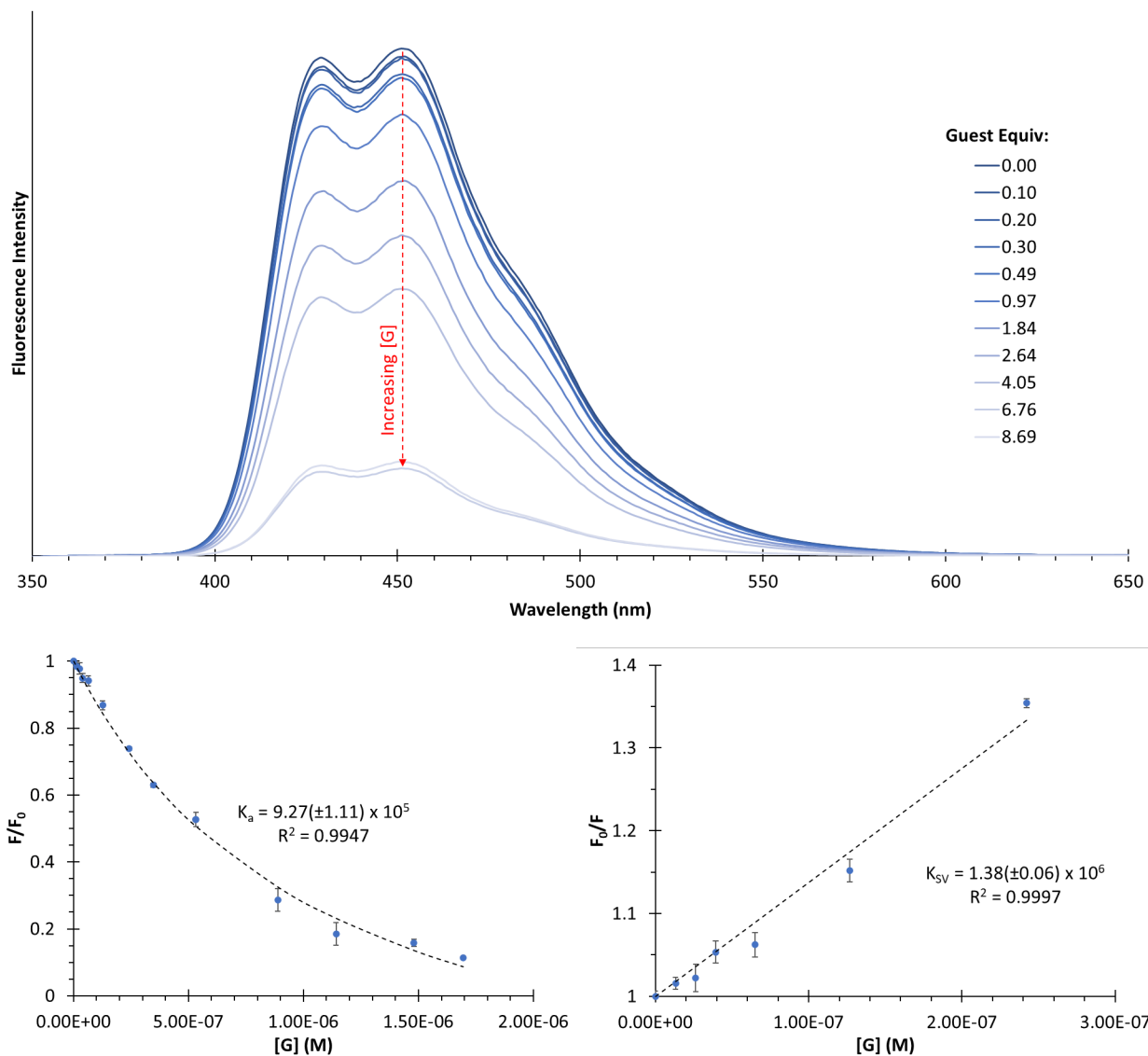


Figure 3.6. Top: fluorescence titration of C_{60} ($[G] = 6.66 \times 10^{-5}$ M) into $[12]CPP$ in toluene ($[H] = 3.29 \times 10^{-6}$ M); the changes in fluorescence intensity of $[12]CPP$ at 450 nm were measured. Bottom: correlations of the fluorescence intensity of $[12]CPP$ in toluene as a function of guest concentration to obtain (left) $K_a = (9.27 \pm 1.11) \times 10^5$ M $^{-1}$ and (right) $K_{SV} = (1.38 \pm 0.06) \times 10^6$ M $^{-1}$ for the system.

3.4.2.3. Functionalized [10]CPP Host Derivatives with Fullerene Guests

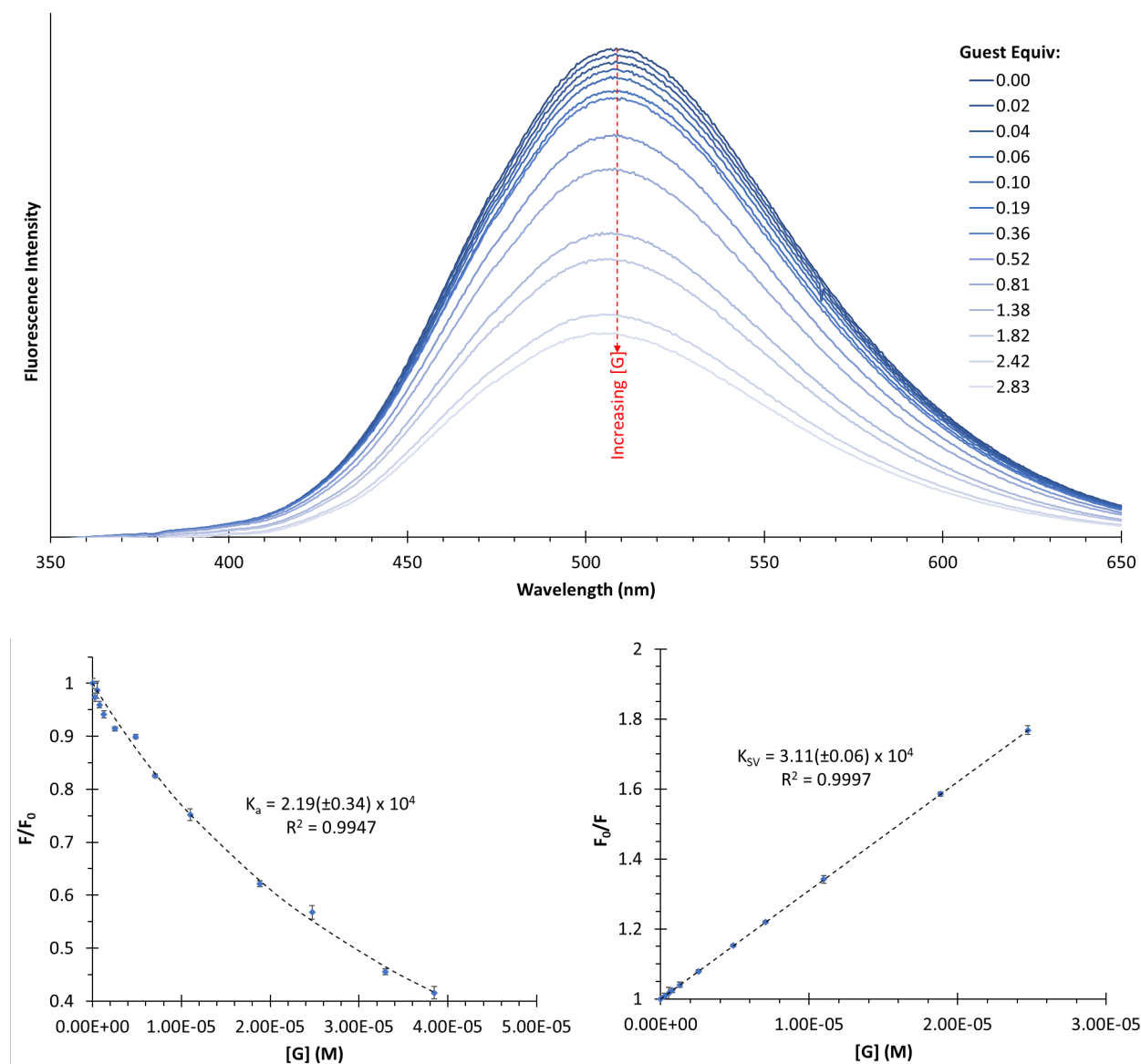


Figure 3.7. Top: fluorescence titration of PCBM ($[G] = 6.59 \times 10^{-5}$ M) into $(\text{CO}_2\text{Et})_4$ -[10]CPP (**III.1**) in DMSO ($[H] = 1.36 \times 10^{-5}$ M); the changes in fluorescence intensity of **III.1** at 509 nm were measured. Bottom: correlations of the fluorescence intensity of **III.1** in DMSO as a function of guest concentration to obtain (left) $K_a = (2.19 \pm 0.34) \times 10^4 \text{ M}^{-1}$ and (right) $K_{sv} = (3.11 \pm 0.06) \times 10^4 \text{ M}^{-1}$ for the system.

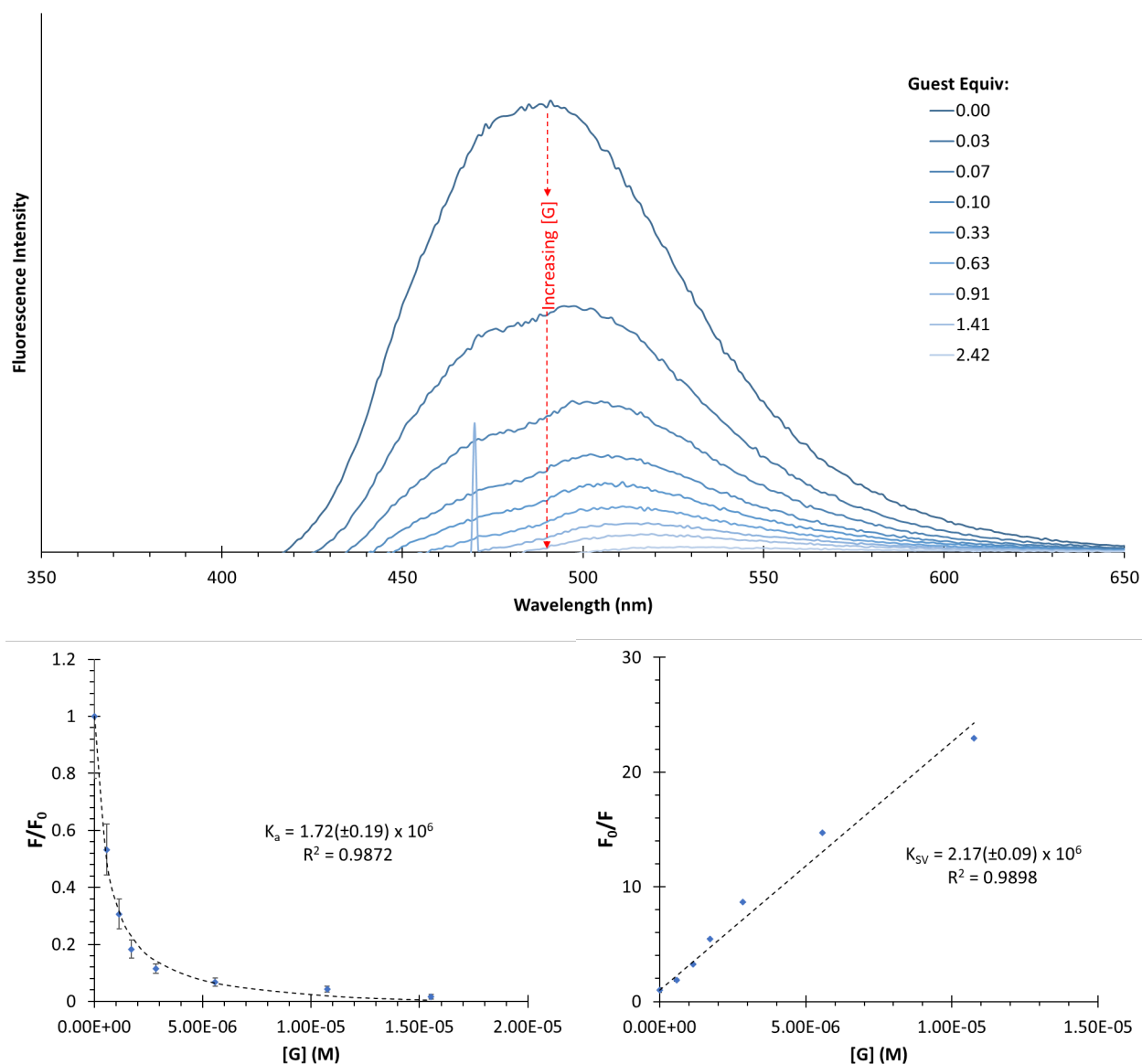


Figure 3.8. Top: fluorescence titration of PCBM ($[G] = 1.45 \times 10^{-4}$ M) into $(\text{CO}_2^-)_4$ -[10]CPP (**III.2***) in DMSO ($[H] = 1.71 \times 10^{-5}$ M); the changes in fluorescence intensity of **III.2*** at 490 nm were measured. Bottom: correlations of the fluorescence intensity of **III.2*** in DMSO as a function of guest concentration to obtain (left) $K_a = (1.72 \pm 0.19) \times 10^6 \text{ M}^{-1}$ and (right) $K_{sv} = (2.17 \pm 0.09) \times 10^6 \text{ M}^{-1}$ for the system.

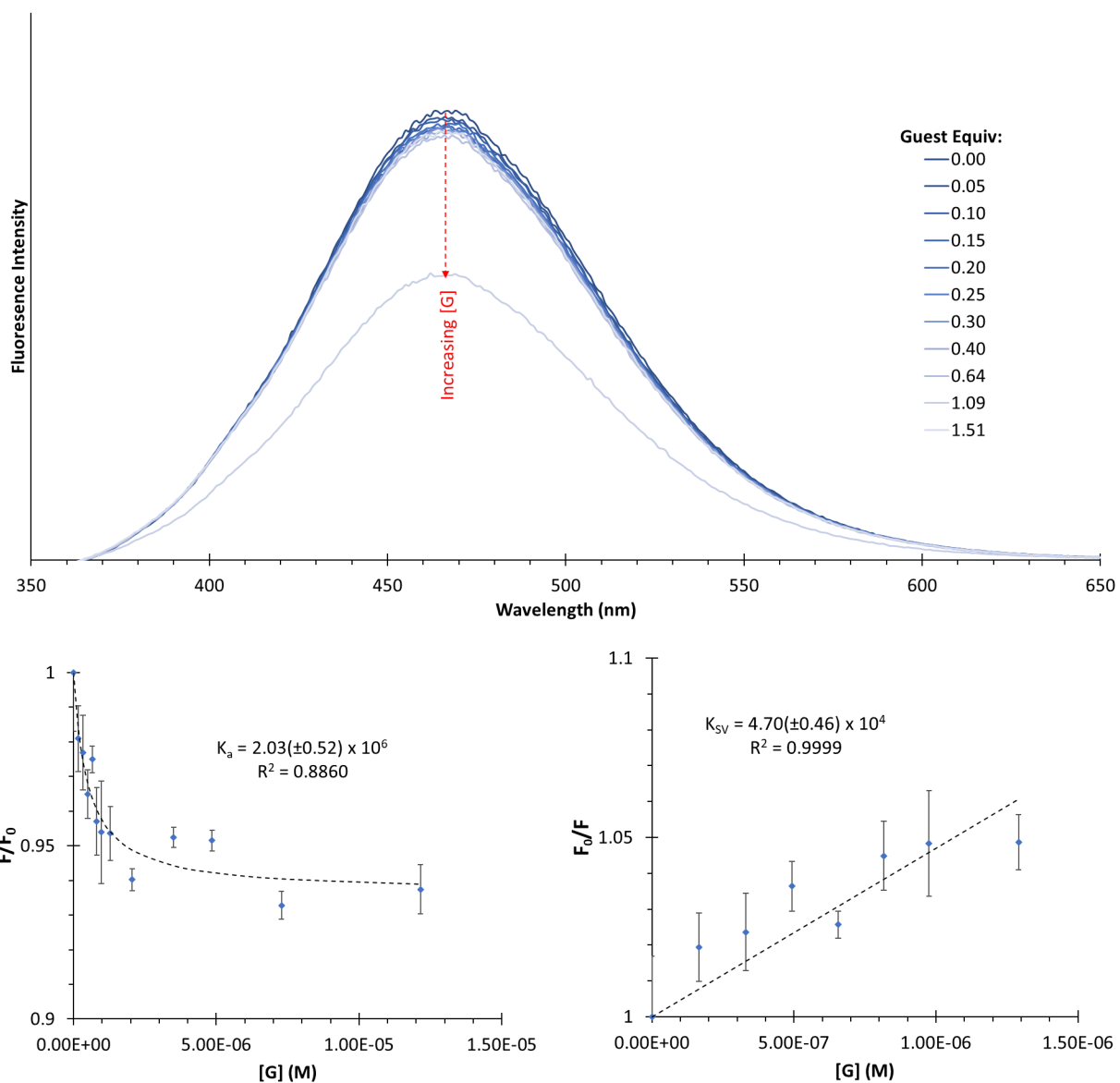


Figure 3.9. Top: fluorescence titration of C_{60} ($[G] = 4.16 \times 10^{-5}$ M) into $(CO_2^-)_4$ -[10]CPP (**III.2***) in 20% EtOH/H₂O ($[H] = 3.20 \times 10^{-6}$ M); the changes in fluorescence intensity of **III.2*** at 470 nm were measured. Bottom: correlations of the fluorescence intensity of **III.2*** in 20% EtOH/H₂O as a function of guest concentration to obtain (left) $K_a = (2.03 \pm 0.52) \times 10^6$ M⁻¹ and (right) $K_{SV} = (4.70 \pm 0.46) \times 10^4$ M⁻¹ for the system.

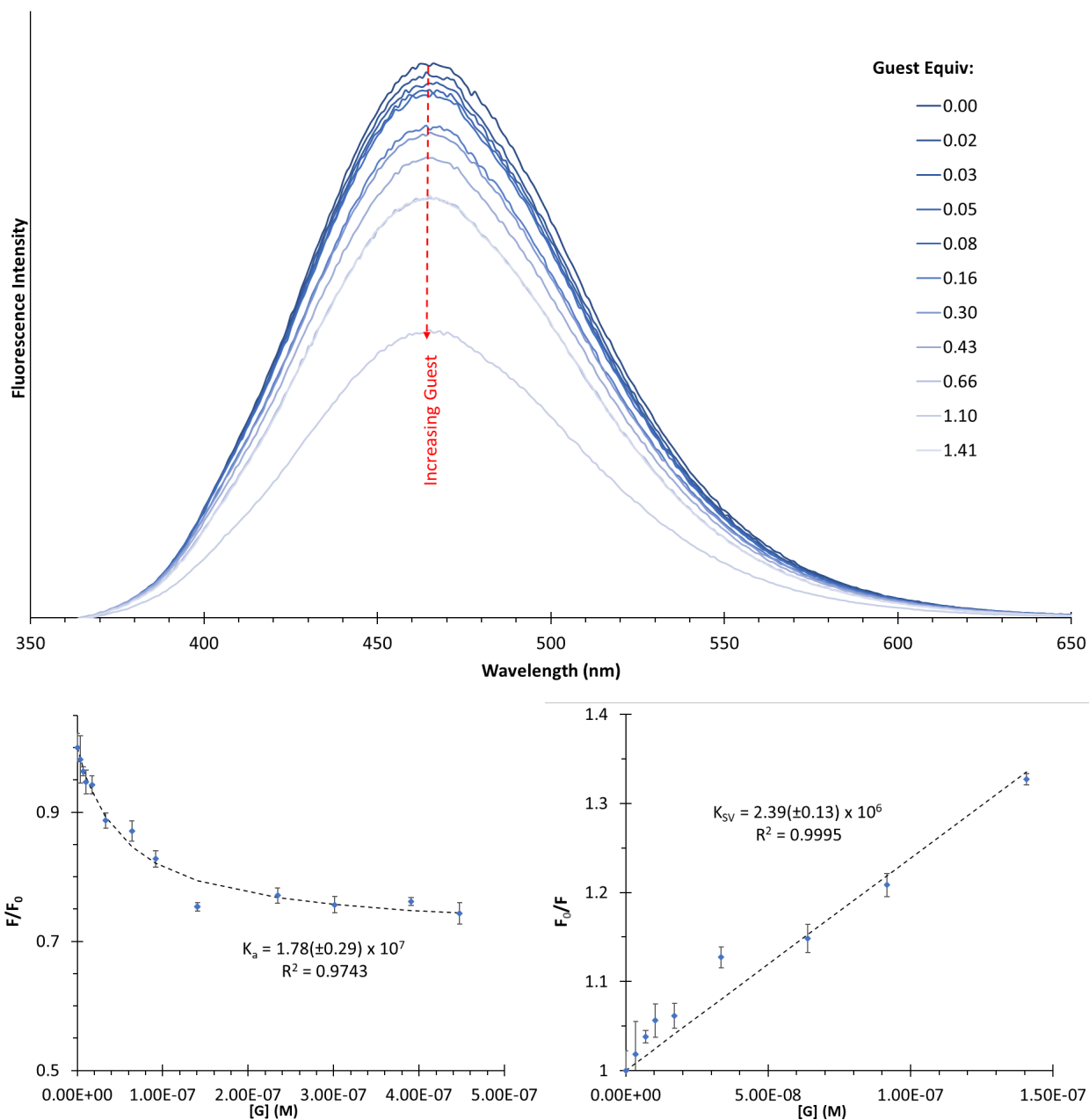


Figure 3.10. Top: fluorescence titration of PCBM ($[G] = 1.76 \times 10^{-5}$ M) into $(\text{CO}_2^-)_4$ -[10]CPP (**III.2***) in 20% EtOH/H₂O ($[H] = 5.43 \times 10^{-6}$ M); the changes in fluorescence intensity of **III.2*** at 470 nm were measured. Bottom: correlations of the fluorescence intensity of **III.2*** in 20% EtOH/H₂O as a function of guest concentration to obtain (left) $K_a = (1.78 \pm 0.29) \times 10^7$ M⁻¹ and (right) $K_{sv} = (2.39 \pm 0.13) \times 10^6$ M⁻¹ for the system.

3.4.2.4. Functionalized [12]CPP Host Derivatives with Fullerene Guests

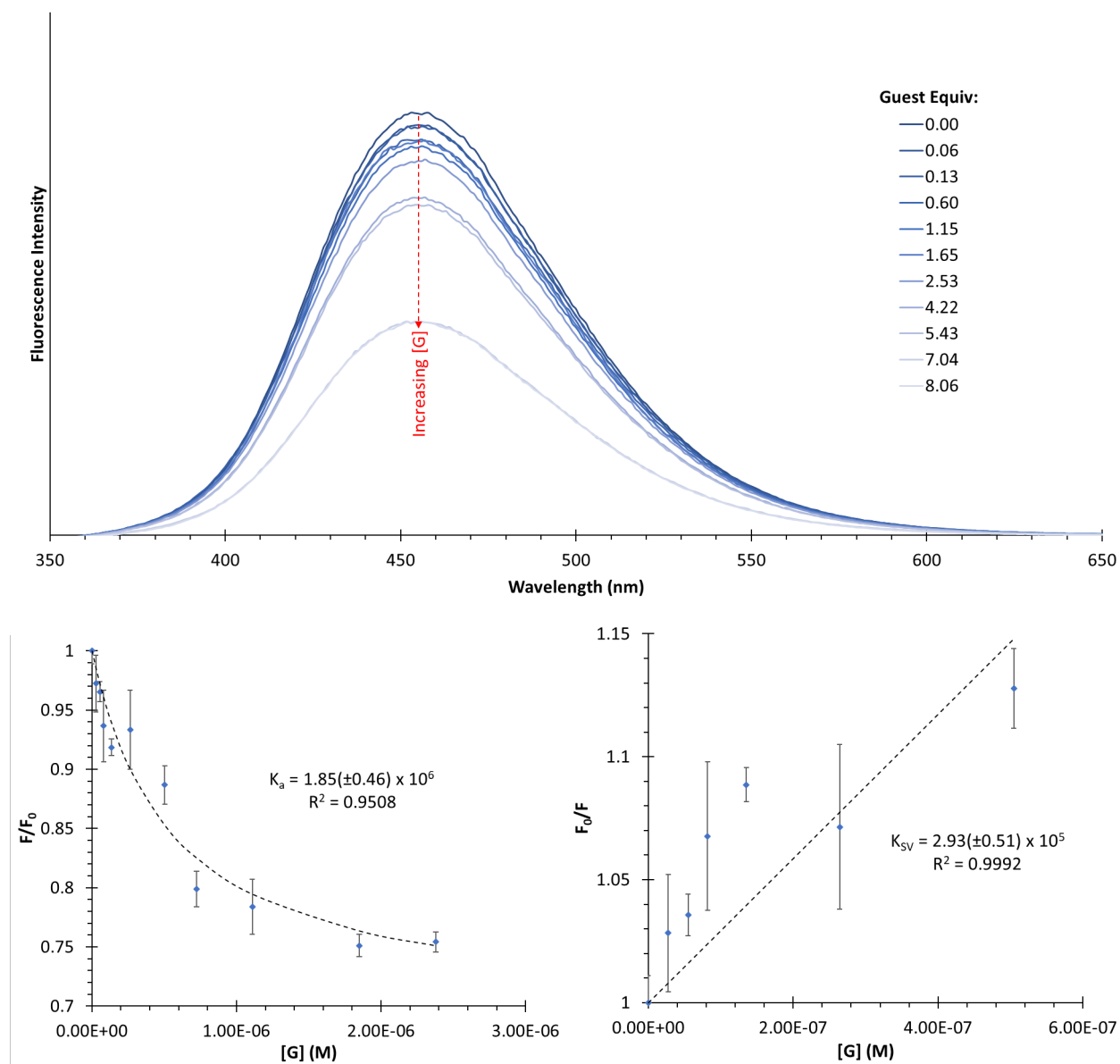


Figure 3.11. Top: fluorescence titration of C_{60} ($[G] = 1.39 \times 10^{-4}$ M) into $(CO_2^-)_6$ -[12]CPP (**III.3***) in 20% EtOH/H₂O ($[H] = 1.09 \times 10^{-5}$ M); the changes in fluorescence intensity of **III.3*** at 455 nm were measured. Bottom: correlations of the fluorescence intensity of **III.3*** in 20% EtOH/H₂O as a function of guest concentration to obtain (left) $K_a = (1.85 \pm 0.46) \times 10^6$ M⁻¹ and (right) $K_{SV} = (2.93 \pm 0.51) \times 10^5$ M⁻¹ for the system.

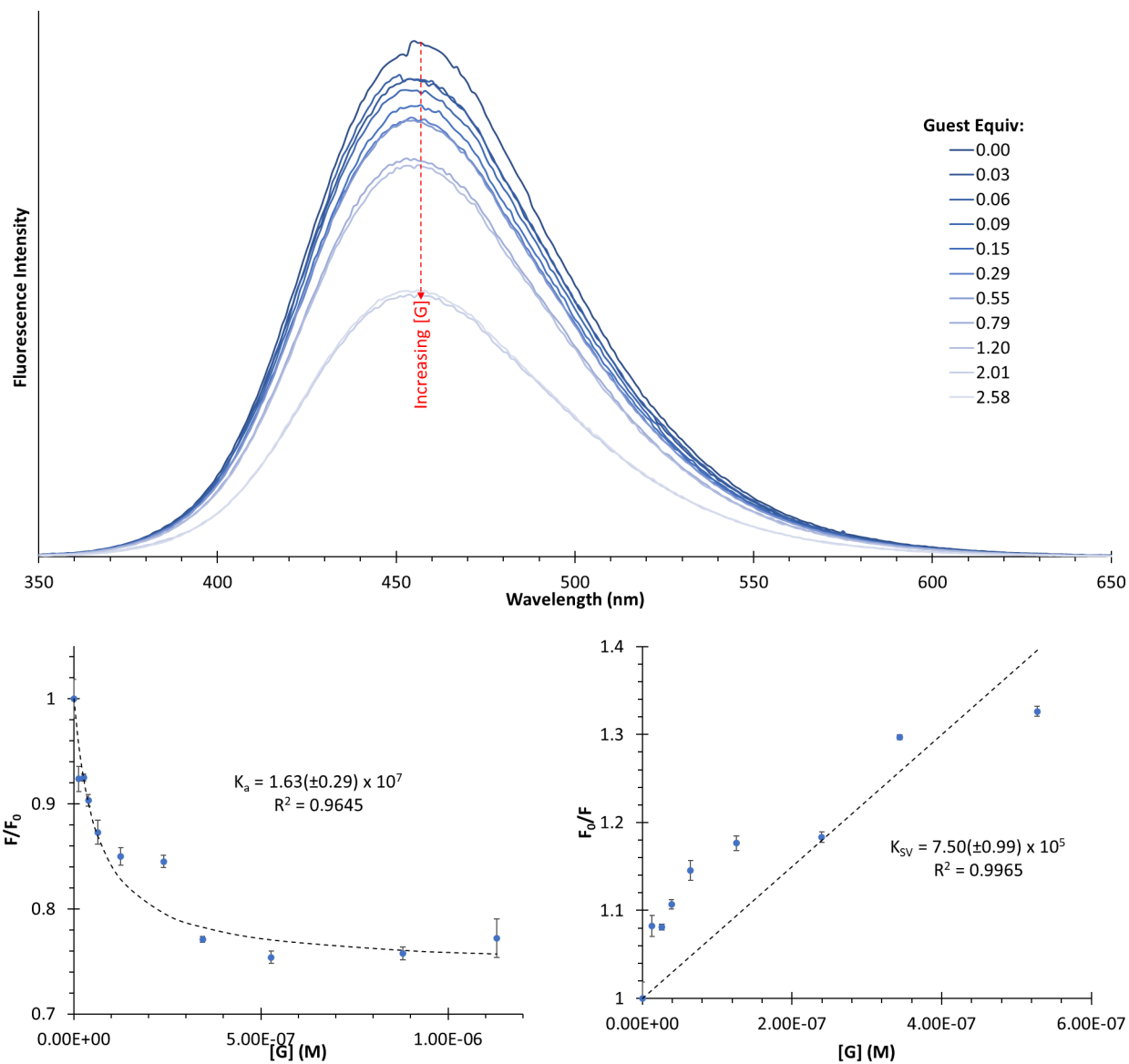


Figure 3.12. Top: fluorescence titration of PCBM ($[G] = 6.59 \times 10^{-5} \text{ M}$) into $(\text{CO}_2)_6$ -[12]CPP (**III.3***) in 20% EtOH/H₂O ($[H] = 1.09 \times 10^{-5} \text{ M}$); the changes in fluorescence intensity of **III.3*** at 455 nm were measured. Bottom: correlations of the fluorescence intensity of **III.3*** in 20% EtOH/H₂O as a function of guest concentration to obtain (left) $K_a = (1.63 \pm 0.29) \times 10^7 \text{ M}^{-1}$ and (right) $K_{SV} = (7.50 \pm 0.99) \times 10^5 \text{ M}^{-1}$ for the system.

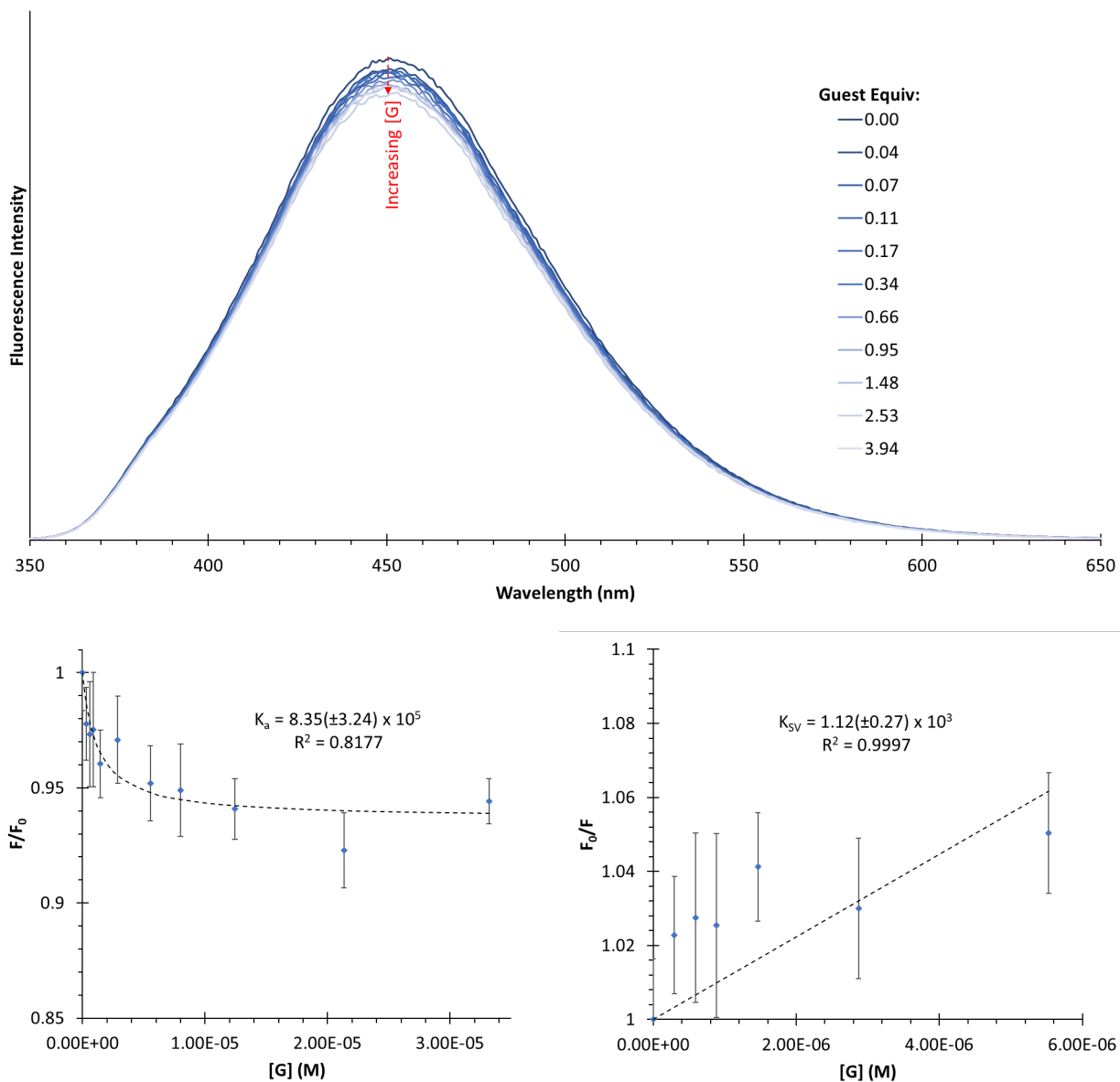


Figure 3.13. Top: fluorescence titration of PCBM ($[G] = 7.47 \times 10^{-5}$ M) into $(\text{CO}_2^-)_6$ -[12]CPP (**III.3***) in H_2O ($[\text{H}] = 8.42 \times 10^{-6}$ M); the changes in fluorescence intensity of **III.3*** at 450 nm were measured. Bottom: correlations of the fluorescence intensity of **III.3*** in H_2O as a function of guest concentration to obtain (left) $K_a = (8.35 \pm 3.24) \times 10^5 \text{ M}^{-1}$ and (right) $K_{SV} = (1.12 \pm 0.27) \times 10^3 \text{ M}^{-1}$ for the system.

3.4.2.5. [10]- and [12]CPP Hosts with CPP Guests

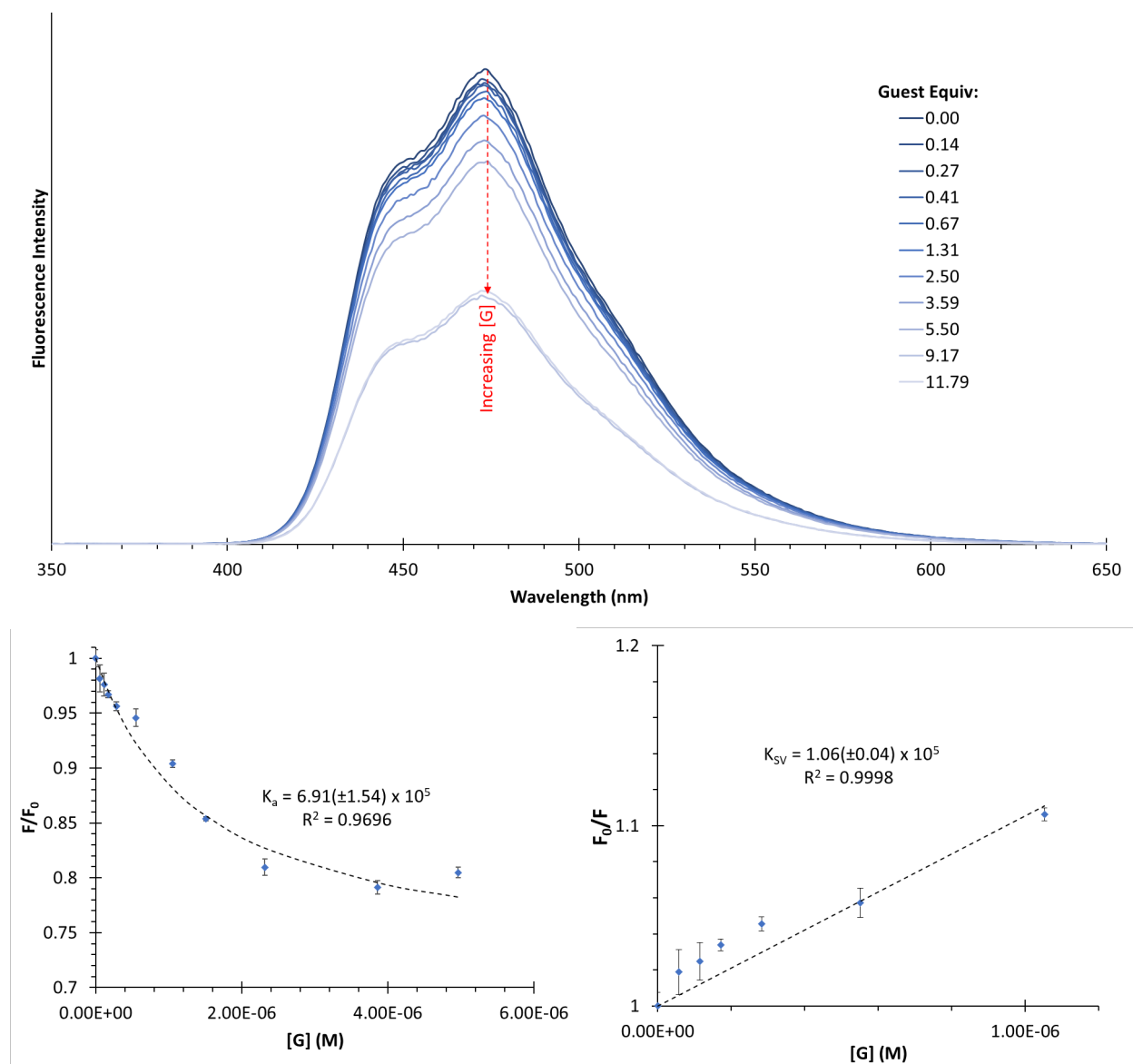


Figure 3.14. Top: fluorescence titration of [5]CPP ($[G] = 1.16 \times 10^{-4}$ M) into [10]CPP in toluene ($[H] = 1.05 \times 10^{-5}$ M); the changes in fluorescence intensity of [10]CPP at 470 nm were measured. Bottom: correlations of the fluorescence intensity of [10]CPP in toluene as a function of guest concentration to obtain (left) $K_a = (6.91 \pm 1.54) \times 10^5$ M $^{-1}$ and (right) $K_{SV} = (1.06 \pm 0.04) \times 10^5$ M $^{-1}$ for the system.

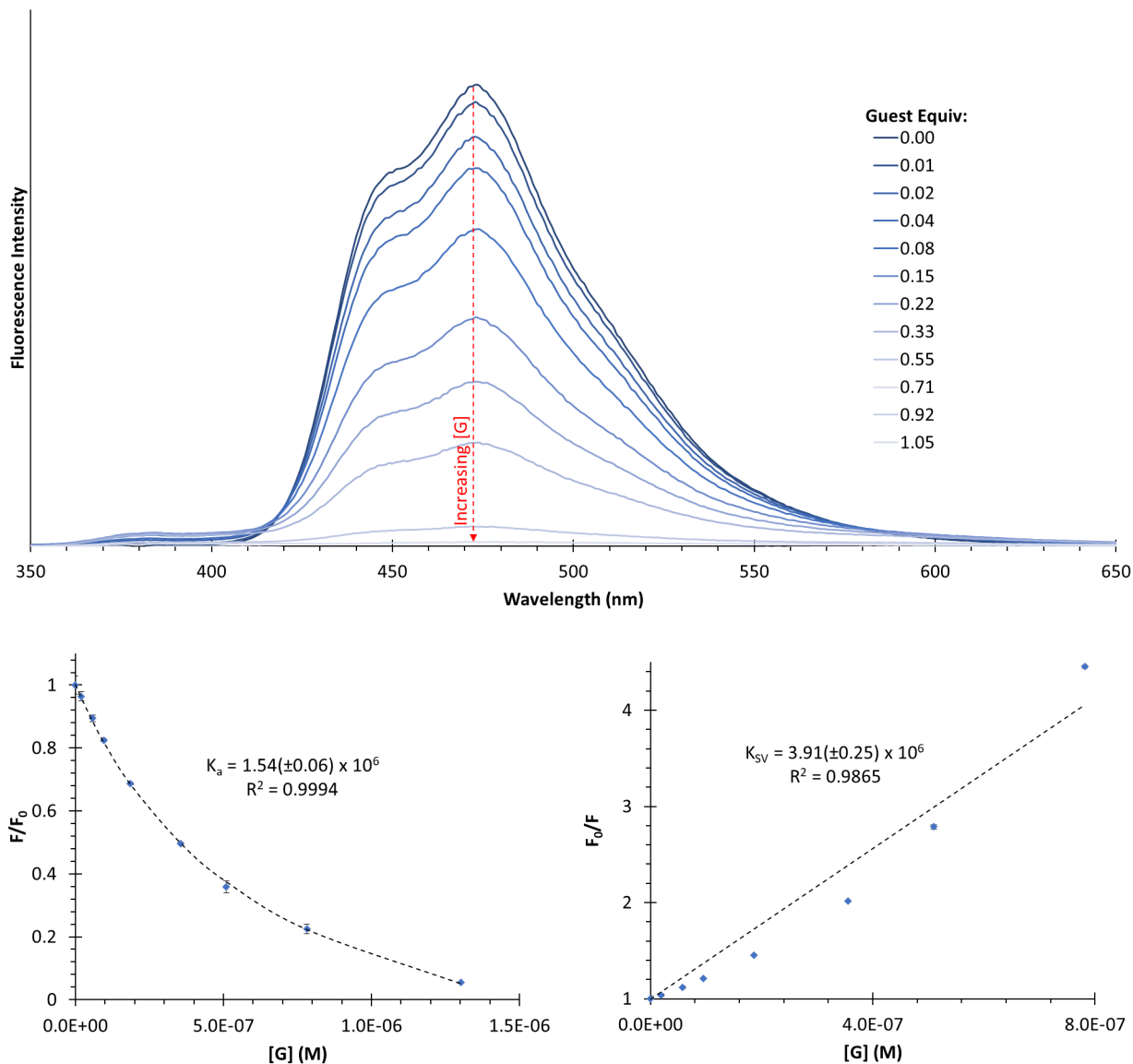


Figure 3.15. Top: fluorescence titration of [7]CPP ($[G] = 9.77 \times 10^{-5}$ M) into [10]CPP in toluene ($[H] = 2.37 \times 10^{-6}$ M); the changes in fluorescence intensity of [10]CPP at 470 nm were measured. Bottom: correlations of the fluorescence intensity of [10]CPP in toluene as a function of guest concentration to obtain (left) $K_a = (1.54 \pm 0.06) \times 10^6$ M⁻¹ and (right) $K_{SV} = (3.91 \pm 0.25) \times 10^6$ M⁻¹ for the system.

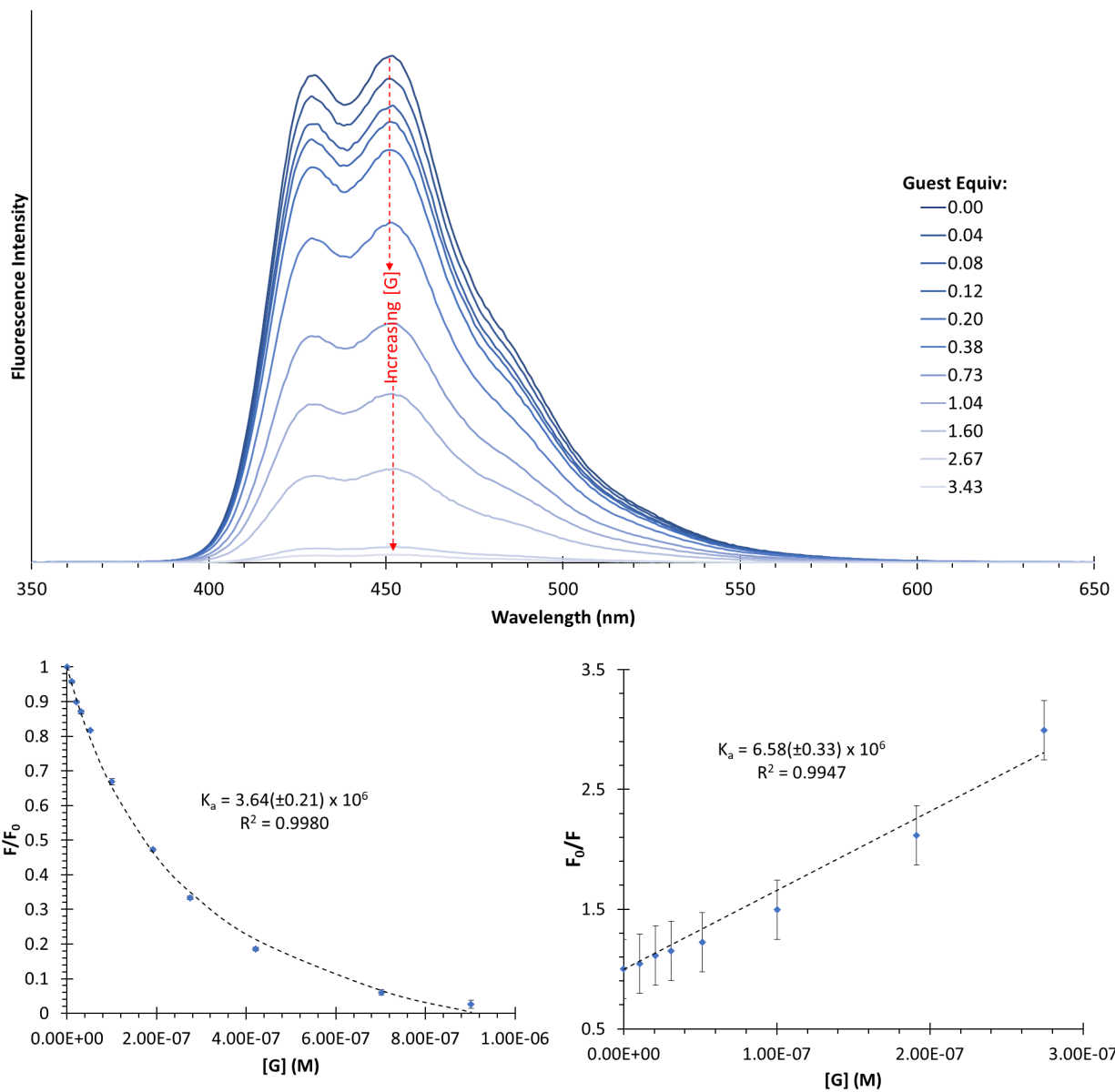


Figure 3.16. Top: fluorescence titration of [7]CPP ($[G] = 5.26 \times 10^{-5}$ M) into [12]CPP in toluene ($[H] = 6.58 \times 10^{-6}$ M); the changes in fluorescence intensity of [12]CPP at 450 nm were measured. Bottom: correlations of the fluorescence intensity of [10]CPP in toluene as a function of guest concentration to obtain (left) $K_a = (3.64 \pm 0.21) \times 10^6$ M⁻¹ and (right) $K_{SV} = (6.58 \pm 0.33) \times 10^6$ M⁻¹ for the system.

3.4.2.6. Functionalized [10] and [12]CPP Host Derivatives with CPP Guests

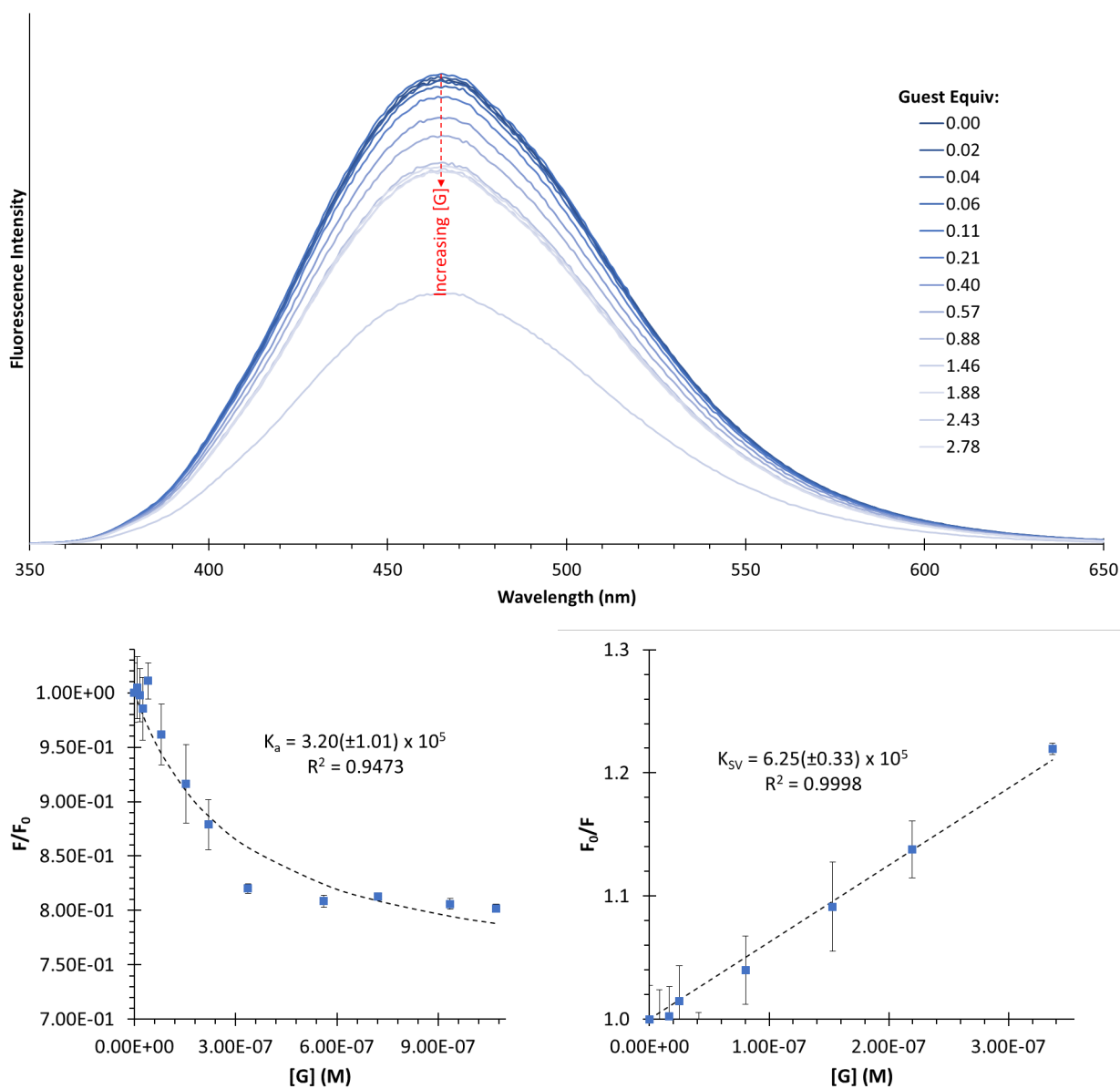


Figure 3.17. Top: fluorescence titration of [5]CPP ($[G] = 4.21 \times 10^{-5}$ M) into $(\text{CO}_2^-)_4$ -[10]CPP (**III.2***) in H_2O ($[\text{H}] = 9.62 \times 10^{-6}$ M); the changes in fluorescence intensity of **III.2*** at 470 nm were measured. Bottom: correlations of the fluorescence intensity of **III.2*** in H_2O as a function of guest concentration to obtain (left) $K_a = (3.20 \pm 1.01) \times 10^5 \text{ M}^{-1}$ and (right) $K_{SV} = (6.25 \pm 0.33) \times 10^5 \text{ M}^{-1}$ for the system.

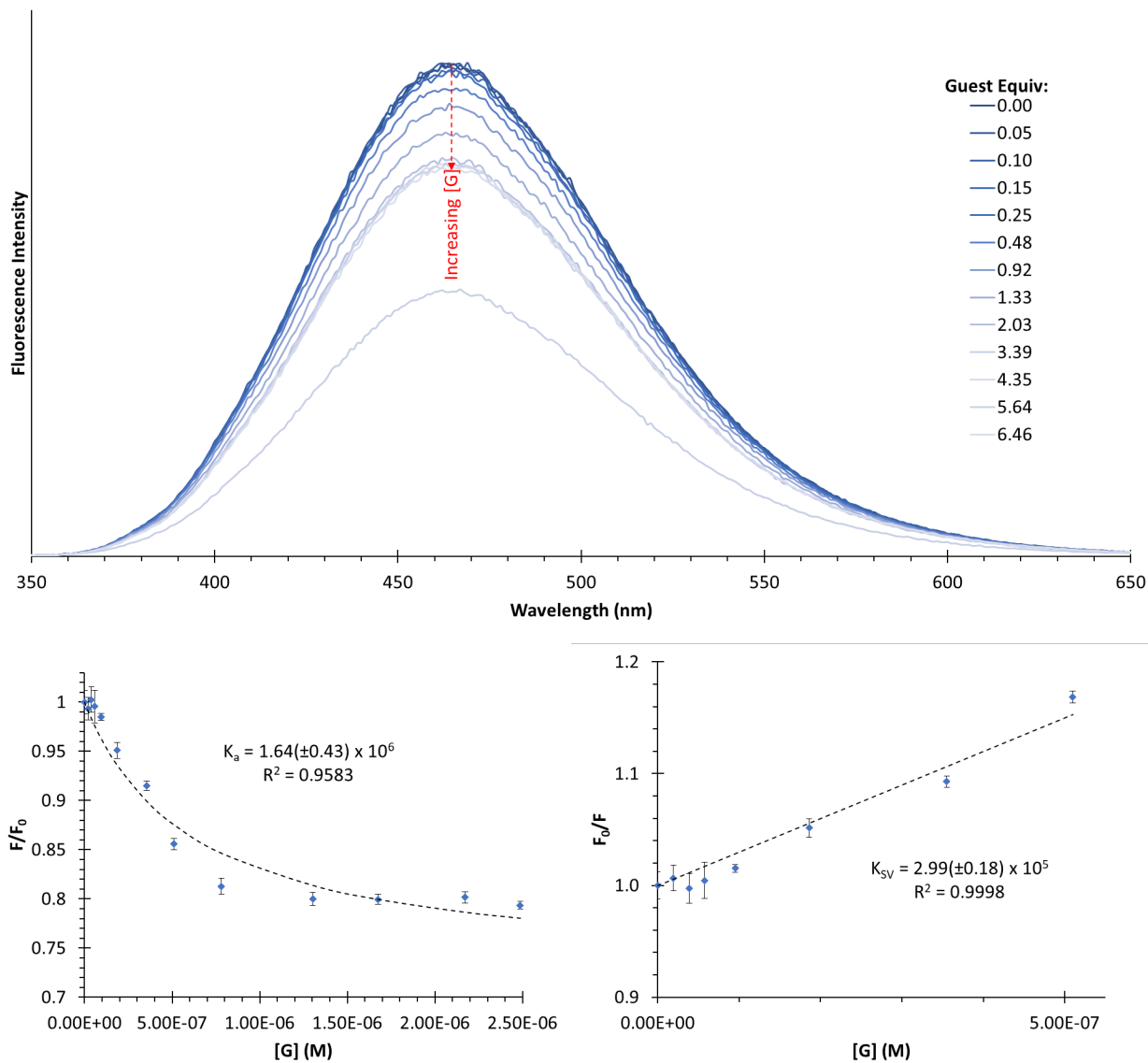


Figure 3.18. Top: fluorescence titration of [7]CPP ($[G] = 9.77 \times 10^{-5}$ M) into $(\text{CO}_2^-)_4$ -[10]CPP (**III.2***) in H_2O ($[H] = 9.62 \times 10^{-6}$ M); the changes in fluorescence intensity of **III.2*** at 470 nm were measured. Bottom: correlations of the fluorescence intensity of **III.2*** in H_2O as a function of guest concentration to obtain (left) $K_a = (1.64 \pm 0.43) \times 10^6 \text{ M}^{-1}$ and (right) $K_{SV} = (2.99 \pm 0.18) \times 10^5 \text{ M}^{-1}$ for the system.

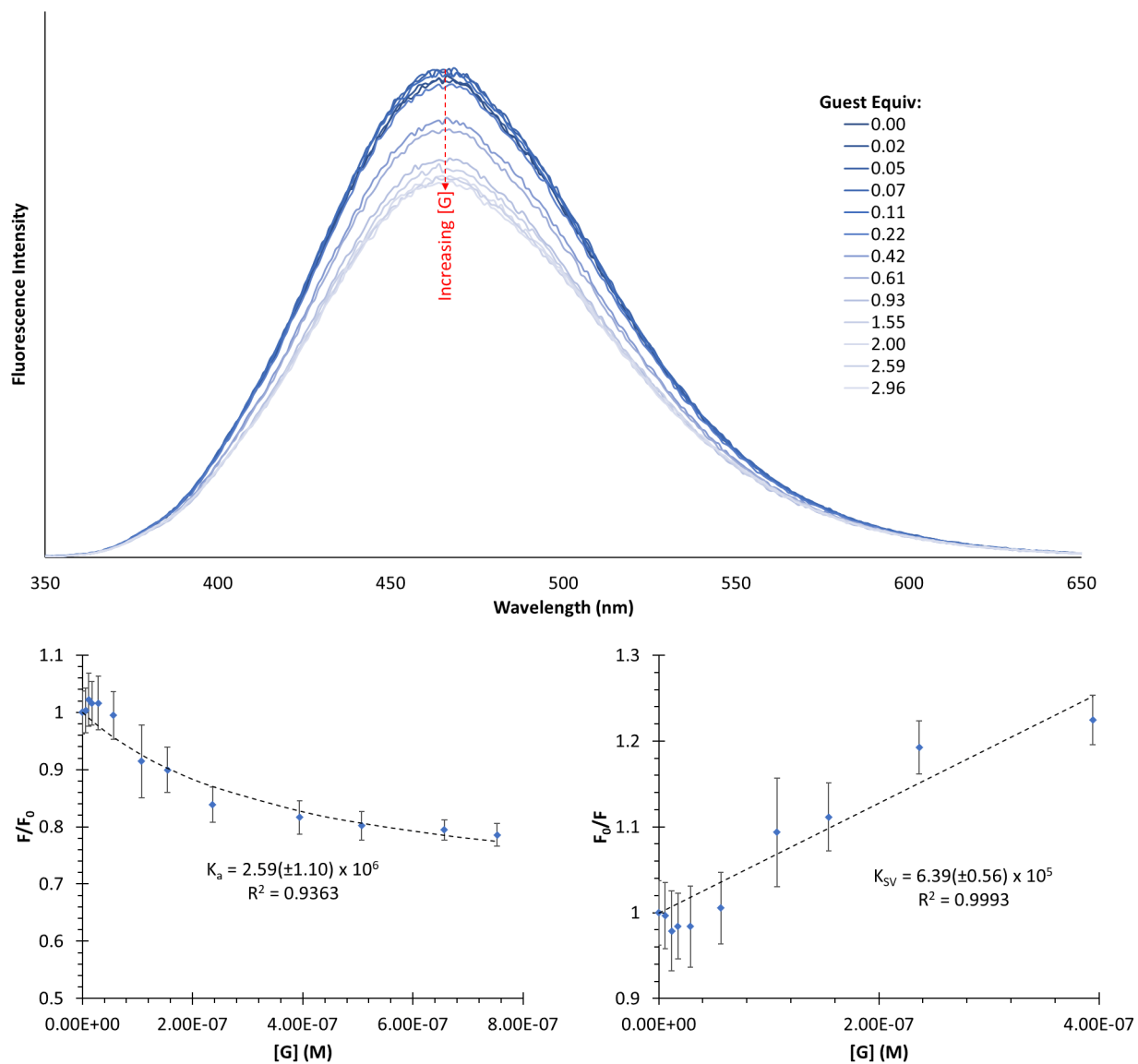


Figure 3.19. Top: fluorescence titration of [8]CPP ($[G] = 2.96 \times 10^{-5}$ M) into $(\text{CO}_2^-)_4$ -[10]CPP (**III.2***) in H_2O ($[\text{H}] = 6.35 \times 10^{-6}$ M); the changes in fluorescence intensity of **III.2*** at 470 nm were measured. Bottom: correlations of the fluorescence intensity of **III.2*** in H_2O as a function of guest concentration to obtain (left) $K_a = (2.59 \pm 1.10) \times 10^6 \text{ M}^{-1}$ and (right) $K_{SV} = (6.39 \pm 0.56) \times 10^5 \text{ M}^{-1}$ for the system.

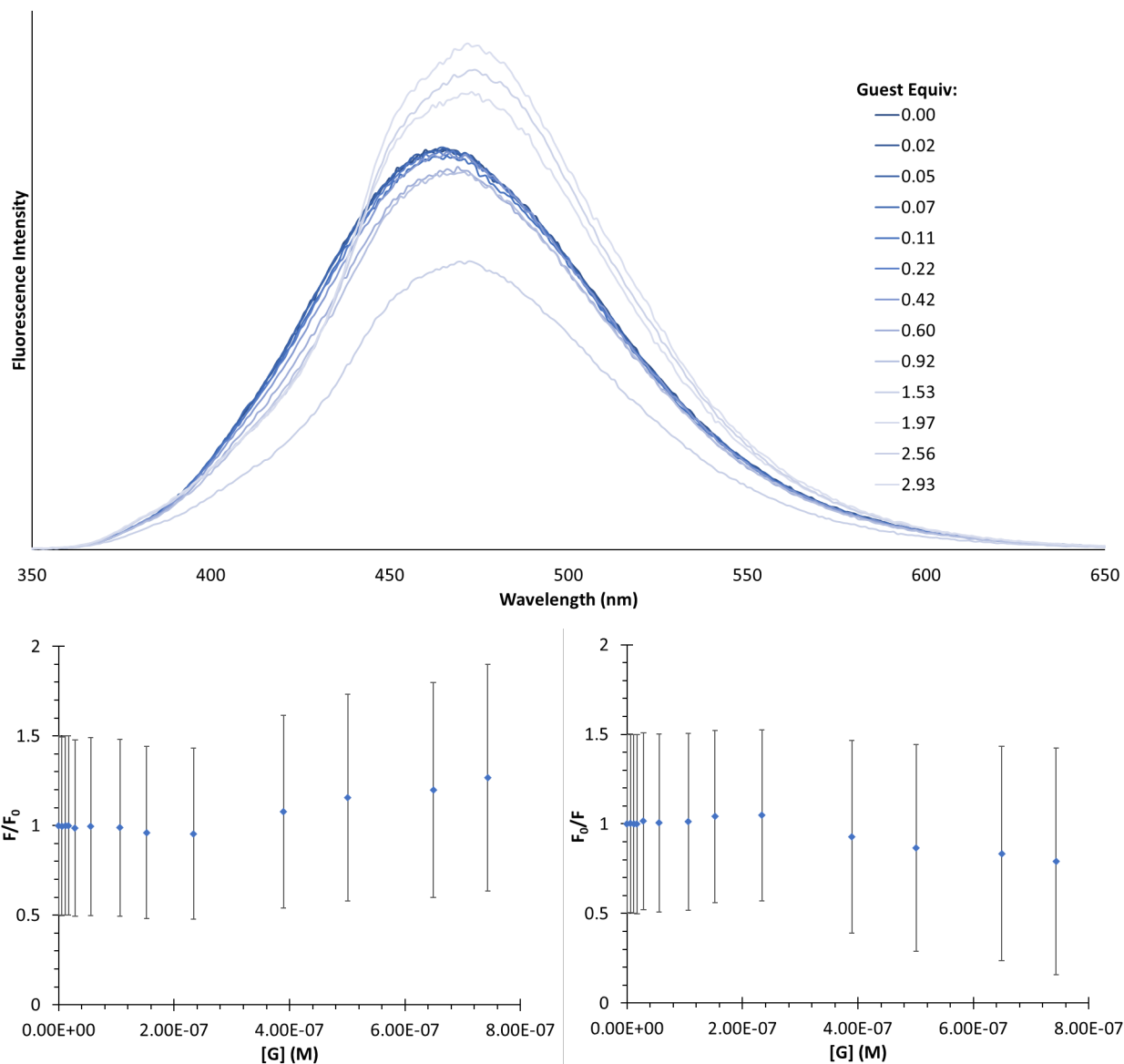


Figure 3.20. Top: fluorescence titration of [9]CPP ($[G] = 2.92 \times 10^{-5}$ M) into $(\text{CO}_2^-)_4$ -[10]CPP (**III.2***) in H_2O ($[\text{H}] = 6.35 \times 10^{-6}$ M); the changes in fluorescence intensity of **III.2*** at 470 nm were measured. Bottom: correlations of the fluorescence intensity of **III.2*** in H_2O as a function of guest concentration could not be reasonably fit to equations *III.1* and *III.2*, respectively.

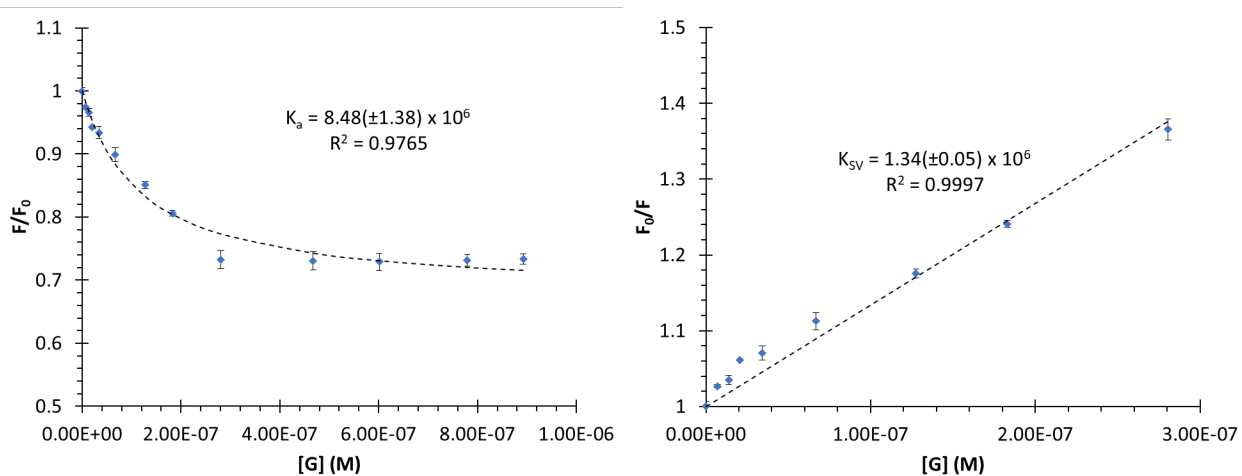
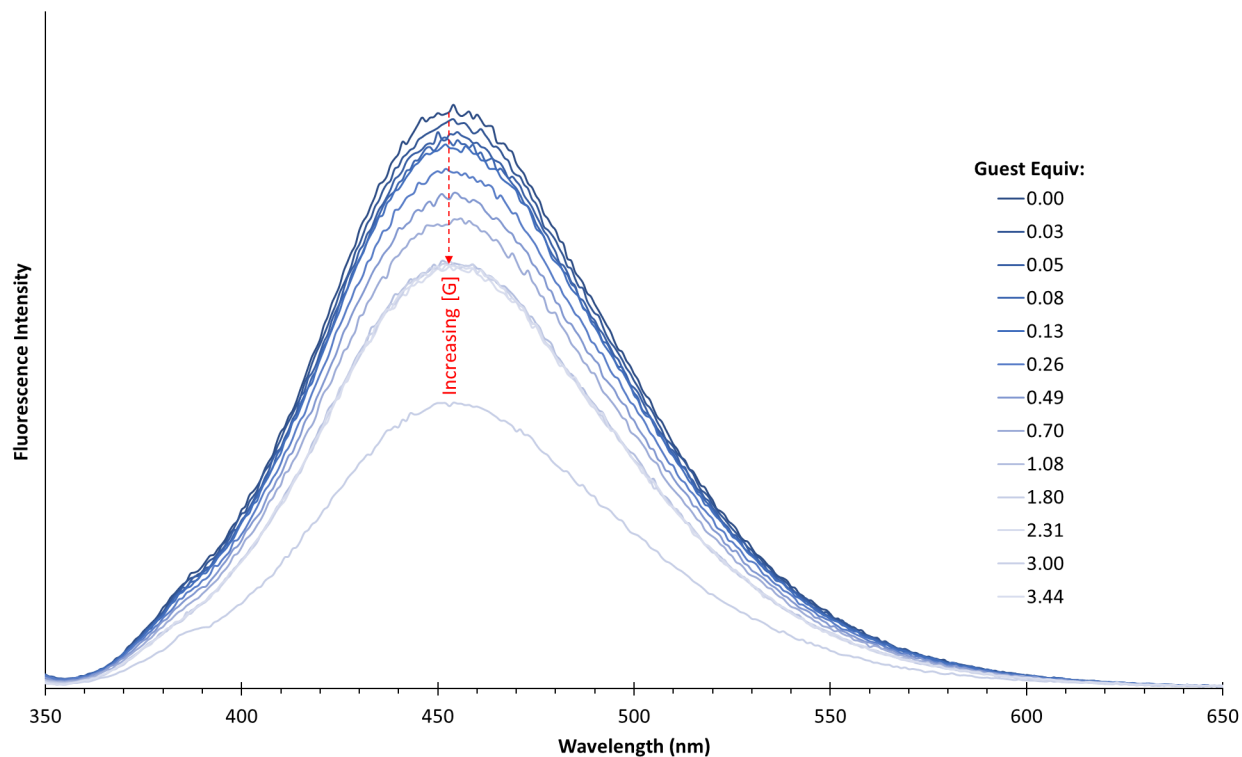


Figure 3.21. Top: fluorescence titration of [6]CPP ($[G] = 3.51 \times 10^{-5}$ M) into $(\text{CO}_2^-)_6$ -[12]CPP (**III.3***) in H_2O ($[\text{H}] = 6.50 \times 10^{-6}$ M); the changes in fluorescence intensity of **III.3*** at 450 nm were measured. Bottom: correlations of the fluorescence intensity of **III.3*** in H_2O as a function of guest concentration to obtain (left) $K_a = (8.48 \pm 1.38) \times 10^6 \text{ M}^{-1}$ and (right) $K_{SV} = (1.34 \pm 0.05) \times 10^6 \text{ M}^{-1}$ for the system.

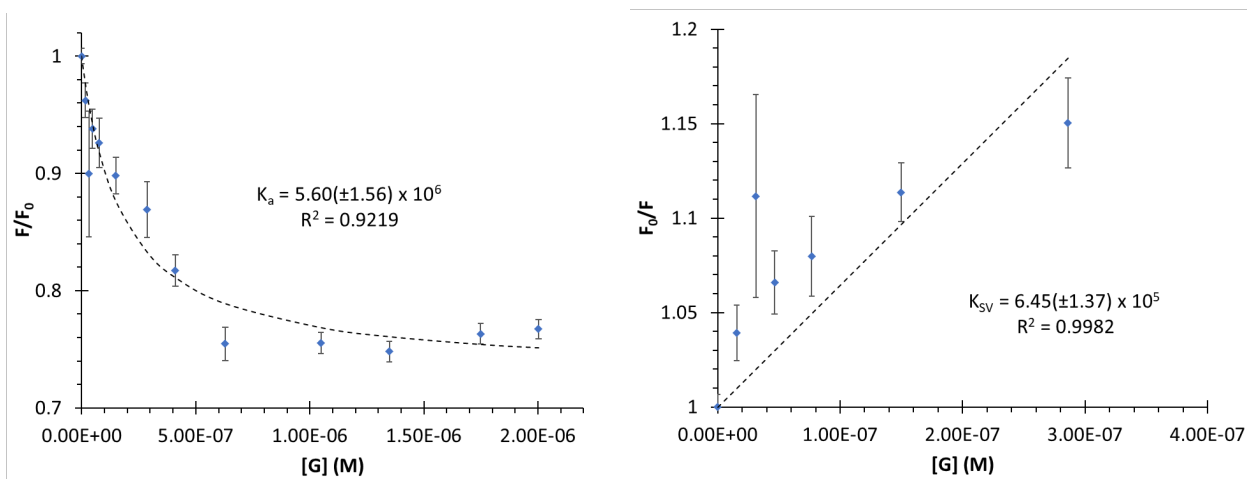
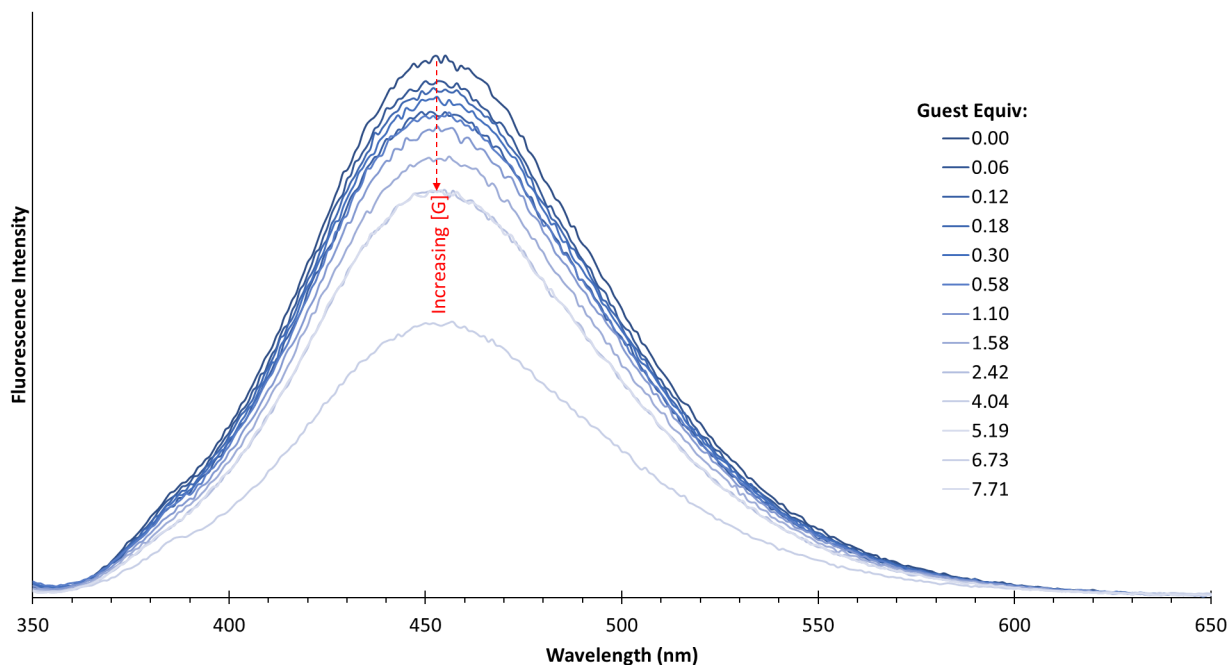


Figure 3.22. Top: fluorescence titration of aza-[6]CPP ($[G] = 7.87 \times 10^{-5}$ M) into $(\text{CO}_2^-)_6$ -[12]CPP (**III.3***) in H_2O ($[\text{H}] = 6.50 \times 10^{-6}$ M); the changes in fluorescence intensity of **III.3*** at 450 nm were measured. Bottom: correlations of the fluorescence intensity of **III.3*** in H_2O as a function of guest concentration to obtain (left) $K_a = (5.60 \pm 1.56) \times 10^6 \text{ M}^{-1}$ and (right) $K_{SV} = (6.45 \pm 1.37) \times 10^5 \text{ M}^{-1}$ for the system.

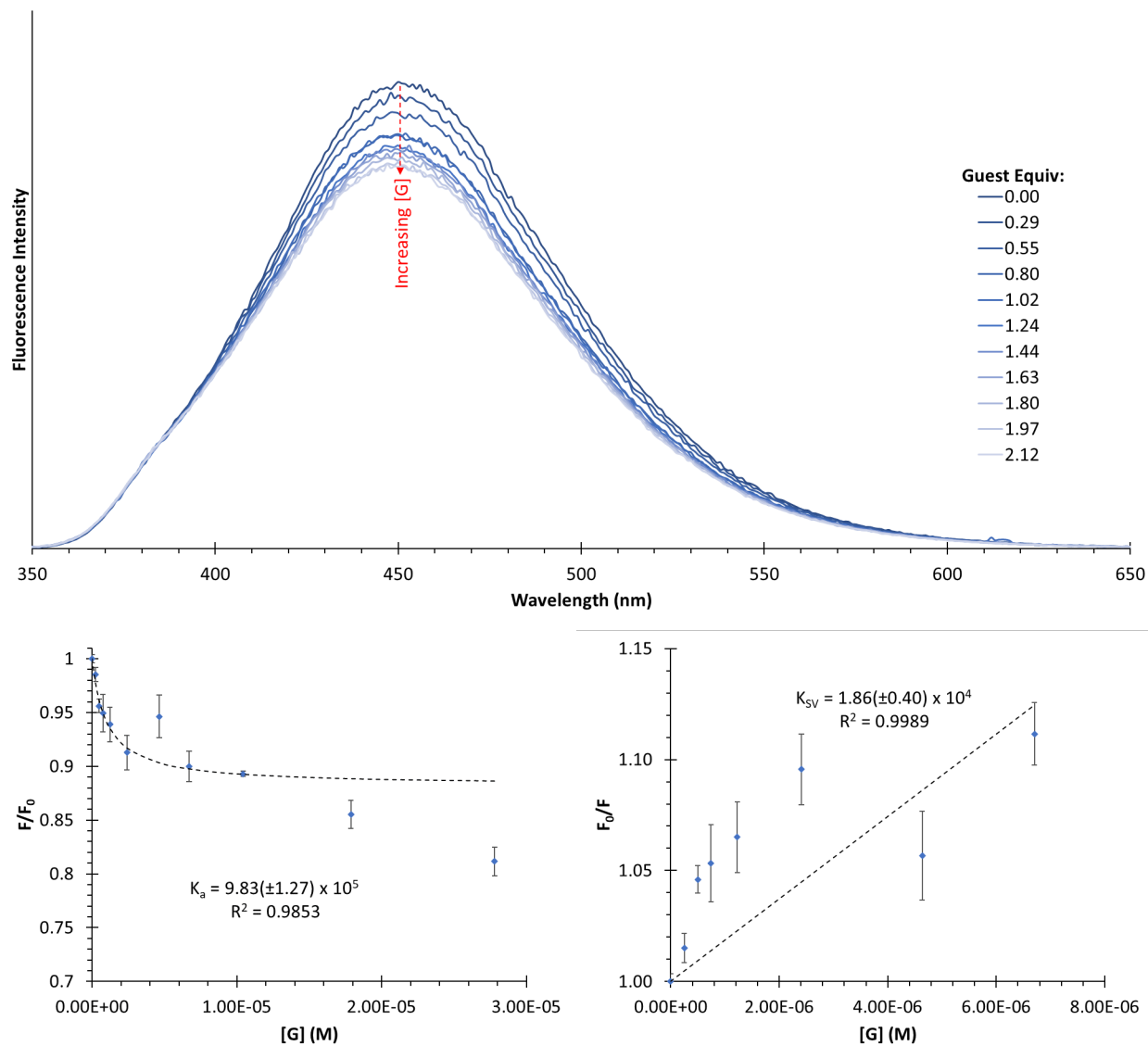


Figure 3.23. Top: fluorescence titration of [7]CPP ($[G] = 6.26 \times 10^{-5}$ M) into $(\text{CO}_2^-)_6$ -[12]CPP (**III.3***) in H_2O ($[\text{H}] = 8.42 \times 10^{-6}$ M); the changes in fluorescence intensity of **III.3*** at 450 nm were measured. Bottom: correlations of the fluorescence intensity of **III.3*** in H_2O as a function of guest concentration to obtain (left) $K_a = (9.83 \pm 1.27) \times 10^5 \text{ M}^{-1}$ and (right) $K_{SV} = (1.86 \pm 0.04) \times 10^4 \text{ M}^{-1}$ for the system.

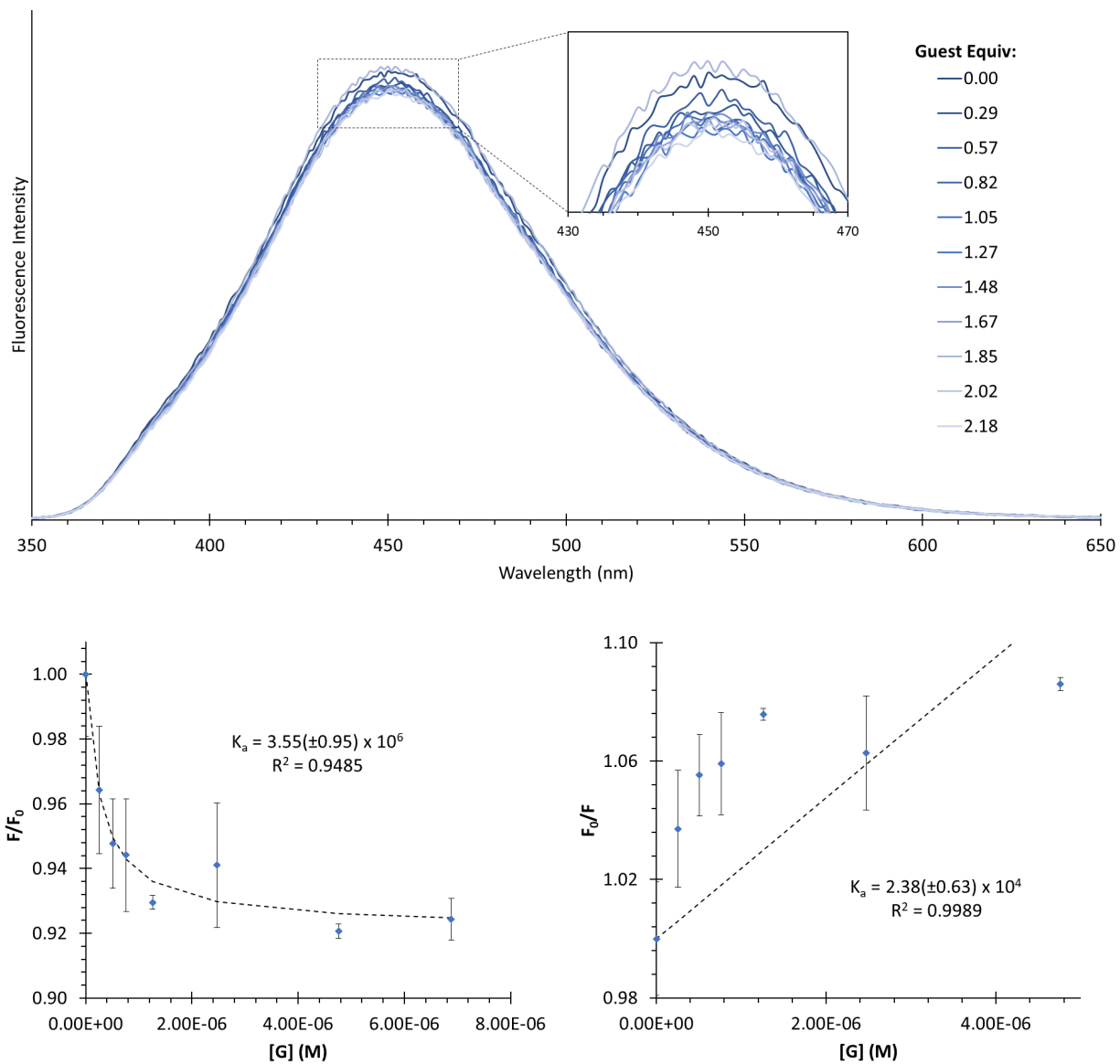


Figure 3.24. Top: fluorescence titration of [9]CPP ($[G] = 6.42 \times 10^{-5}$ M) into $(\text{CO}_2^-)_6$ -[12]CPP (**III.3***) in H_2O ($[\text{H}] = 8.42 \times 10^{-6}$ M); the changes in fluorescence intensity of **III.3*** at 450 nm were measured. Bottom: correlations of the fluorescence intensity of **III.3*** in H_2O as a function of guest concentration to obtain (left) $K_a = (3.55 \pm 0.95) \times 10^6 \text{ M}^{-1}$ and (right) $K_{\text{SV}} = (2.38 \pm 0.63) \times 10^4 \text{ M}^{-1}$ for the system.

3.4.2.7. Functionalized [12]CPP Host Derivatives with CNTs

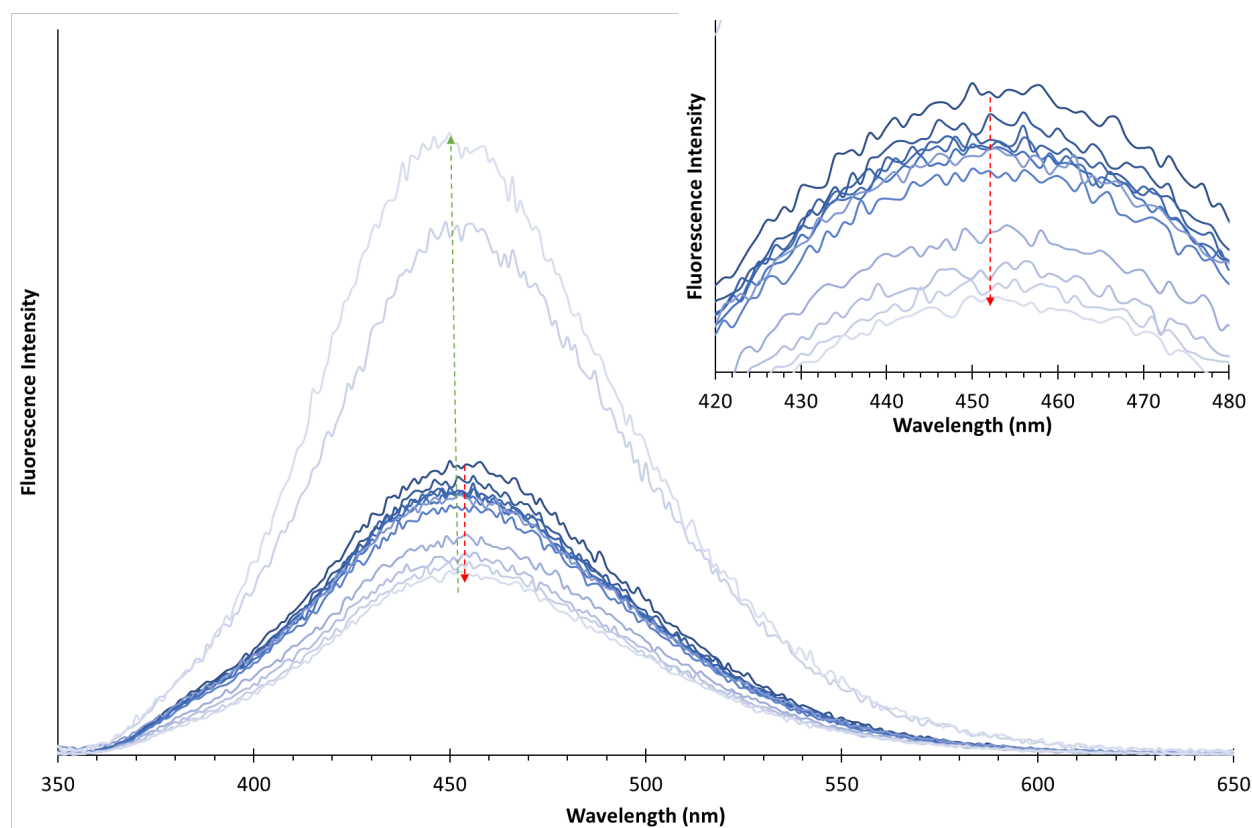


Figure 3.24. Fluorescence titration of [5,6]CNT into $(\text{CO}_2^-)_6$ -[12]CPP (**III.3***) in H_2O ($[\text{H}] = 6.50 \times 10^{-6} \text{ M}$); as guest concentration increases fluorescence is quenched (red arrow, see inlay), however at high concentration of guest fluorescence increases dramatically (green arrow).

3.5. Bridge to Chapter IV

This chapter outlined the supramolecular capabilities of a novel set of water-soluble nanohoop fluorophores, and the broad utility of the hydrophobic effect to drive complexation with a variety of guests. This marks a substantial step in the development of nanohoops towards use in aqueous and biological applications. The next chapter details the development of a nanohoop-based rotaxane probe for use in sensing biologically relevant analytes.

CHAPTER IV

NANOHOOP ROTAXANE DESIGN TO ENHANCE THE SELECTIVITY OF REACTION-BASED PROBES: A PROOF-OF-PRINCIPLE STUDY

From Otteson, C. E.; Levinn, C. M.; Van Raden, J. M.; Pluth, M.; Jasti, R. Nanohoop Rotaxane Design to Enhance the Selectivity of Reaction-Based Probes: A Proof-of-Principle Study. *Org. Lett.* **2021**, *23* (12), 4608-4612. <https://pubs.acs.org/doi/10.1021/acs.orglett.1c01348>. Further permissions related to the use of material excerpted in this chapter should be directed to the ACS. This manuscript was written by myself, with contributions from Carolyn M. Levinn, and with editorial assistance from Professor Ramesh Jasti, and Professor Michael D. Pluth. Experimental work in this chapter was performed by myself, Carolyn M. Levinn, and Jeff M. Van Raden. Experimental guidance was provided by Professor Ramesh Jasti, and Professor Michael D. Pluth.

Mechanical interlocking of a nanohoop fluorophore and a reactive thread couples the benefits of a reaction-based probe with a sterically congested active site for enhanced selectivity. Advantageously, the thread design uses dual function stoppers that act as both a quencher and a trigger for sensing. In progress toward expanding this approach to biologically relevant analytes, this system is used to demonstrate steric differentiation and provide a selective turn-on fluorescent response with size selectivity for HS⁻ rather than larger thiolates.

4.1. Introduction

The development of fluorescent sensors for biologically relevant analytes is a rapidly growing field of research, due in part to the utility, simplicity, and versatility of these systems.¹⁻⁵ These probes are used for detection and quantification of chemical species with documented roles in various disease states and also as tools to obtain a better understanding of biological processes.^{1,4,6,7} In many cases, the effective concentration of a particular analyte can be linked with disease progression, and therefore the ability to study an analyte in a natural biological environment is critical.^{5,7,8} This requirement, however, presents a formidable challenge because probes need to be highly selective due to the large number of reactive species present in complex

biological systems. Simultaneously, heightened sensitivity is required due to the low physiological concentrations of these species, all while operating in a very competitive solvent (water).⁶⁻¹¹ Obtaining analyte selectivity has traditionally relied on the creation of highly specific binding sites; however, these “lock-and-key” systems come with challenges (**Figure 4.1a**).¹² Sensors based solely on supramolecular or coordination-driven interactions can be heavily influenced by solvation effects and changes in pH, issues that are amplified in aqueous media.⁷ Alternatively, reaction-based probes can be designed to contain a “trigger” that reacts with an analyte of interest, and therefore, selectivity is a function of differences in reactivity (**Figure 4.1b**).^{7,13-16} This mode of selectivity, however, can be difficult to achieve when considering a group of analytes with similar reactivity, such as reactive sulfur species (RSS). To our knowledge, a yet unexplored route to enhancing probe selectivity is the pairing of these two powerful methods of analyte sensing by constructing a sterically encumbered reactive probe via mechanical interlocking.

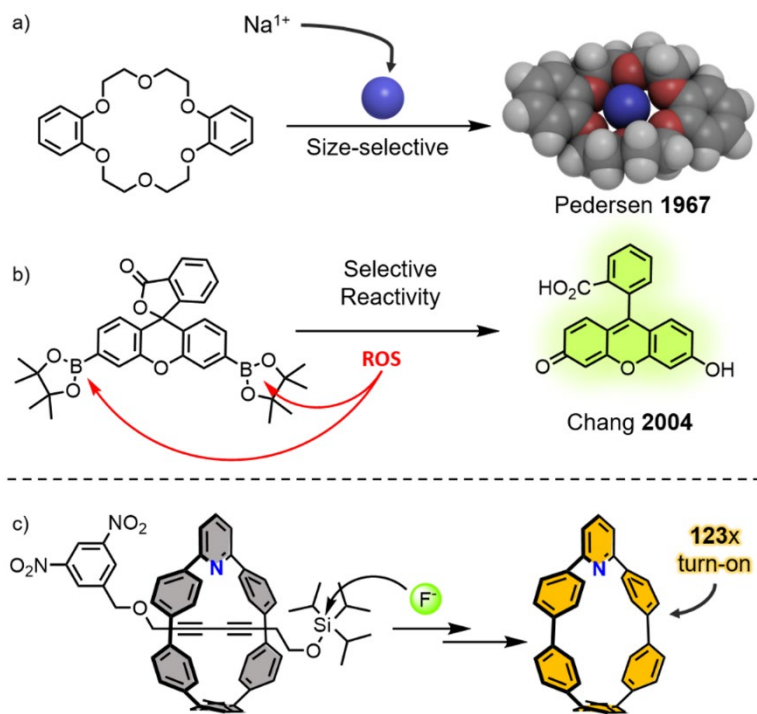


Figure 4.1. Classic examples of (a) size selective¹² and (b) reaction-based sensing platforms.¹⁶ (c) A previously published nanothoop[2]-rotaxane-based fluorescent fluoride sensor.²⁸

Mechanically interlocked molecules (MIMs) have recently garnered interest for a variety of biological applications. The chemistry, which can be useful for sensing, imaging, and drug

delivery.^{17–30} Furthermore, the steric encumbrance provided by the macrocyclic component of rotaxanes has been exploited to protect electron-deficient moieties from nucleophilic attack, modulate the reactivity of the thread component, and enhance the photophysical properties of dye-based axles.^{18,30–33} Nanohoos are unique among macrocycles used for MIM synthesis,^{34–36} due to their inherent fluorescence and highly rigid structure, particularly at small sizes.³⁷ As a consequence, minimal steric bulk is required to prevent dethreading via slippage, allowing for broad flexibility in thread design. Taking advantage of these properties, we recently illustrated the potential of nanohoop [2]rotaxanes as turn-on fluorescent sensors (**Figure IV.1c**).³⁵ Use of an electron-deficient 2,5-dinitrobenzyl alcohol as one of the stoppers quenches the fluorescence of the nanohoop in the interlocked state. A fluoride-triggered silyl deprotection of the triisopropylsilyl ether stopper results in dethreading of the macrocycle, dissociation of the quencher and fluorophore, and ultimately a 123-fold turn-on in fluorescence.

Building from this example, we sought to target a more challenging analyte to demonstrate the advantage of the congested reaction site of the interlocked sensor. As noted above, one group of analytes that has proved challenging to sense selectively is RSS. The smallest species in this family is hydrogen sulfide (H₂S), one of three currently recognized gasotransmitters.³⁸ H₂S is involved in a wide variety of regulatory processes, and the diverse roles in human physiology make it an important target of research.^{39–42} Selective reaction-based probes that rely on H₂S/HS[−] nucleophilicity are often challenging to design because other biologically relevant nucleophilic thiols are present in much greater concentrations (low nM for H₂S vs low mM concentrations for glutathione).^{13,43–51} Herein, we report a novel turn-on fluorescent nanohoop [2]rotaxane⁵² for selective sensing of HS[−] in organic solution based on the well documented S_NAr reaction of thiolates with 2,4-dinitrophenyl (DNP) ethers.^{44–46} We provide a proof-of-principle demonstration that encapsulation of a DNP ether thread within a nanohoop via mechanical interlocking effectively couples the benefits of a reactive probe with a sterically tailored active site, enhancing the selectivity of the probe.

4.2. Results and Discussion

As previously mentioned, our group recently accessed a variety of nanohoop [2]rotaxanes, where “2” denotes the number of component molecules in the MIM. These structures can be prepared by incorporation of a 2,6-pyridine unit into the backbone of a carbon nanohoop that can

then participate in active metal templating via a Cadiot–Chodkiewicz (CC) cross-coupling reaction.^{35,36,53,54} With this methodology in mind, rotaxane sensor **IV.4** was envisioned with **IV.1** as the templating macrocycle, which again is notable for its small size, rigidity, and fluorescence (**Figure 4.2a**). The thread component was designed to have two multifunctional DNP units that serve as stoppers, reactive probes, as well as fluorescence quenchers. To this end, terminal alkyne coupling partner **IV.2** was prepared via deprotonation of DNP alcohol with potassium carbonate and reaction with propargyl bromide. The requisite halo-alkyne coupling partner **IV.3** was then easily obtained in good yield via treatment of **IV.2** with silver nitrite and N-bromosuccinimide. Treatment of both thread components **IV.2** and **IV.3** with $[\text{Cu}(\text{MeCN})_4][\text{PF}_6]$ in the presence of nanohoop **IV.1** delivered the desired interlocked rotaxane **IV.4** in 18% unoptimized yield. Notably, the isolated yellow solid was nonfluorescent in the solid and solution state as predicted. Free thread **IV.5** was prepared as a control compound using similar methods. All compounds were characterized by ^1H and $^{13}\text{C}\{^1\text{H}\}$ NMR spectroscopy, mass spectrometry, and IR spectroscopy.

DNP reacts with HS^- via an $\text{S}_{\text{N}}\text{Ar}$ mechanism.^{44,45} Based on this, we expected HS^- to react with rotaxane **IV.4** to first generate a Meisenheimer complex (**Figure 4.2b**). Collapse of this intermediate would release 2,4-dinitrothiophenol (DNT), an equivalent of diyne, with subsequent dethreading of the nanohoop and a concomitant turn-on in fluorescence (**Figure 4.2b**). We first investigated this process via ^1H NMR spectroscopy. For these studies, we used the organic soluble tetrabutylammonium hydrosulfide (NBu_4SH) because HS^- is the most prevalent protonation state of H_2S under physiological conditions and is the active species responsible for cleavage of DNP groups. **Figure IV.2c** illustrates the immediate response upon treatment of 4.5 mM rotaxane **IV.4** with 1 equiv of NBu_4SH in acetonitrile- d_3 at 25 °C. Consistent with the mechanism in **Figure 4.2b**, we see the return of free macrocycle **IV.1** (resonances outlined in yellow) as well as the appearance of resonances that suggest the formation of $\text{S}_{\text{N}}\text{Ar}$ byproduct DNT. Moreover, at the conclusion of the experiment, the sample showed bright yellow fluorescence under UV irradiation, also consistent with dissociation of the thread from macrocycle **IV.1**.

Next, we investigated the kinetics of the dethreading events using time-course fluorescence and UV–vis experiments. We added 10, 50, or 100 equiv of NBu_4SH to a solution of rotaxane sensor **IV.4** in degassed MeCN and monitored changes in the fluorescence and absorbance spectra over time. Dethreading is complete within 30 min (based on lack of further change in fluorescence

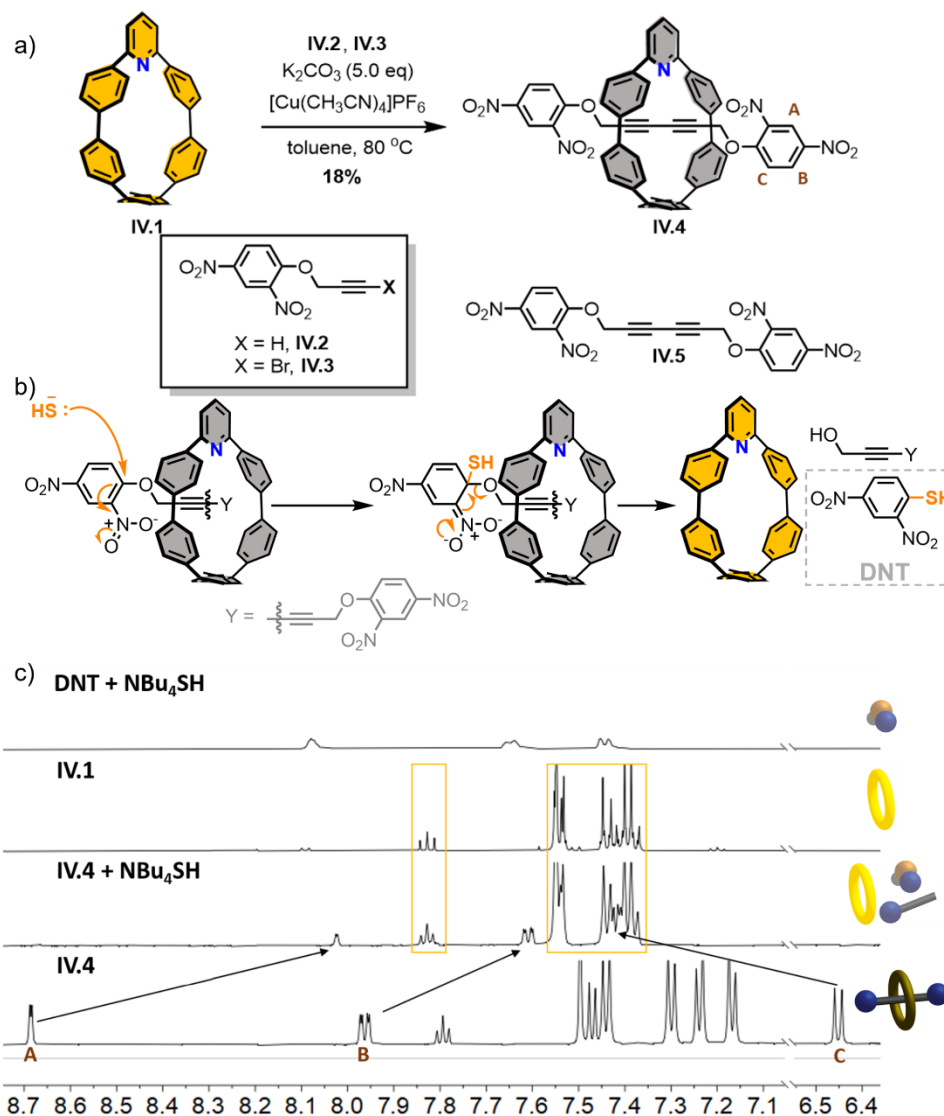


Figure 4.2. (a) Synthesis of rotaxane **IV.4** and free thread **IV.5**, (b) proposed mechanism of rotaxane dethreading in the presence of HS^- , and (c) 1H NMR spectra (aromatic region) of rotaxane **IV.4** in CD_3CN , before and after addition of 1 equiv of NBu_4SH , compared with free macrocycle **IV.1** and DNT in the presence of NBu_4SH .

or UV-vis spectra) when either 50 or 100 equiv of NBu_4SH is introduced. With just 10 equiv of NBu_4SH , we see a 320-fold turn-on in nano hoop fluorescence, with the signal plateauing around 120 min (**Figure 4.3**). It should be noted that the immediate reaction seen by NMR is a consequence of the higher concentration regime utilized for NMR (4.45 mM **IV.4**) versus photophysical (25 μM **IV.4**) studies. The corresponding absorbance spectra show steady consumption of NBu_4SH at 270 nm (**Figures 4.11, 4.13, and 4.15**) along with a steady increase in

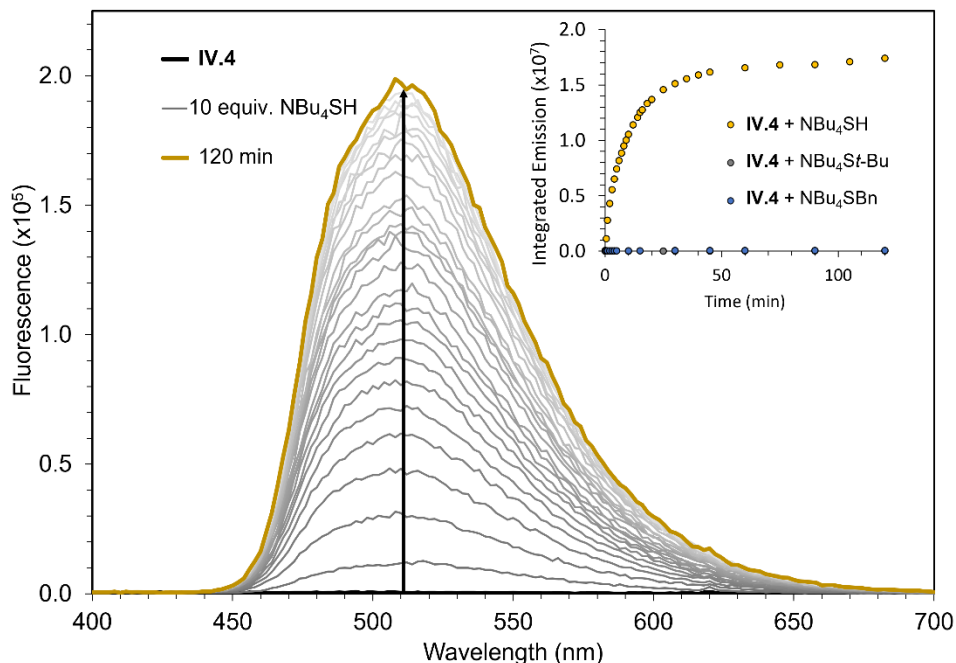


Figure 4.3. Time-course fluorescence (excitation 310 nm) of **IV.4** (25 μ M in acetonitrile) before and after addition of 10 equiv of NBu_4SH over 120 min. Inlay: integrated fluorescence of **IV.4** over 120 min in the presence of 10 equiv of NBu_4SH , $\text{NBu}_4\text{St-Bu}$, or NBu_4SBn .

absorbance around 375 and 425 nm, attributed to formation of DNT (**Figure 4.4**, top). In contrast, the absorbance of the nanohoop (320 nm) remains relatively constant over the course of the experiment, as expected, since **IV.1** and **IV.4** have similar absorption profiles.

Curiously, at the end of experiments using 50 or 100 equiv of the nucleophile, a slightly decreased maximum fluorescence emission is observed. Consistent with this observation, a separate control experiment (**Figure 4.36**) demonstrated a slight decrease in fluorescence when the free nanohoop **IV.1** was treated with 10 equiv of NBu_4SH in the absence of the thread, which may explain the lower overall fluorescence observed with high NBu_4SH concentrations. The same decrease in fluorescence of **IV.1** is not observed when in the presence of up to 100 equiv of NBu_4Cl (**Figure 4.37**) suggesting that high concentrations of HS^- can slightly modulate the fluorescence of the nanohoop. A Stern–Volmer analysis of this system (**Figure 4.38**) suggests this is likely due to dynamic/collisional quenching. These concentrations of NBu_4SH , however, are significantly higher than would be found in biological systems.

At the outset of this work, we hypothesized that the steric hindrance created by interlocking the reactive thread within the compact nanohoop should enhance selectivity for small nucleophiles

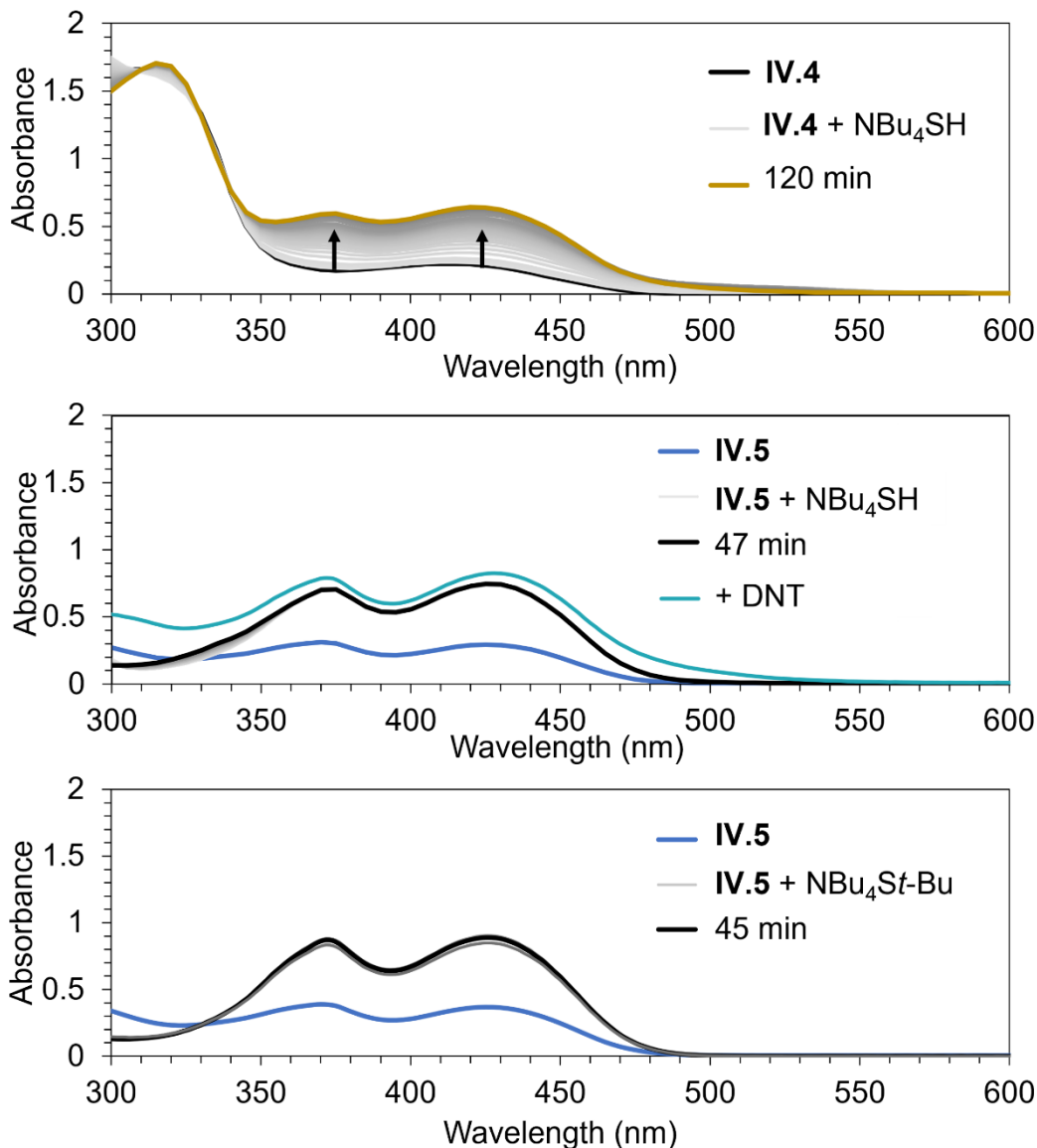


Figure 4.4. Time-course UV-vis spectra of **IV.4** with 10 equiv of NBu_4SH (top) and of **IV.5** with 10 equiv of NBu_4SH followed by addition of DNT (middle) and **IV.5** with 10 equiv of $\text{NBu}_4\text{St-Bu}$ (bottom). All probe concentrations are $25\ \mu\text{M}$ each in acetonitrile.

such as $\text{H}_2\text{S}/\text{HS}^-$. To investigate this size-based selectivity, we next repeated these experiments with both $\text{NBu}_4\text{St-Bu}$ and NBu_4SBn , more sterically demanding thiolates. After 120 min in the presence of the larger nucleophiles, we observed virtually no turn-on fluorescence response, which is consistent with a significant steric selectivity for HS^- (**Figure 4.3**, inlay). To further confirm the effect of interlocking the reactive unit, free thread **IV.5** was also subjected to reaction with NBu_4SH , $\text{NBu}_4\text{St-Bu}$, and NBu_4SBn . In contrast to **IV.4**, free thread **IV.5** shows an immediate

growth of peaks at 375 and 425 (DNT) without change over time (**Figure 4.4**, middle/bottom), suggesting that the free thread reacts nearly instantaneously regardless of nucleophile identity. Finally, in a competition experiment, both **IV.4** and **IV.5** were combined (25 μM each) with $\text{NBu}_4\text{S}t\text{-Bu}$ or NBu_4SBn (125 μM) and observed over time. While there is no change seen in the fluorescence spectrum over 30 min, addition of either thiolate results in the immediate appearance of $\text{S}_{\text{N}}\text{Ar}$ byproduct peaks in the UV-vis spectra, consistent with the breakdown of free thread **IV.5** only. Taken together, these results confirm the successful enhancement of selectivity for this particular reactive probe via mechanical interlocking. We hypothesize that this concept will be broadly applicable to enhancing the selectivity of reaction probes for smaller analytes.

4.3. Conclusion

In summary, we have designed a turn-on fluorescent probe for HS^- that shows excellent selectivity over $t\text{-BuS}^-$ and BnS^- . This study suggests the utility of such rotaxane-based probes to tune the size selectivity of reactive sensors due to the unique steric environment imparted by the mechanical bond. In conjunction with recent work in our laboratory toward creating biocompatible nanohoops for biological imaging/sensing, the development of these rotaxane sensor systems that can operate in aqueous media is an important and feasible next step.⁵⁵ We also note that the sensor reported here contains a symmetric thread where either end can function as a trigger. Future work investigating unsymmetric thread units that impart these nanohoop rotaxane sensors with enhanced function (e.g., payload release) is ongoing and will be reported in due course.

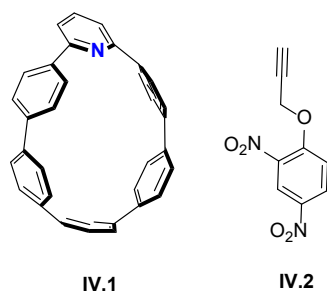
4.4. Experimental Sections

4.4.1. General Experimental Details

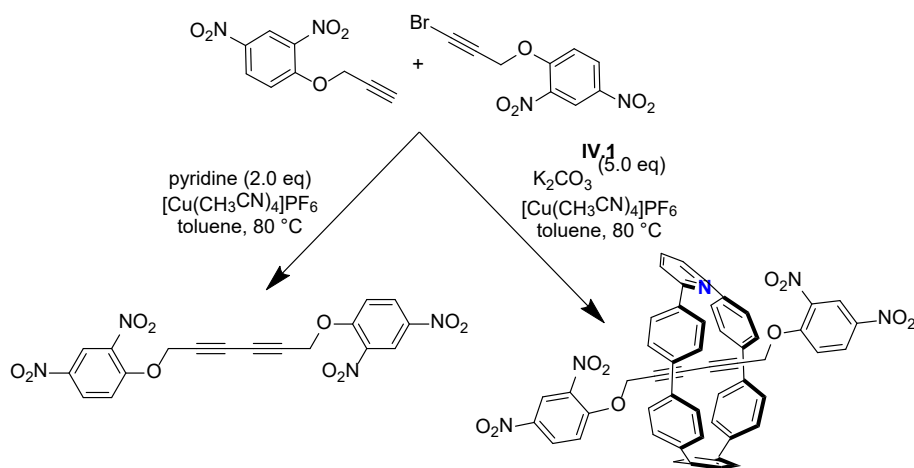
Moisture/air sensitive reactions were carried out under nitrogen atmosphere using standard Schlenk technique with flame-dried glassware cooled under an inert atmosphere of nitrogen. Solvents used for moisture/air sensitive reactions were dried by filtration through alumina and stored under an inert argon atmosphere. Silica column chromatography was conducted with Zeochem Zeoprep 60 Eco 40-63 μm silica gel and automated flash chromatography was performed using a Biotage Isolera One. Recycling gel permeation chromatography (GPC) was performed using a Japan Analytical Industry LC-9101 preparative HPLC with JAIGEL-1H/JAIGEL-2H columns with CHCl_3 . Absorbance and fluorescence spectra were obtained in a 1 cm Quartz cuvette

with dichloromethane, or deionized water using an Agilent Cary 60 or Cary 100 UV-Vis spectrometer and a Quanta Master 40 spectrofluorometer (Photon Technology International) equipped with a Quantum Northwest TLC-50 temperature controller at 25.0 ± 0.05 °C. IR spectra were measured on a Thermo Scientific Nicolet 6700 RT-IR using an ATR attachment.

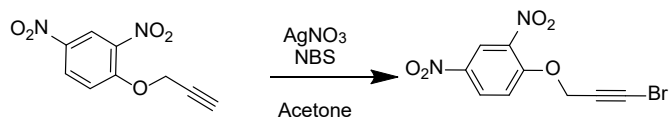
NMR spectra were recorded at 500 MHz or 600 MHz on a Bruker Advance-III-HD NMR spectrometer. All ^1H NMR spectra were taken in $(\text{CD}_3)_2\text{CO}$ (referenced to acetone, δ 2.05 ppm), CD_3CN (referenced to MeCN, δ 1.96 ppm), CDCl_3 (referenced to TMS, δ 0.00 ppm). All ^{13}C NMR spectra are referenced to either residual $(\text{CD}_3)_2\text{CO}$ (29.84), or CDCl_3 (77.16 ppm). Mass spectra for **IV.3** and **IV.4** were acquired at the University of Illinois, Urbana Champaign MS Facility (TOF mass analyzer). Mass spectrum for **IV.5** obtained on a Xevo Waters ESI LC/MS instrument (TOF mass analyzer). All reagents were obtained commercially. Compounds **IV.1**³⁵, **IV.2**⁵⁶, (below) were prepared according to literature procedure.



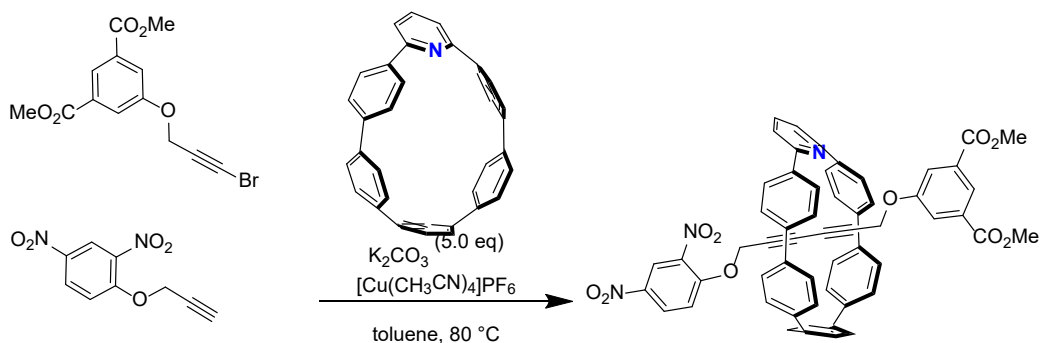
4.4.2. Synthesis and Characterization



Scheme 4.1. Synthesis of thread component **IV.3**, rotaxane **IV.4** (using macrocycle **IV.1**) and free thread **IV.5**.

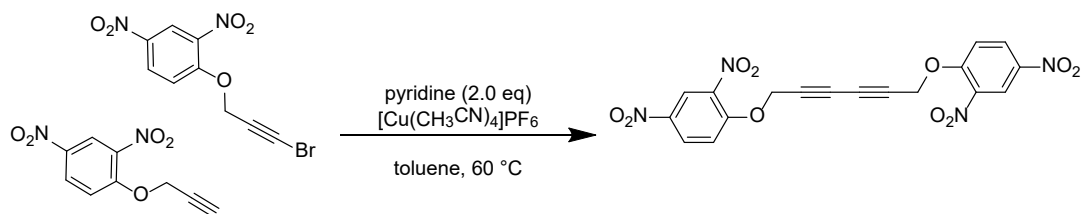


IV.3. To a 50 mL flask equipped with magnetic stir bar was added **IV.2** (0.101 mg, 0.450 mmol, 1.00 equiv.) followed by the addition of AgNO₃ (0.139 mg, 0.473 mmol, 1.05 equiv.) and N-bromosuccinimide (0.121 mg, 0.675 mmol, 1.50 equiv.) and 25 mL acetone. After stirring 1h at room temperature, the solvent was removed under reduced pressure. The resulting brown solid was loaded onto a short SiO₂ plug which was subsequently washed with 100% hexanes before eluting the product in 100% dichloromethane to yield the product as a straw-colored solid (0.132 mg, 95%). IR: 3113.63, 3088.81, 2237.22, 1599.99, 1513.09. ¹H NMR (500 MHz, Chloroform-*d*) δ 8.77 (d, *J* = 2.7 Hz, 1H), 8.47 (dd, *J* = 9.3, 2.8 Hz, 1H), 7.38 (d, *J* = 9.2 Hz, 1H), 5.01 (s, 2H). ¹³C NMR (126 MHz, Chloroform-*d*) δ 155.0, 140.9, 139.4, 128.9, 122.0, 115.1, 72.3, 58.7, 51.7. HRMS (EI⁺) *m/z*: [M]⁺ Calcd for C₉H₅BrN₂O₅, 299.9382; found, 299.9388.



IV.4. To a flame-dried 25 mL round bottom flask equipped with a magnetic stir bar was added **IV.1** (0.0200 mg, 0.0437 mmol, 1.00 equiv.), **IV.2** (0.0146 mg, 0.0656 mmol, 1.50 equiv.), **IV.3** (0.0193 mg, 0.0656 mmol, 1.50 equiv.), oven-dried K₂CO₃ (0.0302 g, 0.218 mmol, 5 equiv.) and [Cu(CH₃CN)₄]PF₆ (0.0155 mg, 0.0415 mmol, 0.950 equiv.), followed by five cycles of evacuation and refill with N₂. A septum was placed on the flask followed by the addition of 10.0 mL toluene. The reaction was heated to 80 °C (via oil bath) with stirring for 48 hours, with reaction progress monitored by TLC. Once complete, the reaction was cooled to room temperature and quenched with a solution of ethylenediaminetetraacetic acid (EDTA) in 15% NH₃ (3 mL) solution then

allowed to stir for 10 min. The layers were separated, and the aqueous phase was washed with dichloromethane (3x 20 mL). The combined organic phase was then washed with H₂O (3x 20 mL) and brine (1x 20 mL) then dried over sodium sulfate, filtered, and concentrated to yield an oily yellow solid. The crude material was purified by automated flash chromatography, eluted with 50-100% dichloromethane and hexanes to separate residual **IV.1** from the product. The resulting yellow solid was then purified via size exclusion chromatography to give the product as a bright yellow solid (7.2 mg, 18%.) IR: 2961.39, 2161.17, 1603.02, 1521.13, 1484.22. ¹H NMR (500 MHz, Chloroform-*d*) δ 8.69 (d, *J* = 2.8 Hz, 2H), 7.99 (dd, *J* = 9.2, 2.8 Hz, 2H), 7.86 (t, *J* = 7.7 Hz, 1H), 7.50 (d, *J* = 8.3 Hz, 6H), 7.41 (d, *J* = 8.8 Hz, 4H), 7.20 (s, 8H), 7.13 (d, *J* = 8.7 Hz, 4H), 6.14 (d, *J* = 9.2 Hz, 2H), 3.60 (s, 4H). ¹³C NMR (126 MHz, Acetone-*d*₆) δ 159.9, 154.6, 141.5, 140.7, 140.5, 139.5, 138.3, 137.9, 136.8, 136.4, 129.7, 128.3, 128.1, 127.9, 127.9, 127.8, 121.1, 116.5, 114.9, 71.7, 70.7, 58.3 ppm. HRMS (ES⁺) *m/z*: [M+H]⁺ Calcd for C₅₃H₃₄N₅O₁₀, 900.2306; found, 900.2304.



IV.5. To a flame-dried 25 mL round bottom flask equipped with a magnetic stir bar was added **IV.2** (0.0295 mg, 0.133 mmol, 1.00 equiv.) **IV.3** (0.0400 mg, 0.133 mmol, 1.00 equiv.) and [Cu(CH₃CN)₄]PF₆ (0.0248 mg, 0.0664 mmol, 0.500 equiv.), followed by five cycles of evacuation and refill with N₂. A septum was placed on the flask followed by the addition of 10.0 mL toluene and the addition of pyridine (0.0210 mL, 0.266 mmol, 2.00 equiv.) The reaction was heated to 80 °C (via oil bath) with stirring for 48 hours, with reaction progress monitored by TLC. Once complete, the reaction was cooled to room temperature and the solvent was removed under reduced pressure. The crude solid was purified by automated flash chromatography, eluted with 100% dichloromethane to obtain the product as a pale brown oily solid (23.1 mg, 39%.) IR: 3261.68, 3109.02, 3920.58, 2873.83, 1746.35, 1624.01, 1593.32, 1514.87, 1478.71. ¹H NMR (500 MHz, Acetone-*d*₆) δ 8.76 (d, *J* = 2.8 Hz, 1H), 8.58 (dd, *J* = 9.3, 2.8 Hz, 1H), 7.72 (d, *J* = 9.3 Hz, 1H), 5.27 (s, 2H). ¹³C NMR (126 MHz, Acetone-*d*₆) δ 155.6, 141.8, 140.5, 129.7, 122.1, 116.7, 74.3, 59.6, 51.3. MS (ASAP⁺) (*m/z*): [M+H]⁺ Calcd for C₁₈H₁₁N₄O₁₀, 443.0475; found, 443.0381.

4.4.3. ^1H NMR Studies

4.4.3.1. Reaction of Rotaxane **IV.4** with varying concentrations of NBu_4SH

Under inert atmosphere, 2.0 mg of **IV.4** was dissolved in 0.5 mL degassed, deut. MeCN in an NMR tube which was capped with a septum top and taped closed. A stock solution of NBu_4SH was also prepared in degassed MeCN under nitrogen immediately prior to use. Spectra were acquired on a 600 MHz Bruker Advance-III-HD. Instrument locked, tuned, and shimmed at 25 °C on the sample of **IV.4**. The sample was then ejected and 1 equivalent of NBu_4SH was transferred to the NMR tube using an air-tight Hamilton syringe and mixed well. Sample turned a red/orange upon addition of thiol. Instrument shimmed with new sample prior to obtaining ^1H spectrum.

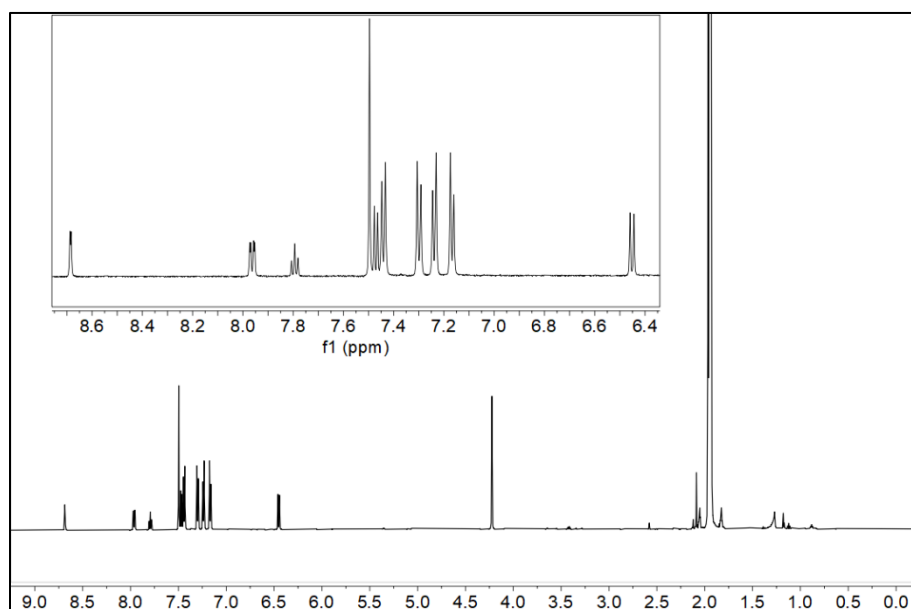


Figure 4.5. Rotaxane prior to addition of NBu_4SH in MeCN-d_3 .

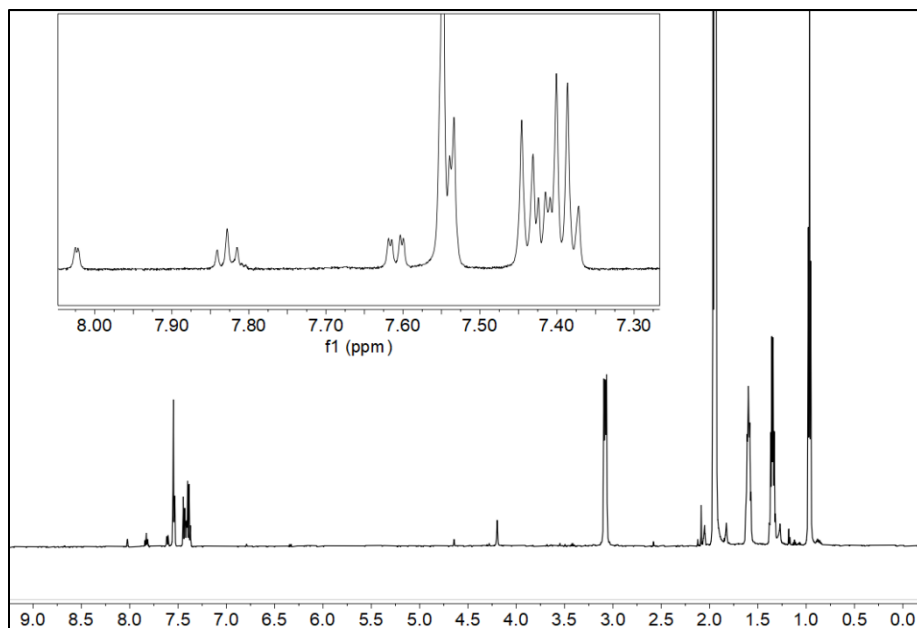


Figure 4.6. Rotaxane after addition of NBu₄SH in MeCN-*d*₃.

4.4.3.2. *S_NAr* Byproduct Studies

Under inert atmosphere, 10.0 mg of 2,4-dinitrothiol (an authentic sample of the expected product of *S_NAr*) was dissolved in 0.5 mL degassed, deut. MeCN in an NMR tube which was capped with a septum top and taped closed. A stock solution of NBu₄SH was also prepared in degassed MeCN under nitrogen immediately prior to use. Spectra were acquired on a 500 MHz Bruker. Instrument locked, tuned, and shimmed at 25 °C on the sample of 2,4-dinitrothiol (DNT). The sample was then ejected and 1 equivalent of NBu₄SH was transferred to the NMR tube using an air-tight Hamilton syringe and mixed well. Sample turned a deeper orange upon addition of thiol. Instrument shimmed with new sample prior to obtaining ¹H spectrum.

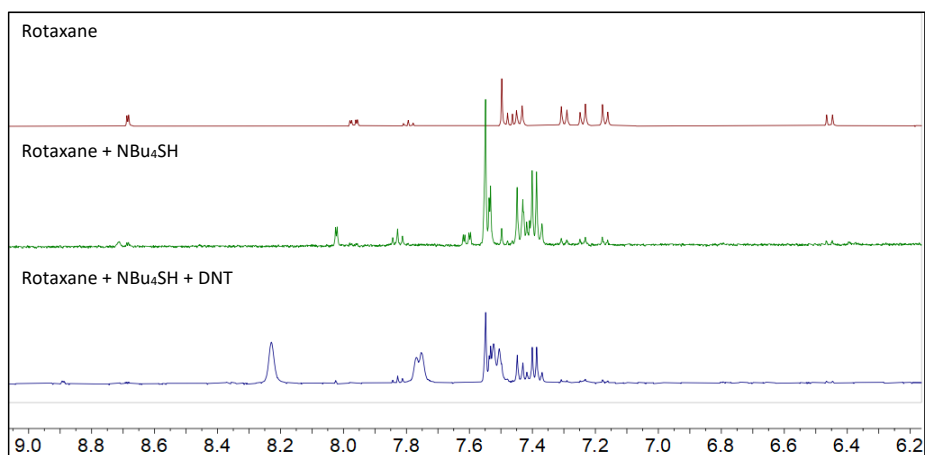


Figure 4.7. Aromatic region of ^1H NMR of (top) **IV.4**, (middle) **IV.4** and NBu_4SH , and (bottom) **IV.4**, NBu_4SH and DNT.

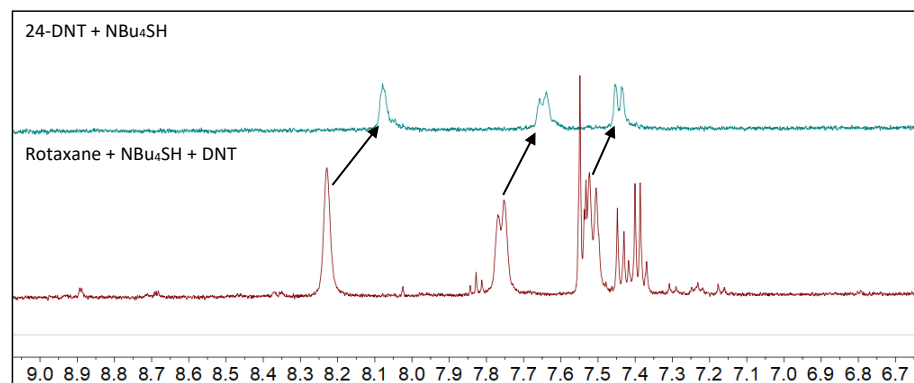


Figure 4.8. Aromatic region of ^1H NMR of (top) DNT and NBu_4SH and (bottom) **IV.4**, NBu_4SH and DNT.

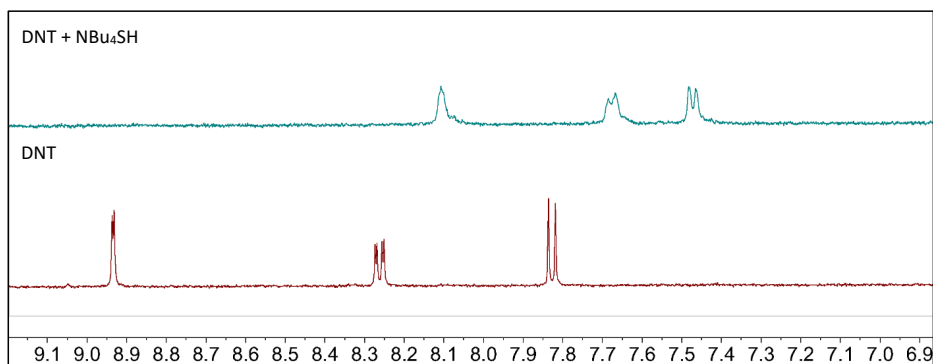


Figure 4.9. Aromatic region of ^1H NMR of (top) DNT in the presence of NBu_4SH and (bottom) DNT.

4.4.4. Photophysical Studies

Stock solutions of the rotaxane probe (**IV.4**), nanohoop (**IV.1**), thread (**IV.5**), and NBu₄SH or NBu₄St-Bu were prepared in degassed DCM or MeCN under nitrogen immediately prior to use and were introduced into cuvettes filled with 3 mL degassed MeCN with an air-tight Hamilton syringe. To ensure accurate measurements and to prevent decomposition of potentially reactive species, all experiments were performed under an inert atmosphere unless otherwise indicated. Fluorescence was measured using a Quanta Master 40 spectrofluorometer (Photon Technology International) equipped with a Quantum Northwest TLC-50 temperature controller at 25.0 ± 0.05 °C. All fluorescence measurements were made under an inert atmosphere in septum-sealed cuvettes obtained from Starna Scientific, with both excitation and emission slit widths set to 0.4 mm. Fluorescence spectra were collected with 0.1 s integration and 2 nm step size. UV/Vis spectra were acquired on an Agilent Cary 60 or Agilent Cary 100 UV/Vis spectrophotometer equipped with a Quantum Northwest TC-1 temperature controller set at 25 ± 0.05 °C. NBu₄SH⁵⁷ was prepared according to the literature, the same approach was used to make NBu₄St-Bu and NBu₄SBn.

4.4.4.1. Reaction of Rotaxane **IV.4** with varying concentrations of NBu₄SH

A 10 mM stock solution of symmetric rotaxane **IV.4** was prepared in DCM and a 100 mM stock solution of NBu₄SH was prepared in MeCN under N₂. 3.0 mL of degassed MeCN in a septum sealed cuvette was scanned as a blank for both fluorescence and absorbance, after which 7.5 μL of the rotaxane solution was added to make a 25 μM solution. 7.5, 37.5, or 75 μL of 100 mM NBu₄SH stock was added for the 10, 50, and 100 equivalent reactions, respectively. For fluorescence, the excitation wavelength was set to 310 nm, and the emission was measured from 350 – 700 nm, with a 2 nm step size. Absorbance was measured from 250 – 700 nm.

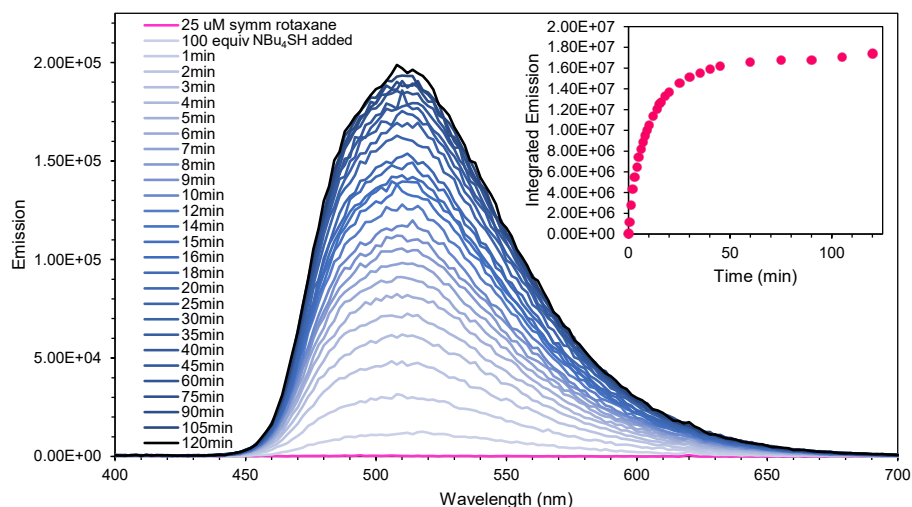


Figure 4.10. Fluorescence of IV.4 over time with 10 equiv of NBu_4SH added.

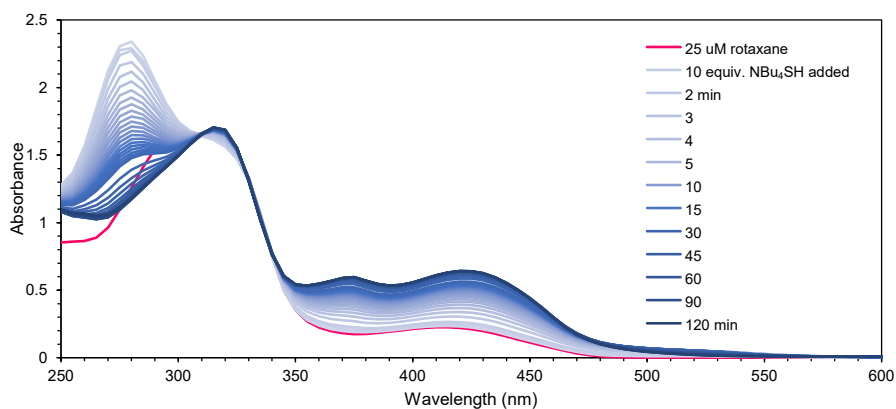


Figure 4.11. Absorbance of IV.4 over time with 10 equiv of NBu_4SH added.

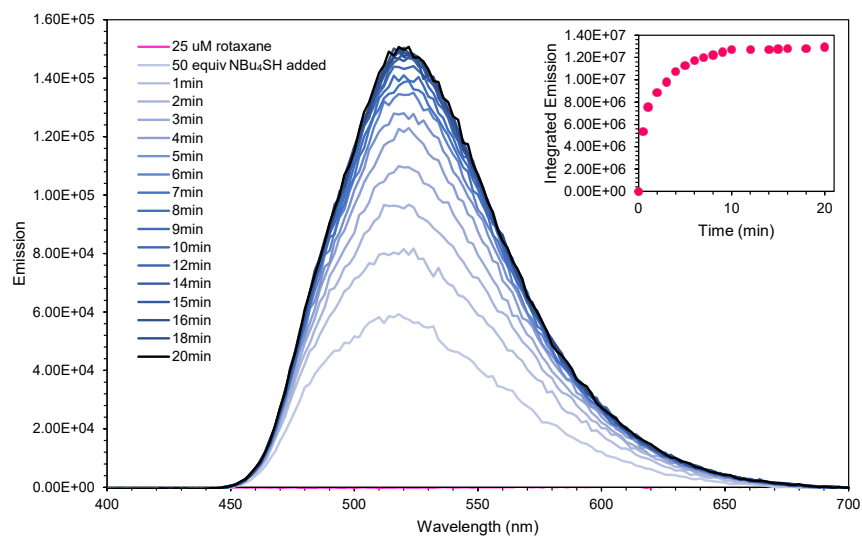


Figure 4.12. Fluorescence of IV.4 over time with 50 equiv of NBu_4SH added.

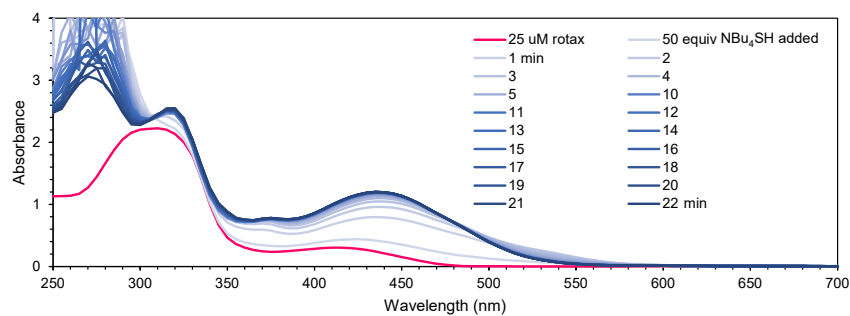


Figure 4.13. Absorbance of IV.4 over time with 50 equiv of NBu₄SH added.

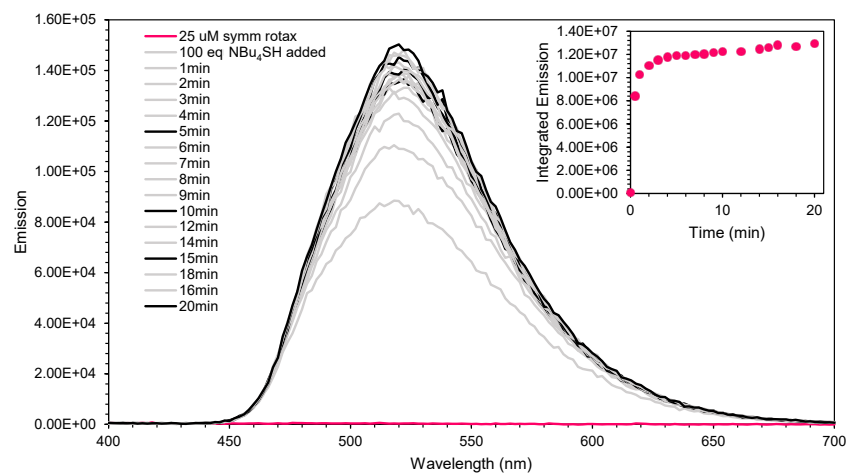


Figure 4.14. Fluorescence of IV.4 over time with 100 equiv of NBu₄SH added.

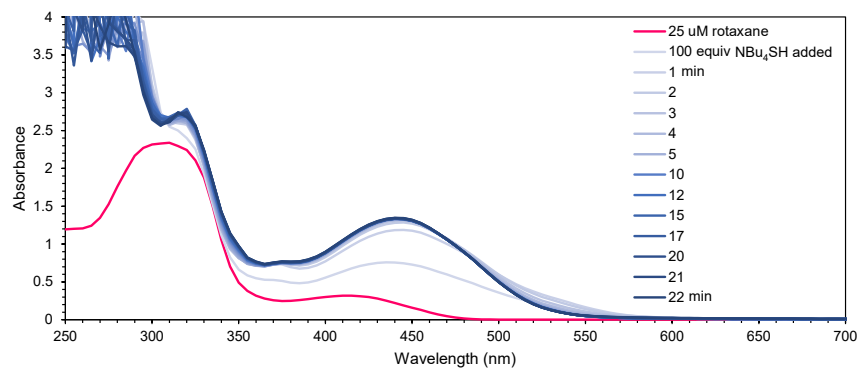


Figure 4.15. Absorbance of IV.4 over time with 100 equiv of NBu₄SH added.

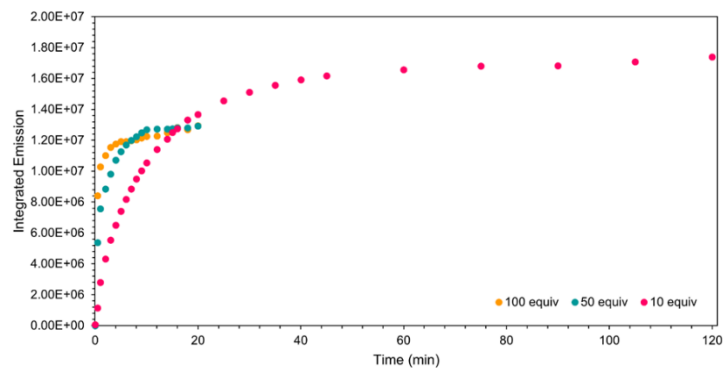


Figure 4.16. Comparison of integrated emission vs. time for **IV.4** with varying concentrations of NBu_4SH .

4.4.4.2. Reaction of Rotaxane **IV.4** with of $\text{NBu}_4\text{St-Bu}$ and NBu_4SBn

A 10 mM stock solution of symmetric rotaxane **IV.4** was prepared in DCM and a 10 mM stock solution of NBu_4SR was prepared in MeCN under N_2 . 3.0 mL of degassed MeCN in a septum sealed cuvette was scanned as a blank for both fluorescence and absorbance, after which 7.5 μL of thread stock was added to make a 25 μM solution, and then 75 μL of NBu_4SR stock was added. For fluorescence, the excitation wavelength was set to 310 nm, and the emission was measured from 350 – 700 nm, with a 2 nm step size. Absorbance was measured from 250 – 700 nm.

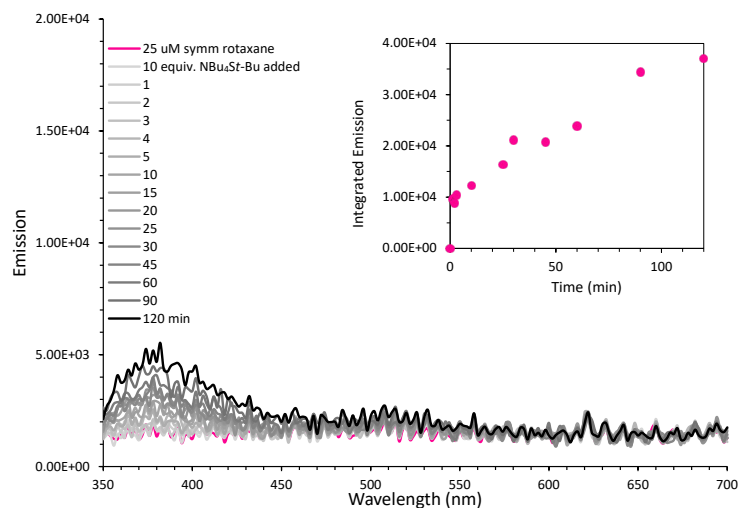


Figure 4.17. Fluorescence of **IV.4** over time with 10 equiv of $\text{NBu}_4\text{St-Bu}$ over time. Inlay: integrated fluorescence over time.

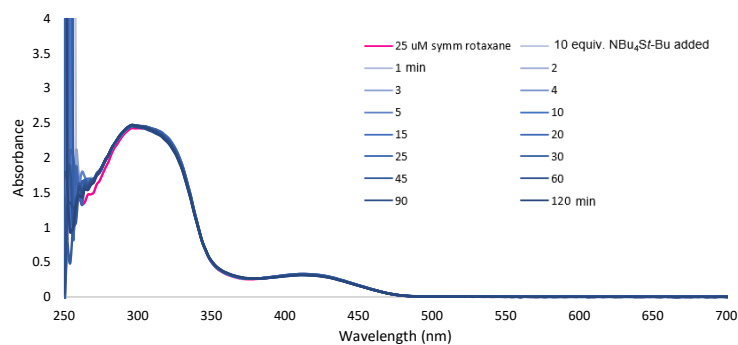


Figure 4.18. Absorbance of IV.4 over time with 10 equiv of $\text{NBu}_4\text{St-Bu}$ over time.

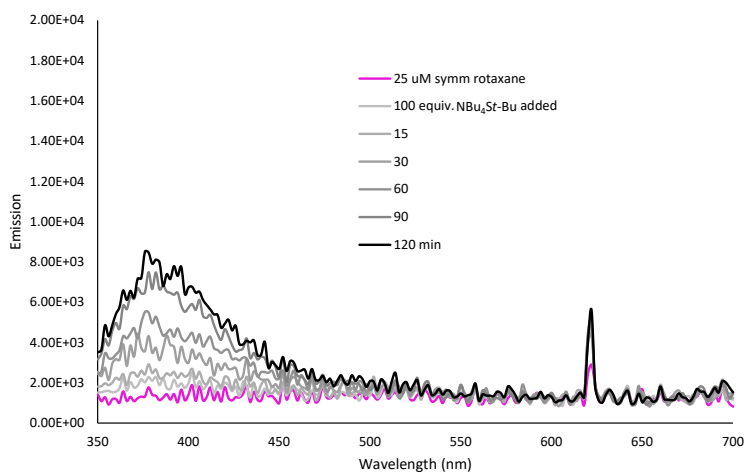


Figure 4.19. Fluorescence of IV.4 over time with 100 equiv of $\text{NBu}_4\text{St-Bu}$ over time. The sharp signal at 620 nm is an artifact of the fluorimeter.

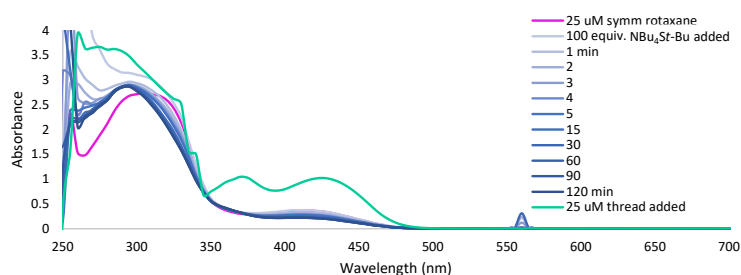


Figure 4.20. Absorbance of IV.4 over time with 100 equiv of $\text{NBu}_4\text{St-Bu}$ over time, spiked with thread IV.5 after 120 minutes to ensure thiolate remains reactive.

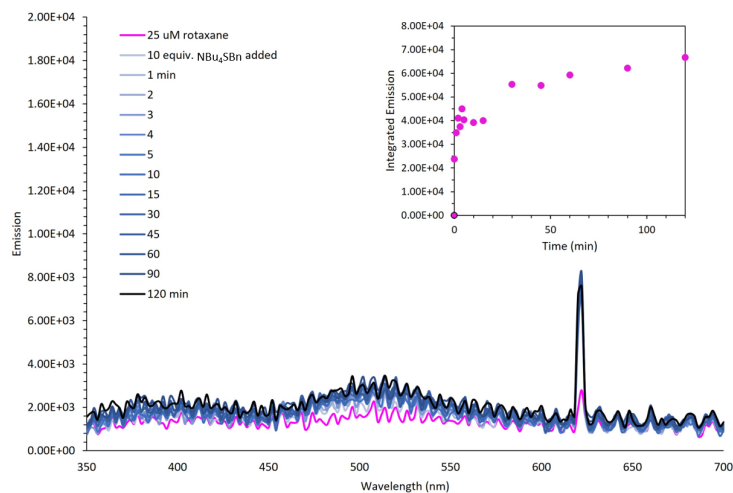


Figure 4.21. Fluorescence of **IV.4** over time with 10 equiv of NBu_4SBn over time. Inlay: integrated fluorescence over time. The sharp signal at 620 nm is an artifact of the fluorimeter.

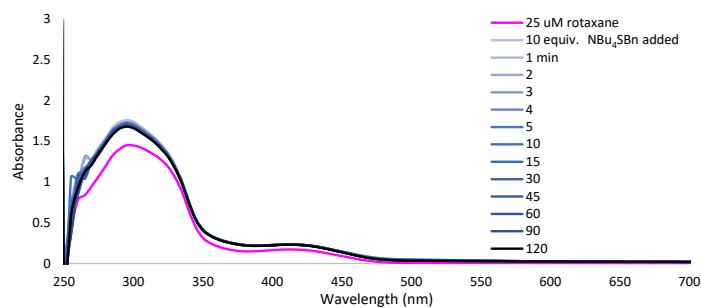


Figure 4.22. Absorbance of **IV.4** over time with 10 equiv of NBu_4SBn over time.

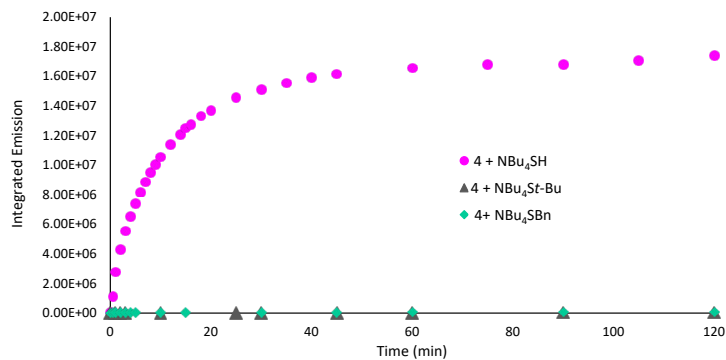


Figure 4.23. Comparison of integrated emission vs. time for **IV.4** with 10 equiv of NBu_4SH , $\text{NBu}_4\text{St-Bu}$, and NBu_4SBn .

4.4.4.3. Reaction of thread **IV.5** with NBu_4SR

A 10 mM stock solution of symmetric thread **IV.5** was prepared in DCM and a 100 mM stock solution of NBu_4SH was prepared in MeCN under N_2 , and 10 mM stock solution of NBu_4SR was prepared in MeCN. 3.0 mL of degassed MeCN in a septum sealed cuvette was scanned as a blank for both fluorescence and absorbance, after which 7.5 μL of the thread stock was added to make a 25 μM solution. 7.5 and 75 μL of 100 mM NBu_4SH and 10 mM NBu_4SR stock were added, respectively. For Fluorescence, the excitation wavelength was set to 310 nm, and the emission was measured from 350 – 700 nm, with a 2 nm step size. Absorbance was measured from 250 – 700 nm.

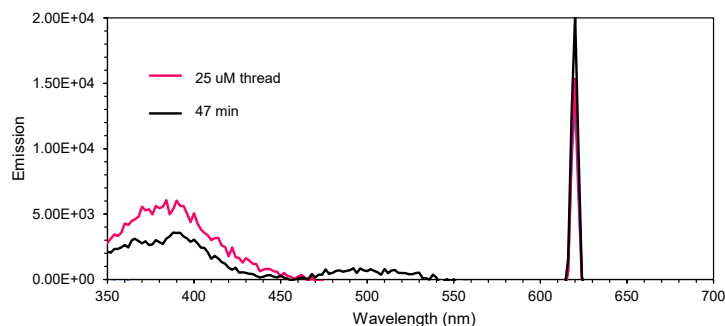


Figure 4.24. Fluorescence of **IV.5** before and after 10 equiv of NBu_4SH was added. The sharp signal at 620 nm is an artifact of the fluorimeter.

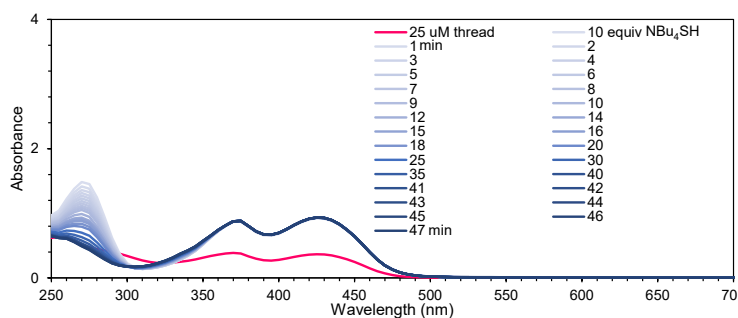


Figure 4.25. Absorbance over time of **IV.5** with 10 equiv of NBu_4SH .

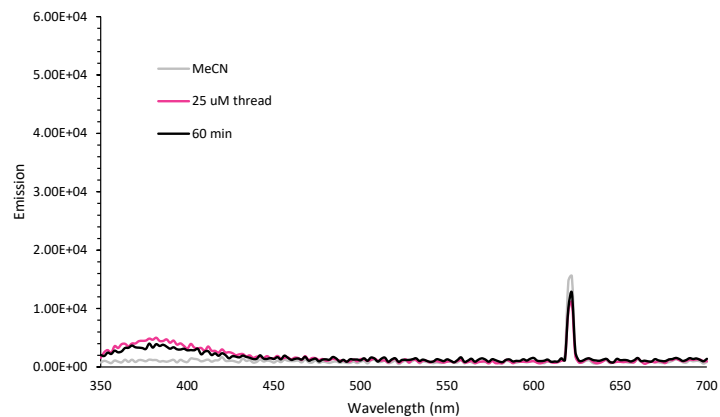


Figure 4.26. Fluorescence of **IV.5** before and after 10 equiv of $\text{NBU}_4\text{St-Bu}$ was added. The sharp signal at 620 nm is an artifact of the fluorimeter.

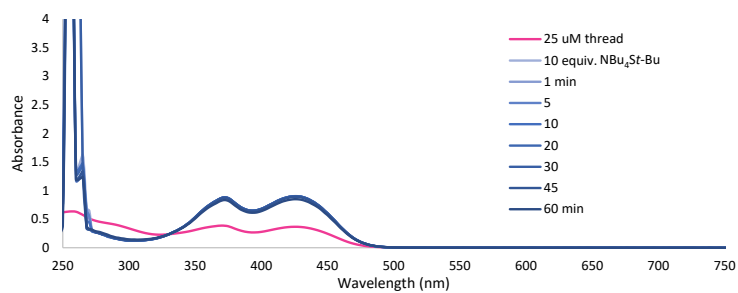


Figure 4.27. Absorbance over time of **IV.5** with 10 equiv of $\text{NBU}_4\text{St-Bu}$ was added.

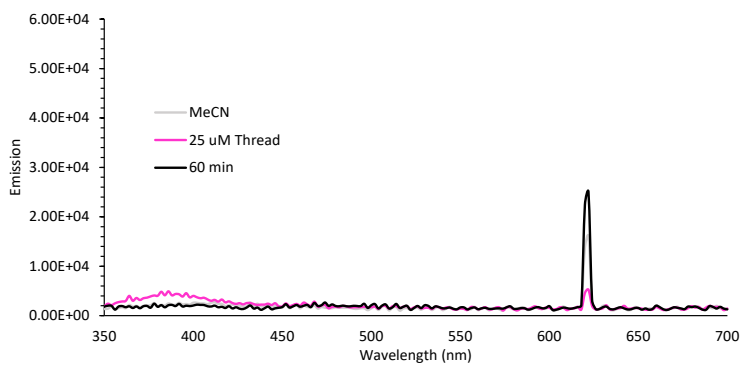


Figure 4.28. Fluorescence of **IV.5** before and after 10 equiv of NBU_4SBn was added. The sharp signal at 620 nm is an artifact of the fluorimeter.

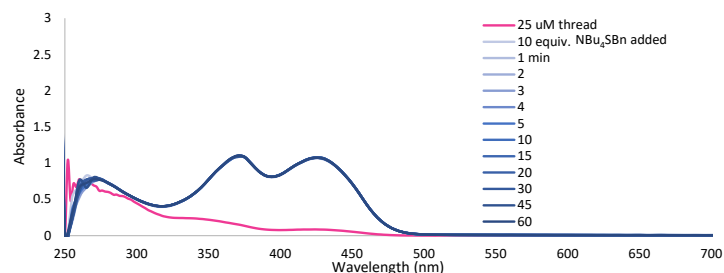


Figure 4.29. Absorbance over time of **IV.5** before and after 10 equiv of NBu_4SBn was added.

4.4.4.4. Rotaxane/Thread Competition Experiment

10 mM stock solutions of **IV.4** and **IV.5** were prepared in DCM and 100 mM stock solutions of NBu_4SR were prepared in MeCN under N_2 . 3.0 mL of degassed MeCN in a septum sealed cuvette was scanned as a blank for both fluorescence and absorbance, after which 7.5 μL of each the rotaxane and thread stocks were added to make a final concentration of 25 μM of each. 37.5 μL of 100 mM NBu_4SR was added for a final concentration of 125 μM . For Fluorescence, the excitation wavelength was set to 310 nm, and the emission was measured from 350 – 700 nm, with a 2 nm step size. Absorbance was measured from 250 – 700 nm.

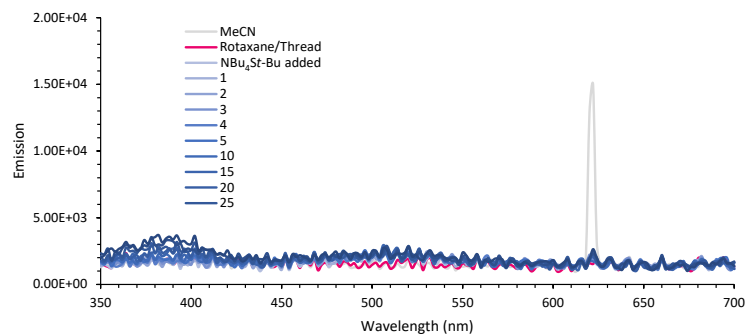


Figure 4.30. Fluorescence over time of **IV.4** and **IV.5** with $\text{NBu}_4\text{St-Bu}$. The sharp signal at 620 nm is an artifact of the fluorimeter.

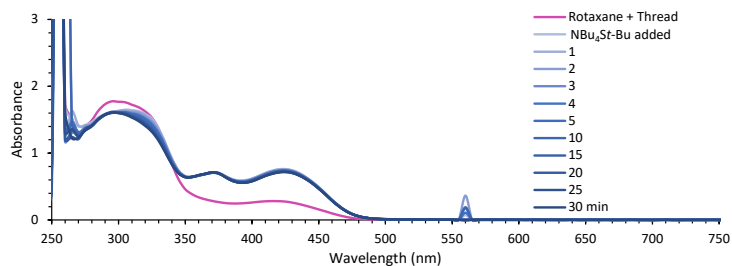


Figure 4.31. Absorbance over time of **IV.4** and **IV.5** with $\text{NBu}_4\text{St-Bu}$.

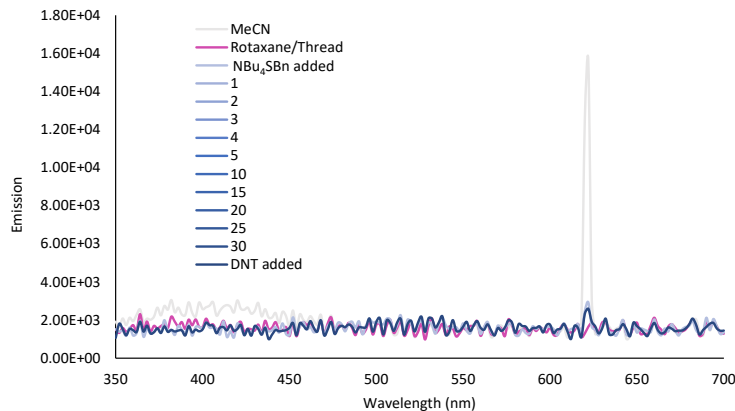


Figure 4.32. Fluorescence over time of **IV.4** and **IV.5** with NBu_4SBn . The sharp signal at 620 nm is an artifact of the fluorimeter.

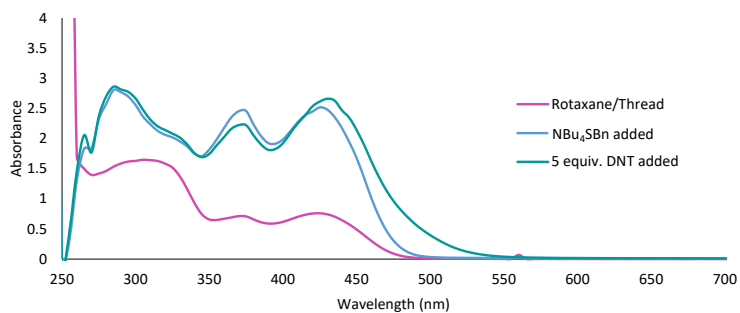


Figure 4.33. Absorbance over time of **IV.4** and **IV.5** with NBu_4SBn . DNT added 30 minutes after the addition of thiolate.

4.4.4.5. S_NAr Byproduct Studies

Stock solutions (10 mM) of thread **IV.5** and DNT were prepared in DCM and MeCN, respectively. Stock solutions (100 mM) of NBu_4SH and $\text{NBu}_4\text{St-Bu}$ were prepared in MeCN under N_2 . 3.0 mL of degassed MeCN in a septum sealed cuvette was scanned as a blank. Absorbance was measured from 250 – 700 nm.

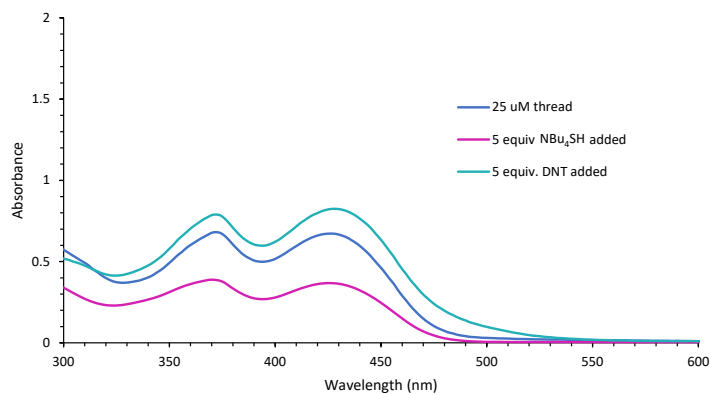


Figure 4.34. Absorbance of thread **IV.5** with NBu_4SH and DNT.

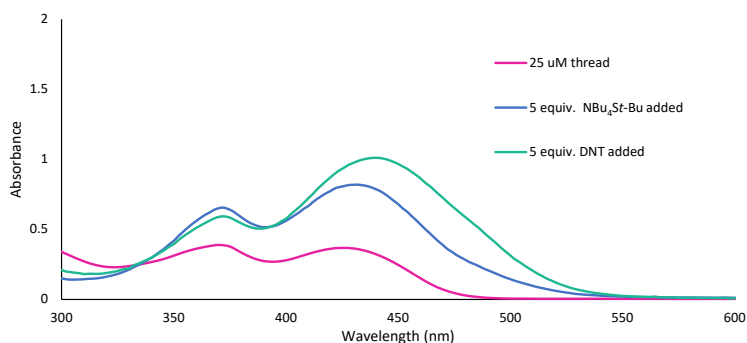


Figure 4.35. Absorbance of thread **IV.5** with $\text{NBu}_4\text{St-Bu}$ and DNT.

4.4.4.6. Control Reactions

A 10 mM stock solution of nanohoop **IV.1** was prepared in DCM, and 100 mM stock solutions of NBu_4SH and NBu_4Cl were prepared in MeCN under N_2 . 3.0 mL of degassed MeCN in a septum sealed cuvette was scanned as a blank for both fluorescence and absorbance. For fluorescence, the excitation wavelength was set to 310 nm, and the emission was measured from 350 – 700 nm, with a 2 nm step size. Absorbance was measured from 250 – 700 nm.

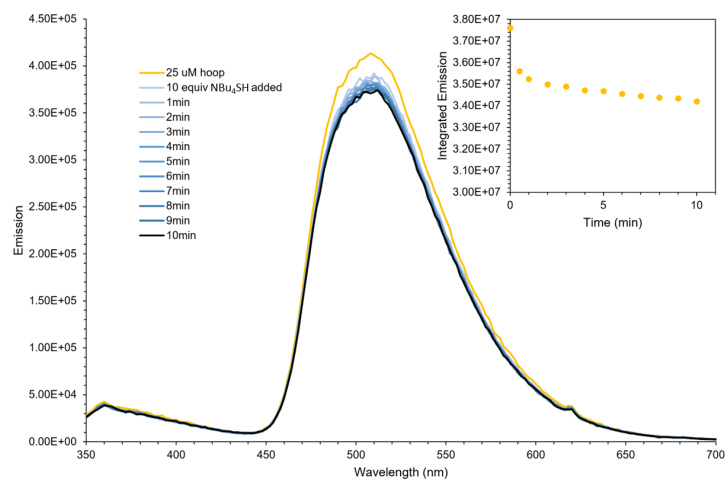


Figure 4.36. Fluorescence of macrocycle **IV.1** with NBu_4SH over time; inlay: integrated fluorescence.

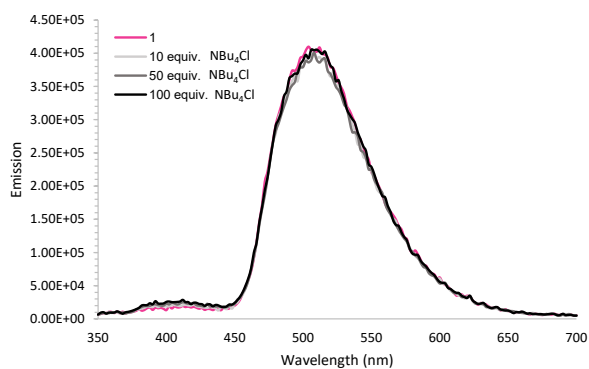


Figure 4.37. Fluorescence of macrocycle **IV.1** with increasing equiv (10-100) of NBu_4Cl .

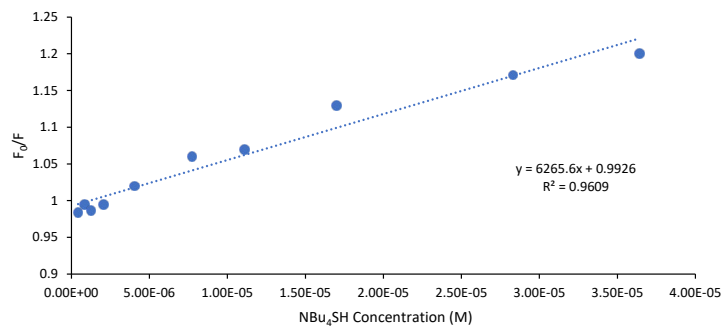


Figure 4.38. Stern-Volmer analysis of fluorescence quenching of **IV.1** of NBu₄SH. Stock solutions of **IV.1** (1.8 μM) in 1% DCM/MeCN and NBu₄SH (8.5 μL) in dry MeCN were prepared. To a 2.0 mL solution of **IV.1** were added aliquots of NBu₄SH and the change in fluorescent intensity of **IV.1** at 520 nm was measured. K_{SV} was determined by using the following **Equation IV.1**

$$\frac{F_0}{F} = 1 + K_{SV}[\text{NBu}_4\text{SH}] \quad \text{(Equation IV.1)}$$

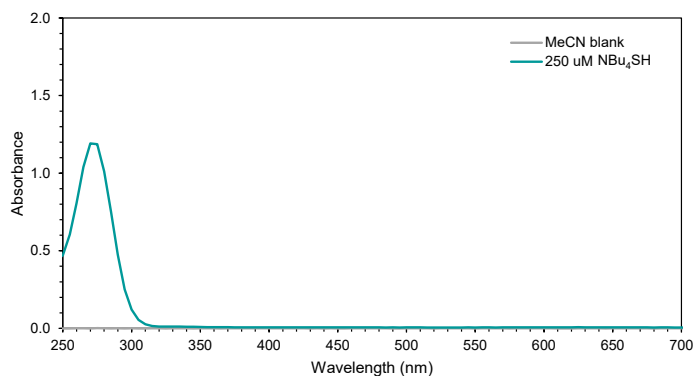


Figure 4.39. Absorbance of 250 μM NBu₄St-Bu in MeCN.

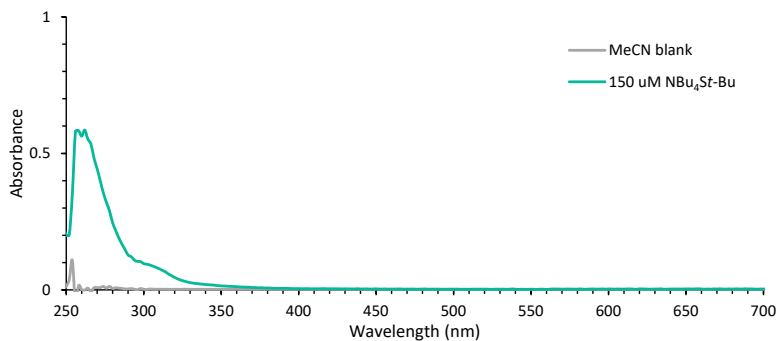


Figure 4.40. Absorbance of 150 μM NBu₄SBn in MeCN.

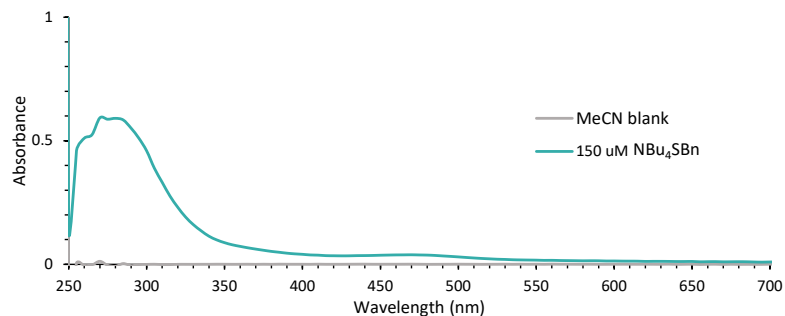


Figure 4.41. Absorbance of 150 μM NBu₄SH in MeCN.

4.5. Bridge to Chapter V

This chapter detailed the development of a nanohoop-based rotaxane probe for use in sensing biologically relevant analytes. Interlocking of a reactive thread unit within a compact nanohoop fluorophore effectively modulated the reactivity of the thread component to greatly enhance the selectivity of our probe for HS⁻ over other sulfide nucleophiles. The following chapter discusses our work towards further developing these nanohoop-[2]rotaxane sensors for use in biological systems via rendering the rotaxanes biologically compatible and exploring alternative trigger motifs to illustrate the modularity of our system.

CHAPTER V

TOWARDS THE DEVELOPMENT OF MODULAR NANOHOOP-[2]ROTAXANES FOR BIOLOGICAL SENSING APPLICATIONS

This chapter includes unpublished co-authored material, it was written by myself, with editorial assistance from Professor Ramesh Jasti. Experimental work in this chapter was performed by myself or Phyllis Liao under my direction, with experimental guidance provided by Professor Ramesh Jasti.

To build off our success in developing a hydrosulfide sensing nanohoop-[2]rotaxane, we have begun to explore the modularity of this scaffold of these architectures towards use in biological sensing. In order to do this, we first explore the biological compatibility and water-solubility of the rotaxane probes via appending solubilizing groups to the nanohoop used for rotaxane synthesis. In addition, we have begun to explore making probes for other biologically relevant species, specifically reactive oxygen species.

5.1. Introduction

Our ability to accurately sense, target, and deliver analytes in vivo inherently limits our spatiotemporal understanding of small-molecule behavior in complex biological systems.¹⁻⁵ The development of sensors for biologically relevant analytes is a continuously growing field of research allowing researchers to better understand disease states, progression, and treatment.^{1,3,6-8} Multifunctional probes designed for these purposes are often based on inclusion or host-guest complexes, however these systems rely on retaining affinity and selectivity in complex biological media, reducing overall fidelity.⁹⁻¹⁰ As previously illustrated by our lab, nanohoops are robust fluorophores poised for use in a biological setting,¹¹⁻¹² and among biologically relevant fluorophores, nanohoops are exceptional in that they are also shape-persistent macrocycles that have found utility in the construction of mechanically interlocked molecules (MIMs) such as rotaxanes and catenanes.¹³ In Chapter 4 of this work, we described the development of a proof-of-concept nanohoop-[2]rotaxane probe which successfully enhanced the selectivity of a reactive probe for the gasotransmitter H₂S (**Figure 5.1a**, right).¹⁴ This work illustrated the advantage of

integrating nano hoops into mechanically interlocked molecules (MIMs) used for sensing, as the small, rigid nature of these macrocycles was key to enhancing the selectivity of the probe. Importantly, MIMs, while similar to the supramolecular systems, generally benefit from the enhanced stability conferred by the mechanical bond, and often serve to protect a reactive thread motif.^{9,15-16} This protective capability was further illustrated in a collaboration with Anderson et. al. in which the same *mN*[6]CPP described in Chapter 4 was used to protect a highly reactive 14-

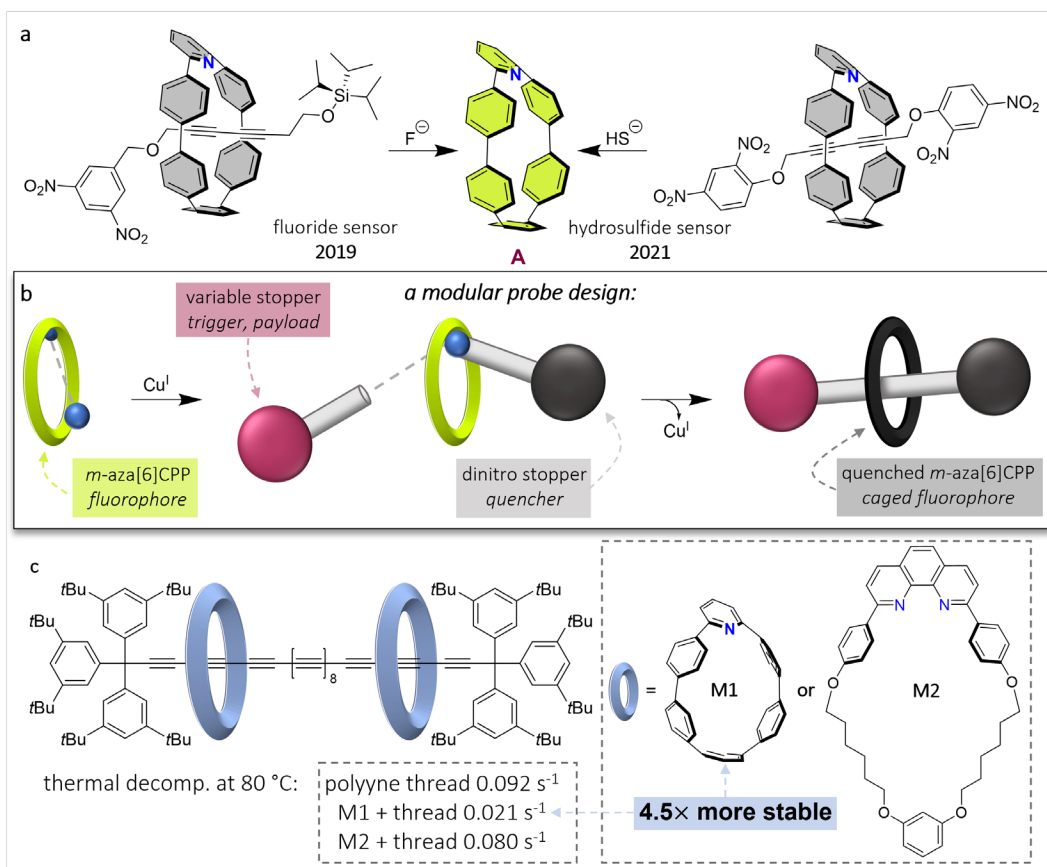


Figure 5.1. A) Previously developed nano hoop-[2]rotaxane sensors for fluoride²⁶ (left) and hydrosulfide¹⁴ (right) highlight the potential for this scaffold in sensing; b) the rotaxane design offers a modular synthesis comprised of three components: a nano hoop fluorophore also serves as protection for a reactive thread, a dinitro-substituted aromatic ring serves as stopper and quencher when interlocked, and a second stopper could serve as a trigger and/or potentially a payload for theranostic applications in the future. C) The small, rigid nano hoop provides substantially better protection for a reactive poly-yne thread than the larger, more flexible **M2**.¹⁷

alkyne thread, even at elevated temperatures, outperforming the alternative, more flexible macrocycle (**Figure 5.1c**).¹⁷

Due to their unique architecture, a great deal of effort has been put forth towards developing MIMs for biomedical research.^{9,18-19} Thus far rotaxanes have been used as biological near-IR squaraine dyes, fluorescent metal ion sensors, hosts for cellular transport, and autonomous peptide delivery, while (pseudo)rotaxane nanovalves for drug delivery have also been heavily developed by Stoddart and coworkers.²⁰⁻²⁴ Still, applying MIMs in biological research remains challenging owing to the difficulty in designing systems that are both soluble and functional in aqueous media.⁹ While our H₂S probe proved successful in organic media, developing this system as a modular family of rotaxane probes for biological species first requires making the system biologically compatible. For this we envision creating a water-soluble version of macrocycle **A** based on recent success with an all-carbon *m*[6]CPP analog used for cell imaging via appendage of a PEG chain with an attached morpholine moiety (**Figure 5.2**, bottom left insert.)²⁵ Additionally, we aim to explore the modularity in rotaxane design beyond our initial proof-of-principle systems (**Figure 5.1**, top) via incorporation of alternative trigger motifs and potential payloads; recent efforts towards these goals are described herein.

5.2. Results and Discussion

5.2.1. Work Towards Biological Compatibility

As mentioned above, *meta*-pyridyl nanohoop **A** used for rotaxane formation is analogous to the all carbon *m*[6]CPP that has successfully been rendered biologically compatible for organelle targeted cell imaging.²⁵ This approach was based on the incorporation of a pendant alkyne on the nanohoop which could be used for late stage conjugation with solubilizing groups via copper-catalyzed azide-alkyne cycloaddition (CuAAC.) Additionally, a similar alkyne-functionalized *mN*[6]CPP (**C**) had previously been synthesized for the development of nanohoop-based daisy chains, which served as a starting point for this synthesis.²⁶ As expected, CuAAC of **C** with an azide-functionalized PEG linker yielded a water soluble nanohoop in good yield (**Figure 5.2**). However, this PEG-functionalized nanohoop was likely to fail at the active template Cadiot-Chodkewitz (ATCC) due to the addition of many heteroatoms which could obscure the macrocycle's pyridine or simply outcompete for coordination of the copper catalyst required for formation of the mechanical bond.

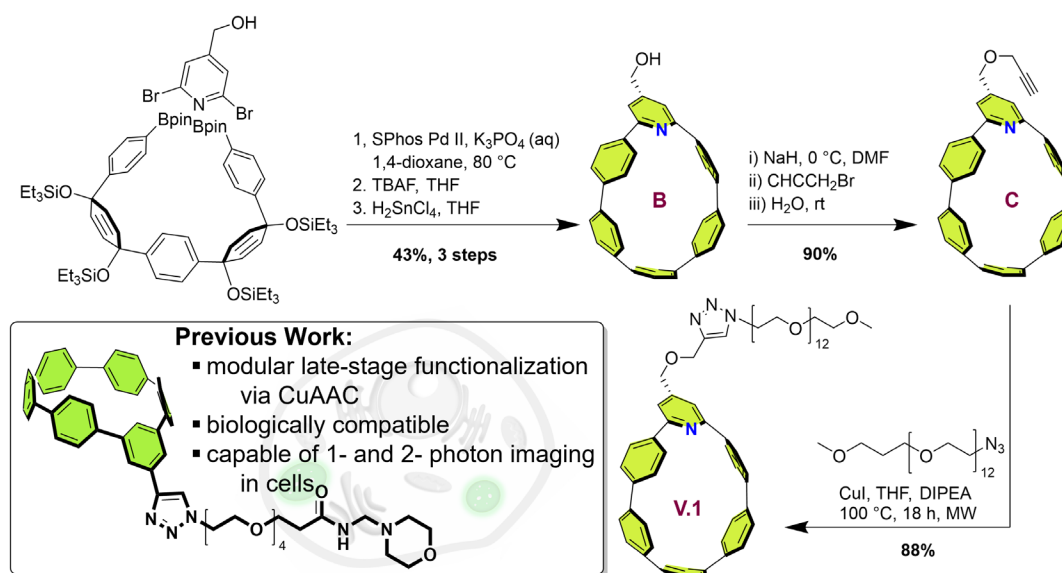
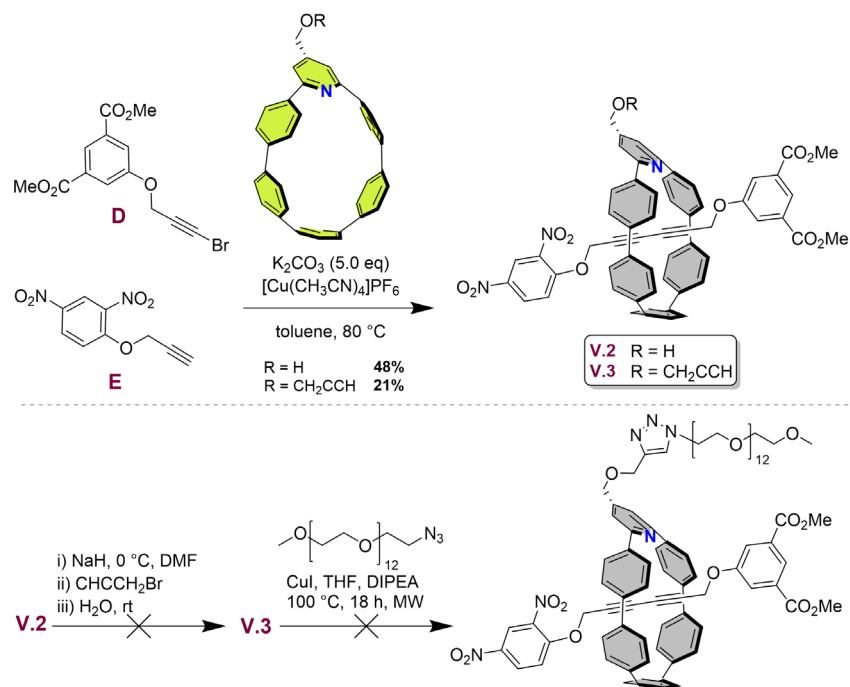


Figure 5.2. Synthesis of a PEG-functionalized water-soluble $mN[6]CPP$ compatible nanohoop, **V.1**, for use in the development of biologically compatible nanohoop-rotaxane sensors based on previous work with m -[6]CPP used for cell imaging.²⁵

Based on this hypothesis, the synthesis of rotaxane **V.2** using **B** as the templating macrocycle was carried out in good yield. Of note, this synthesis made use of a 3,5-dimethyl ether aromatic stopper unit (**D**), which differs from the published symmetric H_2S rotaxane. This was based on preliminary work on this system in which an asymmetric H_2S -sensing rotaxane analogous to **V.2** using the unfunctionalized $mN[6]CPP$ was synthesized and also showed activity in the presence of H_2S . This was chosen for synthetic ease, as the asymmetric rotaxane proved far easier to isolate and broadly more soluble than the symmetric counterpart. While **V.2** was made in good yield, attempts to append an alkyne to the alcohol were unsuccessful post-interlocking. Therefore, we next attempted to carry macrocycle **C** through the synthesis. While the potential interference of the already appended alkyne in the ATCC was considered, previous work on nanohoop-based daisy chains suggested that this short chain length would not be capable of forming daisy chains, and pre-coordination of the copper catalyst with **C** should reduce the potential for side reactivity. This proved to be the case, and **V.3** was isolated in reasonable yield. However, once again attempts to further functionalize the rotaxane were unsuccessful, as the subsequent CuAAC returned only starting **V.3**.

Further attempts to reach a biologically compatible rotaxane remain underway, and alternative approaches have been considered. One approach considered was saponification of the methyl ester groups of the thread, however this requires use of a bulky base, as a small base like hydroxide would be capable of S_NAr with the dinitro-stopper group leading to rotaxane dethreading. It remains unknown whether an already PEGylated nanothread like **V.1** could be used in ATCC reactions. If this is not possible, alternative means of solubilizing the nanothread fluorophore should be explored.



Scheme 5.1. Progress towards synthesizing a biologically compatible nanothread-[2]rotaxane for sensing HS^- in cells has been complicated by challenges with late-stage functionalization of the interlocked system.

5.2.2. Work Towards Exploring Modularity

We are currently exploring the use of alternative trigger motifs to expand the utility of the rotaxane probes to other analytes of interest. In doing so, we hope to capitalize on the inherent modularity of the scaffold's synthesis. Building off our success in tuning the selectivity of our sulfide-sensing rotaxane we next turned to reactive oxygen species (ROS.) Our previous sensor was able to select for HS^- in a sea of larger reactive sulfur species and we are hopeful that we could similarly select for one of the many ROS with implications in a variety of disease states and cell

signaling functions.²⁷⁻³¹ There are many known reactive “trigger” motifs that have been used for the study of various biological analytes³², and for ROS the most common trigger motif is the boronate acid/ester.³³⁻³⁵ Initially, therefore, we sought to incorporate a boronate ester into the thread component of a nanothoop [2]-rotaxane, however all attempts at synthesis of the proposed boronate-containing stopper group were unsuccessful. Therefore, we considered an alternative benzil trigger that should confer specific reactivity with only H₂O₂ via a Baeyer-Villiger type reaction, in a complex biological environment with many reactive oxygen species (**Figure 5.4**, bottom).³⁶

We envisioned that by using the same 3,5-dinitrobenzyl alcohol-based stopper utilized in the synthesis of the previously discussed fluoride sensor (**Figure 5.1**, top left) we could avoid any off-target reactivity we might expect from the 2,4-dinitrophenol stopper used for the H₂S-specific probe. Additionally, using the same unfunctionalized *m*N[6]CPP discussed in Chapter 4, we should be able to quickly obtain our rotaxane with only the synthesis of new stopper **V.6** required before

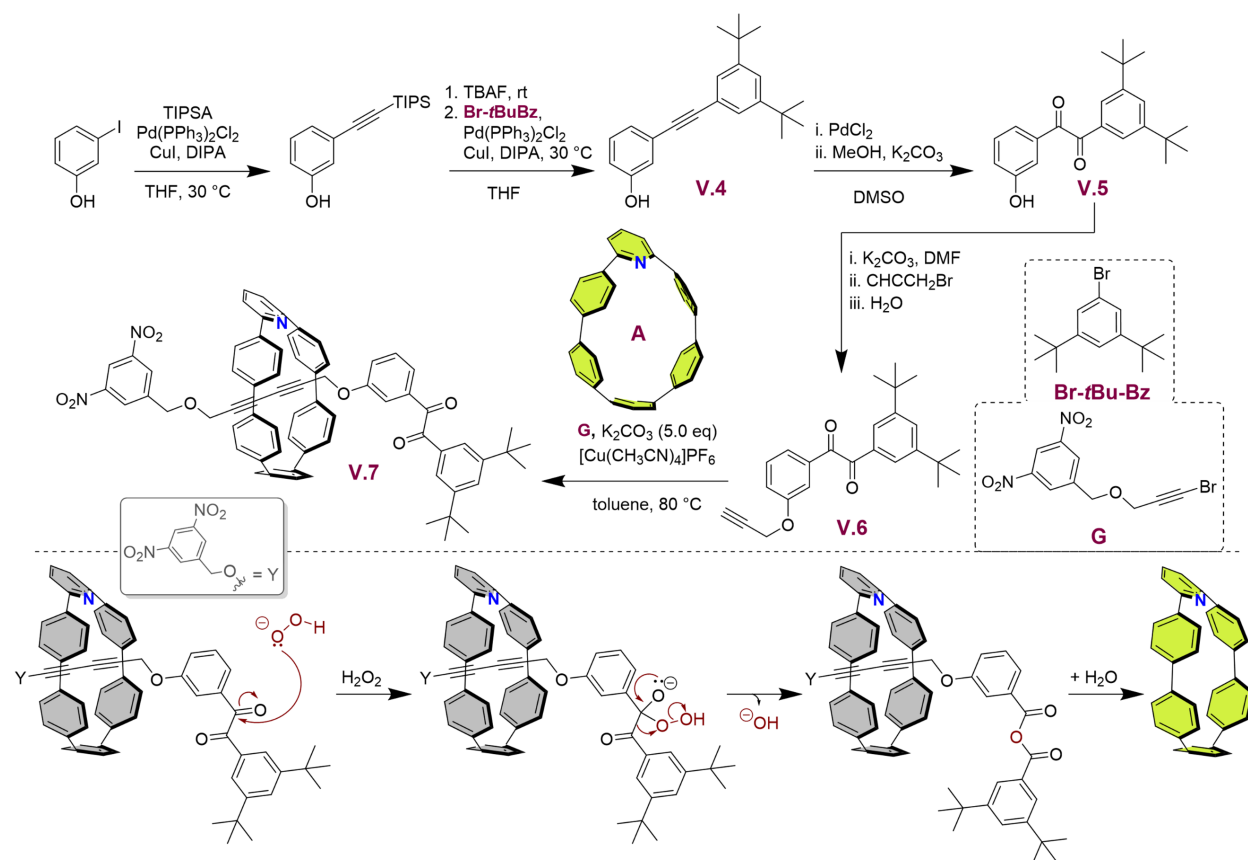


Figure 5.3. Progress towards a nanothoop-[2]rotaxane ROS probe (top) based on a benzil trigger motif (bottom) highlights the potential modularity of the sensing scaffold.

attempting the ATCC reaction. Starting from 3-iodophenol, a Sonogashira coupling with a protected alkyne followed by silyl deprotection and directly subjected to a second Sonogashira coupling with 1-bromo-3,5-di-*tert*-butylbenzene yields **V.4** containing an internal alkyne oxidation to benzil. Following the palladium-catalyzed oxidation, reaction with propargyl bromide yields stopper **V.6** for ATCC. Finally, coupling of **V.6** and **G** within the cavity of macrocycle **A** yields proposed ROS-sensing rotaxane **V.7**. Additionally coupling of **V.6** and **G** without the nano hoop present yields free thread **V.8**, which will be used to assess the influence of interlocking on the probe's reactivity.

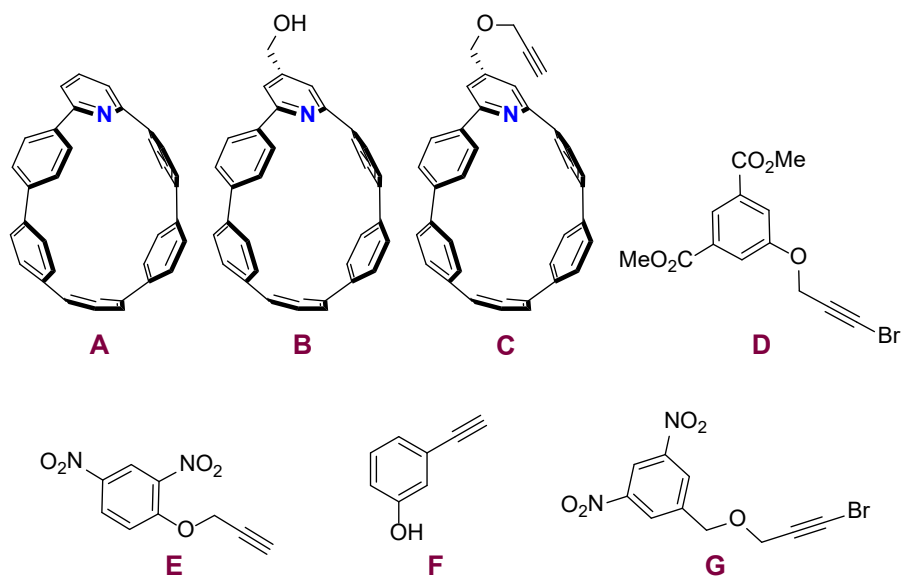
5.3. Conclusion

With the promising development of a proof-of-concept H₂S sensor and successful integration of nano hoops in biological imaging, we have begun to explore the potential of nano hoop-[2]rotaxanes as probes in a biological context. Initial work on rendering the scaffolds biologically compatible has seen some challenges, suggesting that installation of water-soluble groups may be required prior to mechanical interlocking or via alternative strategies that we continue to investigate. In addition, work towards understanding the modularity of the system with an eye toward potential delivery applications is also underway. The synthesis of a probe designed to react with H₂O₂ has recently been completed and work on understanding the reactivity of this new design is now required. The challenges in both syntheses discussed above suggest an alternative means of ATCC may be useful, namely CuAAC which has previously been successfully employed in nano hoop-[2]rotaxane synthesis.²⁶ Another consideration for future synthesis is the use of an alternative quenching agent, as the dinitro-functionalized stopper groups have broadly decreased the solubility of the subsequent rotaxanes which has in turn made both synthesis and isolation of these materials more challenging. Overall, these initial experiments suggesting the promise of nano hoops in the development of more complex scaffolds for sensing and potential for payload delivery.

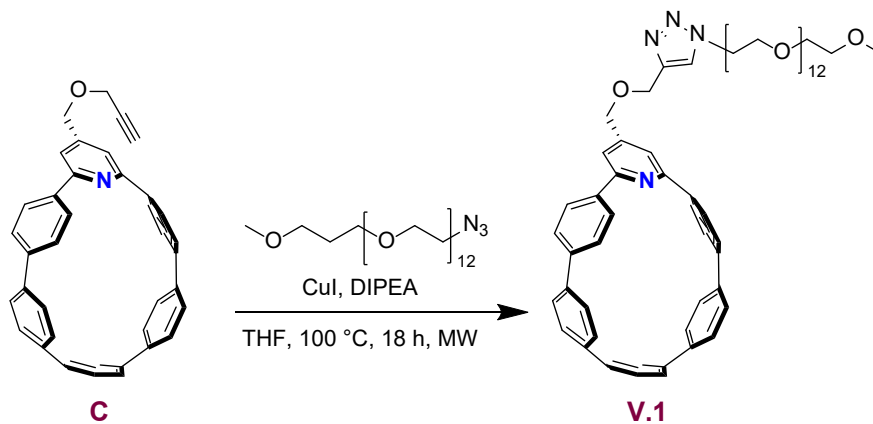
5.4. Experimental Sections

5.4.1. General Experimental Details

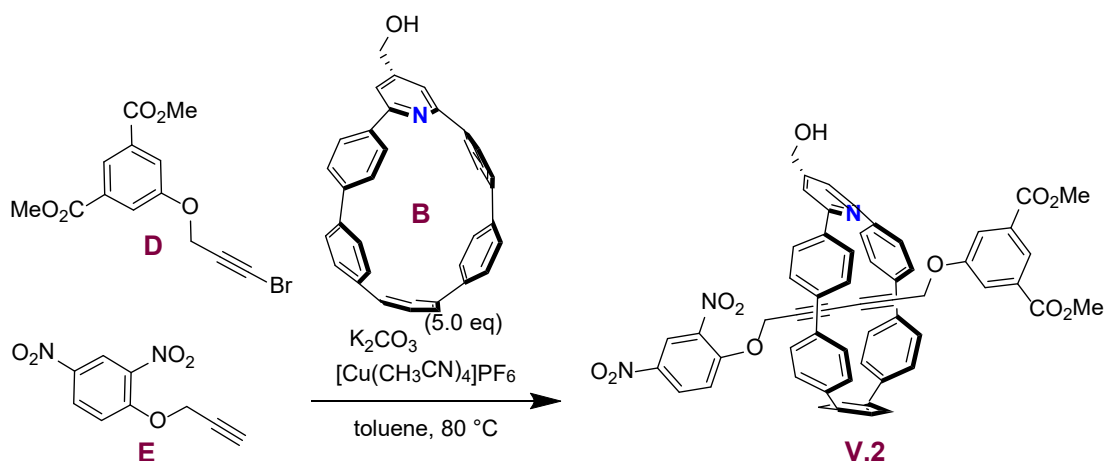
Moisture/air sensitive reactions were carried out under nitrogen atmosphere using standard Schlenk technique with flame-dried glassware cooled under an inert atmosphere of nitrogen. Solvents used for moisture/air sensitive reactions were dried by filtration through alumina and stored under an inert argon atmosphere. Silica column chromatography was conducted with Zeochem Zeoprep 60 Eco 40-63 μm silica gel and automated flash chromatography was performed using a Biotage Isolera One. Recycling gel permeation chromatography (GPC) was performed using a Japan Analytical Industry LC-9101 preparative HPLC with JAIGEL-1H/JAIGEL-2H columns with CHCl_3 . NMR spectra were recorded at 500 MHz or 600 MHz on a Bruker Advance-III-HD NMR spectrometer. All ^1H NMR spectra were taken in CDCl_3 (referenced to TMS, δ 0.00 ppm). All reagents were obtained commercially unless otherwise noted. Compounds **A**²⁶, **B-D**³⁷, **E**¹⁴, **F**³⁸ and **G**²⁶ were prepared according to literature procedure.



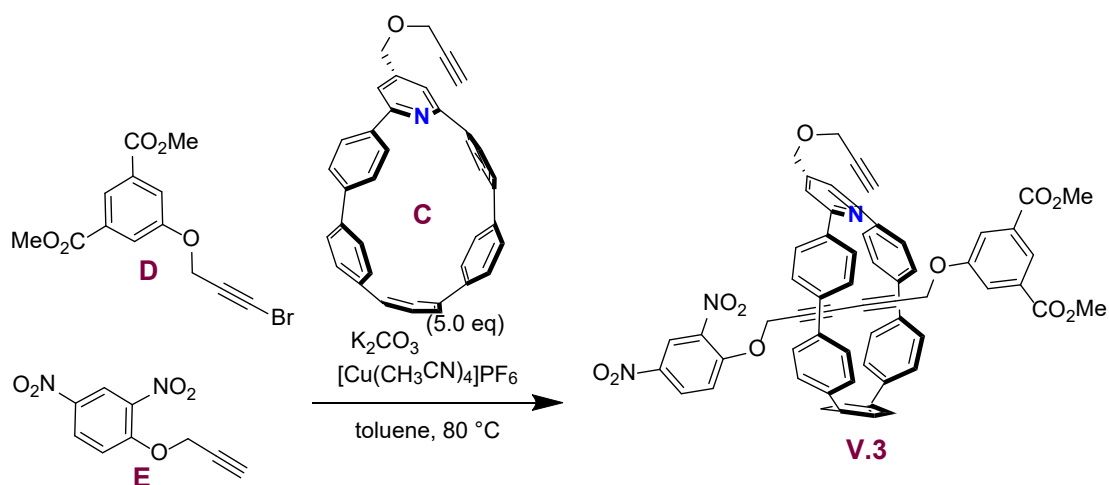
5.4.2. Synthesis and Characterization



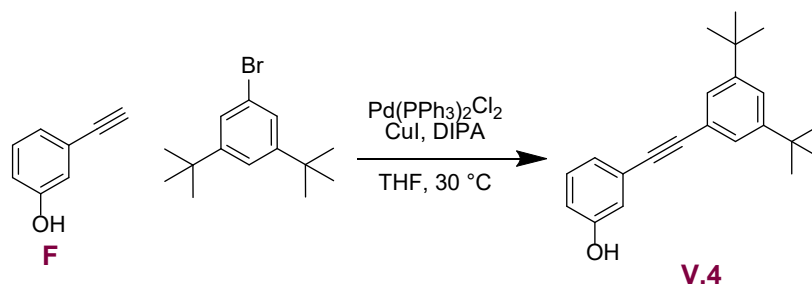
V.1. **C** (20.0 mg, 0.038 mmol, 1.0 equiv), copper iodide (0.001 mg, 0.006 mmol, 0.14 equiv) and m-PEG12-azide (22.0 mg, 0.038 mmol, 1.0 equiv) were added to an oven dried 0.5-2.0 mL microwave vial equipped with a stir bar. The vial was equipped with a septum and was evacuated and purged with nitrogen. Dry diisopropylethylamine (0.25 mL, 1.9 mmol, 50 equiv) and THF (1.9 mL) were added to the vial, which was then sealed and heated to 100 °C in the microwave for 18 hours. The reaction mixture was then cooled to room temperature and concentrated under reduced pressure. Water (5 mL) was added to the resulting oil was extracted with dichloromethane (3 x 10 mL) then dried over sodium sulfate, filtered, and concentrated to yield the product as an orange oil (36.9 mg, 88%). ¹H NMR (500 MHz, Chloroform-d) δ 8.09 (s, 1H), 7.45 (d, J = 9.0 Hz, 4H), 7.43 (s, 4H), 7.39 (d, J = 8.4 Hz, 4H), 7.37 (s, 2H), 7.35 (d, J = 8.7 Hz, 4H), 7.30 (d, J = 8.0 Hz, 4H), 4.77 (s, 2H), 4.69 (s, 2H), 4.57 (t, J = 5.1 Hz, 2H), 3.89 (t, J = 5.1 Hz, 2H), 3.70 – 3.58 (m, 32H), 3.54 (m, 4H), 3.37 (s, 3H).



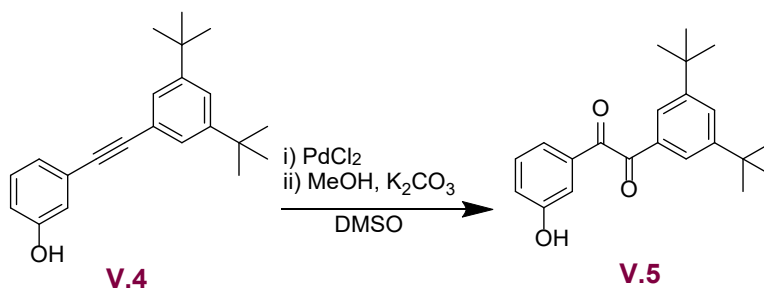
V.2. To a flame-dried 25 mL round bottom flask equipped with a magnetic stir bar was added **B** (20.6 mg, 0.0423 mmol, 1.00 equiv.), **D** (20.0 mg, 0.0635 mmol, 1.50 equiv.), **E** (14.1 mg, 0.0635 mmol, 1.50 equiv.), oven-dried K_2CO_3 (0.044 g, 0.317 mmol, 5.0 equiv.) and $[Cu(CH_3CN)_4]PF_6$ (0.0150 mg, 0.0402 mmol, 0.95 equiv.), followed by five cycles of evacuation and refill with N_2 . A septum was placed on the flask followed by the addition of 10.0 mL toluene. The reaction was heated to 80 °C (via oil bath) with stirring for 48 hours, with reaction progress monitored by TLC. Once complete, the reaction was cooled to room temperature and quenched with a solution of ethylenediaminetetraacetic acid (EDTA) in 15% NH_3 (3 mL) solution then allowed to stir for 30 min. The layers were separated, and the aqueous phase was washed with dichloromethane (3 x 10 mL). The combined organic phase was then washed with H_2O (3 x 10 mL) and brine (1 x 20 mL) then dried over sodium sulfate, filtered, and concentrated to yield yellow oil. The crude material was loaded onto a short silica plug and washed with DCM, then the product eluted with 10% MeOH/DCM, and concentrated. The resulting yellow oil was further purified by silica flash chromatography, (30-50% ethyl acetate/hexanes). Fractions 3-6 were combined and concentrated to obtain free thread (5.9 mg), while fractions 7-13 were combined and concentrated to yield **V.2** as a yellow oily solid (19.2 mg, 48%). 1H NMR (500 MHz, Chloroform-d) δ 8.67 (d, $J = 2.7$ Hz, 1H), 8.30 (t, $J = 1.5$ Hz, 1H), 7.77 (dd, $J = 9.2, 2.8$ Hz, 1H), 7.49 (s, 2H), 7.48 (d, $J = 2.2$ Hz, 2H), 7.46 (d, $J = 2.3$ Hz, 2H), 7.38 (dd, $J = 8.9, 2.3$ Hz, 2H), 7.32 (dd, $J = 8.8, 2.2$ Hz, 2H), 7.29 (dd, $J = 8.4, 2.0$ Hz, 2H), 7.23 (dd, $J = 8.4, 2.0$ Hz, 2H), 7.21 (d, $J = 1.4$ Hz, 2H), 7.16 (dd, $J = 8.9, 2.2$ Hz, 2H), 7.12 (dd, $J = 3.6, 2.0$ Hz, 2H), 7.10 (dd, $J = 3.7, 2.0$ Hz, 2H), 7.02 (dd, $J = 8.9, 2.3$ Hz, 2H), 6.14 (d, $J = 9.3$ Hz, 1H), 4.86 (d, $J = 4.8$ Hz, 2H), 3.96 (s, 6H), 3.78 (s, 2H), 3.10 (s, 2H), 2.40 (t, $J = 4.75$ Hz, 1H).



V.3. To a flame-dried 25 mL round bottom flask equipped with a magnetic stir bar was added **C** (18.0 mg, 0.0423 mmol, 1.00 equiv.), **D** (20.0 mg, 0.0635 mmol, 1.50 equiv.), **E** (14.1 mg, 0.0635 mmol, 1.50 equiv.), oven-dried K_2CO_3 (0.044 g, 0.317 mmol, 5.0 equiv.) and $[Cu(CH_3CN)_4]PF_6$ (0.0150 mg, 0.0402 mmol, 0.95 equiv.), followed by five cycles of evacuation and refill with N_2 . A septum was placed on the flask followed by the addition of 10.0 mL toluene. The reaction was heated to 80 °C (via oil bath) with stirring for 48 hours, with reaction progress monitored by TLC. Once complete, the reaction was cooled to room temperature and quenched with a solution of ethylenediaminetetraacetic acid (EDTA) in 15% NH_3 (3 mL) solution then allowed to stir for 30 min. The layers were separated, and the aqueous phase was washed with dichloromethane (3 x 10 mL). The combined organic phase was then washed with H_2O (3 x 10 mL) and brine (1 x 20 mL) then dried over sodium sulfate, filtered, and concentrated to yield yellow oil. The resulting yellow oil was further purified by silica flash chromatography, (30% ethyl acetate/hexanes). Fractions 1-3 were combined and concentrated to obtain free thread (3.9 mg), while fractions 4-6 were combined and concentrated to yield **V.3** as an oily yellow solid (4.9 mg, 12%.) 1H NMR (500 MHz, Chloroform- d) δ 8.63 (d, $J = 2.7$ Hz, 1H), 8.34 (t, $J = 1.5$ Hz, 1H), 7.83 (dd, $J = 9.2, 2.8$ Hz, 1H), 7.49 (d, $J = 2.2$ Hz, 2H), 7.46 (s, 2H), 7.42 (d, $J = 2.3$ Hz, 2H), 7.41 (dd, $J = 8.9, 2.3$ Hz, 2H), 7.38 (dd, $J = 8.8, 2.2$ Hz, 2H), 7.36 (dd, $J = 8.4, 2.0$ Hz, 2H), 7.35 (dd, $J = 8.4, 2.0$ Hz, 2H), 7.33 (d, $J = 1.4$ Hz, 2H), 7.31 (dd, $J = 8.9, 2.2$ Hz, 2H), 7.24 (dd, $J = 3.6, 2.0$ Hz, 2H), 7.11 (dd, $J = 3.7, 2.0$ Hz, 2H), 7.06 (dd, $J = 8.9, 2.3$ Hz, 2H), 5.93 (d, $J = 9.3$ Hz, 1H), 4.70 (s, 2H), 3.95 (s, 6H), 3.40 (s, 2H), 3.38 (s, 2H), 2.54 (s, 1H).

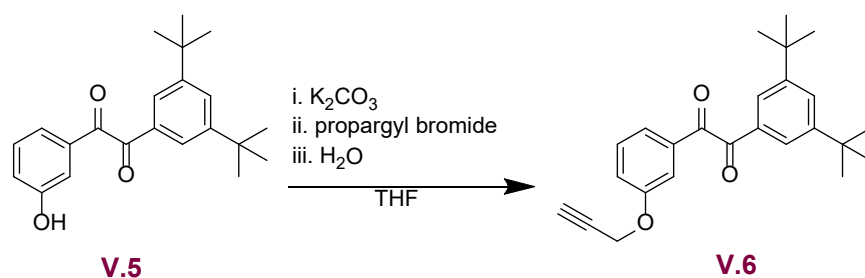


V.4. To a flame-dried 25 mL round bottom flask equipped with a magnetic stir bar was added **F** (50.0 mg, 0.423 mmol, 1.00 equiv.), 1-bromo-3,5-di-*tert*-butylbenzene (125 mg, 0.466 mmol, 1.10 equiv.), copper iodide (4.0 mg, 0.021 mmol, 0.05 equiv.), and Pd(PPh₃)₂Cl₂ (0.003 mg, 0.004 mmol, 0.01 equiv.), followed by five cycles of evacuation and refill with N₂. A septum was placed on the flask followed by the addition of 1.8 mL toluene and distilled diisopropylamine (0.90 mL). The reaction was heated to 30 °C (via oil bath) with stirring for 48 hours. The reaction was cooled to room temperature and water added (5 mL) then the organic solvent was removed under reduced pressure. The resulting solution was washed with diethyl ether (3 x 10 mL) then the combined organic phase was then washed with H₂O (3 x 10 mL) and brine (1 x 20 mL). The organic phase was then dried over sodium sulfate, filtered, and concentrated to yield brown oil which was purified by silica flash chromatography, (25% ethyl acetate/hexanes) to yield **V.4** as an yellow oil (0.10 g, 45%). ¹H NMR (500 MHz, Chloroform-d) δ 7.41 (d, J = 1.9 Hz, 2H), 7.38 (t, J = 1.8 Hz, 1H), 7.21 (dd, J = 7.9, 7.7 Hz, 1H), 7.12 (dt, J = 7.6, 1.2 Hz, 1H), 7.02 (d, 2.6 Hz, 1H), 6.82 (ddd, J = 8.1, 2.6, 1.0 Hz, 1H), 1.33 (s, 18H). ¹³C NMR (126 MHz, CDCl₃) δ 155.42, 150.91, 129.66, 125.94, 124.75, 124.34, 122.91, 122.08, 118.31, 115.67, 90.62, 87.82, 34.87, 31.38, 31.37.



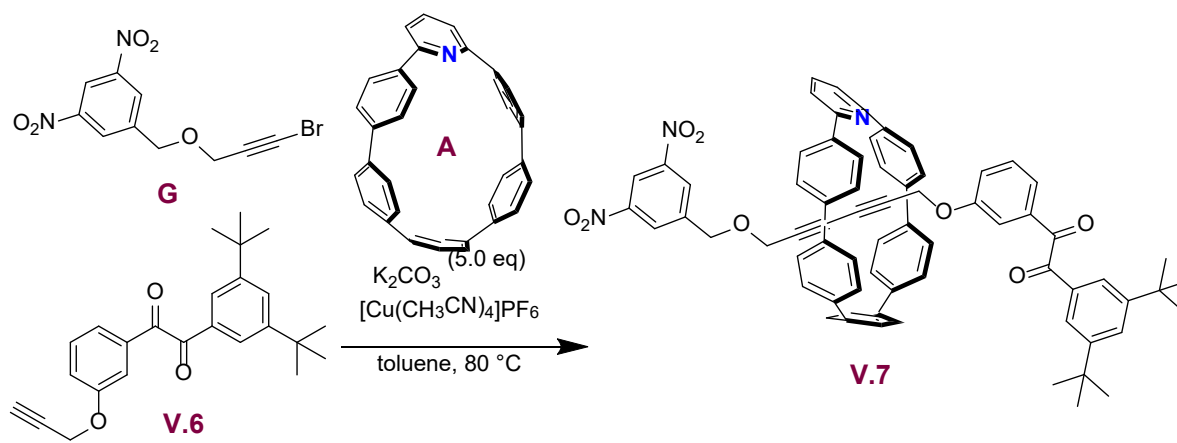
V.5. To a flame-dried 15 mL round bottom flask equipped with a magnetic stir bar was added PdCl₂ (0.0005 mg, 0.29 mmol, 0.01 equiv.) followed by five cycles of evacuation and refill with N₂. A septum was placed on the flask followed by the addition of a solution of **V.4** (90 mg, 0.294 mmol, 1.0 equiv.) in dry DMSO (0.42 mL, 5.8 mmol, 20 equiv.). The reaction was heated to 105

°C (via oil bath) with stirring for 24 hours. While at temperature, solid K_2CO_3 (0.02 g, 0.15 mmol, 0.5 equiv.) was added in one shot under a blanket of N_2 , followed by the addition of MeOH (0.42 mL, 10.3 mmol, 35 equiv.) and allowed to stir 10 minutes while cooling to room temperature. The reaction mixture was diluted with water and extracted with ethyl acetate (3 x 10 mL) then the combined organic phase was washed with brine (1 x 20 mL), dried over sodium sulfate, filtered, and concentrated to yield a yellow oil. The crude oil was purified by silica flash chromatography, (20% ethyl acetate/hexanes) to yield **V.5** as a sticky yellow oil (0.056 g, 56%). 1H NMR (500 MHz, Chloroform- d) δ 7.79 (d, J = 1.8 Hz, 2H), 7.74 (t, J = 1.9 Hz, 1H), 7.51 (dt, J = 7.6, 1.2 Hz, 1H), 7.47 (dd, J = 2.6, 1.6 Hz, 1H), 7.38 (dd, 7.9, 7.7 Hz, 1H), 7.14 (ddd, J = 8.0, 2.6, 1.0 Hz, 1H), 1.33 (s, 18H). ^{13}C NMR (126 MHz, $CDCl_3$) δ 195.16, 194.61, 156.04, 151.89, 134.66, 132.55, 130.38, 129.59, 124.21, 122.99, 122.11, 115.64, 35.04, 31.27.

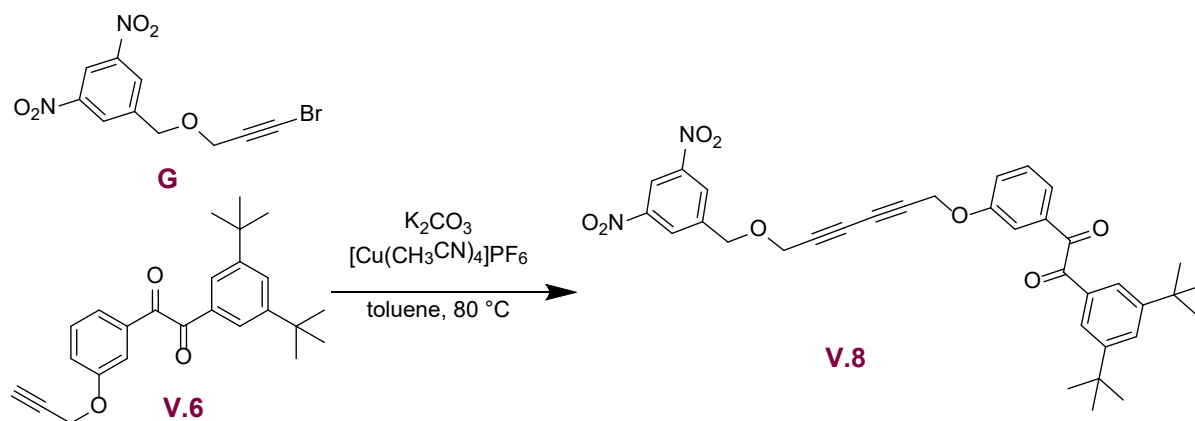


V.6. To a flame-dried 15 mL round bottom flask equipped with a stir bar was added **V.5** (0.30 g, 0.89 mmol, 1.0 equiv.), and oven-dried K_2CO_3 (0.24 g, 1.8 mmol, 2.0 equiv.) followed by five cycles of evacuation and refill with N_2 . A septum was placed on the flask followed by the addition of DMF (1.8 mL). After 15 minutes the dropwise addition of propargyl bromide (0.10 mL, 1.3 mmol, 1.5 equiv.) resulted in a brown solution that was allowed to stir over night at room temperature. The reaction was quenched with excess water (6 mL) followed by extraction of the aqueous suspension with DCM (3 x 30 mL). The combined organic phases were washed with H_2O (3 x 20 mL), LiCl (30 mL) and brine (50 mL) and then dried over sodium sulfate. After removal of DCM under reduced pressure, the resulting brown oil was purified via silica flash chromatography (100% DCM) to yield **V.6** as an orange oil which solidified on standing (0.060 g, 18%). 1H NMR (500 MHz, Chloroform- d) δ 7.80 (d, J = 1.9 Hz, 2H), 7.75 (t, J = 1.9 Hz, 1H), 7.63 (dd, J = 2.6, 1.5 Hz, 1H), 7.56 (dt, J = 7.7, 1.2 Hz, 1H), 7.43 (dd, 8.5, 7.9 Hz, 1H), 7.28 (ddd, J = 8.3, 2.7, 1.6 Hz, 1H), 4.76 (d, J = 2.4 Hz, 2H), 2.53 (d, J = 2.4 Hz, 1H), 1.33 (s, 18H). ^{13}C NMR

(126 MHz, CDCl₃) δ 195.12, 194.62, 157.93, 151.87, 134.58, 132.61, 130.12, 129.54, 124.21, 123.93, 122.19, 114.47, 77.79, 76.18, 56.07, 35.04, 31.28.



V.7. To a flame-dried 25 mL round bottom flask equipped with a magnetic stir bar was added **A** (10.0 mg, 0.022 mmol, 1.00 equiv.), **G** (0.010 mg, 0.033 mmol, 1.50 equiv.), **V.6** (0.012 mg, 0.033 mmol, 1.50 equiv.), oven-dried K₂CO₃ (0.015 g, 0.109 mmol, 5.0 equiv.) and [Cu(CH₃CN)₄]PF₆ (8.0 mg, 0.021 mmol, 0.95 equiv.), followed by five cycles of evacuation and refill with N₂. A septum was placed on the flask followed by the addition of 10.0 mL toluene. The reaction was heated to 80 °C (via oil bath) with stirring for 48 hours, with reaction progress monitored by TLC. Once complete, the reaction was cooled to room temperature and quenched with a solution of ethylenediaminetetraacetic acid (EDTA) in 15% NH₃ (3 mL) solution then allowed to stir for 30 min. The layers were separated, and the aqueous phase was washed with dichloromethane (3 x 10 mL). The combined organic phase was then washed with H₂O (3 x 10 mL) and brine (1 x 20 mL) then dried over sodium sulfate, filtered, and concentrated to yield yellow oil. The resulting yellow oil was further purified by automated flash chromatography (silica, 0-20% ethyl acetate/hexanes). Product containing fractions were combined and concentrated and purified further by preparative TLC (25% ethyl acetate/hexanes) to yield **V.3** as a yellow residue (trace.) ¹H NMR (500 MHz, Chloroform-d) δ 8.94 (t, *J* = 1.9 Hz, 1H), 8.07 (d, *J* = 2.1 Hz, 2H), 7.88 (d, *J* = 1.8 Hz, 2H), 7.79 (t, *J* = 1.7 Hz, 1H), 7.75 (t, *J* = 7.8 Hz, 1H), 7.49 (s, 4H), 7.48 (d, *J* = 1.9 Hz, 2H), 7.44 (d, *J* = 7.7 Hz, 4H), 7.37 (s, 1H), 7.23 – 7.19 (m, 8H), 7.16 (dd, *J* = 8.9, 2.2 Hz, 2H), 7.11 (t, *J* = 8.0 Hz, 1H), 6.95 (dd, *J* = 10.7, 8.4 Hz, 4H), 3.70 (s, 2H), 3.35 (s, 2H), 2.85 (s, 2H), 1.54 (s, 18H).



V.8. To a flame-dried 25 mL round bottom flask equipped with a magnetic stir bar was added oven-dried K_2CO_3 (0.018 g, 0.133 mmol, 5.0 equiv.) and flask flame-dried again. Once cooled, **G** (0.008 g, 0.027 mmol, 1.00 equiv.), **V.6** (0.010 g, 0.027 mmol, 1.00 equiv.) and $[Cu(CH_3CN)_4]PF_6$ (0.010 mg, 0.027 mmol, 1.00 equiv.) were added followed by five cycles of evacuation and refill with N_2 . A septum was placed on the flask followed by the addition of 0.5 mL toluene and the reaction was heated to $80\text{ }^\circ\text{C}$ (via oil bath) with stirring for 48 hours. The reaction was cooled to room temperature and the solvent was removed under reduced pressure. The crude solid was purified by silica flash chromatography, (0-20% ethyl acetate/hexanes) to obtain the product as a pale brown oily solid (-- mg, --%). 1H NMR (500 MHz, Chloroform-d) δ 8.97 (t, $J = 2.1$ Hz, 1H), 8.54 (d, $J = 2.1$ Hz, 2H), 7.80 (d, $J = 1.9$ Hz, 2H), 7.75 (t, $J = 1.9$ Hz, 1H), 7.62 (dd, 2.7, 1.5 Hz, 1H), 7.28 (dt, $J = 7.7, 1.2$ Hz, 1H), 7.44 (dd, $J = 7.9, 7.7$ Hz, 1H), 7.26 (ddd, 8.0, 2.7, 1.6, 1H), 4.85 (s, 2H), 4.80 (s, 2H), 4.42 (s, 2H), 1.33 (s, 18H).

CONCLUDING REMARKS

In summary, the studies discussed in this dissertation provide synthetic methodologies to reach a variety of functionalized nanohoop derivatives with potential in biological/aqueous applications. The methodology was used to prepare the first fully water-soluble nanohoop fluorophores, allowing for the first exploration of nanohoop supramolecular chemistry in water. This work illustrates the broad utility of the hydrophobic effect to drive host-guest interactions in nanohoops for the first time. Further the synthetic methodologies described herein build off of work by former lab mates to develop nanohoop-based fluorescence sensors for biologically relevant analytes, towards furthering the utility of nanohoops in biological applications.

REFERENCES CITED

Chapter I

1. Fischer, E. The influence of configuration on enzyme activity. *Dtsch. Chem. Ges.* **1894**, *27*, 2984.
2. Pederson, C. J. Cyclic polyethers and their complexes with metal salts. *J. Am. Chem. Soc.* **1967**, *89*, 7017.
3. The Nobel Prize in Chemistry 1987. NobelPrize.org. Nobel Prize Outreach AB 2022. Thu. 14 Jul 2022. <https://www.nobelprize.org/prizes/chemistry/1987/summary/>
4. Li, J.; Loh, X. J. Cyclodextrin-based supramolecular architectures: Synthesis, structures, and applications for drug and gene delivery. *Adv. Drug Deliv. Rev.* **2008**, *60*, 1000.
5. Helttunen, K.; Shahgaldian, P. Self-assembly of amphiphilic calixarenes and resorcinarenes in water. *New. J. Chem.* **2010**, *34*, 2704.
6. Bhasikuttan, A. C.; Pal, H.; Mohanty, J. Cucurbit[n]uril based supramolecular assemblies: tunable physico-chemical properties and their prospects. *Chem. Commun.* **2011**, *47*, 9959.
7. Ogoshi, T.; Yamagishi, T. Pillararenes: Versatile Synthetic Receptors for Supramolecular Chemistry. *Eur. J. Org. Chem.* **2013**, *15*, 2961.
8. Rebilly, J.-N.; Reinaud, O. Calixarenes and resorcinarenes as scaffolds for supramolecular metallo-enzyme mimicry. *Supramol. Chem.* **2013**, *26* (7-8), 454.
9. Barrow, S. J.; Kasera, S.; Rowland, M. J.; del Barrio, J.; Scherman, O. A. Cucurbituril-Based Molecular Recognition. *Chem. Rev.* **2015**, *115*, 12320.
10. Healy, B.; Yu, T.; da Silva Alves, D. C.; Okeke, C.; Breslin, C. B. Cyclodextrins as Supramolecular Recognition Systems: Applications in the Fabrication of Electrochemical Sensors. *Materials* **2021**, *14* 1668.
11. Ogoshi, T.; Yamagishi, T.; Nakamoto, Y. Pillar-Shaped Macrocyclic Hosts Pillar[n]arenes: New Key Players for Supramolecular Chemistry. *Chem. Rev.* **2016**, *116* (14), 7937-8002.
12. Wang, M.-X. Coronarenes: recent advances and perspectives on macrocyclic and supramolecular chemistry. *Sci. China Chem.* **2018**, *61*, 993.

13. Gaeta, C.; Wang, D.-X. Editorial: New Macrocycles and Their Supramolecular Perspectives. *Front. Chem.* **2020**, *8*, 128.
14. Yu, J.; Qi, D.; Li, J. Design, synthesis and applications of responsive macrocycles. *Commun. Chem.* **2020**, *3*, 189.
15. Jasti, R.; Bhattacharjee, J.; Neaton, J. B.; Bertozzi, C. R. Synthesis, Characterization and Theory of [9]-, [12]-, and [18]Cycloparaphenylene: Carbon Nanohoop Structures. *J. Am. Chem. Soc.* **2008**, *130*, 17646.
16. Darzi, E. R.; Jasti, R. The dynamic, size-dependent properties of [5]-[12]cycloparaphenylenes. *Chem. Soc. Rev.* **2015**, *44* (18), 6401.
17. Leonhardt, E. J.; Jasti, R. Emerging applications of carbon nanohoos. *Nat. Rev. Chem.* **2019**, *3*, 672.
18. Diederich, F.; Gómez-López, M. Supramolecular fullerene chemistry. *Chem. Soc. Rev.* **1999**, *28*, 263.
19. Pérez, E. M.; Martín, N. Molecular tweezers for fullerenes. *Pure Appl. Chem.* **2010**, *82* (3), 523.
20. García-Simón, C.; Costas, M.; Ribas, X. Metallosupramolecular receptors for fullerene binding and release. *Chem. Soc. Rev.* **2016**, *45*, 40.
21. Smith, B. W.; Monthieux, M.; Luzzi, D. E. Encapsulated C₆₀ in carbon nanotubes. *Nature* **1998**, *396*, 323.
22. Chen, J.; Dong, J. Electronic properties of peapods: effects of fullerene rotation and different types of tube. *Science* **2001**, *292* (5514), 45.
23. Kawase, T.; Tanaka, K.; Fujiwara, N.; Darabi, H. R.; Oda, M. Complexation of a Carbon Nanoring with Fullerenes. *Angew. Chem. Int. Ed.* **2003**, *42* (14), 1624.
24. Kawase, T.; Tanaka, K.; Seirai, Y.; Shiono, N.; Oda, M. Complexation of a Carbon Nanoring with Fullerenes: Supramolecular Dynamics and Structural Tuning for a Fullerene Sensor. *Angew. Chem. Int. Ed.* **2003**, *42* (45), 5597.
25. Iwamoto, T.; Watanabe, Y.; Sadahiro, T.; Haino, T.; Yamago, S. Size-Selective Encapsulation of C₆₀ by [10]Cycloparaphenylene: Formation of the Shortest Fullerene-Peapod. *Angew. Chem. Int. Ed.* **2011**, *50* (36), 8342-8344.
26. Xia, J.; Bacon, J. W.; Jasti, R. Gram-scale synthesis and crystal structures of [8]- and [10]CPP, and the solid-state structure of C₆₀@[10]CPP. *Chem. Sci.* **2012**, *3* (10), 3018-3021.

27. Huang, Q.; Zhuang, G.; Jia, H.; Qian, M.; Cui, S.; Yang, S.; Du, P. Photoconductive Curved-Nanographene/Fullerene Supramolecular Heterojunctions. *Angew. Chem. Int. Ed.* **2019**, *58*, 6244.
28. Xu, Y.; Wang, B.; Kaur, R.; Minameyer, M. B.; Bothe, M.; Drewello, T.; Guldi, D. M.; von Delius, M. A Supramolecular [10]CPP Junction Enables Efficient Electron Transfer in Modular Porphyrin-[10]CPP \supset Fullerene Complexes. *Angew. Chem. Int. Ed.* **2018**, *57* (36), 11549.
29. Lovell, T. C.; Garrison, Z. R.; Jasti, R. Synthesis, Characterization, and Computational Investigation of Bright Orange-Emitting Benzothiadiazole [10]Cycloparaphenylene. *Angew. Chem. Int. Ed.* **2020**, *59*, 14363.
30. Schwer, F.; Zank, S.; Freiberger, M.; Kaur, R.; Frühwald, S.; Robertson, C.; Görling, A.; Drewello, T.; Guldi, D.; von Delius, M. Synthesis and C₆₀ Binding of *N*-Methylaza[10]CPP. *Organic Materials*, **2022**, *4* (2), 7.
31. Bachrach, S. T.; Stück, D. DFT Study of Cycloparaphenylenes and Heteroatom-Substituted Nanohoops. *J. Org. Chem.* **2010**, *75* (19), 6595-6604.
32. Iwamoto, T.; Watanabe, Y.; Takaya, H.; Haino, T.; Yasuda, N.; Yamago, S. Size- and Orientation-Selective Encapsulation of C70 by Cycloparaphenylenes. *Angew. Chem. Int. Ed.* **2013**, *19* (42), 14061.
33. Iwamoto, T.; Slanina, Z.; Mizorogi, N.; Guo, J.; Akasaka, T.; Nagese, S.; Takaya, N.; Kato, T.; Yamago, S. Partial Charge Transfer in the Shortest Possible Metallofullerene Peapod, La@C82 \subset [11]Cycloparaphenylene. *Chem. Eur. J.* **2014**, *20*, 14403.
34. Nakanishi, Y.; Omachi, H.; Matsuura, S.; Miyata, Y.; Kitaura, R.; Segawa, Y.; Itami, K.; Shinohara, H. Size-Selective Complexation and Extraction of Endohedral Metallofullerenes with Cycloparaphenylene. *Angew. Chem. Int. Ed.* **2014**, *53* (12), 3102.
35. Rio, J.; Beeck, S.; Rotas, G.; Ahles, S.; Jacquemin, D.; Tagmatarchis, N.; Ewels, C.; Wegner, H. A. Electronic Communication between two [10]cycloparaphenylenes and Bis(azafullerene) (C₅₉N)₂ Induced by Cooperative Complexation. *Angew. Chem. Int. Ed.* **2018**, *57* (23), 6930-6934.
36. Iijima, S. Helical microtubules of graphitic carbon. *Nature* **1991**, *354*, 56.
37. Fomine, S.; Zolotukhin, M. G.; Guadarrama, P. "Russian doll" complexes of [n]cycloparaphenylenes: a theoretical study. *J. Mol. Model.* **2012**, *18*, 4025.
38. Mizyed, S.; Georghiou, P. E.; Bancu, M.; Cuadra, B.; Rai, A. K.; Cheng, P.; Scott, L. T. Embracing C₆₀ with Multiarmed Geodesic Partners. *J. Am. Chem. Soc.* **2001**, *123* (51), 12770.

39. Hashimoto, S.; Iwamoto, T.; Kurachi, D.; Kayahara, E.; Yamago, S. Shortest Double-Walled Carbon Nanotubes Composed of Cycloparaphenylenes. *ChemPlusChem* **2017**, *82*, 1015.
40. Peña-Álvarez, M.; Fanetti, S.; Falsini, N.; Novelli, G.; Casado, J.; Baonza, V. G.; Taravillo, M.; Parsons, S.; Bini, R.; Citroni. Linear, Non-Conjugated Cyclic and Conjugated Cyclic Paraphenylene under Pressure. *Molecules* **2019**, *24* (19), 3496.
41. Minameyer, M. B.; Xu, A.Y.; Frühwald, S.; Görling, A.; von Delius, M.; Drewello, M. Investigation of Cycloparaphenylenes (CPPs) and their Noncovalent Ring-in-Ring and Fullerene-in-Ring Complexes by (Matrix-Assisted) Laser Desorption/Ionization and Density Functional Theory. *Chem. Eur. J.* **2020**, *26*, 8729.
42. Zhao, C.; Liu, F.; Feng, L.; Nie, M.; Lu, Y.; Zhang, J.; Wang, C.; Wang, T. Construction of a Double-Walled Carbon Nanoring. *Nanoscale* **2021**, *13* (9), 4880.
43. Miki, K.; Saiki, K.; Umeyama, T.; Baek, J.; Noda, T.; Imahori, H.; Sato, Y.; Suenaga, K.; Ohe, K. Unique Tube-Ring Interactions: Complexation of Single-Walled Carbon Nanotubes with Cycloparaphenyleneacetylenes. *Small* **2018**, *14* (26), 1800720.
44. Yumura, T.; Miki, R.; Fukuura, S.; Yamamoto, W. Energetics of Hybrid Structures between Cycloparaphenylene and Carbon Nanotubes: A Dispersion-Corrected Density Functional Theory Study. *J. Phys. Chem. C* **2020**, *124* (32), 17836.
45. Kwon, H.; Bruns, C. J. All-hydrocarbon, all-conjugated cycloparaphenylene-polycyclic aromatic hydrocarbon host-guest complexes stabilized by CH- π interactions. *Nano Res.* **2022**, *15*, 5545.
46. Hermann, M.; Wassy, D.; Esser, B. Conjugated Nanohoops Incorporating Donor, Acceptor, Hetero- or Polycyclic Aromatics. *Angew. Chem. Int. Ed.* **2021**, *60* (29), 15743.
47. Della Sala, P.; Talotta, C.; Caruso, T.; De Rosa, M.; Soriente, A.; Ner, P.; Gaeta, C. Tuning Cycloparaphenylene Host Properties by Chemical Modification. *J. Org. Chem.* **2017**, *82*, 9885.
48. Lu, D.; Zhuang, G.; Jia, H.; Wang, J.; Huang, Q.; Cui, S.; Du, P. A novel symmetrically multifunctionalized dodecamethoxy-cycloparaphenylene: synthesis, photophysical, and supramolecular properties. *Org. Chem. Front.* **2018**, *5*, 1446.
49. Frisch, H.; Martin, I.; Mark, H. Zur Struktur der Polysiloxene. I. *Monatsh. Chem.* **1953**, *84* (2), 250
50. Stoddart, J. D. Mechanically Interlocked Molecules (MIMs)- Molecular Shuttles, Switches, and Machines (Nobel Lecture). *Angew. Chem. Int. Ed.* **2017**, *56*, 11094.

51. Bruns, C. J.; Stoddart, J. F. The Nature of the Mechanical Bond: From Molecules to Machines. *Wiley*, New Jersey, **2016**.
52. Dietrich-Buchecker, C. O.; Sauvage, J. P.; Kintzinger, J. P. Une nouvelle famille de molécules: les metallo-catenes. *Tet. Lett.* **1983**, *24* (46) 5095.
53. Xu, Y.; Kaur, R.; Wang, B.; Minameyer, M. B.; Gsä, S.; Meyer, B.; Drewello, T.; Guldi, D. M.; von Delius, M. Concave-Convex π - π Template Approach Enables the Synthesis of [10]Cycloparaphenylene-Fullerene [2]Rotaxanes. *J. Am. Chem. Soc.* **2018** *140* (41), 13413.
54. Saito, S.; Takahashi, E.; Nakazono, K. Synthesis of [2]Rotaxanes by the Catalytic Reactions of a Macrocyclic Copper Complex. *Org. Lett.* **2006**, *8*, 5133.
55. Aucagne, V.; Hänni, K. D.; Leigh, D. A.; Lusby, P. J.; Walker, D. Catalytic "Click" Rotaxanes: A Substoichiometric Metal Template Pathway to Mechanically Interlocked Architectures. *J. Am. Chem. Soc.* **2006**, *128*, 2186.
56. Crowley, J. D.; Goldup, S. M.; Lee, A.-L.; Leigh, D. A.; McBurney, R. T. Active metal template synthesis of rotaxanes, catenanes and molecular shuttles. *Chem. Soc. Rev.* **2009**, *38* (6), 1530-1541.
57. Denis, M.; Goldup, S. M. The active template approach to interlocked molecules. *Nat. Rev. Chem.* **2017**, *1*, 0061.
58. Hines, D. A.; Darzi, E. R.; Hirst, E. S.; Jasti, R.; Kamat, P. V. Carbon Nanohoops: Excited Singlet and Triplet Behavior of Aza[8]CPP and 1,15-Diaza[8]CPP. *J. Phys. Chem. A* **2015**, *119* (29), 8083.
59. Darzi, E. R.; Hirst, E. S.; Weber, C. D.; Zakharov, L. N.; Lonergan, M.; Jasti, R. Synthesis, Properties, and Design Principles of Donor-Acceptor Nanohoops. *ACS Cent. Sci.* **2015**, *1* (6), 335.
60. Van Raden, J. M.; Louie, S.; Zakharov, L.; Jasti, R. 2,2'-Bipyridyl-Embedded Cycloparaphenylenes as a General Strategy To Investigate Nanohoop-Based Coordination Complexes. *J. Am. Chem. Soc.* **2017**, *139* (8), 2936.
61. Fan, Y.-Y.; Chen, D.; Huang, Z.-A.; Zhu, J.; Tung, C.-H.; Wi, L.-Z.; Cong, H. An isolable catenane consisting of two Möbius conjugated nanohoops. *Nat. Commun.* **2018**, *9*, 3037.
62. Van Raden, J. M.; White, B. M.; Zakharov, L. N.; Jasti, R. Nanohoop Rotaxanes from Active Metal Template Syntheses and Their Potential in Sensing Applications. *Angew. Chem. Int. Ed.* **2019**, *58* (22), 7341.

Chapter II

1. Endo, M.; Strano, M. S.; Ajayan, P. M. Potential Applications of Carbon Nanotubes. In *Carbon Nanotubes*, **2007**, 13.
2. Shulaker, M. M.; Hills, G.; Patil, N.; Wei, H.; Chen, H.-Y.; Wong, H.-S. P.; Mitra, S. Carbon nanotube computer. *Nature* **2013**, *501*, 526.
3. Notarianni, M.; Lui, J.; Vernon, K.; Motta, N. Synthesis and applications of carbon nanomaterials for energy generation and storage. *Deilstein J. Nanotechnol.* **2016**, *7*, 149.
4. Mauter, M. S.; Elimelech, M. Environmental Applications of Carbon-Based Nanomaterials. *Environ. Sci. Technol.* **2008**, *42* (16), 5843.
5. Brennan, L. J.; Byrne, M. T.; Bari, M.; Gun'ko, Y. K. Carbon Nanomaterials for Dy-Sensitized Solar Cell Applications: A Bright Future. *Adv. Energy Mater.* **2011**, *1*, 472.
6. Machado, F. M.; Lima, É. C.; Jauris, I. M. Adebayo, M. A. Carbon Nanomaterials for Environmental Applications. In *Carbon Nanomaterials as Adsorbents for Environmental and Biological Applications*, **2015**, 85.
7. Choudhary, N.; Hwang, S.; Choi, W. Carbon Nanomaterials: A Review. In *Handbook of Nanomaterials Properties*, **2014**, 709.
8. Kroto, H. W.; Heath, J. R.; O'Brien, S. C.; Curl, R. F.; Smalley, R. E. C₆₀: Buckminsterfullerene. *Nature* **1985**, *382*, 162.
9. Tagmatarchis, L. Fullerene-Based Electronics. In *Advances in Carbon Nanomaterials: Science and Applications*, **2012**, 189.
10. Tagmatarchis, L. Cell Biology of Carbon Nanotubes. In *Advances in Carbon Nanomaterials: Science and Applications*, **2012**, 343.
11. Panwar, N.; Soehartono, A. M.; Chan, K. K.; Zeng, S.; Xu, G.; Qu, J.; Coquet, P.; Yong, K. T.; Chen, X. Nanocarbons for Biology and Medicine: Sensing, Imaging, and Drug Delivery. *Chem. Rev.* **2019**, *119*, 9959.
12. Augustine, S.; Singh, J.; Srivastava, M.; Sharma, M.; Dasa, A.; Malhotra, B.D. Recent advances in carbon based nanosystems for cancer theranostics. *Biomater. Sci.* **2017**, *5*, 901.
13. Loh, K. P.; Ho, D.; Chiu, G. N. C.; Leong, D. T.; Pastorin, G.; Chow, E. K.-H. Clinical Applications of Carbon Nanomaterials in Diagnostics and Therapy. *Adv. Mater.* **2018**, *30* (47), 1802368.
14. Hong, G.; Diao, S.; Antaris, A. L.; Dai, H. Carbon Nanomaterials for Biological Imaging and Nanomedicinal Therapy. *Chem. Rev.* **2015**, *115*, 10816.

15. Ajitha, A. R.; Akhina, H.; Aswathi, M. K.; Lovely, M.; Sabu, T. Carbon Nanotubes: An Ideal Candidate for Biomedical Applications. *JSM Nanotechnol. Nanomed.* **2018**, *6* (2), 1605.
16. Hirsch, A. Functionalization of Single-Walled Carbon Nanotubes. *Angew. Chem. Int. Ed.* **2002**, *41* (11), 1853.
17. Nielsen, G. D.; Roursgaard, M.; Jensen, K. A.; Poulsen, S. S.; Larsen, S. T. *In Vivo* Biology and Toxicology of Fullerenes and Their Derivatives. *Basic Clin. Pharmacol. Toxicol.* **2008**, *103* (3), 197.
18. Jia, G.; Wang, H.; Yan, L.; Wang, X.; Pei, R.; Yan, T.; Zhao, Y.; Guo, X. Cytotoxicity of Carbon Nanomaterials: Single-Wall Nanotube, Multi-Wall Nanotube, and Fullerene. *Environ. Sci. Technol.* **2005**, *39*, 1378.
19. Sayes, C. M.; Fortner, J. D.; Wenh G.; Lyon, D.; Boyd, A. M.; Ausman, K. D.; Tao, Y. J.; Sitharaman, B.; Wilson, L. J.; Hughes, J. B. West, J. L.; Colvin, V. L. The Differential Cytotoxicity of Water-Soluble Fullerenes. *Nano. Lett.* **2004**, *4* (10), 1881.
20. Patlolla, A.; Knighten, B.; Tchounwou, P. Multi-Walled Carbon Nanotubes Induce Cytotoxicity, Genotoxicity and Apoptosis In Normal Human Dermal Fibroblast Cells. *Ethn. Dis.* **2010**, *20*, 65.
21. Zhang, Y.; Ali, S. F.; Dervishi, E.; Xu, Y.; Li, Z.; Casciano, D.; Biris, A. S. Cytotoxicity effects of graphene and single-wall carbon nanotubes in neural pheochromocytoma-derived PC12 cells. *ACS Nano.* **2010**, *4* (6), 3181.
22. Wick, P.; Manser, P.; Limbach, L. K.; Dettlaff, Weglikowska, U.; Krumeich, F.; Roth, S.; Stark, W. J.; Bruinink, A. The degree and kind of agglomeration affect carbon nanotube cytotoxicity. *Toxicol. Lett.* **2007**, *168* (2), 121.
23. Kim, J. S.; Song, K. S.; Lee, J. H.; Yu, I. J. Evaluation of biocompatible dispersants for carbon nanotube toxicity tests. *Arch. Toxicol.* **2011**, *85* (12), 1499.
24. Jiang, J. K.; Oberdorster, G.; Biswas, P. Characterization of size, surface charge, and agglomeration state of nanoparticle dispersions for toxicological studies. *J. Nanopart. Res.* **2009**, *11*, 77.
25. Herzog, E.; Byrne, H. J.; Davoren, M.; Casey, A.; Duschl, A.; Oostingh, G. J. Dispersion medium modulates oxidative stress response of human lung epithelial cells upon exposure to carbon nanomaterial samples. *Toxicol. Appl. Pharmacol.* **2009**, *236*, 276.
26. Moore, V. C.; Strano, M. S.; Haroz, E. H.; Hauge, R. H.; Smalley, R. E. Individually Suspended Single-Walled Carbon Nanotubes in Various Surfactants. *Nano. Lett.* **2003**, *3* (10), 1379.

27. Setaro, A.; Adeli, M.; Glaeske, M.; Przyrembel, D.; Bisswanger, T.; Gordeev, G.; Maschietto, F.; Faghani, A.; Paulus, B.; Weinelt, M.; Arenal, R.; Haag, R.; Reich, S. Preserving π -conjugation in covalently functionalized carbon nanotubes for optoelectronic applications. *Nat. Commun.* **2017**, *8*, 14281.
28. Cognet, L.; Tsyboulski, D. A.; Rocha, J.-D. R.; Doyle, C. D.; Tour, J. M.; Weisman, R. B. Stepwise Quenching of Exciton Fluorescence in Carbon Nanotubes by Single-Molecule Reactions. *Science* **2007**, *316* (5830), 1465.
29. Lee, A. J.; Wang, X.; Carlson, L. J.; Smyder, J. A.; Loesch, B.; Tu, X.; Zheng, M.; Krauss, T. D. Bright Fluorescence from Individual Single-Walled Carbon Nanotubes. *Nano Lett.* **2011**, *11* (4), 1636.
30. Sisto, T. J.; Tian, X.; Jasti, R. Synthesis of Tetraphenyl-Substituted [12]Cycloparaphenylene: Toward a Rationally Designed Ultrashort Carbon Nanotube. *J. Org. Chem.* **2012**, *77* (14), 5857.
31. White, B. M.; Zhao, Y.; Kawashima, T. E.; Branchaud, B. P.; Pluth, M. D.; Jasti, R. Expanding the Chemical Space of Biocompatible Fluorophores: Nanohoops in Cells. *ACS Cent. Sci.* **2018**, *4*, 1173.
32. Leonhardt, E. J.; Van Raden, J. M.; Miller, D. J.; Zakharov, L. N.; Alemán, B. J.; Jasti, R. A Bottom-Up Approach to Solution-Processed, Atomically Precise Graphitic Cylinders on Graphite. *Nano Lett.* **2018**, *18*, 7991.
33. Lu, D.; Zhuang, G.; Jia, H.; Wang, J.; Huang, Q.; Cui, S.; Pingwu, D. A novel symmetrically multifunctionalized dodecamethoxy-cycloparaphenylene: synthesis, photophysical, and supramolecular properties. *Org. Chem. Front.* **2018**, *5*, 1446.
34. Peters, G. M.; Grover, G.; Maust, R. L.; Colwell, C. E.; Bates, H.; Edgell, W. A.; Jasti, R.; Kertesz, M.; Tovar, J. D. Linear and Radial Conjugation in Extended π -Electron Systems. *J. Am. Chem. Soc.* **2020**, *142* (5), 2293.
35. Li, K.; Xu, Z.; Deng, H.; Zhou, Z.; Dang, Y.; Sun, Z. Dimeric Cycloparaphenylenes with a Rigid Aromatic Linker. *Angew. Chem. Int. Ed.* **2021**, *60* (14), 7649.
36. Kohrs, D.; Becker, J.; Wegner, H. A. A Modular Synthesis of Substituted Cycloparaphenylenes. *Chem. Euro. J.*, **2022**, *28* (8), e202104239.
37. Iwamoto, T.; Watanabe, Y.; Sadahiro, T.; Haino, T.; Yamago, S. Size-Selective Encapsulation of C₆₀ by [10]Cycloparaphenylene: Formation of the Shortest Fullerene-Peapod. *Angew. Chem. Int. Ed.* **2011**, *50* (36), 8342.
38. Darzi, E. R.; Jasti, R. The Dynamic Size-Dependent Properties of [5]-[12] Cycloparaphenylenes. *Chem. Soc. Rev.* **2015**, *44*, 6401.

39. Kuwabara, T.; Orii, J.; Segawa, Y.; Itami, K. Curved Oligophenylenes as Donors in Shape-Persistent Donor-Acceptor Macrocycles with Solvatochromic Properties. *Angew. Chem. Int. Ed.* **2005**, *54* (33), 9646.
40. Lovell, T. C.; Garrison, Z. R.; Jasti, R. Synthesis, Characterization, and Computational Investigation of Bright Orange Emitting Benzothiadiazole. *Angew. Chem. Int. Ed.* **2020**, *59* (34), 14363.
41. Hermann, M.; Wassy, D.; Esser, B. Conjugated Nanohoops Incorporating Donor, Acceptor, Hetero- or Polycyclic Aromatics. *Angew. Chem. Int. Ed.* **2021**, *60* (29), 15743.
42. Lovell, T. C.; Bolton, S. G.; Kenison, J. P.; Shangguan, J.; Otteson, C. E.; Cevitci, F.; Nan, X.; Pluth, M. D.; Jasti, R. Subcellular Targeted Nanohoop for One- and Two-Photon Live Cell Imaging. *ACS Nano*. **2021**, *15*, 15285.
43. Tsien, R. Y. A non-disruptive technique for loading calcium buffers and indicators into cells. *Nature* **1981**, *290*, 527.
44. Lin, V. S.; Lippert, A. R.; Chang, C. J. Cell-trappable fluorescent probes for endogenous hydrogen sulfide signaling and imaging in H₂O₂-dependant H₂S production. *Proc. Nat. Acad. Sci.* **2013**, *110* (18), 7131.
45. Marshall, J. L.; O'Neal, N. J.; Zakharov, L. N.; Haley, M. M. Synthesis and Characterization of Two Unsymmetrical Indenofluorene Analogues: Benzo[5,6]-s-indaceno[1,2-*b*]thiophene and Benzo[5,6]-s-indaceno[2,1-*b*]thiophene. *J. Org. Chem.* **2016**, *81* (9), 3674.
46. Shaub, T. A.; Margraf, J. T.; Zakharov, L.; Reuter, K.; Jasti, R. Strain-Promoted Reactivity of Alkyne-Containing Cycloparaphenylenes. *Angew. Chem. Int. Ed.* **2018**, *57* (50), 16348.
47. Lovell, T. C.*; Colwell, C. E.*; Zakharov, L. N.; Jasti, R. Symmetry breaking and the turn-on fluorescence of small, highly strained carbon nanohoops. *Chem. Sci.*, **2019**, *10*, 3786.
48. Xue, P.; Sun, J.; Chen, P.; Gong, P.; Yao, B.; Zhang, Z.; Qian, C.; Lu, R. Strong solid emission and mechanofluorochromism of carbazole-based terephthalate derivatives adjusted by alkyl chains. *J. Mater. Chem. C*, **2015**, *3*, 4086.
49. Bruno, N. C.; Tudge, M. T.; Buchwald, S. L. Design and Preparation of New Palladium Precatalysts for C–C and C–N Cross-Coupling Reactions. *Chem. Sci.* **2013**, *4* (3), 916.

Chapter III

1. De Volder, M. F. L.; Tawfick, S. H.; Baughman, R. H.; Hart, A. J. Carbon Nanotubes: Present and Future Commercial Applications. *Science* **2013**, 339, 535.
2. Jariwala, D.; Sangwan, V. K.; Lauhon, L. J.; Marks, T. J.; Hersam, M. C. Carbon nanomaterials for electronics, optoelectronics, photovoltaics, and sensing. *Chem. Soc. Rev.* **2013**, 42, 2824.
3. Zhu, S.; Xu, G. Single-walled carbon nanohorns and their applications. *Nanoscale* **2010**, 2, 2538.
4. Panwar, N.; Soehartono, A. M.; Chan, K. K.; Zeng, S.; Xu, G.; Qu, J.; Coquet, P.; Yong, K. T.; Chen, X. Nanocarbons for Biology and Medicine: Sensing, Imaging, and Drug Delivery. *Chem. Rev.* **2019**, 119, 9559.
5. Augustine, S.; Singh, J.; Srivastava, M.; Sharma, M.; Dasa, A.; Malhotra, B.D. Recent advances in carbon based nanosystems for cancer theranostics. *Biomater. Sci.* **2017**, 5, 901.
6. Liu, Z.; Robinson, J. T.; Tabakman, S. M.; Yang, K.; Dai, H. Carbon materials for drug delivery & cancer therapy. *Mater. Today* **2011**, 14, 316.
7. Wong, B. S.; Yoong, S. L.; Jagusiak, A.; Panczyk, T.; Ho, H. K.; Ang, W. H.; Pastorin, G. Carbon nanotubes for delivery of small molecule drugs. *Adv. Drug Delivery Rev.* **2013**, 65, 1964.
8. Biagiotti, G.; Fedeli, S.; Tuci, G.; Luconi, L.; Giambastiani, G.; Brandi, A.; Pisaneschi, F.; Cicchi, S.; Paoli, P. Combined therapies with nanostructured carbon materials: there is room still available at the bottom. *J. Mater. Chem. B* **2018**, 6, 2022.
9. Saleem, J.; Wang, L.; Chen, C. Carbon-Based Nanomaterials for Cancer Therapy via Targeting Tumor Microenvironment. *Adv. Healthcare Mater.* **2018**, 7, 1800525.
10. Liu Z., Sun X., Nakayama-Ratchford N., Dai H. Supramolecular Chemistry on Water-Soluble Carbon Nanotubes for Drug Loading and Delivery. *ACS Nano* **2007**, 1, 50.
11. Kharissova, O. V.; González, C. M. O.; Kharisov, B. I. Solubilization and Dispersion of Carbon Allotropes in Water and Non-aqueous Solvents. *Ind. Eng. Chem. Res.* **2018**, 57, 12624.
12. Damasceno, J. P. V.; Zarbin, A. J. G. A new approach for the achievement of stable aqueous dispersions of carbon nanotubes. *Chem. Commun.* **2019**, 55, 5809.
13. Al-Hamadani, Y. A. J.; Chu, K. H.; Son, A.; Heo, J.; Her, N.; Jang, M.; Park, C. M.; Yoon, Y. Stabilization and dispersion of carbon nanomaterials in aqueous solutions: A review. *Sep. Purif. Technol.* **2015**, 156, 861.

14. Marcus, Y.; Smith, A. L.; Korobov, M. V.; Mirakyan, A. L.; Avramenko, N. V.; Stukalin, E. B. Solubility of C₆₀ Fullerene. *J. Phys. Chem. B* **2001**, *105*, 2499.
15. Bianco A.; Kostarelos K.; Prato M. Making carbon nanotubes biocompatible and biodegradable. *Chem. Commun.* **2011**, *47*, 10182.
16. Nayagam D. A. X.; Williams, R. A.; Chen, J.; Magee, K. A.; Irwin, J.; Tan, J.; Innis, P.; Leung, R. T.; Finch, S.; Williams, C. E.; Clark, G. M.; Wallace, G. G. Biocompatibility of Immobilized Aligned Carbon Nanotubes. *Small* **2011**, *7*, 1035.
17. Mchedlov-Petrossyan, N. O.; Klochkov, V. K.; Andrievsky, G. V. Colloidal dispersions of fullerene C₆₀ in water: some properties and regularities of coagulation by electrolytes. *J. Am. Chem. Soc., Faraday Trans.* **1997**, *93*, 4343.
18. Andrievsky, G. V.; Kosevich, M. V.; Vovk, O. M.; Shelkovsky, V. S.; Vashchenko, L. A. On the production of an aqueous colloidal solution of fullerenes. *J. Chem. Soc., Chem. Commun.* **1995**, 1281.
19. Mikheev, I. V.; Pirogova, M. O.; Usoltseva, L. O.; Uzhel, A. S.; Bolotnik, T. A.; Kareev, I. E.; Bubnov, V. P.; Lukonina, N. S.; Volkov, D. S.; Goryunkov, A. A.; Korobov, M. V.; Proskurnin, M. A. Green and rapid preparation of long-term stable aqueous dispersions of fullerenes and endohedral fullerenes: The pros and cons of an ultrasonic probe. *Ultrason. Sonochem.* **2021**, *73*, 105533.
20. Afreen, S.; Kokubo, K.; Muthoosamy, K.; Manickam, S. Hydration or hydroxylation: direct synthesis of fulleranol from pristine fullerene [C₆₀] via acoustic cavitation in the presence of hydrogen peroxide. *RSC Adv.* **2017**, *7*, 31930.
21. Hirsch, A. Functionalization of Single-Walled Carbon Nanotubes. *Angew. Chem. Int. Ed.* **2002**, *41* (11), 1853.
22. Cagnet, L.; Tsyboulski, D. A.; Rocha, J.-D. R.; Doyle, C. D.; Tour, J. M.; Weisman, R. B. Stepwise Quenching of Exciton Fluorescence in Carbon Nanotubes by Single-Molecule Reactions. *Science* **2007**, *316* (5830), 1465.
23. Canevet, D.; Pérez, E. M.; Martín, N. Wraparound Hosts for Fullerenes: Tailored Macrocycles and Cages. *Angew. Chem. Int. Ed.* **2011**, *50*, 9248.
24. Andersson, T.; Nilsson, K.; Sundahl, M. Westman, G.; Wennerström, O. C₆₀ embedded in γ -cyclodextrin: a water-soluble fullerene. *J. Am. Chem. Soc., Chem. Commun.* **1992**, (8), 604.
25. Giosia, M. D.; Bomans, P. H. H.; Bottoni, A.; Cantelli, A.; Falini, G.; Franchi, P.; Guarracino, G.; Friedrich, H.; Lucarini, M.; Paolucci, F.; Rapino, S.; Sommerdijk, N. A. J. M.; Soldá, A.; Valle, F.; Zerbetto, F.; Calvaresi, M. Proteins as supramolecular hosts for C₆₀: a true solution of C₆₀ in water. *Nanoscale* **2018**, *10* (21), 9908.

26. Murthy, C. N.; Geckeler, K. E. The water-soluble β -cyclodextrin-[C₆₀]fullerene complex. *Chem. Commun.* **2001**, (13), 1194.
27. Andersson, T.; Westman, G.; Wennerström, O.; Sundahl, M. NMR and UV-VIS Investigation of water-soluble fullerene-60- γ -cyclodextrin complex. *J. Chem. Soc., Perkin Trans.* **1994**, 2, 1097.
28. Suzuki, T.; Nakashima, K.; Shinkai, S. Very Convenient and Efficient Purification Method for Fullerene (C₆₀) with 5,11,17,23,29,35,41,47-Octa-*tert*-butylcalix[8]arene-49,50,51,52,53,54,55,56-octol. *Chem. Lett.* **1994**, 23 (4), 699.
29. Atwood, J. L.; Koutsantonis, G. A.; Raston, C. L. Purification of C₆₀ and C₇₀ by selective complexation with calixarenes. *Nature* **1994**, 368, 229.
30. Pérez, E. M.; Martín, N. Molecular tweezers for fullerenes. *Pure Appl. Chem.* **2010**, 82 (3), 523.
31. Da Ros, T.; Prato, M. Medicinal chemistry with fullerenes and fullerene derivatives. *Chem. Commun.* **1999**, (8), 663.
32. Pérez, E. M.; Martín, N. Curves ahead: molecular receptors for fullerenes based on concave-convex complementarity. *Chem. Soc. Rev.* **2008**, 37 (8), 1512.
33. Smith, B. W.; Monthieux, M.; Luzzi, D. E. Encapsulated C₆₀ in carbon nanotubes. *Nature* **1998**, 396, 323.
34. Iijima, S.; Ichihashi, T.; Ando, Y. Pentagons, heptagons and negative curvature in graphite microtubule growth *Nature* **1992**, 356, 776.
35. Luzzi, D. E.; Smith, B. W. Carbon cage structures in single wall carbon nanotubes: a new class of materials. *Carbon* **2000**, 38 (11-12), 1751.
36. Iwamoto, T.; Watanabe, Y.; Sadahiro, T.; Haino, T.; Yamago, S. Size-selective encapsulation of C₆₀ by [10]cycloparaphenylene: formation of the shortest fullerene-peapod. *Angew. Chem. Int. Ed.* **2011**, 50, 8342.
37. Lu, D.; Huang, Q.; Wang, S.; Wang, J.; Huang, P.; Du, P. The Supramolecular Chemistry of Cycloparaphenylenes and Their Analogs. *Front. Chem.* **2019**, 7 668.
38. Xu, Y.; von Delius, M. The Supramolecular Chemistry of Strained Carbon Nanohoops. *Angew. Chem. Int. Ed.* **2020**, 59 (2), 559.
39. Bachrach, S. M.; Zayat, Z.-C. "Planetary Orbit" Systems Composed of Cycloparaphenylenes. *J. Org. Chem.* **2016**, 81, 4559.

40. Jiang, Y.; Mattioli, E. J.; Calvaresi, M.; Wang, Z. Theoretical design of an ultrafast supramolecular rotor composed of carbon nano-rings. *Chem. Commun.* **2020**, *56*, 11835.
41. Rehman, H. U.; McKee, N. A.; McKee, M. L. Saturn Systems. *Comput. Chem.* **2016**, *37*, 194.
42. Minameyer, M. B.; Xu, Y.; Frühwald, S.; Görling, A.; von Delius, M.; Drewello, T. Investigation of Cycloparaphenylenes (CPPs) and their Noncovalent Ring-in-Ring and Fullerene-in-Ring Complexes by (Matrix-Assisted) Laser Desorption/Ionization and Density Functional Theory. *Chem. Euro. J.* **2020**, *26*, 8729.
43. Hashimoto, S.; Iwamoto, T.; Kurachi, D.; Kayahara, E.; Yamago, S. Shortest Double-Walled Carbon Nanotubes Composed of Cycloparaphenylenes. *ChemPlusChem* **2017**, *82*, 1015.
44. Zhao, C.; Liu, F.; Feng, L.; Mingzhe, N.; Lu, Y.; Zhang, J.; Wang, C.; Wang, T. Construction of a double-walled carbon nanoring. *Nanoscale*, **2021**, *13*, 4880.
45. Hashimoto, S.; Iwamoto, T.; Kurachi, D.; Kayahara, E.; Yamago, S. Shortest Double-Walled Carbon Nanotubes Composed of Cycloparaphenylenes. *ChemPlusChem* **2017**, *82*, 1015.
46. Yumura, T.; Miki, R.; Fukura, S.; Yamamoto, W. Energetics of Hybrid Structures between Cycloparaphenylene and Carbon Nanotubes: A Dispersion-Corrected Density Functional Theory Study. *J. Phys. Chem. C* **2020**, *124* (32), 17836.
47. Miki, K.; Saiki, K.; Umeyama, T.; Baek, J.; Noda, T.; Imahori, H.; Sato, Y.; Suenaga, K.; Ohe, K. Unique Tube-Ring Interactions: Complexation of Single-Walled Carbon Nanotubes with Cycloparaphenyleneacetylenes. *Small* **2018**, 1800720.
48. Kwon, H.; Bruns, C. J. All-hydrocarbon, all-conjugated cycloparaphenylene-polycyclic aromatic hydrocarbon host-guest complexes stabilized by CH- π interactions. *Nano Res.* **2022**, *15*, 5545.
49. Jasti, R. Bhattacharjee, J.; Neaton, J. B.; Bertozzi, C. Synthesis, Characterization, and Theory of [9]-, [12]-, and [18]Cycloparaphenylene: Carbon NanoHoop Structures. *J. Am. Chem. Soc.* **2008**, *130*, 17646.
50. Xia, J.; Bacon, J. W.; Jasti, R. Gram-Scale Synthesis and Crystal Structures of [8]- and [10]CPP, and the Solid-State Structure of C₆₀@[10]CPP. *Chem. Sci.* **2012**, *3*, 3018.
51. Evans, P. J.*; Darzi, E. R.*; Jasti E. Efficient Room Temperature Synthesis of a Highly Strained Carbon NanoHoop Fragment of Buckminsterfullerene. *Nat. Chem.* **2014**, *6*, 404.
52. Kayahara, E.; Patel, V. K.; Xia, J.; Jasti, R.; Yamago, S. Selective and Gram-scale Synthesis of [6]Cycloparaphenylene. *Synlett.* **2015**, *1*, 335.

53. Van Raden, J. M.; Darzi, E. R.; Zakharov, L. N.; Jasti, R. Synthesis and Characterization of a Highly Strained Donor-Acceptor Nanohoop. *Org. Biomol. Chem.* **2016**, *14*, 5721.

Chapter IV

1. Mao, L.; Liu, Y.; Yang, S.; Li, Y.; Zhang, X.; Wei, Y. Recent advances and progress of fluorescent bio/chemosensors based on aggregation-induced emission molecules. *Dyes Pigm.* **2019**, *162*, 611.
2. Zhang, X.-Y.; Yang, Y.-S.; Wang, W.; Jiao, Q.-C.; Zhu, H.-L. Fluorescent sensors for the detection of hydrazine in environmental and biological systems: recent advances and future prospects. *Coord. Chem. Rev.* **2020**, *417*, 213367.
3. Zajac, M.; Chakraborty, K.; Saha, S.; Mahadevan, V.; Infield, D. T.; Accardi, A.; Qiu, Z.; Krishnan, Y. What biologists want from their chloride reporters – a conversation between chemists and biologists. *J. Cell Sci.* **2020**, *133*, 1.
4. Chen, X.; Wang, F.; Hyun, J. Y.; Wei, T.; Qiang, J.; Ren, X.; Shin, I.; Yoon, J. Recent progress in the development of fluorescent, luminescent and colorimetric probes for detection of reactive oxygen and nitrogen species. *Chem. Soc. Rev.* **2016**, *45*, 2976.
5. Jiao, X.; Li, Y.; Niu, J.; Xie, X.; Wang, X.; Tang, B. Small-molecule fluorescent probes for imaging and detection of reactive oxygen, nitrogen and sulfur species in biological systems. *Anal. Chem.* **2018**, *90*, 533.
6. Giepmans, B. N. G.; Adams, S. R.; Ellisman, M. H.; Tsien, R. Y. The fluorescent toolbox for assessing protein location and function. *Science* **2006**, *312*, 214.
7. Chan, J.; Dodani, S. C.; Chang, C. J. Reaction-based small molecule fluorescent probes. *Nat. Chem.* **2012**, *4*, 973.
8. Bai, X.; Ng, K. K.-H.; Hu, J. J.; Ye, S.; Yang D. Small-molecule-based fluorescent sensors for selective detection of reactive oxygen species in biological systems. *Annu. Rev. Biochem.* **2019**, *88*, 605.
9. Zuin, M.; Rigatelli, G.; Faggian, G.; L'Erario, R.; Chinaglia, M.; Roncon, L. Could advanced drug delivery systems be the future in cardiovascular revascularization medicine? *Vascular*, **2017**, *25*, 447.
10. Veisheh, O., Tang, B. C., Whitehead, K. A., Anderson, D. G., Langer, R., Managing diabetes with nanomedicine: challenges and opportunities. *Nat. Rev. Drug Discov.* **2014**, *14*, 45.

11. Timko, B. P.; Dvir, T.; Kohane, D. S. Remotely triggerable drug delivery systems. *Adv. Mater.* **2010**, *22*, 4925.
12. Pederson, C. J. Cyclic polyethers and their complexes with metal salts. *J. Am. Chem. Soc.* **1967**, *89*, 7017.
13. Bezner, B. J.; Ryan, L. S.; Lippert, A. R. Reaction-based luminescent probes for reactive sulfur, oxygen, and nitrogen species: analytical techniques and recent progress. *Anal. Chem.* **2020**, *92*, 309.
14. Cho, D.-G.; Sessler, J. L. Modern reaction-based indicator systems. *Chem. Soc. Rev.* **2009**, *38*, 1647.
15. Jun, M. E.; Roy, B.; Ahn, K. H. "Turn-on" fluorescent sensing with "reactive" probes. *Chem. Commun.*, **2011**, *47*, 7583.
16. Chang, M. C. Y.; Pralle, A.; Isacoff, E. Y.; Chang, C. J. A selective, cell-permeable optical probe for hydrogen peroxide in living cells. *J. Am. Chem. Soc.* **2004**, *126*, 15392.
17. Stoddart, J. F. Mechanically interlocked molecules (MIMs)-molecular shuttles, switches and machines. *Angew. Chem. Int. Ed.* **2017**, *56*, 11094.
18. Pairault, N.; Barat, R.; Tranoy-Opalinski, I.; Renoux, B.; Thomas, M.; Papot, S. Rotaxane-based architectures for biological applications. *Comptes Rendus Chim.* **2016**, *19*, 103.
19. Denis, M.; Qin, L.; Turner, P.; Jolliffe, K. A.; Goldup, S. M. A fluorescent ditopic rotaxane ion-pair host. *Angew. Chem. Int. Ed.* **2018**, *57*, 5315.
20. Denis, M.; Pancholi, J.; Jobe, K.; Watkinson, M.; Goldup, S. M. Chelating rotaxane ligands as fluorescent sensors for metal ions. *Angew. Chem. Int. Ed.* **2018**, *57*, 5310.
21. Lim, Y. C. J.; Marques, I.; Félix, V.; Beer, P. D. A chiral halogen-bonding [3]rotaxane for the recognition and sensing of biologically relevant dicarboxylate anions. *Angew. Chem. Int. Ed.* **2017**, *57*, 584.
22. Knighton, R. C.; Dapin, S.; Beer, P. D. Luminescent anion sensing by transition-metal dipyridylbenzene complexes incorporated into acyclic, macrocyclic and interlocked hosts. *Chem. Euro. J.* **2020**, *26*, 5288.
23. Bak, K. M.; Porfyakis, K.; Davis, J. J.; Beer, P. D. Exploiting the mechanical bond for molecular recognition and sensing of charged species. *Mater. Chem. Front.* **2019**, *4*, 1052.
24. Arunkumar, E.; Forbes, C. C.; Noll, B. C.; Smith, B. D. Squaraine-derived rotaxanes: sterically protected fluorescent near IR-dyes. *J. Am. Chem. Soc.* **2005**, *127*, 3288.

25. Craig, M. R.; Claridge, T. D. W.; Hutchings, M. G.; Anderson, H. L. Synthesis of a cyclodextrin azo dye [3]rotaxane as a single isomer. *Chem. Commun.* **1999**, 1537.
26. Zhai, C.; Schreiber, C. L.; Padilla-Coley, S.; Oliver, A. G.; Smith, B. D. Fluorescent self-threaded peptide probes for biological imaging. *Angew. Chem. Int. Ed.* **2020**, *59*, 23740.
27. Shaw, S. K.; Liu, W.; Gómez Durán, C. F. A.; Schreiber, C. L.; Betancourt Mendiola, M. de L.; Zhai, C.; Roland, F. M.; Padanilam, S. J.; Smith, B. D. Non-covalently pre-assembled high-performance near-infrared fluorescent molecular probes for cancer imaging. *Chem. Commun.* **2018**, *24*, 13821.
28. Ambrogio, M. W.; Thomas, C. R.; Zhao, Y. L.; Zink, J. I.; Stoddart, J. F. Mechanized silica nanoparticles: A new frontier in theranostic nanomedicine. *Acc. Chem. Res.* **2011**, *44*, 903.
29. Barat, R.; Legigan, T.; Tranoy-Opalinski, I.; Renoux, B.; Péraudeau, E.; Clarhaut, J.; Pointot, P.; Fernandes, A. E.; Aucagne, V.; Leigh, D. A.; Papot, S. A mechanically interlocked molecular system programmed for the delivery of an anticancer drug. *Chem.* **2015**, *6*, 2608.
30. Fernandes, A. E.; Viterisi, A.; Coutrot, F.; Potok, S.; Leigh, D. A.; Aucagne, V.; Papot, S. Rotaxane-based propeptides: protection and enzymatic release of a bioactive pentapeptide. *Angew. Chem. Int. Ed.* **2009**, *48*, 6443.
31. Neal, E. A.; Goldup, S. M. Chemical consequences of mechanical bonding in catenanes and rotaxanes: isomerism, modification, catalysis and molecular machines for synthesis. *Chem. Commun.* **2014**, *50*, 5128.
32. Parham, A. H.; Windisch, B.; Vögtle, F. Chemical reactions in the axle of rotaxanes – steric hindrance by the wheel. *Eur. J. Org. Chem.* **1999**, *1999*, 1233.
33. Anderson, S.; Claridge, T. D. W.; Anderson, H. L. Azo-dye rotaxanes. *Angew. Chem. Int. Ed.* **1997**, *36*, 1310.
34. Van Raden, J. M.; Louie, S.; Zakharov, L. N.; Jasti, R. 2,2'-Bipyridyl-embedded cycloparaphenylenes as a general strategy to investigate nanohoop-based coordination complexes. *J. Am. Chem. Soc.* **2017**, *139*, 2936.
35. Van Raden, J. M.; White, B. M.; Zakharov, L. N.; Jasti, R. Nanohoop rotaxanes from active metal template syntheses and their potential in sensing applications. *Angew. Chem. Int. Ed.* **2019**, *58*, 7341.
36. Van Raden, J. M.; Jarenwattananon, N.; Zakharov, L. N.; Jasti, R. Active metal template synthesis and characterization of a nanohoop [c2]daisy chain rotaxane. *Chem. Eur. J.* **2020**, *26*, 10205.
37. Darzi, E.; Jasti, R. The dynamic size-dependent properties of [5]-[12]cycloparaphenylenes. *Chem. Soc. Rev.* **2015**, *44*, 6401.

38. Wang, R. Two's company, three's a crowd: can H₂S be the third endogenous gaseous transmitter? *FASEB J.* **2002**, *16*, 1792.
39. Wu, D.; Hu, Q.; Liu, X.; Pan, L.; Xiong, Q.; Zhu, Y. Z. Hydrogen sulfide protects against apoptosis under oxidative stress through SIRT1 pathway in H9c2 cardiomyocytes. *Nitric Oxide*, **2015**, *46*, 204.
40. Rinaldi, L.; Gobbi, G.; Pambianco, M.; Micheloni, C.; Mirandola, P.; Vitale, M. Hydrogen sulfide prevents apoptosis of human PMN via inhibition of p38 and caspase 3. *Lab. Invest.*, **2006**, *86*, 391.
41. Katsouda, A.; Bibli, S.-I.; Pyriochou, A.; Szabo, C. Regulation and role of endogenously produced hydrogen sulfide in angiogenesis. *Pharmacol. Res.* **2016**, *113*, 175.
42. Kimura, H. Physiological role of hydrogen sulfide and polysulfide in the central nervous system. *Neurochem. Int.* **2013**, *63*, 492.
43. Hartle, M. D.; Pluth, M. D. A practical guide to working the H₂S at the interface of chemistry and biology. *Chem. Soc. Rev.* **2016**, *45*, 6081.
44. Lin, V. S.; Chen, W.; Xian, M.; Chang, C. J. Chemical probes for molecular imaging and detection of hydrogen sulfide and reactive sulfur species in biological systems. *Chem. Soc. Rev.* **2015**, *44*, 4596.
45. Yu, F.; Han, X.; Chen, L. Fluorescent probes for hydrogen sulfide detection and bioimaging. *Chem. Commun.* **2014**, *50*, 12234.
46. Shi, B.; Gu, X.; Fei, Q.; Zhao, C. Photoacoustic probes for real-time tracking of endogenous H₂S in living mice. *Chem. Sci.* **2017**, *8*, 2150.
47. Cao, J.; Lopez, R.; Thacker, J. M.; Moon, J. Y.; Jiang, C.; Morris, S. N. S.; Bauer, J. H.; Tao, P.; Mason, R. P.; Lippert, A. R. Chemiluminescent probes for imaging H₂S in living animals. *Chem. Sci.* **2015**, *6*, 1979.
48. Bailey, T. S.; Pluth, M. D. Chemiluminescent detection of enzymatically produced hydrogen sulfide: Substrate hydrogen bonding influences selectivity for H₂S over biological thiols. *J. Am. Chem. Soc.* **2013**, *135*, 16697.
49. Montoya, L. A.; Pluth, M. D. Selective turn-on fluorescent probes for imaging hydrogen sulfide in living cells. *Chem. Commun.* **2012**, *48*, 4767.
50. Montoya, L. A.; Pearce, T. F.; Hansen, R. J.; Zakharov, L. N.; Pluth, M. D. Development of selective colorimetric probes for hydrogen sulfide based on nucleophilic aromatic substitution. *J. Org. Chem.* **2013**, *78*, 6550.

51. Lei, Y.; Wang, K.-P.; Chen, S.; Zhang, Q.; Hu, Z.-Q. A fluorescent probe based on tetrahydro[5]helicene for highly selective recognition of hydrogen sulfide. *Spectrochim. Acta A*, **2018**, *204*, 295.
52. Otteson, C. E.; Levinn, C. M.; Van Raden, J. M.; Pluth, M. D.; Jasti, R. Nanohoop Rotaxane Design to Enhance Selectivity of Reaction-Based Probes: a Proof-of-Principle Study. *Org. Lett.* **2021**, *23*, 4608.
53. Denis, M.; Goldup, S. M. The active template approach to interlocked molecules. *Nat. Chem. Rev.* **2017**, *1*, 0061.
54. Berná, J.; Goldup, S. M.; Lee, A.-L.; Leigh, D. A.; Symes, M. D.; Teobaldi, G.; Zerbetto, F. Cadiot-Chodkiewicz active template synthesis of rotaxanes and switchable molecular shuttles with weak intercomponent interactions. *Angew. Chem. Int. Ed.* **2008**, *47*, 4392.
55. White, B. M.; Zhao, Y.; Kawashima, T. E.; Branchaud, B. P.; Pluth, M. D.; Jasti, R. Expanding the chemical space of biocompatible fluorophores: nanohoops in cells. *ACS Cent. Sci.* **2018**, *4*, 1173.
56. Archard, T.; Lepronier, A.; Gimbert, Y.; Clavier, H.; Giordano, L.; Tenaglia, A.; Buono, G. A Regio- and Diastereoselective Platinum-Catalyzed Tandem [2+1]/[3+2] Cycloaddition Sequence. *Angew. Chemie Int. Ed.* **2011**, *50* (15), 3552.
57. Hartle, M. D.; Meininger, D. J.; Zakharov, L. N.; Tonzetich, Z. J.; Pluth, M. D. NBu₄SH provides a convenient source of HS⁻ soluble in organic solution for H₂S and anion-binding research. *Dalton Trans.* **2015**, *44* (46), 1978.

Chapter V

1. Giepmans, B. N. G.; Adams, S. R.; Ellisman, M. H.; Tsien, R. Y. The fluorescent toolbox for assessing protein location and function. *Science* **2006**, *312*, (5771), 214.
2. Wang, B.; Hu, L.; Siahaan, T. J. *Drug Delivery: Principles and Applications*, 2nd ed.; Wang, B., Ed.; Wiley: Hoboken, **2016**.
3. Chan, J.; Dodani, S. C.; Chang, C. J. Reaction-based small molecule fluorescent probes for chemoselective bioimaging. *Nat. Chem.* **2012**, *4*, 973.
4. Zuin, M.; Rigatelli, G.; Faggian, G.; L'Erario, R.; Chinaglia, M.; Roncon, L. Could advanced drug delivery systems be the future in cardiovascular revascularization medicine? *Vascular* **2017**, *25* (4), 447.

5. Veiseh, O.; Tang, B. C.; Whitehead, K. A.; Anderson, D. G.; Langer, R. Managing diabetes with nanomedicine: challenges and opportunities. *Nat. Rev. Drug Discov.* **2015**, *14*, 45.
6. Chen, X.; Wang, F.; Hyun, J. Y.; Wei, T.; Qiang, J.; Ren, X.; Shin, I.; Yoon, J. Recent progress in the development of fluorescent, luminescent and colorimetric probes for detection of reactive oxygen and nitrogen species. *Chem. Soc. Rev.* **2016**, *45*, 2976.
7. Jiao, X.; Li, Y.; Niu, J.; Xie, X.; Wang, X.; Tang, B. Small-molecule fluorescent probes for imaging and detection of reactive oxygen, nitrogen and sulfur species in biological systems. *Anal. Chem.* **2018**, *90*, 533.
8. Bai, X.; Ng, K. K.-H.; Hu, J. J.; Ye, S.; Yang D. Small-molecule-based fluorescent sensors for selective detection of reactive oxygen species in biological systems. *Annu. Rev. Biochem.* **2019**, *88*, 605.
9. Pairault, N; Barat R.; Tranoy-Opalinski, I.; Renoux, B.; Thomas, M.; Papot, S. Rotaxane-based architectures for biological applications. *Chim.* **2016**, *19*, (1-2), 103.
10. Braegelman, A. S.; Webber, M. J. A temperature-sensitive drug release system based on phase-change materials. *Theranostics* **2019**, *9*, (11), 3017.
11. White, B. M.; Zhao, Y.; Kawashima, T. E.; Branchaud, B. P.; Pluth, M. D.; Jasti, R. Expanding the Chemical Space of Biocompatible Fluorophores: Nanohoops in Cells. *ACS Cent. Sci.* **2018**, *4* (9), 1173.
12. Lovell, T. C.; Bolton, S. G.; Kenison, J. P.; Shangguan, J.; Otteson, C. E.; Civitci, F.; Nan, X.; Pluth, M. D.; Jasti, R. Subcellular Target Nanohoop for One- and Two-Photon Live Cell Imaging. *ACS Nano* **2021**, *15* (9), 15285.
13. Stoddart, J. F. Mechanically interlocked molecules (MIMs)—molecular shuttles, switches, and machines. *Angew. Chem. Int. Ed.* **2017**, *56*, (37), 11094.
14. Otteson, C. E.; Levinn, C. M.; Van Raden, J. M.; Pluth, M. D.; Jasti, R. Nanohoop Rotaxane Design to Enhance Selectivity of Reaction-Based Probes: a Proof-of-Principle Study. *Org. Lett.* **2021**, *23*, 4608.
15. Arunkumar, E.; Forbes, C. C.; Noll, B. C.; Smith, B. D. Squaraine-derived rotaxanes: sterically protected fluorescent near-IR dyes. *J. Am. Chem. Soc.* **2005**, *127*, (10), 3288.
16. Craig, M. R.; Claridge, T. D. W.; Anderson, H. L.; Hutchings, M. G. Synthesis of a cyclodextrin azo dye [3]rotaxane as a single isomer. *Chem. Commun.* **1999**, *16*, 1537.
17. Patrick, C. W.; Woods, J. F.; Gawal, P.; Otteson, C. E.; Thompson, A. L.; Claridge, T. D. W.; Jasti, R.; Anderson, H. L. Polyynes [3]Rotaxanes: Synthesis via Dicobalt Carbonyl Complexes and Enhanced Stability. *Angew. Chem. Int. Et.* **2022**, *61* (10), e202116897.

18. Cheng, C.; Deng, T.; Lin, F.; Cai, Y.; Zink, J. I. Supramolecular nanomachines as stimuli-responsive gatekeepers on mesoporous silica nanoparticles for antibiotic and cancer drug delivery. *Theranostics* **2019**, *9*, (11), 3341.
19. Simões, S. M. N.; Rey-Rico, A.; Concheiro, A.; Alvarez-Lorenzo, C. Supramolecular cyclodextrin-based nanocarriers. *Chem. Commun.* **2015**, *51*, (29), 6275.
20. Fernandes, A.; Viterisi, A.; Coutrot, F.; Potok, S.; Leigh, D. A. Rotaxane-based propeptides: protection and enzymatic release of a bioactive pentapeptide. *Angew. Chem. Int. Ed.* **2009**, *48*, (35), 6443.
21. Barat, R. Legigan, T.; Tranoy-Opalinski, I.; Renoux, B.; Péraudeau, E.; Clarhaut, J.; Poinot, P.; Fernandes, A. E.; Aucagne, V.; Leigh, D. A.; Papot, S. A mechanically interlocked molecular system programmed for the delivery of an anticancer drug. *Chem. Sci.* **2015**, *6*, (4), 2608.
22. Denis, M.; Pancholi, J.; Jobe, K.; Watkinson, M.; Goldup, S. M. Chelating rotaxane ligands as fluorescent sensors for metal ions. *Angew. Chem. Int. Ed.* **2018**, *57*, (19), 5310.
23. Yu, G.; Wu, D.; Li, Y.; Zhang, Z.; Shao, L.; Zhou, J.; Hu, Q.; Tang, G.; Huang, F. A pillar[5]arene-based [2]rotaxane lights up mitochondria. *Chem. Sci.* **2016**, *7*, (5), 3017.
24. Sojka, M.; Fojtu, M.; Fialova, J.; Masarik, M.; Necas, M.; Marek, R. Locked and loaded: ruthenium(II)-capped cucurbit[n]uril-based rotaxanes with antimetastatic properties. *Inorg. Chem.* **2019**, *58*, (16), 10861.
25. Lovell, T. C.; Bolton, S. G.; Kenison, J. P.; Shangguan, J.; Otteson, C. E.; Civitci, F.; Nan, X.; Pluth, M. D.; Jasti, R. Subcellular Target Nanohoop for One- and Two-Photon Live Cell Imaging. *ACS Nano* **2021**, *15* (9), 15285.
26. Van Raden, J. M.; Jarenwattananon, N. N.; Zakharov, L. N.; Jasti, R. Active Metal Template Synthesis and Characterization of a Nanohoop [c 2]Daisy Chain Rotaxane. *Chem. Euro. J.* **2020**, *26* (45), 10205.
27. Andersen, J. K. Oxidative stress in neurodegeneration: cause or consequence? *Nat. Med.* **2004**, *10*, 18.
28. Finkel, T.; Serrano, M.; Blasco, M. A. The common biology of cancer and ageing. *Nature* **2007**, *448*, 767.
29. Veal, E. A.; Day, A. M.; Morgan, B. A. Hydrogen Peroxide Sensing and Signaling. *Mol. Cell* **2007**, *26* (1), 1.
30. Dickinson, B. C.; Chang, C. J. Chemistry and biology of reactive oxygen species in signaling or stress responses. *Nat. Chem. Biol.* **2011**, *7*, 504.

31. DiMarzo, N.; Chisci, E.; Giovannoni, R. The Role of Hydrogen Peroxide in Redox-Dependent Signaling: Homeostatic and Pathological Responses in Mammalian Cells. *Cells* **2018**, *7* (10), 156.
32. Bezner, B. J.; Ryan, L. S.; Lippert, A. R. Reaction-Based Luminescent Probes for Reactive Sulfur, Oxygen and Nitrogen Species: Analytical Techniques and Recent Progress. *Anal. Chem.* **2020**, *92* (1), 309.
33. Woolley, J. F.; Stanicka, J.; Cotter, T. G. Recent advances in reactive oxygen species measurement in biological systems. *Trends Biochem. Sci.* **2013**, *38* (11), 556.
34. Wang, H.-S. Development of fluorescent and luminescent probes for reactive oxygen species. *Trends Analyt. Chem.* **2016**, *85*, 181.
35. Wang, R.; Bian, Z.; Zhan, D.; Wu, Z.; Yao, Q.; Zhang, G. Boronic acid-based sensors for small-molecule reactive species: A review. *Dyes Pigm.* **2021**, *185*, 108885.
36. Abo, M.; Urano, Y.; Hanaoka, K.; Terai, T.; Komatsu, T.; Nagano, T. Development of a Highly Sensitive Fluorescence Probe for Hydrogen Peroxide. *J. Am. Chem. Soc.* **2011**, *133*, 10629.
37. Van Raden, J. M.; Jarenwattananon, N. N.; Zakharov, L. N.; Jasti, R. Active Metal Template Synthesis and Characterization of a Nanohoop [c 2]Daisy Chain Rotaxane. *Chem. Euro. J.* **2020**, *26* (45), 10205.
38. Oakdale, J. S.; Kwisnek, L.; Fokin, V. V. Selective and Orthogonal Post-Polymerization Modification using Sulfur(VI) Fluoride Exchange (SuFEx) and Copper-Catalyzed Azide-Alkyne Cycloaddition (CuAAC) Reactions. *Macromolecules*, **2016**, *49* (12), 4473.